

**HUMAN LOCOMOTION AND ENERGETICS
IN SIMULATED PARTIAL GRAVITY**

by

DAVA JEAN NEWMAN

B.S., The University of Notre Dame, 1986
S.M., Massachusetts Institute of Technology, 1988
S.M., Massachusetts Institute of Technology, 1989

Submitted in partial fulfillment
of the requirements for the
degree of

DOCTOR OF PHILOSOPHY

in

AEROSPACE BIOMEDICAL ENGINEERING

at the

MASSACHUSETTS INSTITUTE OF TECHNOLOGY

Cambridge, Massachusetts, U.S.A.

June, 1992

© 1992 Massachusetts Institute of Technology
All rights reserved.

Signature of Author _____
Department of Aeronautics and Astronautics, June, 1992

Certified by _____
Professor Harold L. Alexander
Thesis Supervisor, Bradley Career Development Professor of Aeronautics and Astronautics

Certified by _____
Professor Thomas A. McMahon
Professor of Applied Mechanics and Professor of Biology, Harvard University

Certified by _____
Professor Thomas Sheridan
Professor of Mechanical Engineering

Accepted by _____
Professor Harold Y. Wachman, Chairman, Department Graduate Committee

MASSACHUSETTS INSTITUTE
OF TECHNOLOGY

JUN 05 1992

ARCHIVES

HUMAN LOCOMOTION AND ENERGETICS IN SIMULATED PARTIAL GRAVITY
by
Dava Jean Newman

Submitted to the Department of Aeronautics and Astronautics on May 20, 1992 in partial fulfillment of the requirements for the Degree of Doctor of Philosophy in Aerospace Biomedical Engineering

Attempts to investigate lunar locomotion took place in the 1960's. However, over the past two decades little research on human performance in partial gravity environments has been undertaken. Since human locomotion and posture control are consequences of 1 g evolution and development, it is shown that the mechanics of human gait depend upon the prevailing gravity level, and are altered from walking and running in normal gravity to loping at lunar and Martian gravity levels.

This study investigates human locomotion over a full range of partial gravity environments (1/6 g to 1 g), and investigates multiple partial gravity simulation techniques. This comprehensive scientific investigation includes two aspects of partial gravity locomotion, namely, biomechanics and energetic costs. Experimental results from underwater submersion and parabolic flight, are presented, compared, and then interpreted using mathematical models for locomotion. The simulations provide practical, albeit complex, techniques for assessing the mechanics and associated energetics of partial gravity locomotion.

A unique human-rated submersible treadmill with an embedded split-plate force platform and an adjustable ballasting harness were used during the underwater partial gravity simulations. Biomechanics and steady-state workload measurements were taken during the submersion experiments. Complementary biomechanics measurements were recorded aboard NASA's KC-135 aircraft during parabolic flight simulating lunar and Martian gravity levels. Vertical forces exerted by subjects on the treadmill-mounted force platform were sampled and used for gait analysis, and the results indicate that peak vertical force and stride frequency decrease as the gravity level is reduced while ground contact time is independent of gravity level. Subjects tended to lope over a wide range of speeds (~1.5 m/s to ~2.3 m/s) suggesting a change in the mechanics for lunar and Martian locomotion as compared to typical 1 g locomotion.

Steady-state energy expenditures were measured through respiration gas analysis and heart rate measurements. In accordance with theoretical predictions, energy requirements for lunar gravity (1/6 g), Martian gravity (3/8 g), and two-thirds gravity (2/3 g) are significantly less than energy requirements for 1 g locomotion. Oxygen uptake measurements, $\dot{V}O_2$, decrease as gravity level changes from 1 g to 1/6 g, however, the decrease is nonmonotonic in half the subject population for walking at low gravity levels. It is hypothesized that a gravity threshold may exist, below which energy expenditures increase for low speed locomotion as excess energy is spent maintaining posture and stability in addition to the energy expended for walking.

This research effort investigated the gravity dependence of human locomotion and the associated energetics. Recommendations for advanced spacesuit, conceptual space vehicle, and planetary habitat design are suggested. The biomechanics measurements provide an initial partial gravity database for these future designs while the energetics data will help define oxygen requirements for planetary life support systems. Additional applications of the research may include clinical rehabilitation and sports biomechanics.

Thesis Supervisor: Dr. Harold L. Alexander
Title: Bradley Career Development Professor of Aeronautics and Astronautics, MIT
Thesis Advisor: Dr. Thomas A. McMahon
Title: Professor of Applied Mechanics and Professor of Biology, Harvard University

ACKNOWLEDGMENTS

To my advisors and mentors - thank you!

Great teachers live in each one of us who have learned from them, for they have shaped in us that which is internal.
- Fr. T.M. Hesburgh

Professor Alexander, many thanks. I greatly appreciate all of your help. Professor McMahon, you were my saving grace. You stimulated me, challenged me, and gave me hope. Professor Young, it was your vision and accomplishments that enticed me to come to M.I.T. Thank you for letting me be a part of the Man-Vehicle laboratory. Dr. Oman, I appreciate your guidance. Professor Dunne, your life and teachings have truly inspired and shaped me. Professor Kanury, 80% philosophy and 20% thermodynamics - indeed! Thanks. Dr. Dan, for being someone to look up to as well as a great officemate and friend. Dr. Bussolari, Professor Akin, Dr. Churchill, Dr. Lichtenberg, Dr. Arrott, Bob Renshaw, Sherwood Modestino, Kim Tseko, Beverly Linton, Jim Costello, Will Watson, Myra Harrison, and countless others, please accept my gratitude and smiles. I would like to acknowledge the Aeronautics and Astronautics department and the Technology and Policy Program as well as the Dean's office for help with my Interdepartmental Ph.D. program.

The Advanced EVA Systems Branch at NASA Ames made my underwater experiments possible. Dr. Webbon, thanks for your support. Doug, Phil, Jorge, Jerry, Curt, Bernie, Peter, and Becky, I sure appreciate your help and countless hours of support. Vic (my wardroom critic), thanks for everything. Thanks to Remus, Victoria, and the folks in the machine shop and the model shop. I would also like to acknowledge the Advanced Life Support Division and the NASA Graduate Students Researchers' Fellowship Program. Financial support for my studies and research at MIT was also provided by NASA Grant NAG 9-125. Thanks to the folks in the Man-Systems Division at NASA JSC. It was great flying with you. Same time next year? My appreciation and thanks are extended to everyone at ISU.

Your friends are your needs answered. -Anonymous

Thank you all. From my childhood friends to my adult (although we don't act like it most of the time) colleagues - you made it all worthwhile. Kelli, Paula, Cath, my Notre Dame friends, Daph, Steph and Ron, and Dawno. My MIT friends who kept me sane (or are we all insane and just don't know it?). Thanks to Brad, Rich, Divya, Jock, and Keoki. Nick, thanks for all of the programming help. Mark, my UROP, many thanks (SI units, ha). Corrie, I have really enjoyed this semester. Karla, my new officemate, great to know you. Thanks for everything. Mark, Valerie, Glaw, Dave, Juan, Scott, Ted - good luck. To the Baker House tutors and students, it's been a great five years with you all - thanks. Eliot, Liz, Kjirste, and Jim, thank goodness for skiing and biking.

To everyone, listed and unlisted, many thanks!

I wonder what sort of tale we've fallen into?...Don't the great tales never end? -J.R.R. Tolkien

To my family - thanks for your support and love. I am with you.

"The first twenty pages were great, but now... it reminds me when..."

"Two more months to graduation? Well Dave, we just might not have that long."

The heart's desire: Things are meant, there are signs, the heart speaks, there is a way. -J. Dunne & J.R.R. Tolkien

This thesis is dedicated to the one I love. Thank you for happiness, passion, energy, a challenge, truth, and most of all - the trinity of life. Words do no justice!

Love is the subtlest force in the world. - Gandhi

HUMAN LOCOMOTION AND ENERGETICS IN SIMULATED PARTIAL GRAVITY.

TABLE OF CONTENTS

ABSTRACT	2
ACKNOWLEDGMENTS	3
TABLE OF CONTENTS	4
LIST OF FIGURES	6
LIST OF TABLES	8
PREFACE	9
CHAPTER I. INTRODUCTION	11
1.1 MOTIVATION.....	15
1.1.1 Biomechanics Literature	16
1.1.2 Energetics Literature	17
1.2 CONTRIBUTION.....	19
1.3 ROAD MAP TO DISSERTATION	21
CHAPTER II. BACKGROUND	23
2.1 WORK PHYSIOLOGY.....	25
2.1.1 Energetic Processes	25
2.1.2 Hydraulic Analog.....	27
2.1.3 Workload.....	31
2.2 HUMAN LOCOMOTION	33
2.2.1 Introduction to the Determinants of Human Gait	33
2.2.2 The Mechanics of Walking and Running.....	41
2.2.2.1 <i>Inverted Pendulum Model for Walking</i>	42
2.2.2.2 <i>Running Humans and Hopping Kangaroos</i>	43
2.2.2.3 <i>Mechanical Efficiency</i>	44
CHAPTER III. PARTIAL GRAVITY SIMULATION AND MODELING	49
3.1 SIMULATION TECHNIQUES.....	49
3.1.1 Suspension Systems	49
3.1.2 Parabolic Flight.....	52
3.1.3 Water Immersion	55
3.1.3.1 <i>Partial Gravity Ballasting</i>	56
3.1.3.2 <i>Immersion Assumptions</i>	58
3.2 HYDRODYNAMIC MODELING.....	60
3.2.1 Flow Regimes and Calculations	62
3.2.2 The Mathematical Model.....	64
3.2.2.1 <i>Calculating the Drag Energy</i>	67
3.2.2.2 <i>Computer Programs and Output</i>	71
3.2.2.2.1 Program Inputs.....	71
3.2.2.2.2 Drag Calculation.....	72
3.2.2.2.3 Program Output.....	72

CHAPTER IV. METHODS	74
4.1 SUBJECTS	76
4.2 EXPERIMENTAL PROTOCOL.....	77
4.2.1 Immersion Experiments	77
4.2.2 Parabolic Flight.....	78
4.2.3 Rationale.....	78
4.2.4 Personnel.....	79
4.3 EQUIPMENT AND MEASUREMENTS.....	80
4.3.1 Underwater Locomotion Study.....	80
4.3.1.1 <i>Submersible Treadmill</i>	81
4.3.1.2 <i>Video Recordings</i>	87
4.3.1.3 <i>Energetics Equipment</i>	88
4.3.2 Parabolic Flight Pilot Equipment.....	92
4.3.3 Data Acquisition and Analysis.....	94
 CHAPTER V. RESULTS AND DISCUSSION	 100
5.1 RESULTS	100
5.1.1 Biomechanics	101
5.1.1.1 <i>Underwater Locomotion Study</i>	103
5.1.1.1.1 Peak force.....	105
5.1.1.1.2 Stride frequency and contact time	105
5.1.1.1.3 Aerial time.....	106
5.1.1.2 <i>Parabolic Flight Pilot Study</i>	112
5.1.2 Energetics	116
5.1.2.1 <i>Partial Gravity Oxygen Uptake Measurements</i>	116
5.1.2.2 <i>Partial Gravity Heart Rate Measurements</i>	117
5.2 DISCUSSION.....	123
5.2.1 Limitations of Experimental Techniques.....	123
5.2.2 Mathematical Model for Running.....	124
5.2.3 Gravity Threshold and Optimal Gaits.....	132
 CHAPTER VI. SUMMARY AND CONCLUSIONS	 138
 Appendix A: COMPUTER PROGRAMS	 145
A.1 HYDRODYNAMICS MODEL.....	145
A.2 HYDRODYNAMICS MODEL VERIFICATION.....	164
A.3 DATA ACQUISITION PROGRAM.....	166
 Appendix B: SUBJECTS' CONSENT AND ANTHROPOMETRIC DATA	 200
B.1 ANTHROPOMETRIC DATA	200
B.2 INFORMED CONSENT FORM	209
 REFERENCES	 214

LIST OF FIGURES

CHAPTER TWO

2.1 Hydraulic analog of energetic processes during exercise.....	30
2.2 A complete stride cycle for walking.....	35
2.3 Pelvic rotation during walking.....	35
2.4 Depiction of scissors gait during walking.....	35
2.5 Pelvic tilt during walking.....	37
2.6 Heel strike and heel-off interactions with the knee.....	37
2.7 Lateral displacement of the pelvis.....	38
2.8 Inversion-eversion-inversion of the foot.....	40
2.9 Lateral trunk deflection.....	40
2.10 Anteroposterior flexion of the trunk.....	40
2.11 Energy cost for athletes walking at the most economical speed and running as a function of the incline of the ground.....	46

CHAPTER THREE

3.1 Harvard University Field Station (HFS) partial gravity suspension simulator.....	51
3.2 NASA's KC-135 aircraft used for parabolic flight.....	53
3.3 Schematic drawing of lunar parabolic flight.....	54
3.4 Adjustable ballasting harness used for partial gravity immersion experiments.....	57
3.5 Velocity profile of leg assumed during inertial drag calculations.....	59
3.6 Model of leg moving through the water during inertial drag calculations.....	59
3.7 Model of human body used for the hydrodynamic model.....	66

CHAPTER FOUR

4.1 Underwater treadmill 6x6x3 experimental protocol matrix.....	78
4.2 Submersible treadmill in Neutral Buoyancy Test Facility.....	82
4.3 Submersible treadmill-mounted force platform design.....	86
4.4 Submersible treadmill force plate vertical force calibration.....	87
4.5 Commercial diving band mask used in the underwater experiments.....	90
4.6 Gas analysis equipment used for steady-state workload measurements.....	91
4.7 Astronaut N. Sherlock during Martian parabolic flight.....	93
4.8 Del-Mar instrumented treadmill force calibration.....	94
4.9 Data collection on the KC-135 using a TEAC recorder for force and velocity.....	96
4.10 Data acquisition computer program front panel.....	97

CHAPTER FIVE

5.1 Typical traces for vertical ground reaction, vertical velocity, and vertical displacement.....	102
5.2 Biomechanics data of an average stride cycle for an individual subject on the submersible treadmill moving at 2.3 m/s.....	104
5.3 Mean peak force versus gravity level.....	108
5.4 Dimensionless peak force versus gravity level.....	108
5.5 Dimensionless peak force normalized by local gravitational acceleration versus gravity level.....	109
5.6 Stride frequency versus gravity level.....	109
5.7 Contact time versus gravity level.....	110
5.8 Stepping frequency for Apollo 11 data and simulated lunar gravity.....	110

5.9 Aerial time for partial gravity simulation experiments.	111
5.10 Locomotive index versus gravity level.	111
5.11 KC-135 peak force data versus gravity level for a treadmill speed of 2 m/s.	114
5.12 Mean stride frequency versus gravity level for all partial gravity experiments.	114
5.13 Contact time versus gravity level for all partial gravity experiments.	115
5.14 Aerial time versus gravity level for all partial gravity experiments.	115
5.15 Locomotive index versus gravity level including parabolic flight data.	116
5.16 Workload versus gravity level.	119
5.17 Workload versus gravity level for each of the six subjects.	120
5.18 Heart rate versus gravity level.	121
5.19 Individual heart rate versus gravity level.	121
5.20 Linear relationship between oxygen uptake and heart rate.	122
5.21 Schematic drawing of mass-spring model for forward running.	125
5.22 Peak force at midstep for a mathematical spring-model and experimental data.	129
5.23 Leg spring stiffness and vertical stiffness as functions of dimensionless horizontal velocity.	130
5.24 Leg angle and vertical Froude number as a function of treadmill velocity.	131
5.25 Initial leg angle upon landing as a function of gravity for different speeds.	131
5.26 Oxygen uptake for Subjects 1-3 walking versus simulated gravity level.	133
5.27 Cost of Transport versus treadmill velocity.	136
5.28 Cost of Transport versus gravity level.	136
5.29 Cost of Transport minus resting metabolism versus gravity level.	137

LIST OF TABLES

CHAPTER THREE

3.1 Ballasting loads for a 1.8 meter, 74 kg subject.....	56
3.2 Time increments and positions of leg model for swing phase.	59
3.3 Inertial effects due to added ballast and added mass - sample calculations.....	60
3.4 Expected Reynolds numbers for body segments during underwater simulation.	63
3.5 Dimensions of geometric shapes for hydrodynamics model.....	67
3.6 Hydrodynamic Drag Energy - Summary.....	73

CHAPTER FOUR

4.1 Subject database.....	77
4.2 Underwater locomotion and energetics experiment session timeline.....	79
4.3 Submersible Treadmill Parts List.....	85
4.4 Gas Analysis Equipment.....	89
4.5 Basic Statistical Calculations for a Lunar Gravity Simulation.	95

CHAPTER FIVE

5.1 Input Parameters for Mathematical Model for Running.	126
5.2 Statistical Values for Cost of Transport Measures Across Gravity Levels.....	137

PREFACE

Апреля 12, 1961! Юрий Гагарин (Yuri Gagarin), became the first human to leave the confines of our biosphere as he spent 108 minutes in space. Humanity was forever changed. Would access to infinity change *post 1961 A.D. Homo Sapiens*? Space offers a metamorphosis of human philosophy and charges a fee of responsibility for overseeing her exploitation.

Human exploration of space has deep-rooted scientific, literary, and artistic traditions. Ever since Galileo discovered that the moon and planets were actually different worlds, humankind has been obsessed with space travel and exploration of these nether worlds. The great scientists and engineers of rocketry - Tsiolkovsky, Goddard, and Oberth, and their successors Korolev, von Braun, and others, were inspired by the intellectual challenge as well as the dream of spaceflight. Konstantin Tsiolkovsky's passion to conquer the confines of gravity empowered him to calculate the principles of rocket flight in outer space. He dreamt that spaceflight would bring equality and perfection to humankind and its individual members [McDougall, 1985].

Literary and artistic space disciples actually led the scientists by a few hundred years. In 1638 John Wilkins argued that space travel would be possible in *The Discovery of a World in the Moone*, and just a few decades later French satirist Cyrano deBergerac jested that rockets would lift people from Earth in *The Comical History of the States and Empires of the Worlds of the Moon and Sun*. The creative and limitless imaginations of writers paved the way for scientists, and writer Jules Verne is largely credited for putting the science of spaceflight on truly serious footing with his mathematical, scientific, and engineering depiction of spaceflight in *From the Earth to the Moon* written in 1865.

Human exploration of space assumes an understanding of the environment and how humans will perform in this altered environment. Of the four known natural forces: gravity, electromagnetism, the strong force binding atomic nuclei, and the weak force causing radioactive decay, **gravity** is least understood. Attempts to understand the mysterious and evasive gravitational force have resulted in Newton's *Principia* and Einstein's theory of general relativity. Gravity essentially rules the universe; having a pull that keeps the moon orbiting the Earth, the Earth in place around the sun, and the solar system within the galaxy. The Earth spins a thousand miles an hour at the equator, and gravity keeps us from falling off the surface.

The importance of gravity in our lives is eloquently defined below [Boslough, 1989]:

We are children of gravity. We can't touch it or see it. But it has guided the evolutionary destiny of every plant and animal species and has dictated the size and shape of our organs and limbs. Every bone and muscle is aligned to maximize mobility in 1 g. -Dr. R. Pelligra

But yet...it [gravity] is the least understood of the four known natural forces. How does gravity affect our human existence? Suffice it to say, in an omnipresent fashion. I ask a more tangible question, "How does gravity affect human locomotion and what are the associated energetic costs?"

Locomotion is the most common activity of humans, and it is shocking to discover that until the last few decades, scientists and engineers neglected the study of biomechanics of human locomotion. Movement of the body is not only our most characteristic activity, but our relationships with the environment and other people are based on human movement. Locomotion embodies the elegance of ballet and the quintessence of the bushman.

Just as with space, artists provided the first comprehensive works on locomotion. The importance of the various functions of the limbs in locomotion was recognized as early as Aristotle's time. Throughout history, artists such as DaVinci, Durer, and Meissonier were fascinated with locomotion, and Michelangelo not only captured humans in motion, but he understood the effects of gravity on human posture. This is born out in his masterpiece *The Last Judgment* in which he depicts a symphony of human forms, with levitating spirits and free falling bodies assuming the neutral body posture characteristic of the space environment (See Chapter I cover page graphic). Also fundamental in the advancement of locomotion studies are Eadweard Muybridge's monumental photographs from the late 1800's and early 1900's which still serve as the virtuoso on movements and gaits natural to most animals [© 1957]. I believe a Muybridge living in 1992 would depict Martian loping similar to the opening photograph of the Results and Discussion Chapter.

I. INTRODUCTION



KOSMOS

Who includes diversity and is Nature,

*Who is the amplitude of the earth, and the coarseness and sexuality of the earth, and the
great charity of the earth, and the equilibrium also,*

*Who has not look'd forth from the windows the eyes for nothing, or whose brain held
audience with messengers for nothing,*

Who contains believers and disbelievers, who is the most majestic lover,

*Who holds duly his or her triune proportion of realism, spiritualism, and of the aesthetic or
intellectual,*

Who having consider'd the body finds all its organs and parts good,

*Who, out of the theory of the earth and of his or her body understands by subtle analogies
all other theories,*

The theory of a city, a poem, and of the large politics of these States;

*Who believes not only in our globe with its sun and moon, but in other globes with their
suns and moons,*

*Who, constructing the house of himself or herself, not for a day but for all time, sees races,
eras, dates, generations,*

The past, the future, dwelling there, like space, inseparable together.

Walt Whitman, Leaves of Grass

CHAPTER I. INTRODUCTION

Gravity plays a crucial, but poorly understood role in human locomotion. Human evolution in an Earth-normal one gravity (1 g) environment and the development of our 1 g musculoskeletal system have presumably optimized performance under Earth gravity conditions. Theoretical and experimental studies in the literature suggest that locomotion varies in altered gravity, perhaps due to compensating mechanisms taking place in sub-gravity locomotion. If this hypothesis is true, it provides insight into the fundamental dynamics of human locomotion, but controversy abounds and the role of gravitational acceleration in locomotion is still undefined.

There is a scarcity of partial gravity human locomotion studies. Partial gravity (*reduced gravity*, *low gravity*, and *partial gravity* are synonymous throughout the text) refers to the range of gravitational acceleration between 0 g and 1 g (where 'g' refers to the Earth's gravitational acceleration, 9.8 m/s^2). Of the few existing investigations, an overwhelming majority are over 25 years old and these studies singularly assess human performance for lunar gravity omitting Martian gravity and other partial gravity levels.

The impetus of this research effort lies in the need to fill the void of knowledge on human locomotion and the associated energetic costs for the entire range of partial gravity. Unanswered research questions regarding locomotion and energetics include: What is the naturally occurring gait for human motion in a partial gravity environment at a given speed? What are the speeds associated with transitions from walking to running and is the phenomenon gravity dependent? What is the energy cost for work in partial gravity? What are the oxygen requirements for a life support system on another celestial body? This thesis presents gait, transition speed, and oxygen consumption results to begin understanding human performance on other planets.

This dissertation contributes an unprecedented scientific evaluation of locomotion and associated energy costs for the entire range of partial gravity including experiments at simulated lunar gravity (1/6 g), Martian gravity (3/8 g), two-thirds gravity (2/3 g), approximate full gravity (9/10 g), and terrestrial Earth gravity (1 g). The biomechanics analysis identifies gaits, details transition speeds, and presents force measurements, while the energetics investigation yields energy usage via oxygen consumption measurements for partial gravity environments. Advanced spacesuit designs will rely on all of these measurements because they must accommodate astronaut mobility and locomotion as well as provide portable life support systems. Planetary habitat design could incorporate the results to assure ideal astronaut physiological conditioning, comfort, and the necessary amount of oxygen for life support systems. This partial gravity human performance

study could influence space vehicle conceptualization, especially when considering a human mission to Mars, because if an artificial gravity spacecraft is required the results of this study give engineers an initial partial gravity database from which to base their choice of spacecraft gravity level and life support system capacity.

On Earth, humans primarily employ two gaits for locomotion, walking and running. Gait encompasses all types of locomotion and gait analysis distinguishes between the immutable sequence of limb movements used during locomotion (i.e., walk, run, jump, etc.). During walking there is a dual contact phase in the stride cycle when both feet are in contact with the ground at the same time. The distinguishing characteristics of running are that only one foot contacts the ground at a time and there is an aerial phase. While running, humans exert a vertical force on the ground greater than their body weight and become airborne, but while walking they never leave the ground. Loping is a gait uncharacteristic of terrestrial locomotion, but important for partial gravity locomotion. A lope is a specific type of running that includes an extended aerial phase and an increased stride length. A person who is loping propels himself/herself upwards into a floating trajectory. Loping requires different mechanics for progression than walking or running and may prove to be the most efficient means of human self-transportation in partial gravity in terms of biomechanics, energy consumption, and comfort.

A convenient partial gravity environment for locomotion is necessary to study the impending research questions. Suspension systems, aircraft flying parabolic trajectories, and underwater submersion are the most frequently used techniques. Suspension systems tend to inhibit the subject's movement by limiting the degrees of freedom and parabolic flight allows only short periods of partial gravity, thus limiting data collection to biomechanics and excluding the study of steady-state energetics. Water immersion serves as the primary simulation technique for this research effort because it offers the advantages of allowing free motion for a long time which permits assessment of both biomechanics and steady-state energetics. The major disadvantages of immersion are the viscosity and inertia of the water that produce drag and damping on human movements, therefore, the experimental protocol calls for subjects to minimize rapid limb movements and gross translational motions. A hydrodynamic modeling effort verifies the integrity of water immersion as a partial gravity simulation technique (See Section 3.2 Hydrodynamic Modeling). After completion of the underwater experiments, a fortunate opportunity arose to run a pilot study during lunar and Martian parabolic flight. The results from parabolic flight complement the underwater biomechanical and energetics data, thus allowing for comparisons between two partial gravity techniques.

The submersible treadmill and adjustable ballasting harness used in conjunction with a life support system comprise the partial gravity simulation technique for underwater experiments in the Neutral Buoyancy Test Facility (NBTF) at NASA Ames Research Center in California. The underwater experiments assess human performance for the entire range of partial gravity including experiments at simulated lunar gravity (1/6 g), Martian gravity (3/8 g), two-thirds gravity (2/3 g), approximate full gravity (9/10 g), and terrestrial Earth gravity (1 g). The lunar and Martian parabolic flight experiments complement the underwater experiments and were flown out of Ellington Field, Texas, using NASA's KC-135 aircraft. Six healthy subjects, four men and two women, participated as subjects in the underwater locomotion and energetics experiments while two healthy men served as the primary subjects for the parabolic flight experiments.

The novel submersible treadmill and adjustable ballasting harness designs provide a viable research simulation technique to determine how gravity influences human locomotion. This simulation technique unveils the mechanics of biped locomotion through measurements of vertical force, stride frequency, and foot contact time. These measurements are attained from the innovative submersible treadmill design that incorporates an embedded split-plate force platform to analyze both walking and running gaits. The split-plate force platform provides single foot recordings. Therefore, during the dual stance phase of walking, the signals are meaningful rather than being undifferentiable as for a conventional treadmill which fails to distinguish the feet from one another. The adjustable ballasting harness fits anyone from 1.5 meters to 1.9 meters (5 ft. to 6 ft. 2 in.) in height and provides realistic loading (using lead ballast) of the torso and lower limb segments. The subjects are equipped with a commercial diving facemask that provides two-way communications between the test director and subject at all times. The instrumented life support system provides underwater oxygen consumption measurements to determine energy expenditure during partial gravity locomotion. Heart rate measurements are also taken while the subjects exercise underwater.

1.1 MOTIVATION

The goal of the research effort is to assess biomechanics and workload for simulated partial gravity environments, and the motivation for the research stems from a desire to gain further knowledge of physiological functioning and underlying mechanisms of human locomotion. The influence of various gravitational accelerations on humans is questioned. The utility of this research is not only its applicability to the aerospace sciences, but in a broader sense, also to the physiology and modeling of terrestrial locomotion. A review of past research efforts introduces the reader to the

literature, supplies background, and allows for identification of unanswered research questions that this study investigates.

An extensive partial gravity research initiative during the current decade could help accomplish the goal of sending humans back to the moon and onward to Mars. There exists a prominent need to fill the dearth of knowledge on human performance in partial gravity which results from almost twenty years of inactivity in this area. This study contributes to the understanding of human performance in partial gravity. Many experimental studies have investigated either locomotion or energetics at partial gravity conditions, but I believe this study is the first to provide a comprehensive investigation of both biomechanics and energetics for a wide range of partial gravity conditions.

1.1.1 Biomechanics Literature

Current research in terrestrial biomechanics investigates the mechanics of locomotion assuming a constant gravitational acceleration of 9.8 m/s^2 ; this is precisely the parameter that changes for locomotion on other planets. The laws of physics govern locomotion and energy requirements for movement on the Earth as well as in partial gravity. Models exist for walking and running on Earth, but will these models apply to the mechanics of partial gravity locomotion? During 1 g walking muscular energy is used to lift the body in the first phase of the step acquiring maximum gravitational potential energy (PE), while body acceleration in the forward direction is attained by transforming PE to kinetic energy (KE) in the second phase of the step. Section 2.2.2.1, Inverted Pendulum Model for Walking, describes this phasic relationship of efficient energy exchange between PE and KE during walking in more detail and Section 2.2.2.2, Running Humans and Hopping Kangaroos, describes the elastic energy exchange mechanism of running. The goal of this study is to understand the dynamics of motion which govern partial gravity locomotion, and applying 1 g locomotion models is a start.

Margaria and Cavagna [1964, pg. 1144] extrapolate theoretical analysis of the mechanical characteristics of human locomotion in 1 g and apply it to sub-gravity locomotion. During partial gravity walking less gravitational potential energy is available to sustain the forward acceleration during locomotion, and lifting the body requires less energy. Margaria and Cavagna hypothesize that walking should be practically impossible for low gravity levels such as the moon's $1/6 \text{ g}$ environment. However, Roberts' [1963] study of walking responses under lunar gravity conditions proclaims that the gravity level acceptable for normal walking is close to $1/5 \text{ g}$. Mochon and McMahon's [1981] ballistic walking model shows that to follow the same trajectory of motion

on the moon as on Earth, walking speed is reduced by 60% on the moon due to the much increased time for the swing phase. These trends suggest the importance gravity plays in locomotion.

A recent partial gravity running study by He *et al.* [1991] shows that reduced gravity alters the mechanics of locomotion. They use a cable suspension apparatus to simulate partial gravity for running and their analysis of the mechanics of partial gravity running shows a decrease in contact time, stride frequency, vertical landing velocity, and the angle of excursion of the limbs with respect to 1 g locomotion. They define a vertical stiffness parameter which increases slightly with a reduction in gravity. Their results verify the mathematical model for running proposed by McMahon and Cheng [1990]. Chapter IV, Results and Discussion, presents a modified version of McMahon and Cheng's running model that accounts for low gravitational accelerations and this model provides theoretical analysis to supplement the experimental findings.

Studies by Hewes [1969, pp. 419-432] and Seminara and Shavelson [1969, pp. 451-462] assess human performance in simulated lunar environments by paying attention to which gaits produce effective means of locomotion as well as the energy expenditures associated with the gaits. Seminara and Shavelson [1969] conclude that the combined effect of simulated lunar environment variables substantially degrades certain categories of astronaut performance. Hewes and Spady [1964, pp. 1-34] found that subjects tend to stand on their tiptoes and walk with a longer, stiffer gait in simulated 1/6 g. Unfortunately, the last three references report more subjective findings than quantitative results. Nonetheless, the research questions of Seminara and Shavelson address both aspects of the partial gravity experiments central to this thesis. The following Section highlights the important partial gravity energetics studies of the past.

1.1.2 Energetics Literature

Contradiction abounds in the literature regarding energy expenditures during partial gravity activities. With 90% of the research conducted over twenty years ago, there is an obvious void in understanding how humans might function on the moon or Mars. Reports from a few authors in the mid-1960s show metabolic expenditures to increase in simulated weightlessness and partial gravity [Lomonaco, 1962; Springer *et al.*, 1962; and Wortz *et al.*, 1966]. However, the majority of publications state that energy expenditures at various levels of reduced gravity show a decrease in metabolic rate for walking [Hewes and Spady, 1964; Robertson and Wortz, 1968; and Sanborn and Wortz, 1967]. The studies of Hewes [1967]; Hewes *et al.* [1966]; Kuehneggar *et al.* [1965]; Letko *et al.* [1966]; and Spady and Krasnow [1966], further substantiate the trend of decreased

metabolic expenditure for microgravity and partial gravity environments for walking, loping, and running.

Distinguishing between upper and lower body exercise helps resolve the apparent controversy of increased or decreased workload for humans working in altered gravitational fields reported in the literature. Tasks involving only the small muscles of the upper body could elicit an increase in energy consumption due to greater recruitment of fast twitch motor units. It is known that heart rate is higher when mostly small muscle groups, such as in arm work, are used rather than large muscles in leg work at the same workload [Åstrand and Rodahl, 1977, pg. 457]. Assuming that energy expenditure is a function of the muscular force required to support the weight of the body during lower body exercise, a reduction in energy expenditure makes sense for partial gravity locomotion because less weight has to be supported, therefore, less leg muscle recruitment is necessary. On the basis of the previous argument, a decrease in energy consumption from 1 g to 0 g is anticipated for the partial gravity locomotion study presented in this thesis.

The observer may glean insights from the actual lunar data of the Apollo missions. Only sparse scientific data exists because the primary goal of Apollo was to survive a round trip journey rather than to pursue scientific studies of human performance on the lunar surface. However, a report by Waligora and Horrigan assesses metabolic cost of Apollo EVA tasks [1977, pp. 395-399]. They note that the most energy-consuming tasks are those classified as overhead tasks (i.e., egress, off-loading and setup of equipment, and ingress). Peak metabolic rates (350-450 kcal/hr) occur during steep uphill walking traverses [1977, pg. 396]. Section 2.2.2.1, Mechanical Efficiency, delineates the reason for increased energy expenditures for inclined locomotion. It makes sense that the lowest metabolic rates appear when astronauts ride the lunar rover. The Apollo spacesuits tended to limit astronaut mobility and may have affected the data. Unfortunately, not enough lunar data exists to shed light on the question of energy expenditures for the entire range of partial gravity from 1 g to 0 g. Future partial gravity simulation studies will afford plausible scientific answers.

Given the limited number of partial gravity reviews and the fact that the studies are dated, a review of 1 g energetics and locomotion papers is necessary. Sawka *et al.* [1982, pp. 354-359] investigate energy expenditures at a variety of metabolic intensities and report typical 1 g results for upper and lower body exercise. Their subjects perform submaximal exercise for arm crank and cycle ergometry. Compared to cycle exercise, arm crank exercise elicits higher oxygen uptake (denoted as \dot{V}_{O_2}) and heart rate values for a specified power output level. The authors anticipated these findings based on similar results obtained by Åstrand *et al.* [1965, pp. 253-255], Sternberg *et al.* [1967, pp. 61-70], and Wahren and Bygdeman [1971, pp. 432-441]. Possible physiological

mechanisms responsible for the elevated \dot{V}_{O_2} responses include additional postural muscle activation, a greater recruitment of fast twitch motor units, and a greater static exercise component from gripping the arm crank [Sawka *et al.*, 1982]. The elevated heart rate responses during arm crank ergometry could be the result of increased \dot{V}_{O_2} level, a greater static exercise component, or increased sympathetic output. Peak oxygen uptake and maximal heart rates are lower for upper body tasks than lower body tasks. The authors conclude that energetic responses depend on exercise intensity rather than the muscle groups employed [Sawka *et al.*, 1982]. Their conclusion contradicts speculation by other scientists [Asmussen, 1965; DeJours, 1964; and Levine, 1978] that the magnitude of exercise hypernea depends on the muscle groups involved. Contradiction in the 1 g further substantiates the importance of initiating current research efforts on partial gravity energetics.

Another approach to study performance in partial gravity is to view performance at reduced gravity as a continuum of effects that are consistent from Earth gravity (1 g) through Mars gravity (3/8 g) to lunar gravity (1/6 g) and weightlessness (0 g). Wortz [1969, pp. 433-440] tries to explain the apparent contradiction in energy expenditures for simulated partial gravity environments by pointing out the different mechanisms involved. He suggests that the increased metabolic cost of work in weightlessness is due to the muscular work required to provide necessary reactive forces. Furthermore, he acknowledges that metabolic rates for upper torso work increase systematically with reduction in traction. For locomotion in reduced gravity, substantially less energy consumption is seen in comparison to energy consumption at Earth gravity. Wortz [1969, pg. 438] concludes that the reduction in energy expenditures for locomotion in simulated lunar gravity is a weight-carrying phenomenon, which he describes as being "analogous to locomotion while carrying less weight." Wortz and Prescott [1966] substantiate Wortz's previous results with a study showing a decrease in metabolic rate for walking in the lunar gravity when compared to that of the Earth.

1.2 CONTRIBUTION

This research effort is novel as it marks the first time human locomotion has been studied across the full range of partial gravity between 0 g and 1 g. An unprecedented attempt to compare simulation techniques is undertaken. In this study, experiments are performed using two partial gravity simulation techniques and experimental results are compared to theoretical analysis and published results from a third technique. The primary partial gravity simulation technique, water immersion, mandated the design of a submersible treadmill. The patent-pending treadmill design is unique as it provides comprehensive locomotion analysis for every gait. This research effort

answers numerous outstanding questions regarding biomechanics and oxygen requirements, such as which gaits are natural for partial gravity and what are the oxygen requirements for partial gravity environments (including both the moon and Mars).

This dissertation contributes a scientific evaluation of locomotion and the associated energetics for the entire range of partial gravity including experiments run at simulated lunar gravity ($1/6$ g), Martian gravity ($3/8$ g), two-thirds gravity ($2/3$ g), nine-tenths gravity ($9/10$ g), and terrestrial Earth gravity (1 g). The novel submersible treadmill and an adjustable ballasting harness designs provide a viable research simulation technique to determine how gravity influences human locomotion. These devices unveil the mechanics of locomotion by providing measurements of vertical force, stride frequency, and foot contact time. All of these measurements are attained from the split-plate force platform underneath the belt of the motorized treadmill. In typical laboratory walkway experiments where subjects pass over a ground-mounted force platform as they progress, measurements are time consuming to gather and difficult to reproduce. Whereas, a treadmill-mounted force platform design overcomes these problems by allowing an unlimited number of measurements over a full range of speeds. The adjustable loading harness designed specifically for this study provides realistic loading (using lead ballast) of the torso and lower limb segments by distributing from 0% to 90% of the subject's body weight throughout the harness and ballast pockets.

Distinguishing between gaits for various treadmill speeds is a primary biomechanics contribution especially since the gait distinctions unveil a change in mechanics for partial gravity locomotion as compared to terrestrial locomotion. Pinpointing the naturally occurring gait for various gravity levels allows predictions of astronaut performance in the *shirt-sleeve environment* rather than introducing the confounding effects that spacesuits and life support systems have on human performance.

This research effort should contribute to and influence planetary extravehicular activity (EVA) spacesuit design, vehicle design, and planetary habitat design. This research also has applications in the non-space related areas of clinical rehabilitation and sports biomechanics. Incorporating the appropriate characteristics of gait into advanced spacesuit design is essential in order for crewmembers to walk on the lunar or Martian surface. Suggestions resulting from this study include: incorporating waist bearings into the design of advanced spacesuits to allow for pelvic rotation and pelvic tilt, and providing boots made of flexible materials to ensure ankle plantar flexion. Spacesuit life support systems provide oxygen to the astronaut and data presented in this thesis can be used to specify some of the EVA oxygen requirements. This is an important

contribution because there is a drastic reduction in oxygen consumption for partial gravity, such as the Martian environment, and life support systems should be designed accordingly rather than accommodating terrestrial oxygen needs.

The debate on the necessity of artificial gravity vehicles for a Martian mission should be influenced by scientific data rather than political preferences. Do we need artificial gravity for a human mission to Mars? There is no definitive answer, but the biomechanics data presented in this thesis yields expected Martian musculoskeletal loads. This data can influence the artificial gravity debate and is most beneficial if acknowledged in the space vehicle conceptualization phase. Planetary habitats should be designed for partial gravity rather than 1 g taking into account the different mechanics of locomotion for the lunar and Martian environments. Relying on the data presented herein the reality of financial constraints is bound to dictate the final design of habitats. Underwater locomotion provides an efficient means of exercise for athletes without stressing the skeletal system. Clinics are turning to underwater locomotion for patient rehabilitation. The underwater partial gravity simulation technique offers an ideal method for exercise and rehabilitation.

1.3 ROAD MAP TO DISSERTATION

Chapter Two provides background on work physiology and human locomotion. Section 2.1, Work Physiology, begins by delineating energetic processes and then presents a hydraulic analog. This Section concludes by defining workload and metabolic expenditure nomenclature. Section 2.2, Human Locomotion, acquaints the reader with the characteristics of gait, then describes the mechanics of walking and running, and finally, presents models for walking and running.

Partial gravity simulation techniques and the hydrodynamics modeling effort comprise Chapter Three. Sections 3.1.1 and 3.1.2 introduce suspension systems and parabolic flight, respectively. Section 3.1.3 presents the water immersion technique and discusses the partial gravity ballasting harness. The constraints of the partial gravity immersion technique are acknowledged and discussed. The second main Section in Chapter Three, Hydrodynamic Modeling, describes the mathematical modeling effort that verifies underwater treadmill locomotion as a valid partial gravity simulation technique. This Section introduces flow regimes and calculations and then describes the mathematical model of a subject's limbs moving through water.

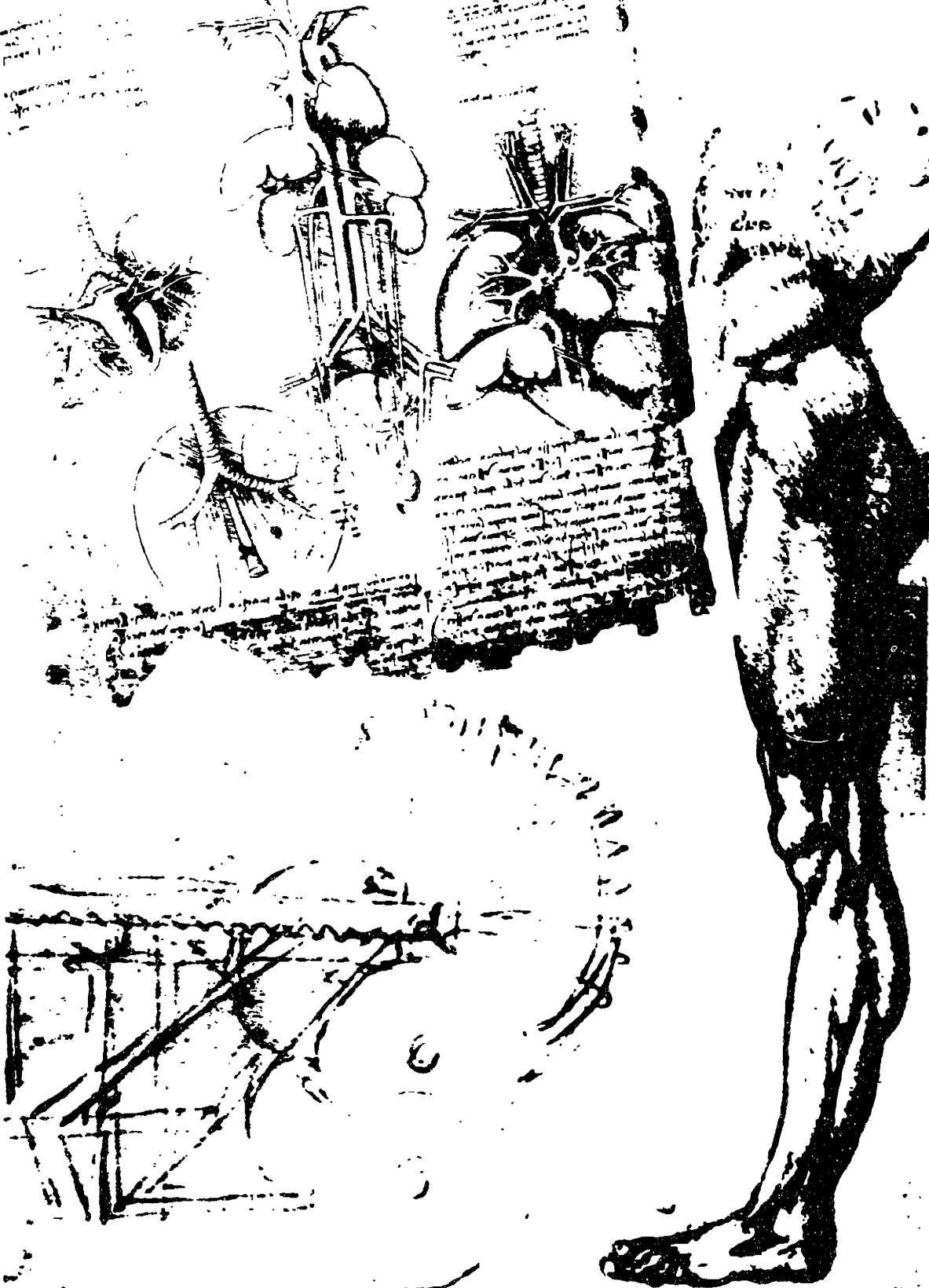
Chapter Four highlights the experimental methods of the partial gravity simulations and contains three main sections. Section 4.1 describes the subjects who participated in the study. Section 4.2

describes the experimental protocol followed in the underwater experiments and during parabolic flight. Section 4.3 describes the experimental apparatus used for the partial gravity locomotion study and highlights the design of the submersible treadmill.

Chapter Five presents the experimental results of the partial gravity locomotion and energetics study and then provides a detailed discussion of the results. The Chapter presents biomechanics results for both immersion and parabolic flight and then presents the results of the energetics measurements for the immersion experiments. Section 5.2, Discussion, starts off by outlining the limitations of the experimental techniques. The biomechanics discussion is based on an existing conceptual locomotion model. This mathematical model substantiates and brings together the hypotheses of the experimental results. The discussion of energetics verifies the hypothesis that suggests a decrease in oxygen consumption at reduced gravity levels. Minimum cost of locomotion is calculated from the metabolic expenditures and reveals a change in the most economical gait for partial gravity locomotion as compared to terrestrial locomotion.

Chapter Six presents the Summary and Conclusions of the partial gravity locomotion and energetics study. This Chapter addresses the applications of the research and reiterates the experimental contributions. This partial gravity locomotion and energetics research effort along with future efforts may influence advanced spacesuit design, vehicle conceptualization, and planetary habitat design as well as having sports biomechanics and clinical rehabilitation implications.

II. BACKGROUND



This unimaginably great and diverse universe, in which we occupy one fragile bubble of air, is not destined to remain forever silent. It will one day be ... throbbing with the pattering of little human feet.

- Freeman J. Dyson

*Looking at the stars always makes me dream,
as simply as I dream over the black dots
representing towns and villages on a map.
Why, I ask myself, shouldn't the shining dots
of the sky be as accessible as the black dots on
the map of France?*

- Vincent van Gogh

CHAPTER II. BACKGROUND

This Background Chapter reviews work physiology and human locomotion with the central theme of defining the role of gravity in locomotion. Section 2.1, Work Physiology, introduces the energetic processes and metabolic costs associated with ambulating, and then an hydraulic analog of energetic processes to describe the body's metabolic physiology. Section 2.1 concludes by quantifying workload and then discussing workload measurement techniques. An important research goal is to quantify the workload associated with human locomotion in partial gravity. The review of work physiology provides a background on energetic processes, workload, and measurements to enrich the discussion of experimental results in Chapter Five. The Background Section on human locomotion starts by defining the specific characteristics of walking, then outlines the mechanics of walking and running through physical laws and energy requirements governing locomotion, and finally reviews existing models.

2.1 WORK PHYSIOLOGY

This Chapter introduces both metabolic expenditures and the mechanics of locomotion because these two aspects of human performance are integrally related. A review of energetic processes sets the foundation for the steady-state workload analysis of the underwater locomotion study.

2.1.1 Energetic Processes

The physiology of muscular work during exercise depends on the ability of muscle cells to transform chemically bound energy into mechanical energy for muscular work. Similarities exist between the human engine and the human built combustion engine. In the combustion engine, a spark from the stored energy in the battery initiates an explosive combustion between gasoline and air and transforms chemical energy into heat and pressure which are transformed by the mechanical action of the engine to kinetic energy. Food plus oxygen provide the combustible material in the human engine and the cell's battery pack is a high-energy phosphate compound called adenosine triphosphate (ATP). In the combustion engine, the expansion of gas causes the pistons to move providing useful mechanical energy. In the human engine, muscle fibers are the pistons. The engine runs as long as it has fuel. "Living organisms, like machines, conform to the laws of conservation of energy, and must pay for all their activities in the currency of metabolism" [Baldwin, 1967]. High-energy phosphate compounds represent the currency for energy transfer within living organisms. The following paragraphs summarize the chemical processes involved in

where GP is phosphagen, ADP is adenosine diphosphate, PC_r is phosphocreatine, ATP is adenosine triphosphate, C_r is creatine, P is inorganic phosphate, E is energy (with subscripts: P-phosphagen, O-oxygen, and L-Glycolysis), O_2 is oxygen, CO_2 is carbon dioxide, and H_2O is water. The three exergonic reactions are a, c, and d, while b and f are endergonic reactions.

Margaria [1976, pg. 7] simplifies the reactions by using capital letters A, B, C, etc. to represent the energy liberated or absorbed during the reactions a, b, c, etc. Then the total amount of energy consumed, E, can be expressed by Equation 2.4:

$$E = A - B + C + D - F \quad (2.4)$$

The amount of energy released or absorbed in each of the reactions can be determined by measuring the phosphagen in the muscle for reactions a and b, the lactic acid in the body for reactions d and f, and the consumption of oxygen for reaction c. After one minute or less of constant intensity exercise, the phosphagen content in the muscle reaches equilibrium. In other words, the amount of energy liberated equals the amount of energy absorbed, or $A = B$. During submaximal work there is no production of lactic acid, therefore, D and F are zero. Work in which a person requires less than maximal oxygen consumption is defined as submaximal and is the case during most partial gravity exercises of this study. Under these conditions, since $A = B$ and $D = F = 0$, Equation 2.4 is simplified to:

$$E = C = MV_{O_2} \quad (2.5)$$

where M is the energy equivalent of one liter of oxygen, and V_{O_2} is the volume of oxygen consumed in milliliters. The energy equivalent of 1 liter of oxygen used in the combustion of food amounts to about 5 kcal. The power, P, is the energy transformed in unit time and is written as:

$$P = \dot{E} = M\dot{V}_{O_2} \quad (2.6)$$

where \dot{E} is energy required per minute and \dot{V}_{O_2} is oxygen consumption per minute, often referred to as *oxygen uptake*. Measuring the oxygen uptake of a person performing work is an accurate method for measuring total aerobic metabolic rate, and the primary method used in the underwater experiments.

2.1.2 Hydraulic Analog

Building on Margaria's work [1976, pg. 53], McMahan [1984] offers a hydraulic analogy which is quite beneficial for comprehending the energetic processes in muscle. McMahan's hydraulic

model represents the flow of energy in the contractile machinery of muscle. ATP is the high energy phosphate compound that muscles use as fuel to perform work. Almost every energy-demanding process in the cell relies on ATP. The ATP battery pack has a limited amount of energy which must be continuously recharged (analogous to the automobile battery). In McMahon's model, ATP replenishment is accomplished by the ATP float dropping, causing the needle valve to open and energy to flow from the phosphocreatine, PC_r , tank to restore the ATP level. Physiologically, the charging consists of combining ADP and phosphate in an endergonic reaction. ATP is the intracellular vehicle of chemical energy transferring energy to processes requiring energy within the cell such as muscle contractions [Åstrand and Rodahl, 1977, pg. 528]. For normal muscle contractions the PC_r supply keeps the ATP concentration at a constant level. PC_r acts as an immediate store for ATP regeneration, but is rapidly depleted (lasting only seconds or minutes during strenuous exercise) and thus the resynthesis of ATP is continuous.

At the start of exercise anaerobic processes may provide support energy to the aerobic metabolic processes, while the oxygen supply to the active muscles is being regulated to meet energy demands. In other words, during the first 30-90 seconds of exercise the cardiac output changes from a resting level to the level mandated by the work rate. Lactic acid concentration in the blood rises a bit due to anaerobic metabolic processes meeting energy demand requirements while the oxidative mechanisms reach a steady-state. After this time delay, the oxidative mechanisms supply the required energy with no further lactic acid build up for a submaximal work rate. McMahon's Figure 2.1 shows the steady-state condition for moderate exercise, the aerobic recovery phase, the heavy exercise condition, and the anaerobic recovery phase (See Figure 2.1 A, 2.1 B, 2.1 C, and 2.1 D, respectively). During the steady-state condition (Figure 2.1 A), check valves A and B are closed because the oxidative mechanisms are able to supply the necessary energy.

Aerobic recovery is illustrated in Figure 2.1 B. Once the muscle contraction is finished and the muscle is at rest, the human engine no longer uses ATP. Since the PC_r supply is lower than the oxidative supply, check valve A is forced open as the alactacid reaction of Equation 2.1 runs in reverse to replenish the PC_r supply. The initial lactic acid build up is reduced as it is transformed into glycogen, and this anaerobic pathway is shown as high resistance flow through check valve C. It takes about 30 minutes for the lactic acid to be resynthesized into glucose.

During heavy exercise, the PC_r stores drop at a rapid rate until the supply is almost exhausted. The ATP level drops more than it did for the light exercise scenario and the oxidative reservoir operates at maximum flow capacity (maximum aerobic rate). The increased demand is met by anaerobic glycolysis which causes an increase in muscle lactate concentration. The flow of energy

during heavy exercise is shown in Figure 2.1 C. McMahon points out that the "anaerobic glycolytic mechanism uses glucose much less efficiently than the aerobic mechanism in rephosphorylating ADP" [1984, pg 46].

Figure 2.1 D) shows anaerobic recovery which completes the energetics cycle. The energetic processes in muscle require anaerobic recovery to replenish the PC_r supply. Both check valves are forced open as energy is provided directly from the anaerobic reservoir.

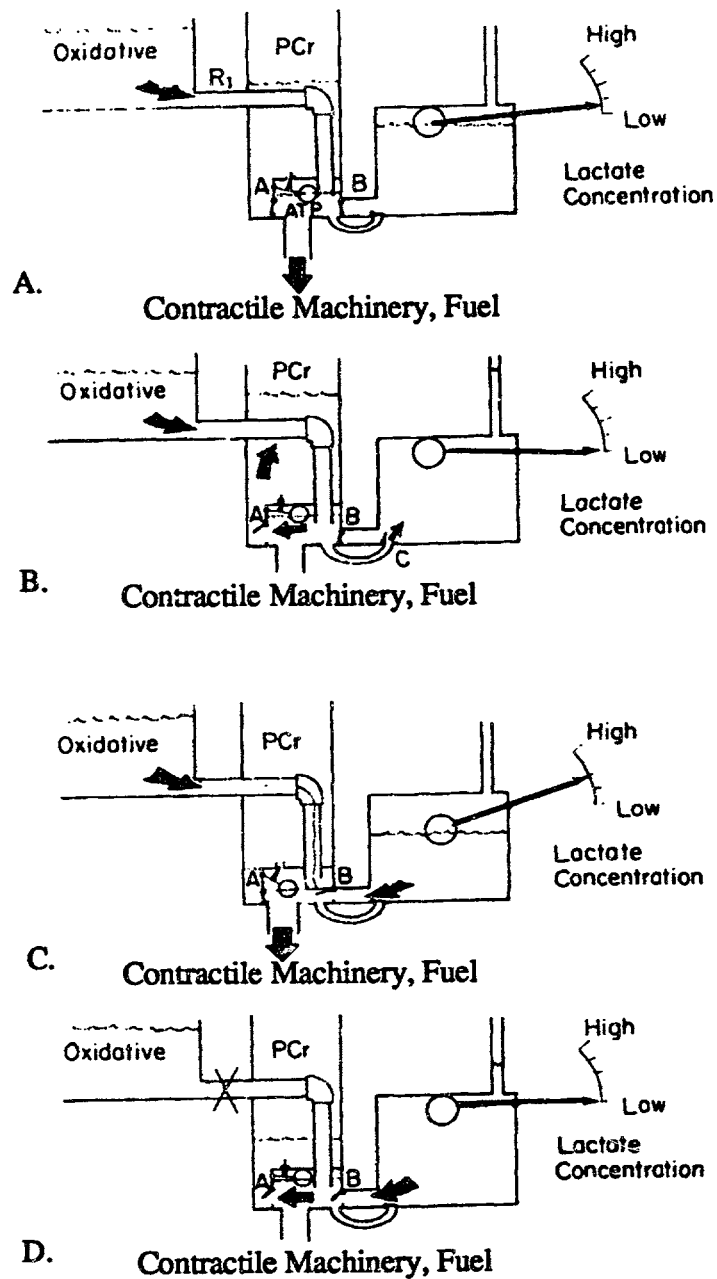


Figure 2.1 A) Light exercise. Aerobic sources only, after transient lactate production. B) Aerobic recovery. The higher level in the oxidative pool forces check valve A open. Lactate is slowly rebuilt into glycogen in specialized tissues via energy flow through check valve C. C) Heavy exercise. The flow of energy from the oxidative pool has reached a maximum. The PCr level is stationary at a low value, but the level in the anaerobic reservoir is continually falling. Note that in the model, the ATP float valve is open to atmospheric pressure. D) Anaerobic recovery. Even when oxygen is excluded, the PCr stores may be rebuilt by anaerobic glycogen splitting (From McMahon, 1984, pg 42)

2.1.3 Workload

An all-encompassing measure of mental and physical workload does not exist. However workload may be thought of as a measurement of the rate at which work is performed by a person.

Subjective rating evaluations often formulate workload as an entity. However, subjective ratings address the symptoms, rather than the causes of task performance achievement. Metabolic measures of workload quantify the physical component of performance. Section 2.1, Energetic Processes, states that the capability to perform physical work depends on the ability of the muscle cell to transform chemically-bound energy into mechanical energy for muscular work. Expressing workload as a percentage of an individual's maximum aerobic power implies that an individual's maximum oxygen uptake, $\dot{V}_{O_2}^{\max}$, is useful in evaluating his/her rate of work.

Gas analysis of the oxygen consumed during exercise and heart rate measurements are two methods of assessing physical workload. Both measurement techniques are used in the underwater experiments; the following paragraphs familiarize the reader with these techniques. Gas analysis offers high precision workload measurements; while heart rate is less precise, it offers other researchers an alternative measurement to compare partial gravity results if they are unable to acquire gas analysis equipment.

Introduction to Gas Analysis

Gas analysis is a common method used to measure oxygen uptake and carbon dioxide output. Metabolic energy expenditure is easily measured in real time and has been used to quantify overall physical workload of space activities since the Gemini program [Cousins, 1987].

Steady-state workload is measured during the underwater partial gravity experiments and these measurements represent the total energy required for locomotion since non-aerobic pathways appear to contribute a negligible amount. Unfortunately, steady-state workload measurements were not taken on the parabolic flights aboard the KC-135 aircraft due to the experimental time limitation.

From onset of activity, the rate of oxygen consumption increases to a steady-state level which is below the maximum oxygen consumption level. A sluggishness in the respiratory/circulatory systems reflects a start up adjustment time for the oxygen-transporting systems. Physiological measures reach steady-state levels one to two minutes into the exercise. Steady-state \dot{V}_{O_2} levels correspond to workload situations where oxygen uptake equals the oxygen requirement of the tissues. The average resting \dot{V}_{O_2} for the underwater experiments is 0.06 ml/(kg·sec) (0.25 liters per minute).

Heart Rate Measurements

Heart rate is most useful as a secondary measure of energy expenditure to supplement \dot{V}_{O_2} measurements. In general, there is a linear relationship between oxygen uptake and heart rate [Åstrand and Rodahl, 1977]. Heart rate can be used to estimate workload assuming that a workload/heart rate relationship is established for an individual subject. This relationship is often established for the large muscles by bicycle ergometry and for smaller arm muscles by arm ergometry. For example, an exercise profile might call for an initial low load of 50 Watts to be maintained for five minutes; then the required power might increase in 50 Watt increments for consecutive five minute intervals until the heart rate reaches 150 beats per minute (bpm).

Inaccuracies may exist while estimating oxygen uptake from heart rate measurements. Rodahl *et al.* [1974] compare \dot{V}_{O_2} to heart rate estimations of \dot{V}_{O_2} and find deviations up to 15%, although they note remarkably consistent day-to-day results for the same individuals doing the same work. Rodahl *et al.* conclude that estimating workload based on heart rate measurements is valid when the large muscles of the legs are used, as is the case in this study.

The heart rate measurements for the simulated partial gravity experiments offer future scientists a metric to compare results if gas analysis equipment is unavailable to them. Continuous heart rate recordings provide uninterrupted data collection which reflect the workload for the entire experimental session. Quantitative numerical analysis of the recorded data, supplemented by visual analysis of heart rate curves permits a "comprehensive and dynamic evaluation of the circulatory strain imposed by workloads of varying intensity" [Åstrand and Rodahl, pg. 458]. Finally, in assessing the validity of heart rate measurements as estimations of oxygen uptake, Rodahl *et al.* state, "in most cases, the reliability of the conversion is adequate for all practical purposes of field investigation" [1974].

The next Section, Human Locomotion, complements this discussion of energetics for human locomotion by delineating the determinants of gait and introducing the mechanics of locomotion. The discussion of mechanics of locomotion contains subsections on models for walking and running and the mechanical efficiency of locomotion.

2.2 HUMAN LOCOMOTION

Locomotion is the most common activity of humans and it is quite surprising that the discipline of biomechanics has only been around for a few decades. Movement of the body is not only our most characteristic activity, but our relationships with the environment and other people are based on human movement. The following Section entitled Introduction to the Determinants of Human Gait reveals the characteristics of walking. The intent of this Section is to provide the reader with an understanding of the characteristics of gait from which to interpret the biomechanics results of the partial gravity experiments. Engineers need to heed the recommendations concerning the essential determinants of walking described below in order to design the most efficient locomotion spacesuits and planetary habitats.

2.2.1 Introduction to the Determinants of Human Gait

Locomotion is an uniform sequence of limb movements and the determinants, or characteristics, of gait serve as a basis for comparison between 1 g locomotion and partial gravity locomotion throughout this thesis. For normal 1 g locomotion, humans primarily use two gaits: walking and running. During walking the subject has at least one foot in contact with the ground and both feet make ground contact during the mid-phase of a stride cycle. The center of mass is highest at mid-step when the hip of the stance leg is directly over the ankle [Mochon and McMahon, 1990]. The typical rhythm or cadence of walking is 60 to 70 strides per minute. A complete stride cycle (Figure 2.2) consists of a stance (or support) phase which is initiated at heel strike and then a swing phase from heel off to the next heel contact of the same foot. During running there is foot contact with the ground before and after an aerial flight phase, but there is never ground contact by both feet at the same time and the center of mass is lowest at mid-step during foot contact. Loping, an extension of running, is not a characteristic 1 g gait, but is common in low gravity environments. Loping includes a step length increase and an increase in aerial time during the stride cycle (Section 5.1.1.1 further discusses loping).

The notions of minimizing energy expenditure and forces are basic hypotheses behind human movement. The functional significance of the determinants of gait is to minimize vertical and lateral oscillations of the center of gravity (CoG) during walking, thus minimizing energy expenditures and perhaps minimizing muscular force generation. The location of the CoG of the body is just anterior to the second sacral segment. The oscillations of the CoG are typically 5 cm for normal walking. There are numerous descriptions of the motions of the limbs during locomotion, but Jenkins' succinct presentation is reiterated herein to familiarize the reader with the

nine determinants of walking [1991]. These components of gait should be kept in mind when comparing Earth-normal 1 g locomotion to partial gravity locomotion as well as for specifying the necessary characteristics of gait to incorporate into spacesuit and habitat design.

Jenkins' determinants of gait [1991] include:

- | | |
|---|---|
| 1) Pelvic rotation | 6) Lateral displacement of the pelvis |
| 2) Pelvic tilt | 7) The inversion-eversion-inversion sequence
at the subtalar joint |
| 3) Knee flexion during the stance phase | 8) Trunk lateral flexion |
| 4) Heel strike | 9) Trunk anteroposterior flexion |
| 5) Heel-off interactions with the knee | |

The first distinguishing characteristic, pelvic rotation, describes the pelvis rotating from side to side about the body's longitudinal (vertical) axis for normal walking. During the swing phase, medial rotation at the weight-bearing (stance) hip advances the contralateral (swing phase) hip. Another way to think of it is that during the stance phase the pelvis passes from relative internal to external rotation. Figure 2.3 illustrates pelvic rotation and Figure 2.4 illustrates a scissors gait in which only hip movement (without a knee joint) is allowed. The pelvis moves through a series of arcs that are determined by leg length. The effective increased leg length from pelvic rotation lengthens the step and flattens out the arcuate trajectory of the CoG insuring a smoother ride as the radii of the arcs of the hip increase.

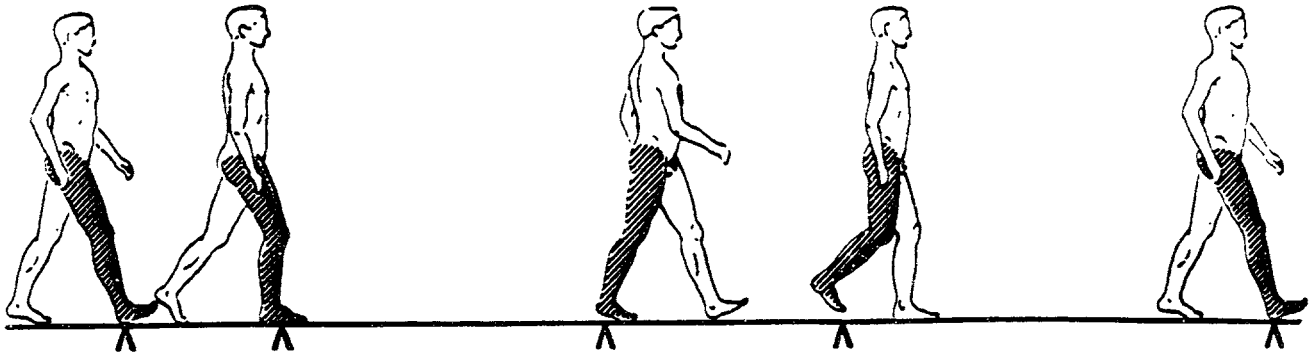


Figure 2.2 A complete stride cycle is shown. The stance phase leg is initiated at heel strike, and at 8% of the stride cycle the foot is flat; then heel off occurs after 43% of the cycle. The swing phase is characterized by toe-off which occurs after 62% of the stride cycle. The stride cycle is complete once the heel strikes again.

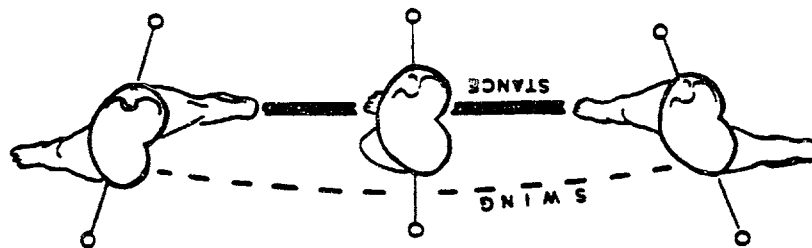


Figure 2.3 Pelvic rotation during walking. The pelvis is rotated for side-to-side about the longitudinal axis of the body.

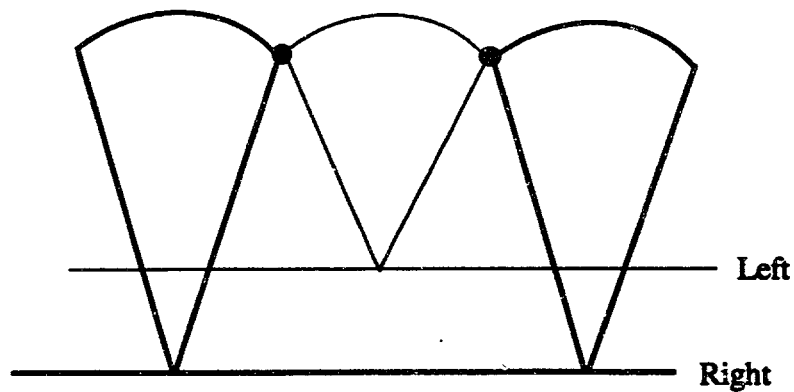


Figure 2.4 Depiction of scissors gait. Models the leg without a knee and allows only hip movements as the pelvis moves through a series of arcs.

The pelvis is tilted downward about 5° on the swing phase side. This occurs as pelvic adduction at the hip joint on the stance phase side (See Figure 2.5). Pelvic tilt further flattens the arcs of the hip allowing for a smooth ride during walking. This mechanism reduces the vertical displacement of the CoG. A simple test of standing on one foot exaggerates the displacement of the CoG to compensate for weak gluteals and shows hip adduction and apparent pelvic tilt.

The third determinant of gait is knee flexion during the stance (support) phase. At heel strike the knee is extended, but then begins to flex. At heel-off just prior to the middle of the support phase the knee extends again. This extension-flexion-extension sequence reduces the excursion of the CoG's arcuate trajectory and further flattens the arcs. Knee flexion on heel strike also absorbs shocks during a stride cycle. The effect of minimizing the arc of CoG trajectory is to reduce energy expenditure during locomotion. During a scissors gait when the knee joint is absent the travel of the CoG is not reduced. This model for locomotion (i.e., peg leg) is very costly in terms of energy expenditure.

Heel strike and heel-off interactions with the knee comprise the fourth and fifth determinants of gait. At heel strike the foot plantar flexes (rotating downward about an axis formed at heel contact) thus lowering the ankle as the foot makes full contact with the ground. A fused ankle joint (immobile) without plantar flexion would cause the CoG to rise as if the leg were a stilt. Ankle plantar flexion affects gait similarly to determinant three; the trajectory of the CoG is reduced and shock absorption is noted at heel strike. The fifth determinant of gait, heel-off, provides a horizontal CoG trajectory as the ankle rotates upwards about an axis formed at the ball of the foot. If the heel is not permitted to rise the leg rotates forward about the ankle joint and the CoG falls abruptly. Heel-off prevents a steep descent of the CoG keeping the excursion of the CoG to a minimum. McMahon [1984] points out the significance of plantar flexion in establishing the initial velocities of the shank and thigh for the swing phase. Figure 2.6 A) and 2.6 B) show heel strike and heel-off interactions with the knee, respectively.

Lateral displacement of the pelvis occurs during the stance phase as the pelvis shifts about 2 cm towards the stance phase (weight bearing) limb. Lateral shift is minimized due to the adducted femora (i.e., The femoral shafts are not sagittally aligned with respect to a sagittal plane; the knees are medial to the hips [Jenkins, 1991]). Lateral shift keeps us from toppling over and prevents a lurching-type gait as seen in monkey locomotion. Figure 2.7 illustrates this sixth determinant of gait.

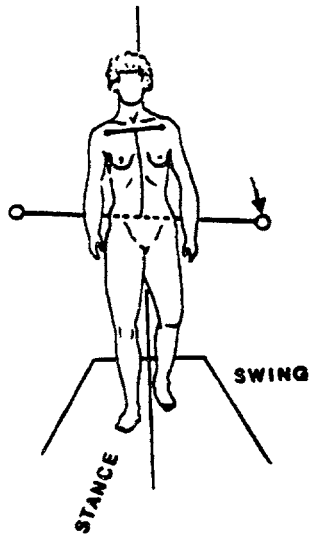


Figure 2.5 Pelvic tilt during walking. A 5° downward tilt of the pelvis is seen on the swing phase side.

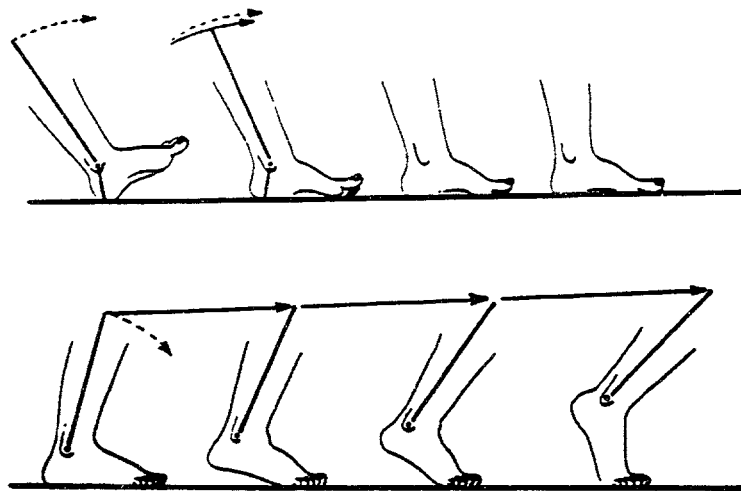
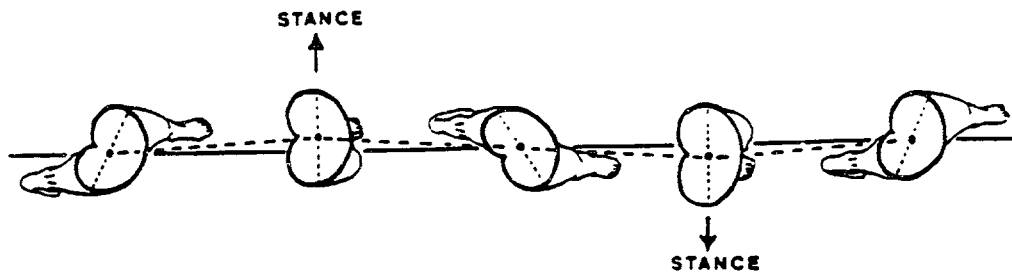


Figure 2.6 A) Heel strike. The foot plantar flexes which lowers the ankle as the foot contacts the ground. B) Heel-off interactions with the knee. Heel-off keeps the excursion of the center of gravity to a minimum.



The degree of lateral shift is minimized by the fact that the femoral shafts are not sagittally aligned. The knees are medial to the hips with respect to the sagittal plane.

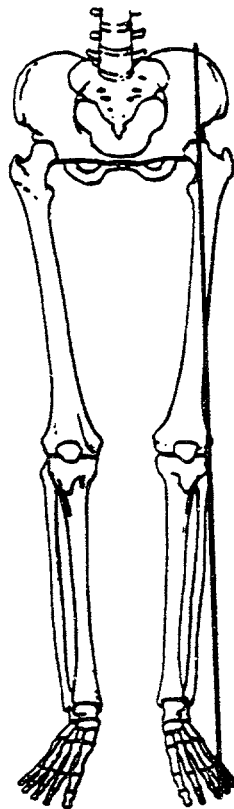


Figure 2.7 Lateral displacement of the pelvis prevents toppling over during walking and minimizes lurching-type of gait.

Inversion-eversion-inversion of the foot is the seventh determinant of gait. For a normal step, slight inversion occurs at heel strike, followed by pressure exerted toward the outside of the foot (eversion) during most of the stance phase. Inversion is seen again after heel-off. See Figure 2.8 for the pressure distribution at the subtalar joint. The effect of subtalar motion is to absorb shock by flattening of the longitudinal arch and to accommodate the 10° to 20° rotation and counter rotation of the tibia during foot contact.

The trunk flexes both laterally and anteroposteriorly during walking to make up the eighth and ninth determinants of gait, respectively. The ipsilateral flexion of the vertebral column toward the stance phase side causes a 1 to 2 cm displacement. The anteroposterior flexion of the trunk shows maximum backward flexion at the beginning of the support phase and maximum forward flexion towards the end of the support phase. Figures 2.9 and 2.10 show small 1 to 2 cm deflections.

For slow walking, the arms are in phase with the load bearing side, but for fast walking, the arms are opposite in phase to the load bearing (stance) leg. This contralateral pendulum action may minimize energy requirements during the stride cycle. In human biped walking, consider the culmination of the swing of the arm as the equivalent of placing a forefoot on the ground for comparisons of biped and quadruped walking.

In sum, the determinants of gait minimize oscillations of the CoG during walking optimize our efficiency during locomotion due to minimum energy expenditure. Many of the characteristics of gait absorb shock during a stride cycle which has the effect of reducing the force exerted on the ground, therefore, equivalently reducing the reactionary force on the skeletal system and human body. These characteristics of walking will be kept in mind during partial gravity gait analysis and are especially pertinent to incorporate into the design of advanced locomotion spacesuits. The following Section defines the mechanics of walking and running.

Pressure distribution on the plantar surface of the foot.



Figure 2.8 Inversion-eversion-inversion of the foot. At heel strike inversion is seen, then during stance, pressure is exerted toward the outside of the foot, and after heel-off, inversion is seen again.

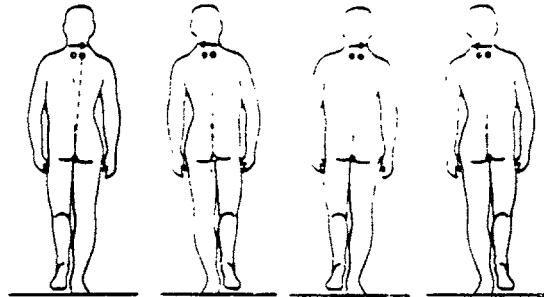


Figure 2.9 Lateral trunk deflection. An ipsilateral flexion of the vertebral column to the stance phase side (in the coronal plane).

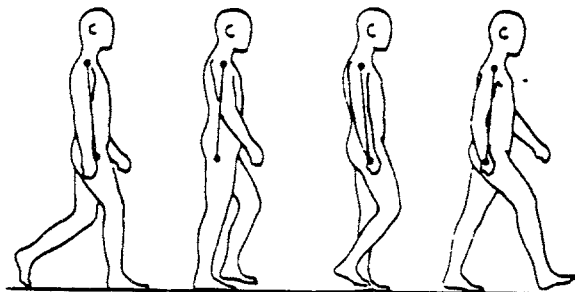


Figure 2.10 Anteroposterior flexion of the trunk. Maximum backward flexion occurs at the beginning of the support phase. Maximum forward flexion occurs toward the end of the support phase.

2.2.2 The Mechanics of Walking and Running

The laws of physics govern walking and running and mechanical analysis reveals the energy requirements of these activities. Theoretical mathematical analysis along with experiments yields insights into the mechanics of walking and running in 1 g as well as partial gravity. This Section on the mechanics of locomotion consists of three subtopics: a model of walking, a running analogy, and a description of the mechanical efficiency of locomotion. An inverted pendulum suggested as a model for human walking and running is likened to a kangaroo jumping. Defining mechanical efficiency helps show the significance of gravity in locomotion.

To what extent does gravity affect locomotion? Two forces, inertial and body weight, govern locomotion. The inertial forces arise from changes of motion of a system, and body weight is determined by mass and the gravitational acceleration. Theoretically, inertial forces are unaffected by a change in gravitational acceleration. Margaria and Cavagna point out that the mechanics of locomotion for a 35 kg subject are substantially the same as for a 70 kg subject; the only difference being the value of the forces [1964]. The energy cost of walking varies from subject to subject in relation to body weight. If the energy cost of walking is referenced to 1 kg of body weight, then the measures are consistent among individuals. Gravity is of paramount importance in locomotion because the phenomenon of lowering the CoG during the second phase of the step, in both walking and running, depends on the acceleration of gravity and is independent of body mass. Gravitational effects may also govern transition time and the mechanics of gait.

Transitions between locomotive gaits occur with increasing speed. On Earth, transitions from walking to running occur when the forward acceleration is too great to be wholly sustained by changes in gravitational potential energy. Running requires muscular force at step initiation producing a simultaneous increase in KE and PE. Margaria and Cavagna [1964, pg. 1141] point out that the "maximal speed of running is lower on the moon because, for the lower weight of the subject, the vertical component of the force may be too low to maintain the adherence of the foot on the ground and prevent skidding." They conclude that a higher speed could be obtained by jumping on the moon and calculate a maximal jump of 4 m. This jumping locomotion requires increased muscular force and suggests a change in mechanics for partial gravity locomotion. Hewes and Spady [1964] demonstrate that vertical jumps of 3.7 to 4.3 m (12 to 14 ft) are possible experimentally which agree quite nicely with Margaria and Cavagna's theoretical predictions.

Researchers undertake modeling efforts in order to provide an analytical link to observed phenomena. We conclude from the previous discussion, that gravity is a crucial parameter for

locomotion modeling efforts. Cavagna *et al.* [1977, pp. 243-261] detail two basic mechanisms for minimizing energy expenditures during terrestrial locomotion. They model the exchange between gravitational potential energy and kinetic energy as a swinging pendulum in walking, and the exchange between mechanical energy stored in muscle's elastic elements and recovered as both gravitational and kinetic energy as a spring mechanism in running. Many authors suggest similar models. The following two Sections present these models of walking and running. An important question to ask when reading about these models is if these models which were established for terrestrial locomotion apply for locomotion in partial gravity environments.

2.2.2.1 *Inverted Pendulum Model for Walking*

Theoretical models are useful in defining the influence of gravity on locomotion. The notion underlying a theoretical model for partial gravity walking is to extrapolate the governing physics of 1 g locomotion and apply them to human movements in partial gravity. During walking, bipeds use an energy conserving mechanism which is analogous to an inverted swinging pendulum [Blickhan and Full, 1987; Cavagna *et al.*, 1977; and Heglund *et al.*, 1982]. By using this pendulum mechanism for walking gravitational PE and KE are exchanged and not lost.

The pendulum walking model suggests that the body vaults, in a similar manner as an inverted pendulum, over the stance limb. The energy required for forward progression during walking is provided by the transformation of gravitational potential energy into kinetic energy. Gravitational potential energy is stored as the body is lifted during the first phase of the gait cycle and can be written as:

$$\dot{W}_v = PE = mgy \quad (2.7)$$

where \dot{W}_v is gravitational potential energy (PE), m is body mass, g is acceleration of gravity, and y is the vertical displacement of the center of gravity of the body. When the leg is vertical maximum gravitational PE is reached, and the maximum horizontal speed is attained when the center of gravity of the body is at its lowest. Therefore, an oscillation between maximum PE and maximum kinetic energy (KE) is seen in the inverted pendulum model.

Vaulting over a stiff leg (recall the scissors gait of Section 2.2.1) conserves up to 70% of the mechanical energy required for progression [Full, 1991]. In walking the muscular force generation at step initiation is mainly directed vertically to raise the body and attain maximum gravitational PE. In the second phase of the stride cycle when KE reaches a maximum, the falling

forward of the body is assisted by the skeletal system and muscles in order to accelerate and decelerate the center of gravity as the alternate foot strikes the ground.

When gravitational PE decreases there is a complementary decrease in walking speed. The lunar surface has a 1/6 g gravitational field, therefore, the PE stored during each step will decrease compared to the PE for locomotion in the Earth's 1 g gravitational field. Forward progression (kinetic energy) is given by:

$$\dot{W}_H = KE = \frac{1}{2}mv^2 \quad (2.8)$$

where \dot{W}_H is kinetic energy (KE) and v is velocity. Assuming a totally efficient system in which all the gravitational potential energy is transformed into kinetic energy,

$$\dot{W} = mgy = \frac{1}{2}mv^2 \quad (2.9)$$

it can be seen that alterations in the gravity field result in speed changes for progression.

Theoretically, energy cost of locomotion in partial gravity will be less than the 1 g case because less muscular activity is required to produce the potential energy in the initial phase of raising the body center. The muscles have less force to generate at reduced gravity, but an ineffective pendulum mechanism may alter the workload and biomechanics of walking. Running entails different energy exchange mechanisms as described in the following Section.

2.2.2.2 Running Humans and Hopping Kangaroos

Fluctuations in gravitational potential energy and forward kinetic energy for running are different than for walking. The initial force of the foot on the ground is directed both upward and forward in running, not solely upward as in walking. Gravitational PE and forward KE are in phase during running which suggests that the energy conserving inverted pendulum mechanism used in walking is not a valid model for human running. The lack of an energy conserving mechanism explains why running elicits twice the energy consumption of walking on the level. For 1 g locomotion walking is the most economical means of transportation; is this true for partial gravity locomotion?

Muscles, ligaments, and tendons are recruited during running as humans spring off the ground similar to a hopping kangaroo. Elastic storage of energy seems to govern running. Mass-spring models emulate the storage and releasal of elastic energy during running. In order to support the weight of the body, muscles are activated and the associated energetic cost is proportional to the amount of force generated [Farley, 1991; McMahon and Cheng, 1990; and Full, 1991]. Taylor *et*

al. [1980] suggest that the total amount of muscle force production during running determines the energetic cost of locomotion in their load carrying experiments. Assuming that force generation reflects metabolic cost, then the energetics of running should vary directly with the gravitational acceleration.

2.2.2.3 Mechanical Efficiency

A description of mechanical efficiency signifies the importance of gravity's effect on locomotion and provides a conversion from mechanical work to an equivalent energy consumption measurement. This conversion is used to convert the calculated mechanical energy of the hydrodynamic drag model to units of energy consumption (See Section 3.2 Hydrodynamic Modeling). Equation 2.10 defines mechanical efficiency as the ratio of mechanical work to energy consumption:

$$\text{Mechanical Efficiency} = \frac{\text{Mechanical Work}}{\text{Energy Consumption}} \quad (2.10)$$

Mechanical work is characterized by the change in average potential energy of a body progressing at a constant speed and is solely a function of the vertical displacement of the body. The constructs of positive and negative work help to further explain mechanical efficiency. The mechanical energy required for walking on a level surface is zero because the overall potential energy at a constant average speed does not change, therefore, no mechanical work is accomplished. Muscles perform positive work during uphill motions and negative work during downhill motions. The displacement of the body is in the same direction as the gravitational force during downhill motions and opposite to the direction of the force developed in the muscles. In this case, the final energy level of the body is lower than the initial energy level, therefore, this is defined as negative work. Energy consumption is always positive because both uphill and downhill movements require muscular activity.

Margaria and his colleagues [referenced in his book, 1976, pg. 143] performed an extensive battery of experiments that lead him to conclude

that the energy cost turns out to be a linear function of the work performed as given by the body lift in uphill walking at gradients greater than about 20 per cent.

This gradient coincides with the 0.25 mechanical efficiency isopleth (See Figure 2.11) [Margaria, 1976, pg. 76]. A similar linear relationship is seen for walking downhill at gradients greater than -10 per cent. Downhill walking coincides with a mechanical efficiency isopleth of -1.2. These observations are for whole body muscle activity, but it is noteworthy that single isolated muscle samples yield similar mechanical efficiencies.

Margaria [1976, pg. 77] defines energy consumption for given workload production as:

$$E = \frac{E_{MEC}}{0.25} \quad \text{for uphill walking} \quad (2.11)$$

$$\text{and } E = \frac{-E_{MEC}}{-1.2} \quad \text{for downhill walking} \quad (2.12)$$

where E is the energy consumed and E_{MEC} is the positive or negative work performed. He then defines energy for walking on the level as:

$$E = \frac{E_{MEC}}{0.25} + \frac{-E_{MEC}}{-1.2} = \frac{E_{MEC}}{0.207} \quad (2.13)$$

giving the rationale that at constant average speed, positive and negative work are equal. When energy consumption is known, Equation 2.13 may be used to calculate the mechanical work effectively performed walking or running on the level, and as previously mentioned, will be revisited in the discussion of drag energy in the Hydrodynamic Modeling Section.

Even though all of the partial gravity experiments entail only horizontal locomotion and not inclined locomotion, there is a point to be made from this delineation of mechanical efficiency. The reason for detailing Margaria's theory is to provide background and to emphasize his observations in which he proclaims that [1976, pg. 77],

the energy consumed depends only on the work performed against gravity, positive or negative, any other factor being negligible.

This powerful statement serves as a driving force and justification for investigating the sensitivity of human locomotion to various gravitational fields. By understanding the energy requirements during locomotion for 1 g, we gain insight into the same physics that may govern locomotion in a reduced gravitational field.

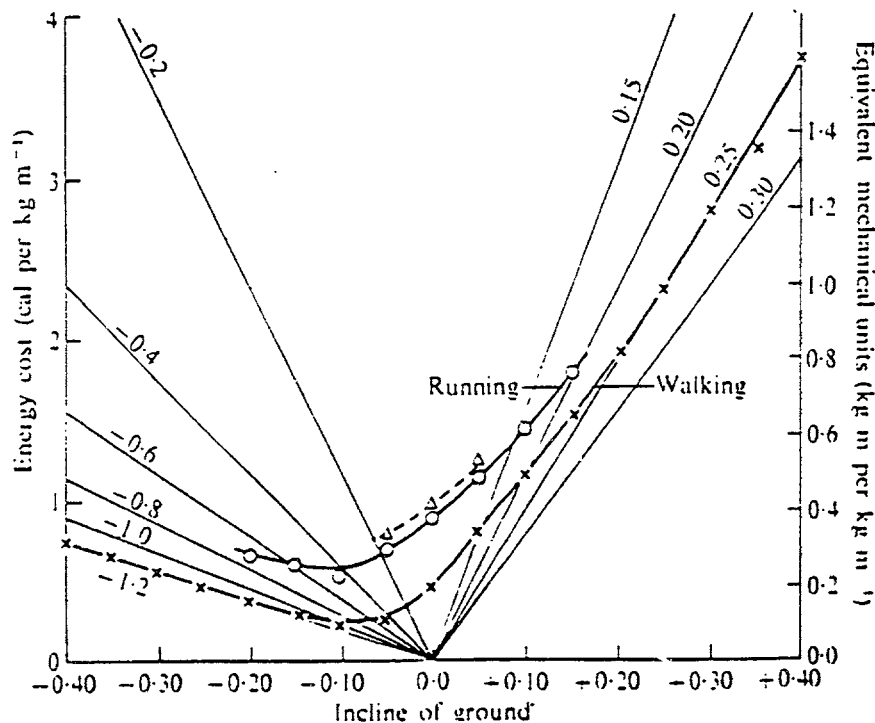
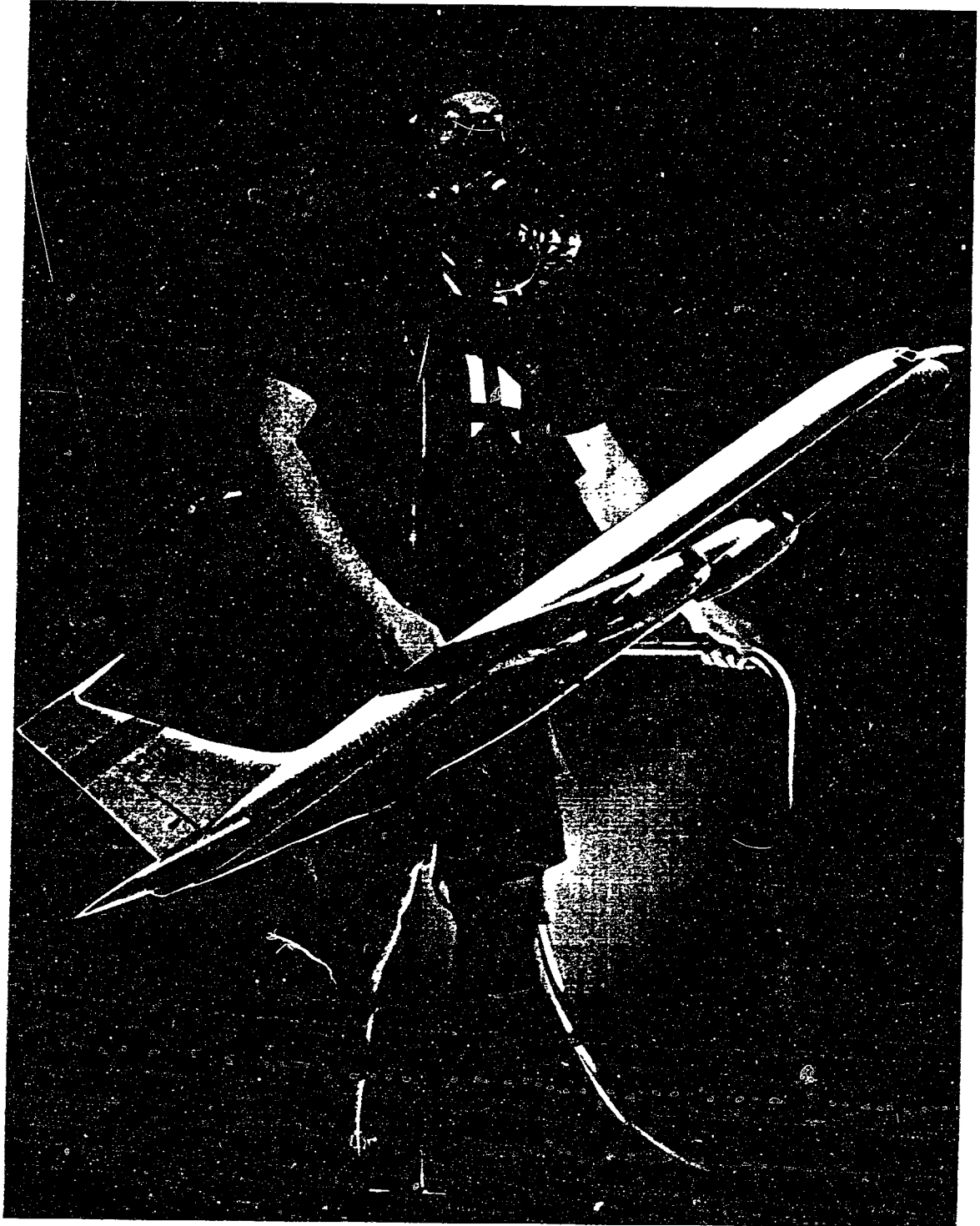


Figure 2.11 Energy cost (cal/kg, ordinate at left; cal/(kg·m), ordinate at right) for athletes walking at the most economical speed and running as a function of the incline of the ground; (dotted line nonathletes). The mechanical efficiency as given by the isopleths irradiating from the origin varies from 0.25 walking uphill to -1.2 walking downhill. (From Margaria, 1963).

This Chapter emphasizes the role of gravity in locomotion and provides background on the two primary areas of interest for the partial gravity research endeavor. The work physiology aspect defines the energetic processes involved in locomotion. Relevant questions for the energetics analysis investigate the workload associated with human locomotion in partial gravity. The work physiology review attempted to provide sufficient background on energetic processes, workload, and measurements in order to enrich the discussion of experimental results. The second aspect, biomechanics of locomotion, defined the specific characteristics of walking; then outlined the mechanics of walking and running via models in order to highlight the physical laws and energy requirements governing locomotion.

Throughout the experiments, an attempt is made to clarify some of the controversial findings in the literature and to verify enhanced published results with a wide range of partial gravity simulations. Based on the literature for lower leg exercise, a decrease in workload is expected for a given reduction in gravity level. Altered gravity is also expected to change the mechanics of locomotion. Chapter Three describes partial gravity simulation techniques, reviews the method of partial gravity loading for the underwater experiments, and discusses the hydrodynamic modeling effort.

III. PARTIAL GRAVITY SIMULATION AND MODELING



*The most beautiful thing we can experience is the mysterious.
It is the source of all true art and science.*
- Albert Einstein, *What I Believe* (1930)

Rules and models destroy genius and art.
- William Hazlitt, *On Taste*

CHAPTER III. PARTIAL GRAVITY SIMULATION AND MODELING

This dissertation is primarily an experimental work which incorporates modeling techniques as necessary. The experimental protocol calls for an investigation of biomechanics and workload in partial gravity environments to assess locomotion and energy expenditures. The three main techniques for simulating partial gravity environments are: cable suspension rigs, parabolic flight, and water immersion. Data from all three techniques is used in this study, however water immersion is the primary technique used and constitutes the major effort. After describing the partial gravity ballasting method used during immersion, the constraints of this technique are delineated. The second main Section of the Chapter describes the hydrodynamic modeling effort which entails a theoretical analysis. The goal of the model is to quantify the magnitude of drag and damping effects encountered by subjects during underwater partial gravity simulation. The theoretical model calculates the mechanical energy needed to overcome water drag during locomotion. It is helpful in estimating the drag constraint in the underwater partial gravity simulation technique.

3.1 SIMULATION TECHNIQUES

Research and astronaut training are the two traditional purposes for weightlessness and partial gravity simulations [Deutsch, 1969]. The three main simulation techniques are: cable suspension systems, parabolic flight, and water immersion. Gimballed systems and air bearing systems can also be used to simulate partial gravity. Each simulation technique offers unique advantages and disadvantages. A brief description of the various methods follows.

3.1.1 Suspension Systems

The cable suspension method typically uses vertical cables to suspend the major segments of the body and relieve some of the weight exerted by the subject on the ground, thus simulating partial gravity. Suspension systems often afford the most economical partial gravity simulation technique, but limited degrees of freedom for movement are often encountered with this technique. The possible mobility constraint of suspension systems is incompatible with the research goal of providing subjects with unlimited mobility during partial gravity locomotion.

Gimbals that allow up to three degrees of rotational freedom can be coupled with suspension systems in order to enhance the simulation technique. Suspension systems and suspension/gimbal/air bearing hybrid simulators for lunar gravity were developed during the

Apollo era in order to try to assess human performance for the lunar missions. Duddy's annotated bibliography gives details on these simulators [1969, pp. 507-540].

Water immersion serves as the primary partial gravity simulation technique of this study. Parabolic flight is used to complement the lunar and Martian locomotion experiments, however, results from these two techniques are compared with results from suspension systems whenever possible. In fact, the author participated in experiments using the Harvard University Field Station (HFS) suspension system (See Figure 3.1), and results from the HFS suspension system partial gravity experiments augment the energetics discussion in Chapter Five.

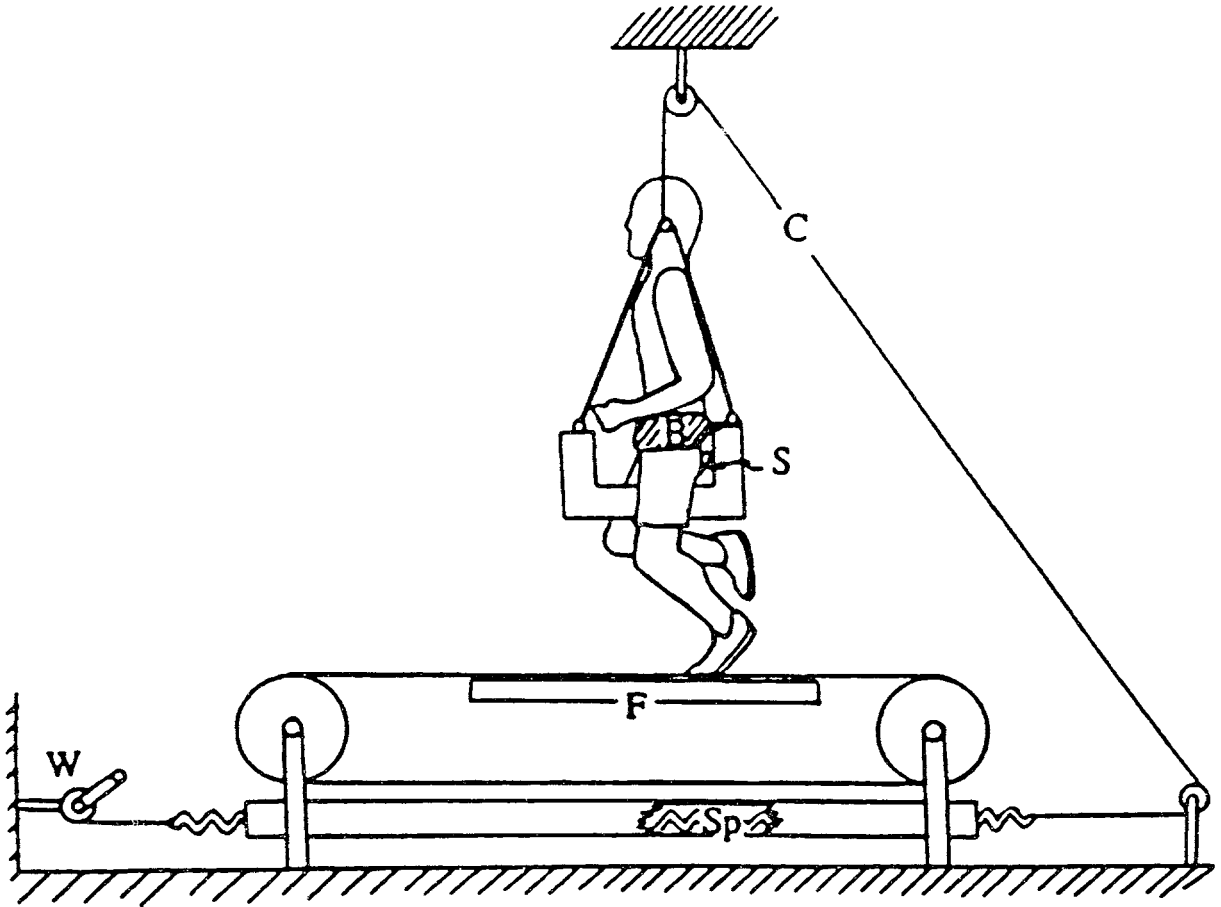


Figure 3.1 Harvard University Field Station (HFS) partial gravity suspension simulator. The device consists of a series of springs (Sp) which apply a nearly constant upward force to the subject through a bicycle saddle (S). The motorized treadmill includes a force platform (F) under the tread. This is the apparatus used by He *et al.* [1991] and Farley [1991] (See references for complete description.).

3.1.2 Parabolic Flight

True simulations of partial gravity can be effected in an aircraft flying Keplerian trajectories. Parabolic flight is capable of imposing partial gravity on the objects within the aircraft and provides up to 25 seconds of 0 g, 30 seconds of lunar gravity, and 40 seconds of Martian gravity for each of the 40 to 50 parabolas per experimental session. Figure 3.2 illustrates NASA's KC-135 aircraft used for parabolic flight research. It is possible to fly lunar and Martian gravity parabolas, but the vast majority of time the aircraft is used for microgravity flights to train astronauts and conduct 0 g research. Parabolic flight offers the advantage of producing the same physical conditions as orbital space flight and planetary environments. The high cost, limited availability, and limited experimental time duration are the disadvantages of the parabolic flight simulation technique. Moran [1969, pp. 463-472] gives a thorough review of reduced gravity human factors research with aircraft.

A fortunate opportunity arose to collaborate with engineers from the Man-Systems Division at Johnson Space Center (JSC) and conduct experiments onboard the KC-135. Four parabolic sessions were flown, two lunar (See Figure 3.3) and two Martian, in which the underwater locomotion study is replicated as closely as possible. Biomechanics measurements are recorded, but steady-state workload could not be recorded because the time limitation of the parabolas prevents energetic measurements.



Figure 3.2 The most common type of aircraft used for parabolic flight is NASA's KC-135.

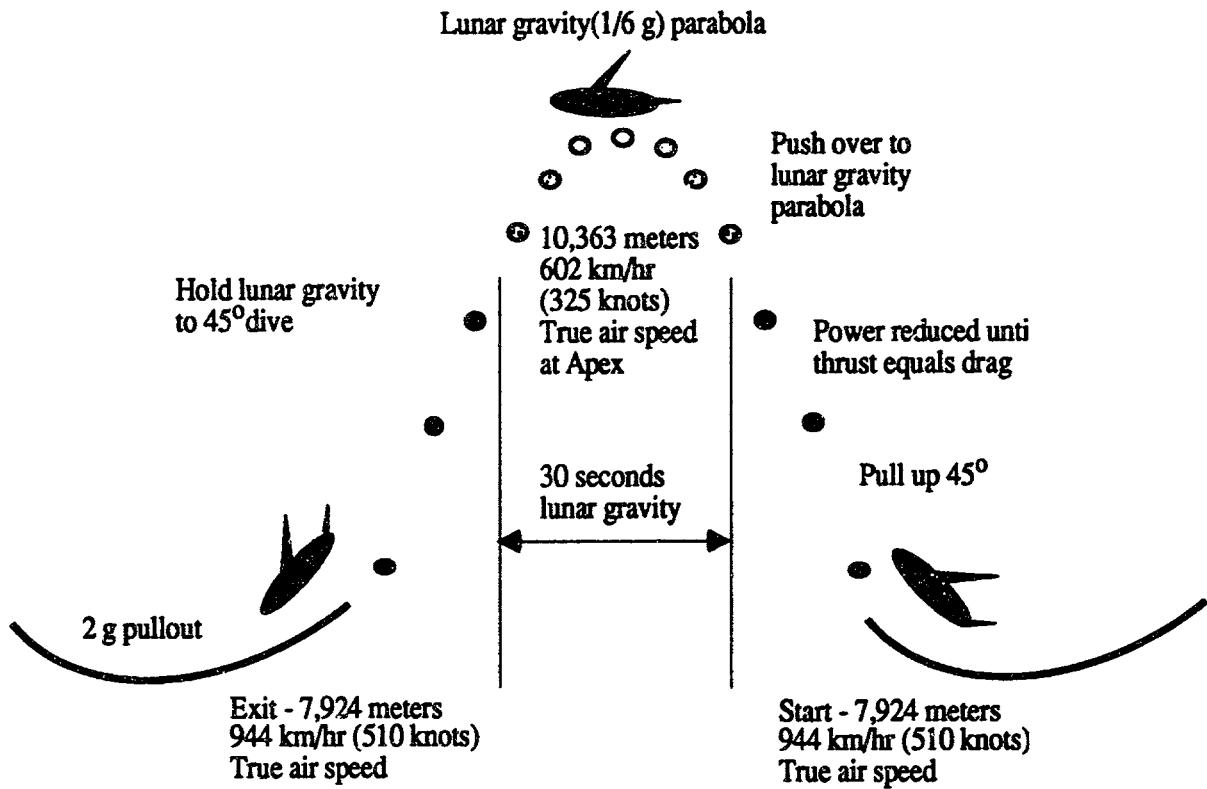


Figure 3.3 Schematic drawing of NASA's KC-135 aircraft flying a lunar gravity parabola.

3.1.3 Water Immersion

Water immersion has been used extensively for over 25 years for astronaut extravehicular activity training, and has been used for zero gravity simulation research [Schilling *et al.*, 1976 and Trout and Bruchey, 1969] during the past 4 decades. A study by Lilly suggested that in terms of sensory deprivation and isolation from physical and mental stimuli, similarities exist between the condition of a body freely floating in space and a body suspended in water [referenced by Duddy, 1969]. Duddy [1969] points out the significant contribution water immersion studies have had on the national space program objectives for pre-flight training and task time lining. The experience gained by the Gemini XII crew in their underwater training was a significant factor in the successful accomplishment of EVA mission objectives and the entire Gemini project. While water immersion has demonstrated its usefulness for training and simulation, it needs to be verified as a valid partial gravity simulation technique for analysis of motion and energy usage.

Buoyancy is responsible for space-like simulations underwater. When an object is submerged in a fluid there is a displacement of fluid by the object and an upward force on the submerged object results from the differential pressures on the top and bottom horizontal surfaces of the object. The weight of the displaced fluid and the loss of weight of the submerged object are equivalent, thus, neutral buoyancy is attained. An object which shows positive buoyancy has specific gravity less than that of the fluid medium in which it is submerged. Negative buoyancy, or simulated partial gravity, can be attained when the object's specific gravity is greater than that of the fluid medium, and can be achieved by adding ballast to a submerged subject.

Two types of water immersion exist, namely, total body immersion and immersion to the neck (which leaves the head out of the water). When immersion is only to the neck, negative-pressure breathing results which has the undesirable effects of exertion and dieresis [Di Giovanni, 1964]. Total body water immersion is recommended and is assumed throughout the remainder of the thesis.

Water immersion serves as the primary experimental technique used in this study since it allows free motion for a long time period. This permits assessment of both biomechanics and steady-state workload. Parabolic flight provides only short periods of true partial gravity and prevents most physiological measurements from being taken. Suspension systems provide limited degrees of freedom for locomotion. The underwater partial gravity simulation technique was found to be practical and establishes a convenient means of partial gravity simulation for future research

efforts. The major disadvantage of the immersion technique is the drag and damping on human movements [Akin *et al.*, 1988] and is addressed in Section 3.2 Hydrodynamic Modeling.

3.1.3.1 Partial Gravity Ballasting

In the underwater experiments, partial gravity loads are provided by an adjustable ballasting (loading) harness that distributes ballast (lead weights) on a subject ranging from 0% to 90% of their dry body weight. The subjects body-segment masses and inertial properties (based on standard models [Wortz *et al.*, 1966; and Chakraborty, 1990] determine the amount of weight required to simulate partial gravity loading. Weights are distributed on five body regions and balanced across the mass center of each: the left and right lower legs, the left and right thighs, and the torso (chest and backside). A 1.8 meter, 74 kg subject is ballasted according to Table 3.1 for the underwater experiments.

The adjustable ballasting harness designed for these experiments provides realistic loading for the entire range of hypogravity from 1/6 g through 9/10 g and is shown in Figure 3.4. The harness provides a novel method of ballasting the subject's torso and lower limbs. Rather than strapping on weight belts and applying all of the load around the waist, the adjustable partial gravity harness provides a high fidelity simulation. Torso and head weight are applied to the upper body through the chest harness and ballast is distributed around the circumference of the upper and lower leg segments via ballasting pockets. Subjects' limb segments are measured and the ballasting pockets are affixed to the thigh and lower leg at approximately the center of mass of the limb, thus a realistic loading of the limbs is provided.

Table 3.1 Ballasting loads for a 1.8 meter, 74 kg subject.

Body segment	Lunar, 1/6 g [kg]	Martian, 3/8g [kg]	2/3 g [kg]	9/10 g [kg]
torso	7.3	16.4	29.1	43.7
left thigh	1.3	2.8	5.1	7.6
right thigh	1.3	2.8	5.1	7.6
left lower leg	0.5	1.2	2.1	3.1
right lower leg	0.5	1.2	2.1	3.1

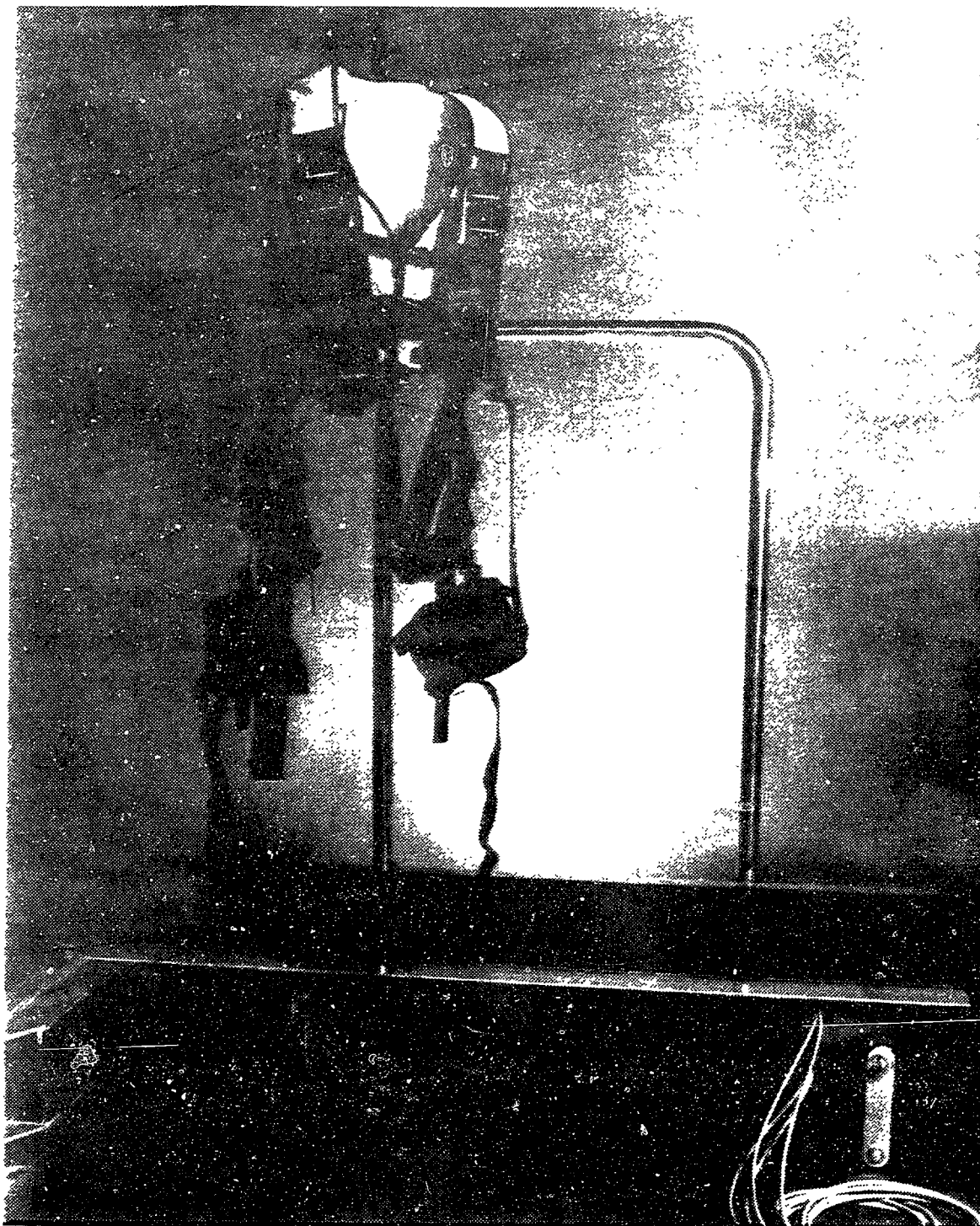


Figure 3.4 Adjustable ballasting harness used for partial gravity immersion experiments.

3.1.3.2 Immersion Assumptions

The first assumption of the immersion technique is that the pressure encountered by a subject underwater does not inadvertently alter his/her physiological measurements. There is no significant difference in subjects' resting metabolism while submerged (0.062 ± 0.013 ml/(kg·s)) or dry (0.06 ± 0.01 ml/(kg·s)). Subjects wear similar equipment and are supplied surface air for both conditions. Since the subjects' heads are only 0.61 meters (2 ft) underwater during treadmill locomotion, pressure increases by as little as 6.144 kN/m² (0.891 psi). This does not significantly alter the gas analysis measurements. The partial pressure of supply O₂ increases 5.7% at this 0.61 meter depth according to Dalton's Law which states that the total pressure exerted by a mixture of gases is the sum of the pressures that would be exerted by each of the gases if it alone were present and occupied that total volume. This O₂ partial pressure level is well within accepted operational limits.

The hydrodynamics model of Section 3.2 assumes steady flow. The actual flow in the submersion experiments is unsteady, but the steady flow assumption is justified because the inertial effects contribute a negligible amount to the measured metabolic expenditure. The total energy required to overcome the inertial forces depends on the energy requirements of moving the mass added to the subjects' limbs for ballast and the apparent added mass of the water displaced by the moving limbs.

The leg is modeled as a uniform cylinder with a linearly increasing and then decreasing velocity profile as it moves through the swing phase of a stride. Figures 3.5 and 3.6 show the velocity profile and the leg modeled as a cylinder, respectively. The figures represent the idealized case of a simple geometric shape moving through the water in order to quantify the order of magnitude of the inertial effects. The hydrodynamics model (See Section 3.2) assumes a more detailed geometric model and incorporates actual velocities obtained from the position histories of the video data of subjects moving through water. The hydrodynamic model also accounts for limb translations and rotations in three dimensions.

For the following idealized inertial drag calculation below, the swing phase of the stride is used to quantify the drag and can be doubled to approximate the drag during the entire stride. The leg starts at rest and reaches maximum velocity half way through the swing phase. Velocity slows down to zero by the end of the swing phase. Table 3.2 lists the parameters for the swing phase simulation.

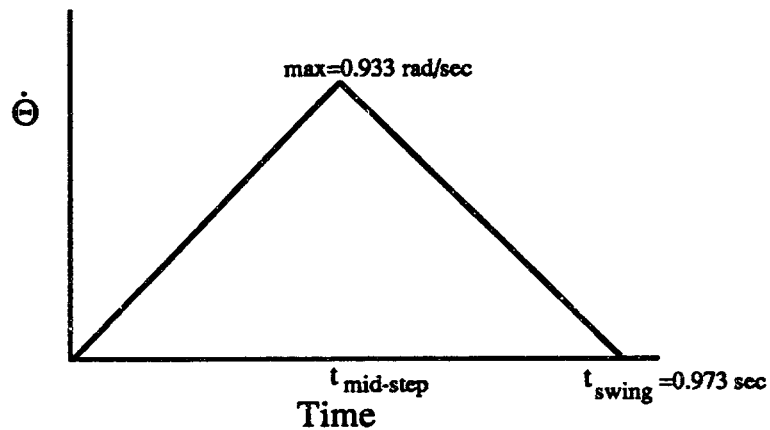


Figure 3.5 Velocity profile of the swing phase of the leg assumed during calculations of the inertial effects of added ballast and added mass due to moving the legs through a fluid medium.

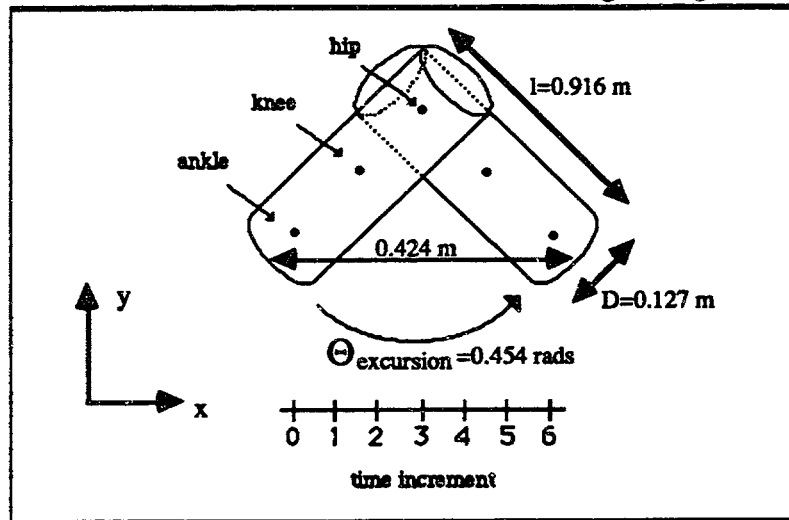


Figure 3.6 Model of the leg as a cylinder moving through the water. This simplified geometric model is assumed in the calculations of the inertial forces, but the hydrodynamics model of Section 3.2 assumes a more detailed geometric model and incorporates actual velocities obtained from video data of subjects moving through the water.

Table 3.2 Time increments and positions of leg model for swing phase.

Time increment	0	1	2	3	4	5	6
Elapsed time (sec)	0.0	0.162	0.324	0.487	0.649	0.811	0.973
<i>Theta dot</i> (rads/sec)	0.0	0.311	0.621	0.933	0.621	0.311	0.0
hip x, (meters)	0.212	0.212	0.212	0.212	0.212	0.212	0.0212
knee x (meters)	0.098	0.136	0.174	0.212	0.259	0.302	0.0325
ankle x (meters)	0.0	0.070	0.141	0.212	0.292	0.368	0.424
hip y (meters)	0.916	0.916	0.916	0.916	0.916	0.916	0.916
knee y (meters)	0.451	0.449	0.445	0.438	0.445	0.449	0.451
ankle y (meters)	0.024	0.016	0.008	0.0	0.008	0.016	0.024

Table 3.3 shows the calculations to determine the magnitude of the inertial acceleration energy. The reason to perform the calculation was to determine if the inertial effects would contribute a significant amount to the (steady flow) hydrodynamic drag energy per stride. The calculations assumed that the stride was only the forward swing of the leg, from the point the toe leaves the ground the point where the heels strikes the ground. The second assumption was that the leg is a uniform cylinder and pivots from the hip. The third assumption was that the angular velocity (Θ) is a ramp up and down. The energy required to overcome the inertial forces depends upon the added lead weight used for ballast and the added mass of the water displaced by the leg (assumed to be the same as the weight of the leg).

Table 3.3 Inertial effects due to added ballast - sample calculations.

Gravity level	Lunar (1/6 g)	Martian (3/8 g)	2/3 g	9/10 g
Ballast (kg)	1.36	3.63	5.9	7.71
F_{lead} (N)	0.28	0.76	1.23	1.60
E_{lead} (J/stride)	0.48	1.28	2.08	2.71
$E_{lead\ adjust}$ (J/stride)	2.31	6.18	10.05	13.11
% Met. Workload	0.7%	1.5%	2.8%	4.2%

Percentage of E_{H_2O} as compared to measured metabolic rate is 3.6% for a complete stride.

The theoretical calculations yield energy requirements attributable to the added lead ballast ($E_{lead\ adjust}$) and apparent added mass of moving a limb through water (E_{H_2O}) which are less than 4.3% of the metabolic energy consumed. Therefore, it is concluded that the unsteady flow effects are negligible and steady flow is assumed in the hydrodynamic modeling effort. The value of F_{lead} was calculated by assuming a constant acceleration of $0.208\ m/s^2$ (refer to Figure 3.6). The first E_{lead} term gives mechanical energy in Joules per stride and the second $E_{lead\ adjust}$ term gives an adjusted energy equivalent to metabolic expenditure in Joules per stride (calculated by applying Equation 2.13). The remainder of this Chapter presents a mathematical model which estimates the magnitude of the drag energy lost in overcoming the hydrodynamic forces of a subject's limbs moving through water.

3.2 HYDRODYNAMIC MODELING

The underwater experiments use water immersion to simulate partial gravity environments. Water immersion simulation offers several advantages: six degrees of freedom, long experimental test times, unrestricted body motions, a stable reference frame, and accommodation of large masses. An inherent simulation weakness is the viscosity encountered while moving through water. The difference between the underwater simulation technique and the actual environments of space or

partial gravity is that the workload measurements for a subject working underwater may be composed of the energy required to perform the task in space and the energy required to overcome the drag effects of the water. As suggested by Wortz *et al.* [1967], one application of an appropriate mathematical model is to reduce the metabolic rates taken from subject's working underwater by the amount of energy required to overcome the drag effects.

The hydrodynamic modeling effort entails a theoretical analysis with the goal of quantifying the magnitude of drag and damping effects encountered by subjects during underwater partial gravity simulation. The development of a mathematical model is necessary to assess the inherent drag constraint in underwater simulations. In the space environment, little additional energy is required to sustain a constant velocity motion because there is virtually no retarding force. The majority of muscle activity, and therefore metabolic energy, is elicited at the beginning of the motion for acceleration of the limbs and at the end of the motion for deceleration. Underwater there is a steady loss of momentum to neighboring fluid layers; the damping forces imposed by the water tend to decelerate the subject's legs while walking. In lieu of this fact, the assumption is made that the metabolic rates measured during the underwater locomotion study include the additional energy required to overcome the drag effects of the viscous medium as well as the energy required to perform locomotion at partial gravity. The theoretical model calculates the mechanical energy needed to overcome water drag and is helpful in estimating the magnitude of the drag constraint in the underwater partial gravity simulation technique.

In order to calculate the drag force, a history of limb positions and velocities is needed. Limb segments are modeled as simple geometric shapes, such as cylinders and conic frustums similar to models in the literature [Wortz *et al.*, 1966; Whitsett, 1963; and Hanavan, 1964]. The limb positions are attained by digitizing video data in two dimensions. The mathematical model can perform three dimensional analysis, however, the small size of the Neutral Buoyancy Test Facility (3.35 meter diameter) and window placement currently prevent three dimensional video recordings of subjects on the treadmill. These two factors also limit video images to the lower legs, excluding total body video. Limb velocities are calculated by differentiating successive limb positions. From these measurements, segment translations and pure rotations about the centroid are determined. Analytical drag values of the geometric model (See Figure 3.7) moving through water help assess the magnitude of the metabolic energy needed to overcome the drag of the water during partial gravity treadmill locomotion.

3.2.1 Flow Regimes and Calculations

This Section briefly describes the principles needed for the mathematical drag calculations. Then Reynolds number calculations for the limb segment model are given, followed by a discussion of hydrodynamic drag forces. Real fluid flow, including viscosity effects, is accounted for in the boundary layer and wake regions of limb segments moving through water. In other parts of the flow field, however, potential flow approximations hold because the body essentially behaves as if immersed in an inviscid fluid. The compressibility property of water is not relevant to the water immersion experiments because a one atmosphere pressure change for every 10.06 m (33 ft) depth of water causes a relative change in volume of 5×10^{-5} [Paines, 1986]. The underwater locomotion experiments were performed in the NBTf with subjects standing at a depth of 2.4 m (8 ft), in which the pressure change is less than one-third of an atmosphere; therefore, water is assumed to be incompressible.

Viscous drag depends on the viscosity of the fluid. Due to the viscosity the fluid literally sticks to the surface forming a very thin boundary layer. Pressure depends on the relative velocity of the object in the fluid. The total drag appears partly as viscous drag and partly as pressure drag. The former results from the viscous resistance of the water molecules against displacement in relation to the surface of the solid body and to each other, and the latter results from the distribution of forces normal to the body surface [Wortz *et al.*, 1967]. The Reynolds number, used to distinguish between laminar, partially turbulent, and fully turbulent flow, signifies whether the resistance of motion through a fluid is dominated by viscous drag or pressure drag. The factors which determine the Reynolds number of a body moving through a fluid are: size of the body, body shape, surface roughness of the body, viscosity of the fluid, and fluid flow velocity. The Reynolds number, or dimensionless ratio of pressure forces to friction forces, is denoted by the following equation:

$$R = \frac{\bar{u}D\rho}{\eta} = \frac{\bar{u}D}{\nu} \quad (3.1)$$

where: \bar{u} = freestream flow velocity
 D = object diameter
 ρ = fluid mass density (kg/m^3)
 η = fluid viscosity of water = $1.0 \text{ kg}/(\text{m}\cdot\text{s})$ at 1 atm. and 20°C
 ν = kinematic viscosity = $1.01 \times 10^{-6} \text{ m}^2/\text{sec}$

Wortz and Duddy [Wortz *et al.*, 1967; Duddy, 1969] found tasks performed at velocities less than a value of 0.61 m/s to be uninhibited by drag. For the underwater experiments, diameters of body segments could range from 6.33 cm for the forearm of a fifth percentile female to 53.2 cm for the

bideltoid (shoulder breadth) of a ninety-fifth percentile male [NASA, 1987]. Table 3.4 shows calculated Reynolds numbers for the water immersion simulations.

Table 3.4 Expected Reynolds numbers for body segments during underwater simulation.

Reynolds number definition,		$R = \frac{\bar{u}D\rho}{\eta} = \frac{\bar{u}D}{\nu}$ where, $\nu = 1.01 \times 10^{-6} \text{ m}^2/\text{sec}$				
Percentile	Body Dimensions, cm (inches)					
	5th %	50th %	95th %	5th %	50th %	95th %
Reynolds Number ($R_{1,2} \times 10^3$) associated with $\bar{u}_1 = 3.05 \times 10^{-3} \text{ m/s}$ and $\bar{u}_2 = 1.5 \text{ m/s}$ treadmill speeds, respectively.						
Female			Male			
Bideltoid	35.60 (14.00)	38.90 (15.30)	42.10 (16.60)	44.60 (17.60)	48.90 (19.30)	53.20 (20.90)
$R_{1,2} = \frac{\bar{u}D}{\nu}$	0.94, 460.34	1.02, 503.02	1.11, 544.40	1.17, 576.72	1.28, 632.33	1.40, 687.93
Biceps	6.94 (2.74)	8.12 (3.21)	9.33 (3.66)	8.69 (3.41)	9.93 (3.92)	11.17 (4.39)
$R_{1,2} = \frac{\bar{u}D}{\nu}$	0.18, 89.74	0.21, 105.00	0.25, 120.65	0.23, 112.37	0.26, 128.41	0.29, 144.83
Forearms	6.33 (2.48)	7.00 (2.77)	7.67 (3.02)	8.72 (3.44)	9.58 (3.76)	10.41 (4.11)
$R_{1,2} = \frac{\bar{u}D}{\nu}$	0.17, 81.85	0.18, 90.52	0.20, 99.18	0.23, 112.76	0.25, 123.88	0.27, 134.61
Hip Breadth	30.50 (12.00)	32.90 (12.90)	35.30 (13.90)	32.70 (12.90)	35.80 (14.10)	39.00 (15.40)
$R_{1,2} = \frac{\bar{u}D}{\nu}$	0.80, 394.40	0.86, 425.43	0.93, 456.47	0.86, 422.84	0.94, 462.93	1.02, 504.31
Thigh	14.52 (5.70)	16.43 (6.46)	18.37 (7.23)	16.71 (6.59)	19.10 (7.51)	18.37 (7.23)
$R_{1,2} = \frac{\bar{u}D}{\nu}$	0.38, 187.50	0.43, 212.07	0.48, 237.54	0.44, 215.95	0.50, 246.98	0.56, 236.64
Calf	9.64 (3.79)	10.85 (4.27)	12.03 (7.23)	10.79 (4.23)	11.97 (4.71)	13.18 (5.19)
$R_{1,2} = \frac{\bar{u}D}{\nu}$	0.26, 124.66	0.29, 140.30	0.32, 155.56	0.28, 139.53	0.31, 154.78	0.35, 170.43

Overall, the calculated range of Reynolds numbers characteristic of the underwater partial gravity simulations is $R = 0.17 \times 10^3 \leftrightarrow 6.88 \times 10^5$. In this range of Reynolds numbers all three flow regimes (laminar, partially turbulent, and turbulent) are seen. However, the design choice of using a submersible treadmill for the locomotion study eliminates full-body translation through the water, therefore, locomotion is modeled simply as limb segments moving through the water. For the limb segments, the Reynolds number range is $R = 0.17 \times 10^3 \leftrightarrow 2.37 \times 10^5$. Both viscous drag and

pressure drag are present at this range of Reynolds numbers, but for the larger numbers, pressure drag dominates the partially turbulent flow.

Large normal pressure drag exists for blunt bodies moving at velocities associated with the calculated Reynolds numbers due to separation of the boundary layer. The surface friction from viscous drag contributes a very small portion of the total drag. These complex drag force interactions require consideration of many factors in determining the damping effects of the water during the underwater partial gravity locomotion study. In order to understand the pressure drag the variation in pressure distribution around the limb segment must be classified. Separation of the boundary layer and wake formation behind the moving body suggest that two critical parameters, dynamic pressure and the projected area normal to the limb motion, are essential for calculating the drag energy for the model. Drag is generally expressed as:

$$D = C_D q A \quad (3.2)$$

where dynamic pressure is $q = \frac{1}{2} \rho v^2$, C_D is the drag coefficient, v is the velocity of the moving limb segment, ρ is the density of water, and A is the projected area of the body normal to v . Drag area, A_D , is defined as:

$$A_D = C_D A = \frac{D}{q} \quad (3.3)$$

The drag coefficient is a nondimensional, experimentally determined constant. Coefficients of drag are readily available for airfoils and simple geometric shapes, but limited research on the coefficients of drag exists for the human body. Unidirectional acceleration of a human body in a stationary fluid has been conducted [Hoerner, 1958; Keim, 1956; Trout *et al.*, 1966; and Sarpkaya and Garrison, 1963]. Hoerner gave drag coefficients between 1.0 and 1.3. Keim analyzed cylinders and a disk accelerated vertically from rest in a water tank. Trout *et al.* gave drag versus velocity curves for pressure-suited subjects performing both aircraft zero gravity trajectories and water immersion tasks with resulting drag coefficients of 1.15 and 1.2, respectively. The drag coefficient for a human body immersed in water is assumed to be between 1.0 and 1.3 and an average is used in this model analysis. It is recommended that accurate C_D values for the human body in water be attained.

3.2.2 The Mathematical Model

Modeling a person moving on a submersible treadmill is an exceptionally complex task, and by using simplifying assumptions and relying on references this Section models the hydrodynamic forces of a person moving his/her limbs through water. The mathematical model and computer

program are edited and enhanced versions of a concept put forth by Wortz and his colleagues [Wortz *et al.*, 1967]. The desired total drag force can be defined in terms of the equivalent instantaneous velocity at the mass center of the body, therefore, limb position and velocity measurements are required for each segment at each time increment. The damping effects are calculated on a limb by limb basis and superposition is used to calculate the total drag for all the limbs.

Figure 3.7 illustrates the eight limb segments of the mathematical model:

- | | |
|-------------------------------------|-------------------------------------|
| 1. Left thigh segment | 5. Left upper arm segment |
| 2. Right thigh segment | 6. Right upper arm segment |
| 3. Left lower leg and foot segment | 7. Left lower arm and hand segment |
| 4. Right lower leg and foot segment | 8. Right lower arm and hand segment |

The model could be enhanced to include a head, torso, and spacesuit backpack if EVA tasks or translation through the tank were experimental objectives. Lower arm/hand and lower leg/foot segments assume that the relative motion between the lower arm and hand and the lower leg and foot contribute a negligible amount to the drag and lumped segments are used. This assumption seems justified for arm/hand motions during locomotion, but is suspect for relative motions between the lower leg and foot (i.e. plantar flexion). The segments are assumed to be rigid and input dimensions (i.e., leg circumference, height, etc.) are required to calculate the dimensions of the geometric model segments. Table 3.5 delineates the required model dimensions.

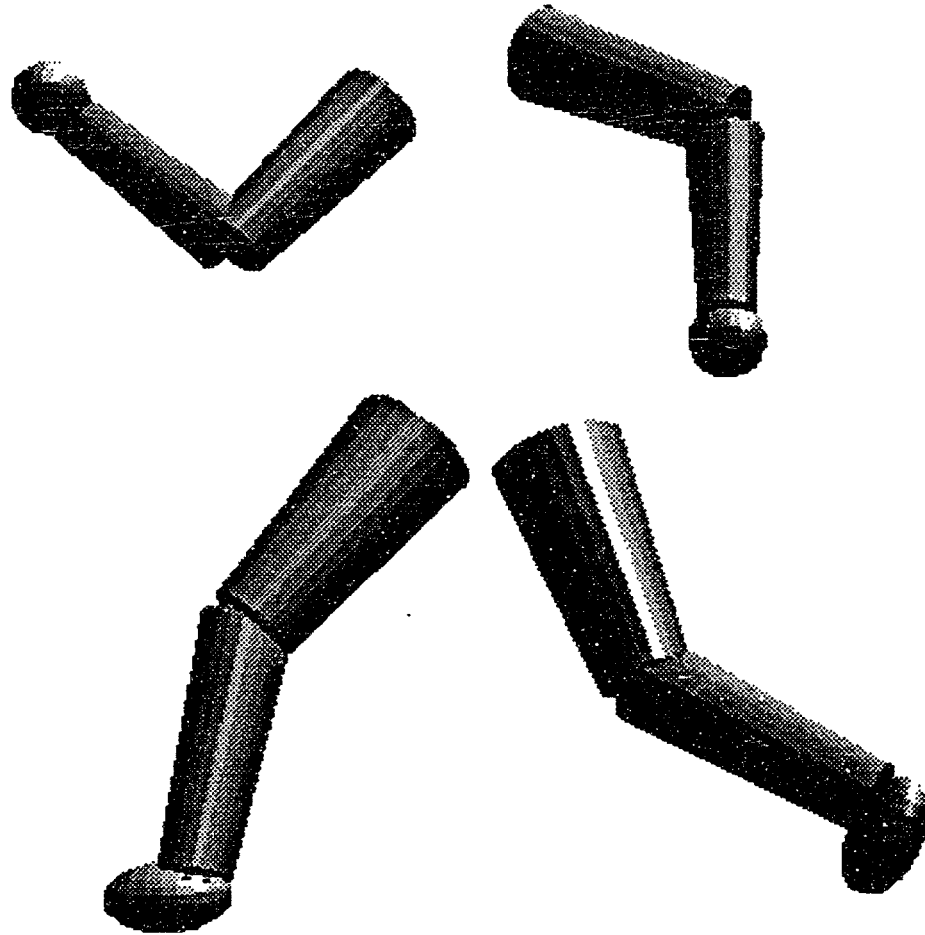


Figure 3.7 Model of the human body for the hydrodynamic model. Limb segments are modeled as conic frustums.

Table 3.5 Dimensions of Geometric Shapes for Hydrodynamics Model

Nomenclature	Description	Segment (1-8)	Model Geometry
ANKC	Ankle Circumference	3, 4	$D_{ll} = \frac{1}{\pi}(\text{ANKC})$
ELBWC	Elbow Circumference	5,7 and 6,8	$D_{ea} = \frac{1}{\pi}(\text{ELBWC})$
FISTC	Fist Circumference	7, 8	$D_h = \frac{1}{\pi}(\text{FISTC})$
FOOTC	Foot Circumference	3, 4	$D_f = \frac{1}{\pi}(\text{FOOTC})$
LAL	Lower Arm (Conic Frustum) Length	7, 8	$l_{7,8} = \text{LAL}$
UAL	Upper Arm (Conic Frustum) Length	5, 6	$l_{5,6} = \text{UAL}$
LLL	Lower Leg (Conic Frustum) Length	3, 4	$l_{3,4} = \text{LLL}$
ULL	Upper Leg (Conic Frustum) Length	1, 2	$l_{1,2} = \text{ULL}$
THIGHC	Thigh Circumference	1, 2	$D_{ul} = \frac{1}{\pi}(\text{THIGHC})$
UAC	Upper Arm Circumference	5, 6	$D_{ua} = \frac{1}{\pi}(\text{UARMC})$
WRISC	Wrist Circumference	7, 8	$D_{la} = \frac{1}{\pi}(\text{WRISTC})$
KNEEC	Knee Circumference	1, 3 and 2, 4	$D_{kl} = \frac{1}{\pi}(\text{KNEEC})$

Where D is the segment diameter in meters and l is the segment length in meters.

3.2.2.1 Calculating the Drag Energy

Metabolic energy expenditure for the steady-state condition is calculated via gas analysis and computer programs for each subject at all three speeds on the submersible treadmill. Ideally, these measurements could be compared to a subject suspended in air using the same limb motions as in the underwater partial gravity experiments, and the difference in energy expenditures would yield the additional energy (drag energy) caused by the underwater partial gravity simulation technique. However, replicating the underwater locomotion experiments in air using a suspension system with the identical equipment was not possible. In lieu of this, the mechanical energy of the drag encountered by the modeled limb segments moving through water is calculated. The relationship between the mechanical drag energy and the measured metabolic expenditures is approximated using Equation 2.13 [Margaria, 1976]. Section 2.2.2.1 gave the rationale for using this equation to convert from mechanical energy to metabolic energy.

Drag energy needed to overcome the hydrodynamic force of the partial gravity submersion technique is derived from the drag equation (Equation 3.2). The geometric model coupled with the recorded motion histories of the limb segments provide the necessary inputs for calculating the drag force encountered by the subject. Consequently, the drag energy is calculated by integrating

the drag force over the distance the segments traverse [Wortz *et al.*, 1967]. The derivation of equations for the model is highlighted below.

Using the position and velocity vectors $\bar{X}_i(t)$ and $\bar{V}_i(t)$, respectively, over the time course of a complete stride, the drag energy can be calculated for each limb segment. The total drag energy of the simulation may be calculated with the following summation $\sum_{i=1}^8 D_i$, where D_i is the drag on segment i . A typical segment AB of length l is shown in Figure 3.8. Digitized video data yields the position vectors from which the velocity vectors are calculated by differentiation. Once the velocity vectors at ends A and B are known, the velocity vector of a differential segment a distance x away from end A is given by:

$$\bar{V}_x = \frac{l-x}{l}\bar{V}_A + \frac{x}{l}\bar{V}_B \quad (3.4)$$

The drag force acting on the surface of the differential segment is:

$$\Delta D = \frac{1}{2}\rho C_D |\bar{V}_x|^2 \Delta A_x \quad (3.5)$$

where ΔA_x is the projected area of the differential lateral surface normal to \bar{V}_x . The segments are modeled as conic frustums and are assumed to have varying cross-sections. The velocity and cross-section variations along the axis of a limb segment are illustrated in Figure 3.8.

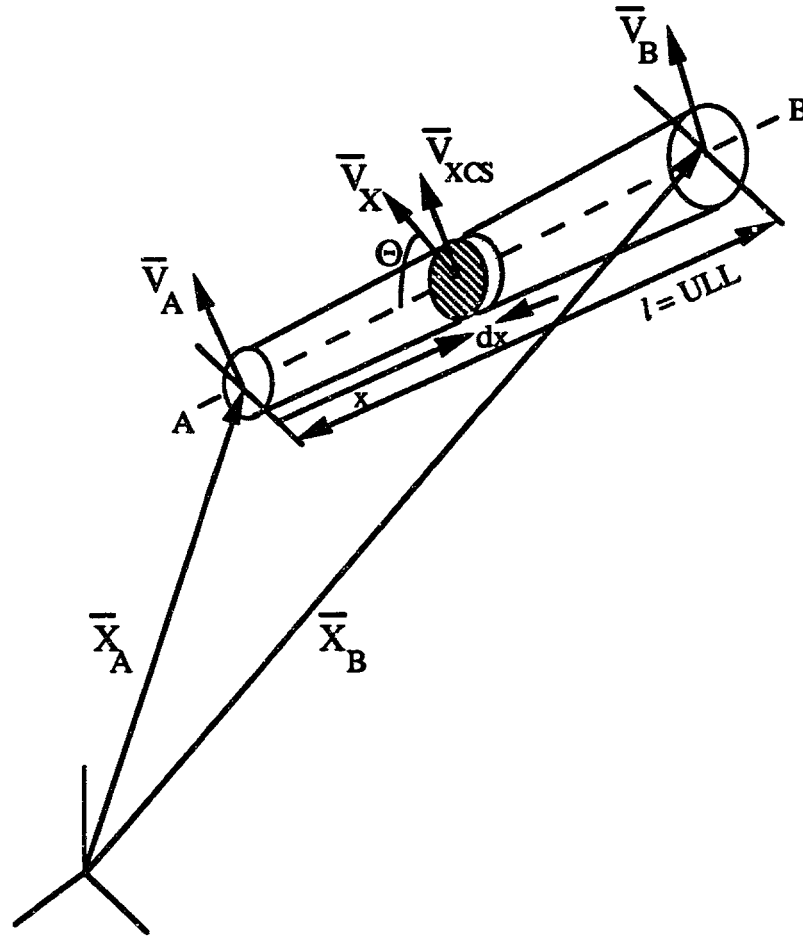


Figure 3.8 Velocity and cross-section variations along the axis of a limb segment.

Given the previous definitions, the projected area is written as:

$$\Delta A_x = w(x) \Delta x \cdot \sin \Theta = \frac{w(x)}{x} \frac{|\vec{V}_x \times \frac{x}{l} \vec{X}_{AB}|}{|\vec{V}_x|} \Delta x \quad (3.6)$$

where $w(x)$ is the projected width of the perimeter of the cross-section and $\vec{X}_{AB} = \vec{X}_B - \vec{X}_A$. The drag energy for segment AB during Δt is:

$$(\Delta E_D)_j = \sum_l \frac{1}{2} C_D \rho |\vec{V}_x|^2 (\Delta A_x) \cdot (\Delta S_x) \quad (3.7)$$

where ΔS_x is the distance traversed by ΔA_x in the direction of \vec{V}_x . The energy expended during

$$\begin{aligned} \left(\frac{\Delta E_D}{\Delta t} \right)_j &= \int_0^l \frac{1}{2} C_D \rho w(x) \frac{|\vec{V}_x \times \frac{x}{l} (\vec{X}_B - \vec{X}_A)|}{x} |\vec{V}_x|^2 dx \\ \text{time increment } \Delta t \text{ is:} & \\ &= \frac{1}{2l} C_D \int_0^l w(x) |\vec{V}_x|^2 |\vec{V}_x \times \vec{X}_{AB}| dx \end{aligned} \quad (3.8)$$

Recall that $\bar{V}_x = \frac{l-x}{l}\bar{V}_A + \frac{x}{l}\bar{V}_B = \bar{V}_A - \bar{V}_A\frac{x}{l} + \bar{V}_B\frac{x}{l}$.

\bar{V}_x^2 is expressed in terms of \bar{V}_A , \bar{V}_B , \bar{X}_A , and \bar{X}_B as:

$$|\bar{V}_x|^2 = (\bar{V}_A - \bar{V}_A\frac{x}{l} + \bar{V}_B\frac{x}{l})^2 = (\bar{V}_A + (\bar{V}_B - \bar{V}_A)\frac{x}{l})^2 \quad (3.9)$$

or re-written as:
$$|\bar{V}_x|^2 = \frac{1}{l^2}(\bar{V}_B - \bar{V}_A)^2 x^2 + \frac{2}{l}\bar{V}_A(\bar{V}_B - \bar{V}_A)x + \bar{V}_A^2 \quad (3.10)$$

which simplifies to:
$$|\bar{V}_x|^2 = Ax^2 + Bx + C \quad (3.11)$$

$|\bar{V}_x \times \bar{X}_{AB}|$ is expressed in terms of \bar{V}_A , \bar{V}_B , \bar{X}_A , and \bar{X}_B as:

$$|\bar{V}_x \times \bar{X}_{AB}| = \sqrt{\left[\left[\bar{V}_A + (\bar{V}_B - \bar{V}_A)\frac{x}{l} \right] \times \bar{X}_{AB} \right]^2} \quad (3.12)$$

or written as:
$$|\bar{V}_x \times \bar{X}_{AB}| = \sqrt{\left[(\bar{V}_A \times \bar{X}_{AB}) + (\bar{V}_B - \bar{V}_A)\frac{x}{l} \times \bar{X}_{AB} \right]^2} \quad (3.13)$$

and re-written as:

$$|\bar{V}_x \times \bar{X}_{AB}| = \sqrt{\frac{1}{l^2}(\bar{V}_B - \bar{V}_A)(\bar{X}_B - \bar{X}_A)^2 x^2 + \frac{2}{l}[\bar{V}_A \times (\bar{X}_B - \bar{X}_A)][(\bar{V}_B - \bar{V}_A) \times (\bar{X}_B - \bar{X}_A)]x + |\bar{V}_A \times (\bar{X}_B - \bar{X}_A)|^2}$$

which simplifies to:
$$|\bar{V}_x \times \bar{X}_{AB}| = \sqrt{ax^2 + bx + c} \quad (3.14)$$

The total drag energy of the mathematical model is the summation of the eight segments obtained by integrating the time variable over the duration of a complete stride and is represented as:

$$E_D = \frac{1}{2}\rho \sum_1^8 \int_0^{t_s} C_D(t) \int_0^l w(x) \frac{1}{l^2}(\bar{V}_B - \bar{V}_A)^2 x^2 + \frac{2}{l}\bar{V}_A(\bar{V}_B - \bar{V}_A)x + \bar{V}_A^2 * \sqrt{\frac{1}{l^2}(\bar{V}_B - \bar{V}_A)(\bar{X}_B - \bar{X}_A)^2 x^2 + \frac{2}{l}[\bar{V}_A \times (\bar{X}_B - \bar{X}_A)][(\bar{V}_B - \bar{V}_A) \times (\bar{X}_B - \bar{X}_A)]x + |\bar{V}_A \times (\bar{X}_B - \bar{X}_A)|^2} dx dt$$

which simplifies to:
$$E_D = \frac{1}{2}\rho \sum_1^8 \int_0^{t_s} C_D(t) \int_0^l w(x)(Ax^2 + Bx + C) \sqrt{ax^2 + bx + c} dx dt \quad (3.15)$$

where l is the length of the segments. The C_D is actually a function of attitude and velocities of limb segments, but is assumed constant in the model because of the lack of data on humans moving through water. Various limb segments may have different cross-section variations and the position and velocity histories of their ends certainly differ; these variations are reflected in A, B, C, a, b, c, and w. Obviously, all variables are functions of time. Equation 3.15 is approximate as it only reflects the drag along the lateral surfaces of the segments [Wortz *et al.*, 1966].

3.2.2.2 Computer Programs and Output

A computer program (partially translated from [Wortz *et al.*, 1966]) written in the C programming language implements the previously defined drag energy calculations for the geometric model of a human during underwater locomotion. The program, named "Legs," conducts its calculations based on input data from subjects' anthropometric measurements and digitized video images of underwater locomotion. It then outputs the amount of drag energy expended by the model for a complete stride. The three main sections of the program are input, drag calculation, and output. These sections are briefly described below. See Appendix A for computer program listing.

3.2.2.2.1 Program Inputs

Model Dimensions

There are four anthropometric dimensions necessary for input into Legs. Those dimensions are height, thigh circumference, knee circumference, and ankle circumference. Leg measurements need be made for one leg only. Legs only indirectly uses the height of the subject in calculating drag; by using relevant anthropometric ratios, Legs calculates the length of the upper leg and lower leg from the height. There are five main model dimensions that are important for a drag calculation: three circumferences and two lengths. Doubling the drag over one leg yields the drag for the entire stride cycle.

Motion History

Digitization of locomotion video images enables the capturing of screen pixel positions of the hip, knee, and ankle for a subject's leg. These coordinates reflect a coordinate system not necessarily correspondent to that of the physical world; for this reason, Legs converts the pixel positions of the digitized images to positions in meters relative to an arbitrary origin (which is held constant throughout the drag calculation). The program captures the coordinates for the hip, knee, and ankle positions for each frame of the videotape; in doing so, the program constructs an array of positions for each of the frames of the video sequence. Positions for each of the frames later become positions for individual *time increments* of the drag calculation.

Legs fills the position array and the velocity array from the hip, knee, and ankle positions for a subject. These two arrays are global and accessible by any procedure in the program; however, once filled in the input section of the program, these arrays remain unchanged throughout the program. Both of the arrays are three dimensional: the three dimensions are JNT, DIR, and MAXT, where JNT equals the number of joints in the drag calculation (in this case, two — the upper leg and the lower leg), DIR equals the number of Cartesian directions involved in the simulation (constant at three), and MAXT, which is the number of time increments in the simulation. An external library contains values for JNT, DIR, and MAXT which the user may easily access and change from simulation to simulation.

3.2.2.2.2 Drag Calculation

Using the five model dimensions and the position and velocity arrays, the program calculates the drag energy for each time increment. To calculate the drag for the entire simulation, the program calculates and sums the drag for each limb segment according to Equations 3.2 - 3.17 over each of the several time increments of the simulation. More specifically, in calculating the drag over a segment for one time increment, the program divides the segment into a specified number of *differential* segments, and uses Simpson's method to carry out the integrations in Equations 3.2 - 3.17. The variable specifying the number of differential segments to be used, NUMPOINTS (currently set at 21), is a global variable in the external library. Another important variable in the drag calculation is DT_SIZE (also included in the external library), which specifies the size (in seconds) of each time increment. For input data from a standard videotape DT_SIZE equals 0.033 seconds because the tape runs at 30 frames per second.

Accuracy of the Drag Calculation

Three variables determine the accuracy of a calculation: NUMPOINTS, DT_SIZE, and the number of time increments in the simulation. A large NUMPOINTS yields a highly accurate solution, since dividing a segment into a large number of differentials yields a more accurate solution to Simpson's method. The error-inducing effects of discrete-time motion input are minimized by using a small DT_SIZE. A large number of time increments also yields highly accurate output.

3.2.2.2.3 Program Output

Legs saves all relevant output in an output file with a user-specified name. The output file contains all the input data needed to repeat the simulation. Raw video data is not saved, but the file contains position and velocity arrays, model dimensions, and all of the variables listed above. Finally, the

output file contains the drag energy expended over each individual time increment and the total drag energy for the simulation.

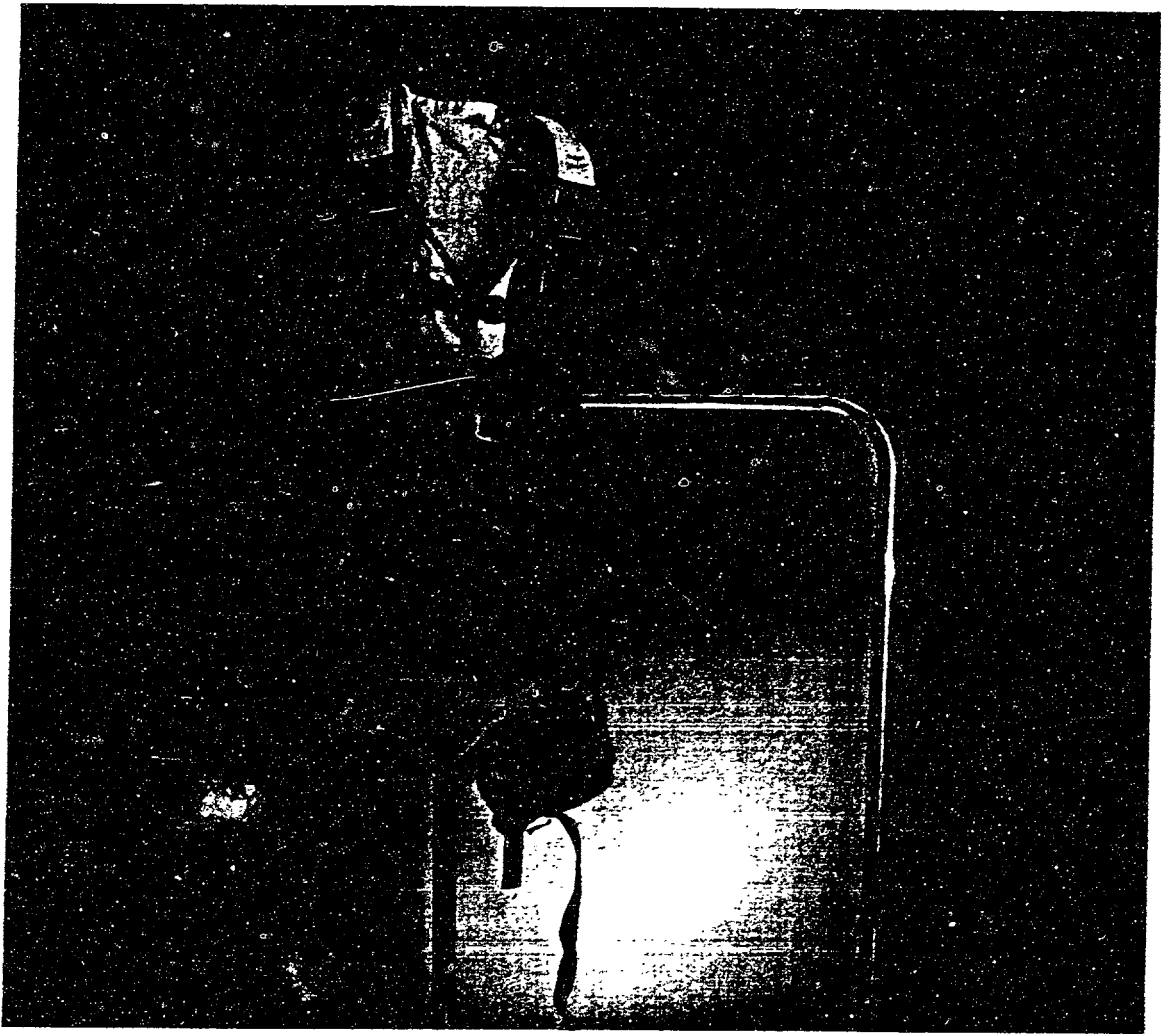
Table 3.6 shows the drag energy output of the Legs program for partial gravity locomotion. The first drag energy value is the output of the hydrodynamic computer model in Joules. This measure of mechanical energy expended during the underwater simulations is adjusted to metabolic energy expenditure by applying Equation 2.13. The large increase for drag at the 2/3 g simulation compared to the other gravity levels is explained by the errors in manually digitizing the video data. For this stride file, larger digitization errors are noted, but all data points are included in the drag simulation. Smoothing the digitized position points would reduce the drag calculation.

The purpose of the hydrodynamic modeling effort in this Chapter was to assess the magnitude of the drag force on the workload measurements. All of the calculated drag energy values are negligible compared to the measured metabolic expenditures (< 6 %). Hence the hydrodynamic effects of moving the legs through the water during underwater treadmill locomotion has an inconsequential affect on the energetic measurements for the experimental protocol of this study. A comparison between an analytical solution (using the Bernoulli equation) and the mathematical computer analysis validates the computer program. The simplified geometric model introduced in Section 3.1.3.2, Immersion Assumptions, is used for the comparison and results are within a factor of 2.6 (See Appendix A.2 for calculations). Another means of validation for the underwater submersion technique is revealed in the Results Section. Oxygen uptake measurements for the 9/10 g simulation underwater and 1 g terrestrial locomotion are seen to vary by less than one standard deviation.

Table 3.6 Hydrodynamic Drag Energy - Summary

Subject	S6	S3	S4	S4
Gravity Level	1/6 g	3/8 g	2/3 g	9/10 g
Velocity (m/s)	1.5	2.3	1.5	1.5
Drag Energy				
E_D (Joules/stride)	8.2	10.8	22.8	18.6
% Met. Workload	2.8%	2.4%	5.7%	4.7%

IV. METHODS



*We shall not cease from exploration
And the end of all our exploring
Will be to arrive where we started
And know the place for the first time.*

- T. S. Eliot, Four Quartets

CHAPTER IV. METHODS

This Chapter describes the methods of the partial gravity locomotion experiments. First, the subjects who participated in the underwater and parabolic flight experiments are mentioned. Then the Chapter outlines the experimental protocol employed during the underwater and parabolic flight experiments. Finally, the equipment that was designed for the study is described, all experimental apparatus used during both experiments is detailed, and the measurements taken with all of the equipment are revealed.

4.1 SUBJECTS

Six healthy paid subjects, four men and two women, participated in the underwater locomotion and energetics experiments while two healthy males volunteered to serve as the primary subjects in the complementary parabolic flight experiments. Subjects range in age from 24 to 39 years, height from 1.66 to 1.83 m, and weight from 578 to 801 N (See Table 4.1 and Appendix B for subjects' anthropometric data). To qualify for participation, each subject passed a physical examination consisting of a general checkup, an ECG test, and a treadmill stress test. Additionally, all subjects were experienced treadmill runners and qualified scuba (self-contained underwater breathing apparatus) divers so they were extremely comfortable underwater. The two KC-135 subjects had previously experienced parabolic flight on numerous occasions (> 6). Subjects were free from any known orthopedic problems. Informed consent for all experiments was obtained and subjects were permitted to withdraw from the study at any time for any reason. Appendix B includes a copy of the informed consent form that was signed by all subjects once the study commenced.

Subjects participated in underwater experiments at the Neutral Buoyancy Test Facility (NBTF) located at NASA Ames Research Center (ARC), Moffett Field, California. The NBTF is a cylindrical tank with a 9 foot depth and an 11 foot diameter [Webbon, 1987]. After pilot studies conducted in the summer of 1990, formal data collection for the underwater locomotion experiments took place during January of 1991. The underwater experiments assess human performance for numerous partial gravity levels (1/6 g, 3/8 g, 2/3 g, and 9/10 g) and are complemented by parabolic flight experiments for lunar (1/6 g) and Martian (3/8 g) gravity levels. Parabolic flights using NASA's KC-135 aircraft took place in July and August of 1991 in conjunction with NASA Johnson Space Center (JSC) and were flown out of Ellington Field, Texas.

Table 4.1 Subject Database.

Subject	Gender	Age [yr]	Height [m]	Mass [kg]	Weight [N]
Subject 1, S1	M	24	1.78	73.3	718
Subject 2, S2	M	31	1.80	73.5	720
Subject 3, S3	M	30	1.78	74.0	725
Subject 4, S4	M	39	1.83	81.7	801
Subject 5, S5	F	32	1.70	61.5	603
Subject 6, S6	F	31	1.66	59.0	578
KC-135, S1	M	34	1.74	73.8	723
KC-135, S2	M	37	1.78	69.9	685

4.2 EXPERIMENTAL PROTOCOL

The experimental protocol provides a strategy for assessment of biomechanics and steady-state energy expenditures for locomotion in partial gravity. During submersion experiments, both biomechanics and steady-state workload are measured. The lunar and Martian parabolic flights provide biomechanics measurements, but the short time duration of each parabola prohibits steady-state oxygen analysis.

4.2.1 Immersion Experiments

The protocol for biomechanics measurements and the associated workload for locomotion in partial gravity environments is described in this Section. For the underwater experiments, each subject participated in six experimental sessions after being fully trained on the treadmill. Subjects were trained on the device until their biomechanics and energy expenditure measurements reach a plateau, and were repeatable. A typical training period consisted of three complete, three-hour experimental sessions. Once data collection began, a different gravity level was simulated in each of six experimental sessions. One session was a 1-g control experiment with subjects exercising on the treadmill outside the NBTF. The remaining five sessions took place underwater in the NBTF. Five gravity conditions are simulated by ballasting the subjects with weights. The five conditions were: 0 g, 1/6 g, 3/8 g, 2/3 g, and approximate full body loading (90% - 100%, or 9/10 g). Subjects move at three speeds (0.5 m/s, 1.5 m/s, and 2.3 m/s) until they reach steady-state oxygen consumption levels (3-5 minutes). The only instruction given to the subjects is to "locomote naturally." The same model AquaSox™ booties were supplied to all subjects and worn for all tests on the submersible treadmill. Figure 4.1 contains an experimental protocol matrix.

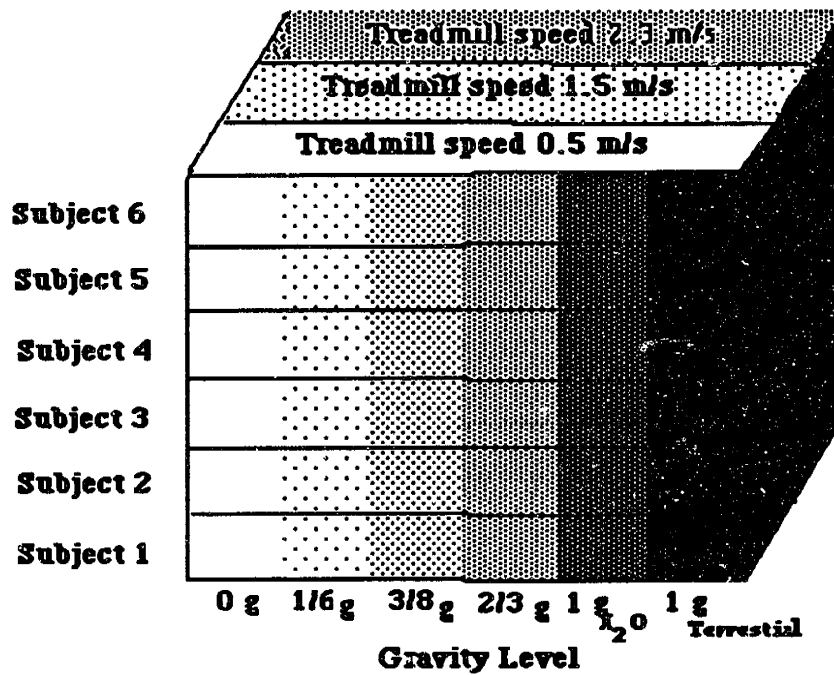


Figure 4.1 Underwater treadmill 6 x 6 x 3 experimental protocol matrix.

4.2.2 Parabolic Flight

During the parabolic flight experiments, the underwater protocol is replicated as closely as possible. The flight experiments include a total of four parabolic sessions, two flights in which lunar gravity (1/6 g) was flown and two flights in which Martian gravity (3/8 g) was maintained. Each session consisted of an average of 50 parabolas. The parabolic experimental protocol called for subjects to ambulate at the same speed as the underwater subjects (0.5 m/s, 1.5 m/s, and 2.3 m/s), but after recalibration of the treadmill, speeds inflight were actually found to be 0.7 m/s, 1.5 m/s, and 2.0 m/s.

4.2.3 Rationale

Treadmill velocities for both experiments elicit low, medium, and high workload levels from subjects. The three velocities correspond to approximately 10%, 40%, and 70% of subjects' maximum oxygen uptake and they also produce different gaits. Walking and running were expected at the low and high speeds during underwater locomotion, respectively. The middle speed was chosen to elicit a transitional gait. These workload levels have practical significance because it is anticipated that astronauts performing planetary EVA will be required to maintain a

workload of 40% for a nominal 8 hour workday. It is also expected that slow and rapid locomotion will be prevalent during EVA. A typical underwater experimental session timeline is shown in Table 4.2.

Table 4.2 Underwater Locomotion and Energetics Experiment Session Timeline.

Elapsed Time (minutes)		Underwater Locomotion and Energetics Sessions
0-20	(20)	Set up - Test director and safety diver Subject preparation - weigh-in, put-on heart monitor Ballast the subject to required simulated gravity level
20-30	(10)	Exercise at 10% workload level
30-35	(05)	Rest (if needed)
35-45	(10)	Exercise at 40% workload level
45-50	(05)	Rest (if needed)
50-60	(10)	Exercise at 70% workload level
60-65	(05)	Cool down period
65-75	(10)	Terminate experimental session, unballast subject
75-105	(30)	Rest, subject remains in laboratory setting, debrief and questions

Measurements of vertical force and steady-state workload are taken during underwater locomotion and only force traces are measured during parabolic flight. The short duration of partial gravity during each parabola prevents energetics measurements, especially steady-state workload measurements because it takes a few minutes to reach a steady-state level. Vertical forces exerted by subjects on the treadmill-mounted force platforms are sampled and low-pass filtered and then the force traces are used for gait analysis. Oxygen uptake measurements, $\dot{V}O_2$, taken during the underwater experiments constitute the energetics data for the entire study. Section 4.3, Equipment and Measurements, explains the experimental measurements in detail.

4.2.4 Personnel

The personnel involved in running the underwater experiments and their responsibilities are described below. Besides the subject, two or three additional people were required to run the experiments. A test director and a safety diver were essential and an optional third person served as test monitor. The test director (or experiment director) was the person responsible for the all aspects of the test and has responsibility for overseeing the power system controls. The test director controlled the treadmill velocity from the control panel and insured that the range of workload values was safely realized. The subject simply kept pace with the treadmill belt. The test director had two-way communication links to the subject and the safety diver throughout the test. The test director had sole authority for initiation and implementation of any contingency or emergency procedures. During an emergency, the test director would instruct all other personnel

of their responsibilities and then monitor and assist in the operation. A safety diver was required throughout the entire experimental session and had responsibility for the test subject and underwater equipment. The safety diver's responsibilities included: verifying that subjects properly donned their equipment, directing the entry and exit of the subject into and out of the tank, and providing emergency support and recovery assistance to the subject, if needed.

The experimental protocol and all equipment for the underwater experiments were approved by the NASA Ames Human Research Experiments Review Board (HRERB), the NASA Ames Man-Rating Review Board; and a comprehensive safety analysis for this experimental protocol is filed as Hazard Report #ARCX-01-NB01 [Newman, 1990]. The parabolic flight protocol and equipment gained NASA JSC KC-135 safety review board approval.

4.3 EQUIPMENT AND MEASUREMENTS

The following Sections describe the equipment and experimental measurements used for both the underwater experiments and the parabolic flights. First, the equipment used and measurements taken during the underwater tests are detailed. Then the equipment and measurements used during parabolic flight are described. The underwater experiments necessitated the design of a submersible treadmill, a partial gravity ballasting harness (previously described in Section 3.1.3.1), and a life support system. The major design contribution of this research effort is the patent-pending human-rated submersible treadmill.

4.3.1 Underwater Locomotion Equipment

A submersible treadmill with a split-plate force platform embedded under the belt provides the capability to perform biomechanics analysis for partial gravity locomotion. The split-plate design allows for a complete biomechanics analysis of all gaits. In other words, peak force, stride length, contact time, and aerial time measurements can be made from the force traces of a subject walking, loping, or running. The following Section describes the design of the treadmill. A video camera records locomotion in two dimensions during the experimental sessions, and measurements are discussed in Section 4.3.1.2. During the experiments, subjects wear a full-face diving mask and are supplied with air from surface tanks. The mask is instrumented to measure energy expenditures. A flow meter coupled with tygon tubing running between the mask and gas analysis equipment provide measurements of \dot{V}_{O_2} and carbon dioxide production.

4.3.1.1 Submersible Treadmill

A human-rated submersible treadmill equipped with a force platform was designed and fabricated for this study. Electric, pneumatic, and hydraulic power systems were all considered for the treadmill drive system, and an electric motor drive was chosen due to its high performance, affordability, and cleanliness of operation. The low-torque, high-speed characteristics of pneumatic motors are undesirable for underwater treadmill operation. Hydraulic motors provide the advantages of high torque and fine control at slow speeds, but the possibility of hydraulic fluid-leaks in the water tank favors the electric-motor option. The motor is mounted on the elevated wooden platform of the NBTF and connected to the submersible treadmill by a 5 meter flexible stainless steel shaft (See Figure 4.2).

A 3 hp, 480 Volt, 3 phase motor powers the treadmill and triply redundant electrical isolation assures subject safety. The allowable ground resistance value for protection from the 480 V source is set at 10 W. Motor induced vibrations do not reach the treadmill force platform due to the distance from the drive pulley and because a flexible rubber coupling at the motor-end of the flexible shaft attenuates vibrations. Flexible shaft alignment is accomplished at the motor-end by a delron clamp that is affixed to the base of the motor platform. The flexible shaft is mated to the treadmill at the drive pulley through a gearbox that provides a 2:1 gear reduction.

Treadmill speed remains constant at foot strike due to the gearbox and the heavy stainless steel pulleys. The drive pulley and idler pulley drums are solid and act as flywheels which in turn assure constant treadmill speed throughout the entire foot strike. Two treadmill handrails are available at the subject's request, and at least one handrail is affixed to the treadmill at all times to assure subject safety. Table 4.3 shows a parts list for the submersible treadmill and the next Section details the treadmill force platform.

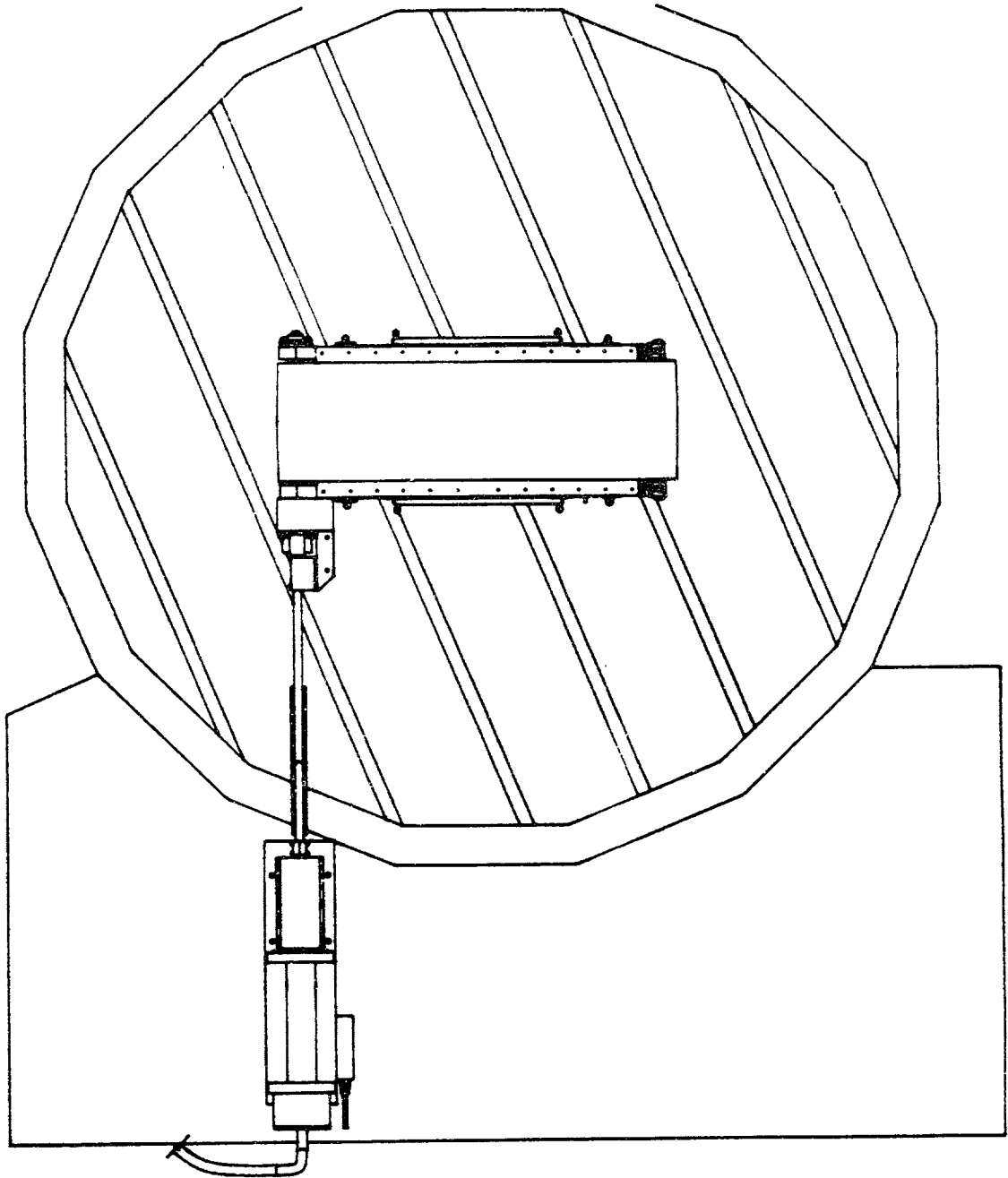


Figure 4.2 Submersible treadmill in Neutral Buoyancy Test Facility (NBTF) located at NASA Ames Research Center (ARC), Moffett Field, California. The NBTF is a cylindrical tank that is 9 feet deep and 11 feet in diameter. The 3 hp, 480 Volt, 3 phase motor is mounted on an elevated platform and connected to the submersible treadmill by a 5 meter flexible stainless steel shaft.

Treadmill-Mounted Force Platform

The treadmill is equipped with a force platform in order to provide ground reaction force measurements from which gait can be determined. In typical laboratory walkway experiments, where subjects pass over a force platform as they progress, measurements are time consuming to gather and difficult to reproduce. In this design these limitations are overcome by mounting a force platform directly under the belt of the motorized submersible treadmill. The design allows for an unlimited number of force measurements over a full range of steady speeds. Design guidelines came from personal communication and two documented treadmill-mounted force platforms [Kram and Powell, 1989; Thornton, 1990].

The force platform consists of base frame supports, 4 water resistant load cells with mounting supports¹, and a suspended split-plate underlying the treadmill belt. The upper surface of the force platform incorporates a split-plate design in order to collect force traces for both walking and running gaits which is an enhancement over single plate treadmill-mounted force platforms that only allow for the analysis of running. This novel design offers flexibility because the four load cells can be located in any of eight positions (See Figure 4.3 A) Topview.) Force traces for running or loping are easy to analyze because only one foot makes contact with the ground at a time. However, during walking the dual contact phase when both feet are in contact with the ground requires the force traces to be differentiated between left and right foot. This is accomplished by the split-plate design which allows all four load cells to be placed under either the left or right half of the treadmill. Each load cell requires a 5 Volt DC input, and its output signal is amplified and transmitted to a microcomputer for recording and analysis. See Figure 4.3 for a CAD drawing of the submersible treadmill.

An ultra-smooth surface (coefficient of friction < 0.12) covers the upper split-plate of the force platform to minimize any frictional forces, or cross-talk, between the platform and the treadmill belt. This low friction surface is flush with the treadmill frame so no erroneous vertical forces are exerted on the force platform by the treadmill belt. If the top surface of the force platform were higher than the treadmill frame, additional vertical forces would be measured due to the treadmill belt exerting a downward force on the force platform. If the force platform surface were lower than the treadmill frame, the vertical force exerted on the force platform would be erroneously reduced.

A test was performed in order to verify that frictional forces were not causing inaccurate vertical force signals. A human subject stood stationary on the treadmill and force output was recorded.

¹ Water resistant load cells, Wagezelle™, HBM, Inc., Marlboro, MA.

Similar measurements were taken for a moving treadmill belt; the subject remained on the treadmill without translating by wearing roller-skates. The roller-skate wheels created localized friction between the treadmill belt and the smooth surface of the force plate. There is no significant difference ($p < 0.05$) in vertical force signal output for the stationary or moving treadmill belt conditions, thus cross-talk is minimized.

A 1.12 m (3.67 ft) force platform assures that vertical force traces are recorded the entire time the foot is in contact with the treadmill belt; this is true for all gaits. Kram and Powell [1989] refer to a contact distance, D_c , parameter for sizing force platforms. Contact distance is a function of single foot contact distance and a velocity dependent term. Equations 4.1 and 4.2 are taken from Kram and Powell [1989] and reveal D_c for human walking and running, respectively.

$$D_{c \text{ walk}} = 0.665 + 0.25 \cdot v \quad (4.1)$$

$$D_{c \text{ run}} = 0.530 + 0.095 \cdot v \quad (4.2)$$

where v is the velocity of locomotion in m/s. Using these equations, the 1.48 m (4.86 ft) submersible treadmill which incorporates a 1.12 m force plate is designed for terrestrial walking speeds close to 2 m/s and running speeds up to 6.2 m/s.

All test equipment was calibrated and treadmill frequency response and force platform nonlinearities were measured before experimentation commenced. The natural frequency of the treadmill was measured by quickly rapping the belt with a hammer and collecting the ground reactions at 10 kHz. The natural frequency of the force platform is well above the frequency band of the force trace signal. The first resonance is extremely well damped and attenuated, and appears at a frequency over 60 Hz, while the energy of the vertical force signals, identified using a fast Fourier transform, is concentrated below 5 Hz. Static linearity was measured by applying known loads from 0 N to 981 N (0 to 100 kg) on the surface of the treadmill and measuring the load cell output. The curve fit for applied load versus force output is linear, deviating less than 0.2%. Figure 4.4 shows the linear vertical force calibration for the treadmill-equipped force platform.

Table 4.3. Submersible Treadmill Parts List.

Part	Quantity	Description
Treadmill Frame		Aluminum 6061-T5 (hard anodized), 2in. x 5in. x 1/8in. Rectangular Tube
Crossbars		Aluminum 6061-T5 (hard anodized), 2in. x 4in. x 1/8in. Rectangular Tube
Bearings	4	Pillow blocks, UHM plastic, ultra D paramount
Seamless Belt	~ 10.83 ft.	Water immersible treadmill belt, L10M, 18in. width, green, 2-ply.
Crowned Stainless Pulley (Drive)		5in. diameter, 18in. long (face width) with shafts that are 1in. diameter (non-removable) and 4in. and 6in. long; stainless steel spray friction coating.
Crowned Stainless Pulley (Idler)		5in. diameter, 18in. long (face width) with shafts that are 1in. diameter and both 4in. long
Screws & Mounts	2	Screws for Idler Pulley take-up
Handrails	2	Stainless steel bent tubing approx. 3 ft. high, pin connection (removable)
Removable Feet	6 pair	Stainless steel, Adjust treadmill front-end height by 0, 5, 10, 15, and 20 degrees.
Split-plate Force Platform		
Top Plate	2	Aluminum 6061-T5 (hard anodized), 1/4in. plate, 9 1/2 in. x 43in.
Bottom Frame		Aluminum 6061-T5 (hard anodized), 2in. x 5in. x 1/8in. Rectangular Tube,
Low Friction Surface	1/8in..	Nylatron GS sheet to provide low friction between force platform and treadmill
Load Cells	4	Wagezelle™ C2/100 kilogram load cells with 15 ft. cables for static and dynamic compressive loads, stainless steel, waterproof
Load Cell Supports	4	EPO3/200 kilogram pendle bearing support for use with C2 load cells.
Amplifier for load cells		IG 2612-K4 amplifier with four channels to allow individual O/P of (0-10V dc) for each load cell, calibrated by manufacturer.
Electric Motor/Control Station System [Motion Industries, Inc., Tracy, CA]		
Eaton Eddy Current Drive		
Chassis Control		
Process Control Speed Indicator w/ Digital Readout		
NEMA size O magnetic starter with 115 V coil and thermal overloads		
KVA transformer with fused 460 V primary, 115 V secondary		
One control relay and base		
Red Pilot light "off"		
Green Pilot light "on"		
Control speed potentiometer with legend		
Start push button		
Mushroom head stop kill button		

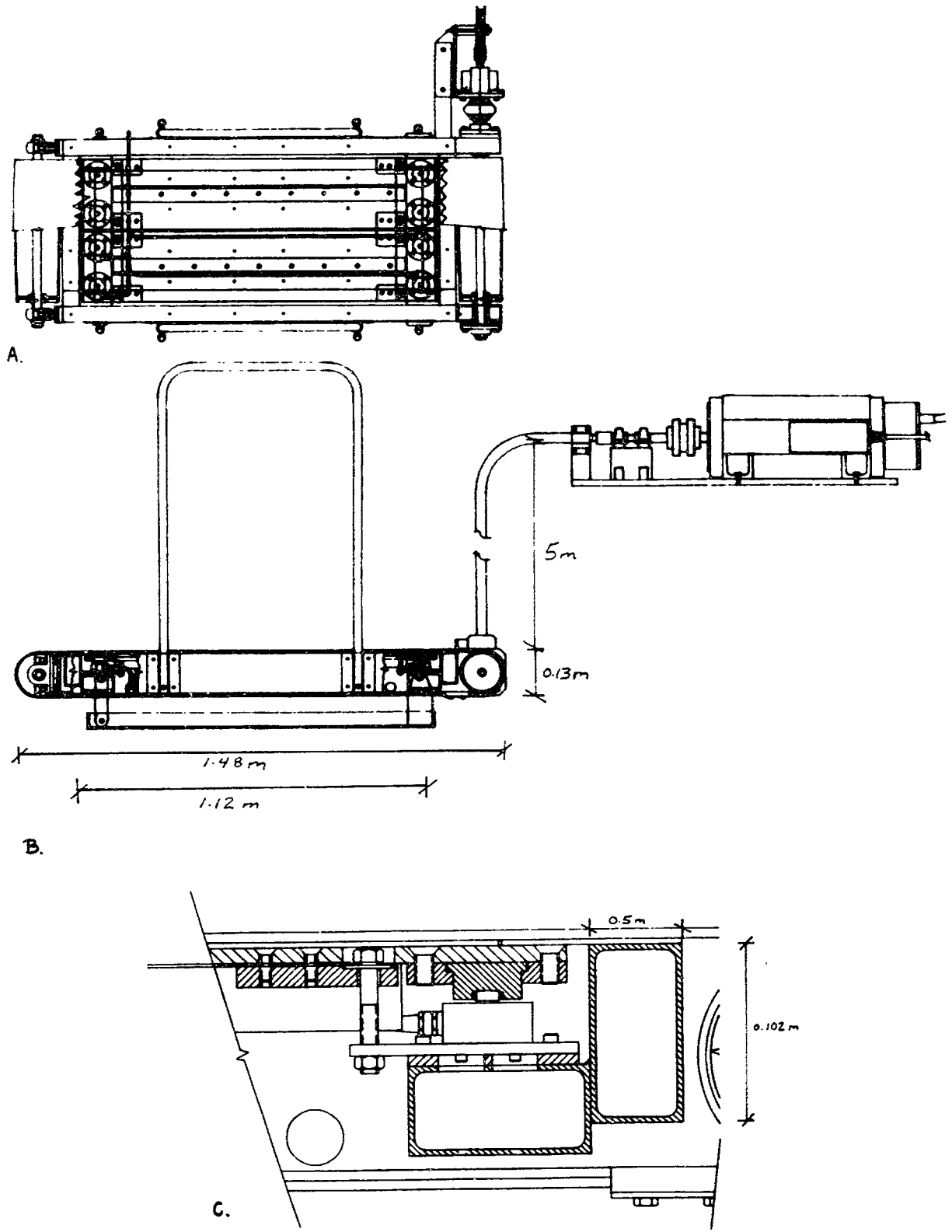


Figure 4.3 Submersible treadmill-mounted force platform design for partial gravity simulation. A) Topview B) Sideview and C) Load cell close-up.

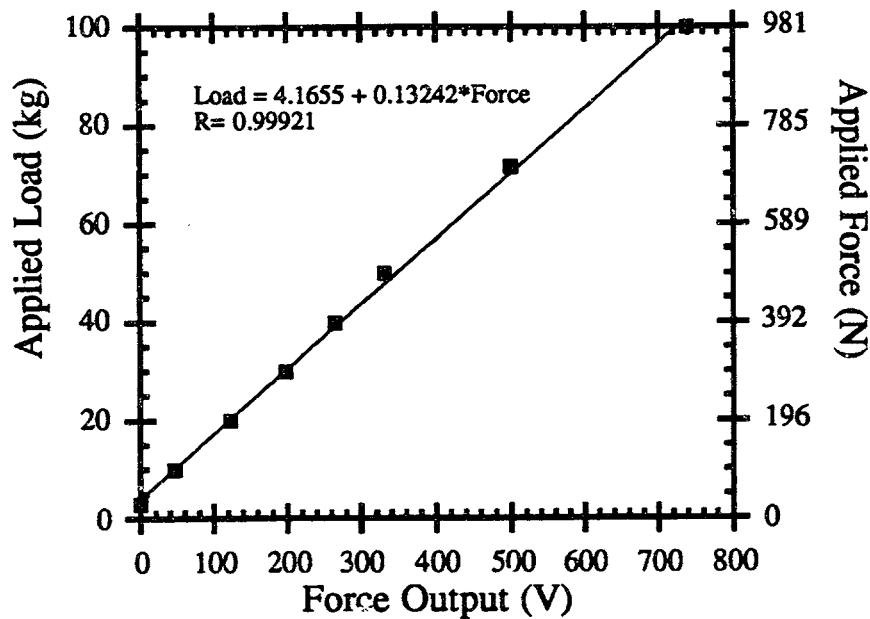


Figure 4.4 Submersible treadmill force plate vertical force calibration. The force platform shows a linear output response to applied load.

4.3.1.2 Video Recordings

Quantifying human biomechanics and gait for this partial gravity study has applications in future human space missions as well as in clinical rehabilitation and sports biomechanics. The treadmill-mounted force platform previously described provides real-time data gathering, but another method to quantify human movement is to use video cameras. Typically, locomotion is filmed and then the video data is hand digitized using a computer interface [Lombrozo *et al.*, 1988]. For this study, video data is recorded on a VHS camcorder during the underwater and parabolic flight partial gravity experiments.

Time histories of the lower limbs are a necessary input to the model (See Section 3.2 Hydrodynamic Modeling). The filmed locomotion data is hand digitized at the rate of 30 frames per second. For each frame, three leg points are digitized: the ankle, the knee, and the hip. The video data is two dimensional because the small size of the NBTF limits data acquisition to a single camera located outside of the tank windows. During the KC-135 experiments, the film captures a two dimensional view of the subject's entire body on the treadmill. Video film is downloaded using equipment at the MIT Media Laboratory and then a computer program written in the C

computer language helps to finalize the digitizing effort. The understanding of biomechanics is enhanced by recording the associated energy costs for partial gravity locomotion and the energetics equipment and measurements are described in the following Section.

4.3.1.3 Energetics Equipment

Subjects performing the underwater experiments were outfitted with a commercial diving mask² and surface air was supplied through an umbilical hose and a demand breathing regulator. Figure 4.5 shows the diving mask. Subjects were not outfitted with a spacesuit because emphasis was placed on unencumbered performance rather than the hardware design or degree to which the pressure suit and gloves affect performance. The experimental protocol called for steady-state workload measurements, thus, gas samples were continuously collected and monitored throughout the experimental session and once the oxygen concentration was seen to plateau flow rate was sampled. This procedure was followed while subjects exercise at each of the treadmill speeds.

Gas analysis equipment³ is used for measuring oxygen and carbon dioxide concentrations and is illustrated in Figure 4.6. Gas samples are routed via a Tygon sample line from the facemask to the analyzers. Oxygen concentration is continuously monitored and displayed on the control unit with an accuracy of $\pm 0.01\%$. Carbon dioxide (CO_2) is measured by the analyzer at an accuracy of $\pm 0.02\%$. The CO_2 sensor utilizes a thermal infrared source, optical filters, and a preamplifier. Table 4.4 lists the gas analysis system components.

A subject's expired air passes through a turbine flow meter⁴ before being vented to the surface. The flow meter is encased in a waterproof housing and attached to the diving mask (Refer to Figure 4.5). Flow is proportional to the volume pulse frequency of the turbine. The specifications of the flow meter state that 1% accuracy is maintained during measurements, however, calibration of the flow meter in the underwater configuration revealed errors to 15%. Errors for flow measurements encountered during the experimental protocol are typically between 5-12%. Coupling flow rate and gas concentrations, oxygen uptake, \dot{V}_{O_2} (volumetric rate of oxygen consumption), and rate of carbon dioxide production, \dot{V}_{CO_2} , are calculated according to Equations 4.3-4.5. Standard room air is assumed to contain 20.94% O_2 and 0.04% CO_2 .

$$20.94\% \text{ O}_2 \text{ air} - \% \text{ O}_2 \text{ measured} = \% \text{ O}_2 \text{ consumed} \quad (4.3)$$

² EOX-26 Commercial diving bandmask, Diving Systems International, Santa Barbara, CA.

³ Ametek™ gas analysis equipment, Pittsburgh, PA.

⁴ Turbine flow meter, KL Engineering, Sylmar, CA.

$$\dot{V}_{O_2} \text{ (lpm)} = [\% O_2 \text{ consumed} / 100] \times \text{Flow Rate (lpm)} \quad (4.4)$$

$$\dot{V}_{CO_2} \text{ (lpm)} = [\% CO_2 \text{ measured} - 0.04 \% CO_2 \text{ air}] / 100 \times \text{Flow Rate (lpm)} \quad (4.5)$$

From onset of activity the rate of oxygen consumption increases to a steady-state level. A sluggishness in the respiratory/circulatory systems reflects a start up adjustment time for the oxygen-transporting systems, and physiological measures reach steady-state levels one to two minutes into the exercise. Steady-state flow rates are sampled between the fourth and fifth minute of exercise to guarantee that the oxygen consumption measurement corresponds to a workload situation where oxygen uptake equals the oxygen requirement of the tissues. A 27 second lag time exists during initiation of exercise for the sampled gas concentrations to reach the gas analysis equipment due to the 6 m long sample line from the submerged subject to the analyzers.

Table 4.4 Gas Analysis Equipment.

Description	Model
Oxygen analyzer	S-3A
Single-cell zirconia sensor	N-22M
Flow control unit	R-1
Carbon dioxide analyzer	CD-3A
Sensor	P-61B
Turbine Flow Transducer	K-520, 60 mA
Kozak Turbine Interface	KTC-3-D

Heart rate is taken as a secondary measure of workload during the underwater locomotion experiments. An underwater wireless exercise computer that senses the electrical signals generated by the heart in the same manner as an electrocardiogram (ECG) was used to measure heart rate in beats per minute⁵, however, no intrusive wires were attached to the subject's body. A comfortable rubber belt with sealed electrodes is strapped around the subject's chest. The receiver is affixed to the ballasting harness and heart rate measurements are stored in memory during the experiment and later downloaded to a computer for analysis.

⁵ Heart Monitor, UNIQTTM CIC Heartwatch, Swimmer's model 8799, Hempstead, NY.

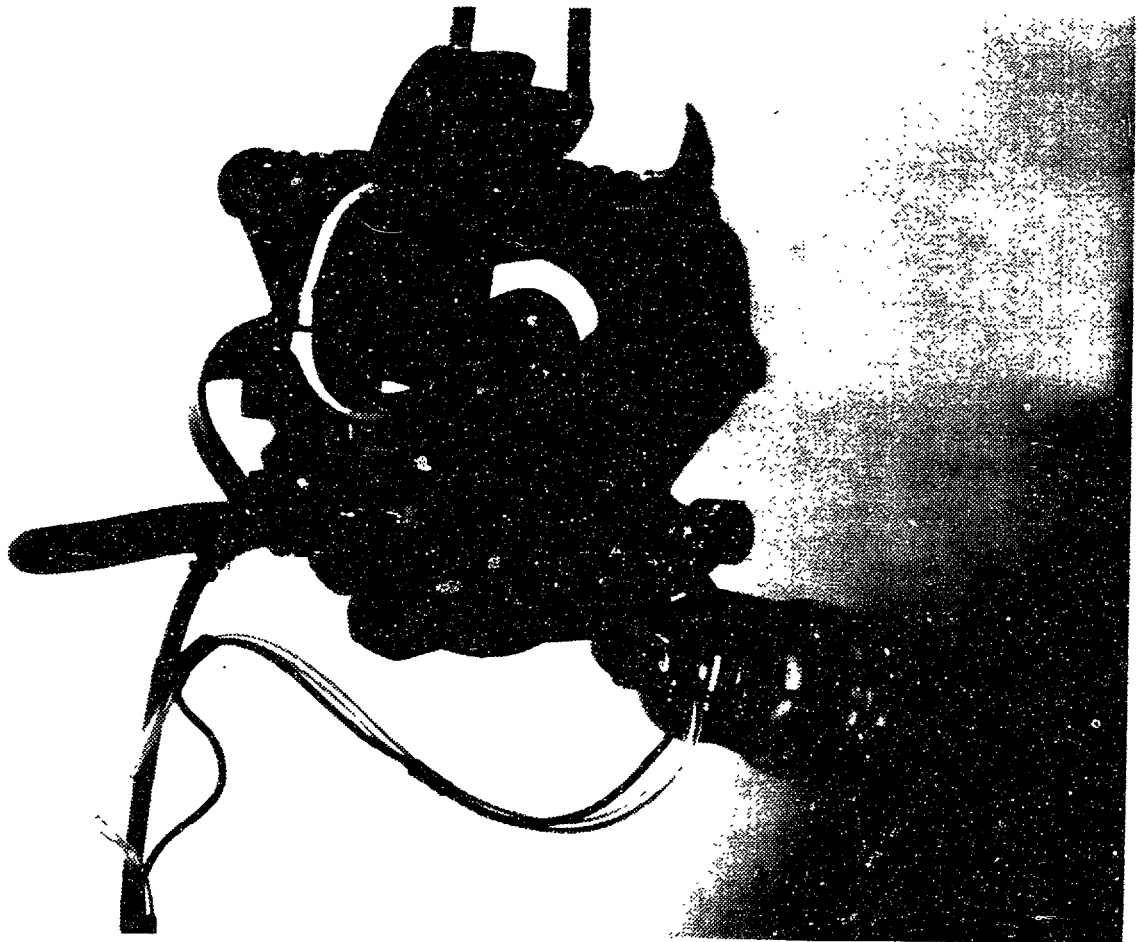


Figure 4.5 Commercial diving band mask used in the underwater experiments. Oxygen uptake measurements rely on gas concentrations from the subject's expired air sampled through the Tygon sample line and expired air flow rate measurements from the flow meter affixed to the mask. Subjects have two-way communication with the test director at all times.

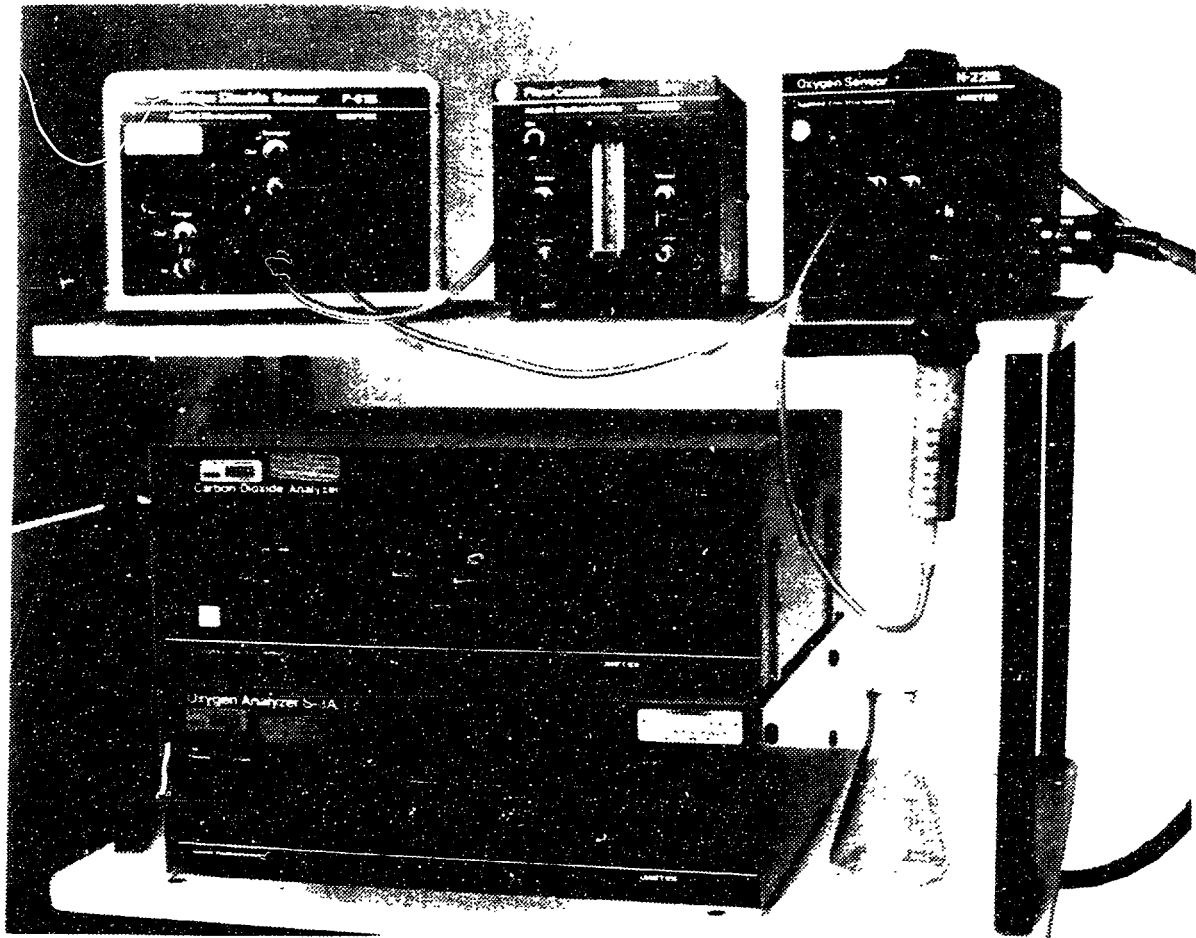


Figure 4.6 Gas analysis equipment used for steady-state workload measurements during the partial gravity underwater locomotion experiments.

4.3.2 Parabolic Flight Pilot Equipment

Lunar and Martian gravity levels were flown during parabolic flight on NASA's KC-135 aircraft, and data from this pilot study complements the full range of partial gravity experiments conducted on the submersible treadmill in the NBTF at NASA ARC. It is not possible to collect steady-state oxygen consumption measurements during parabolic flight due to the time limitation of each parabola. An instrumented treadmill was borrowed from the Anthropometry and Biomechanics Laboratory (ABL) at NASA JSC in order to collect biomechanics data during the parabolic flights (See Figure 4.7). The commercial Del-Mar Avionics treadmill is described below. Two video cameras were flown, one to record video images of subjects on the treadmill and the other to record the consistency of the gravity level throughout each parabola.

Del-Mar Avionics Treadmill [Thornton et al., 1990]

The specifications reported herein for the Del-Mar Avionics treadmill are taken from a NASA JSC technical report [Thornton et al., 1990]. The Del-Mar treadmill is instrumented with four beam load cells to measure vertical foot reaction forces during locomotion. Each rectangular load cell is "bolted to the treadmill frame at one end of the cell with the force application point from the platform supporting the tread belt at the other end." These load cells are located near the four corners of the running surface, therefore, only running gaits can be analyzed for all of the biomechanical measurements mentioned previously (i.e., peak force, stride length, contact time, and aerial phase). Recall that during walking there is a dual stance phase in which both feet are on the ground so force traces from both feet are recorded and independent measures of heel contact and toe-off for the right foot and left foot can not be differentiated with this type of instrumented treadmill system. However, peak forces can be measured for all gaits with this treadmill.

The Del-Mar treadmill was calibrated the week before the initial Martian parabolic flight and exhibited excellent linear response (See Figure 4.8). Static linearity of the treadmill was measured using weights known to within 1% of their weight. Frequency response tests show that the instrumented Del-Mar treadmill acts as a simple spring-mass-damper system with an unloaded resonance of approximately 80 Hz, which is shifted to 40 Hz by a fixed mass of 70 kg [Thornton, 1990, pg. 2]. Using the same argument as for the submersible treadmill, the natural frequency of the force platform is well above the frequency band of a force trace signal. The energy of the vertical force signals can be conservatively assumed to always be below 30 Hz. However, precise measurements of transients which occur above 30 Hz may not be possible.

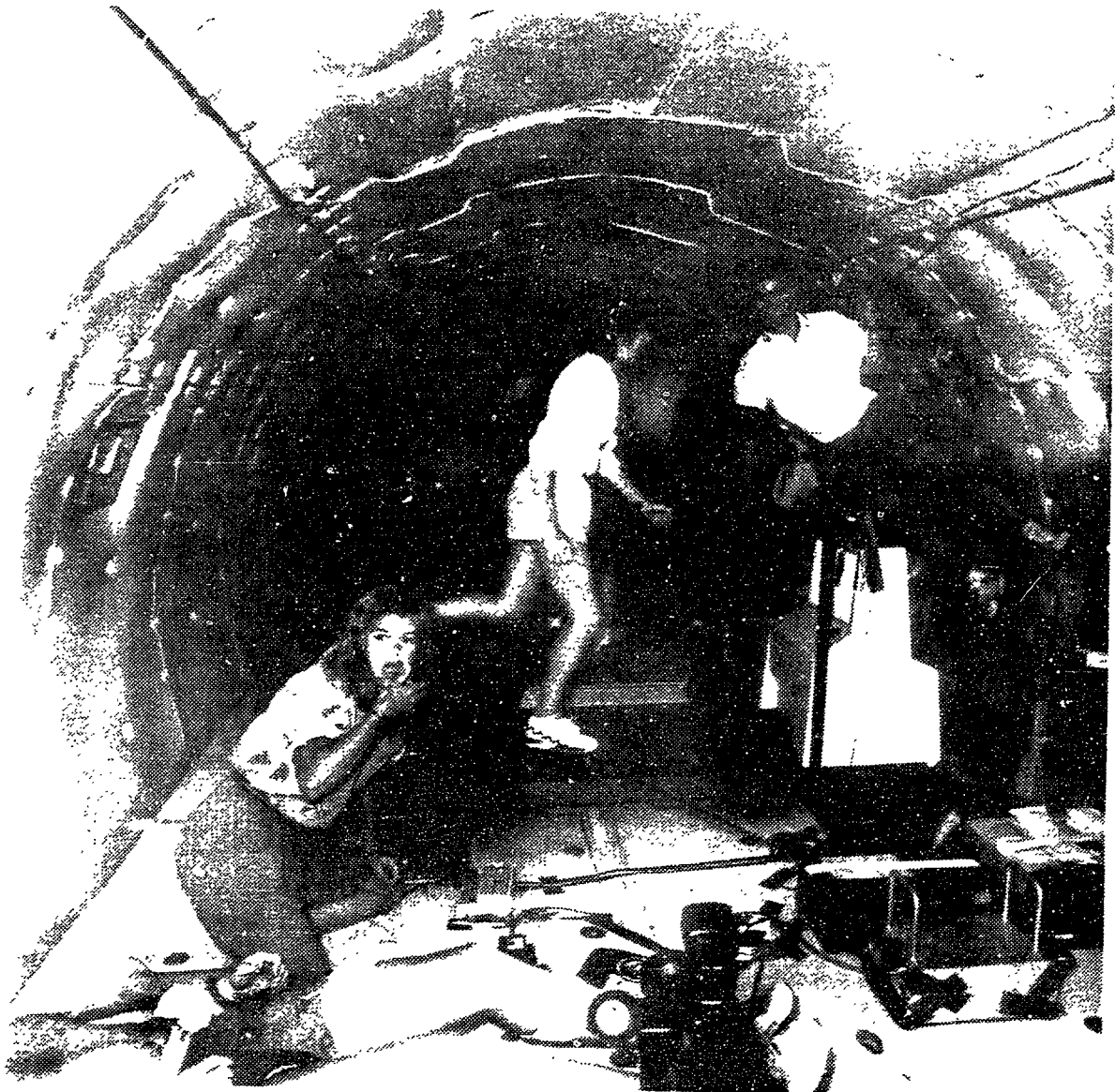


Figure 4.7 Astronaut N. Sherlock during Martian parabolic flight on the Del-Mar treadmill.

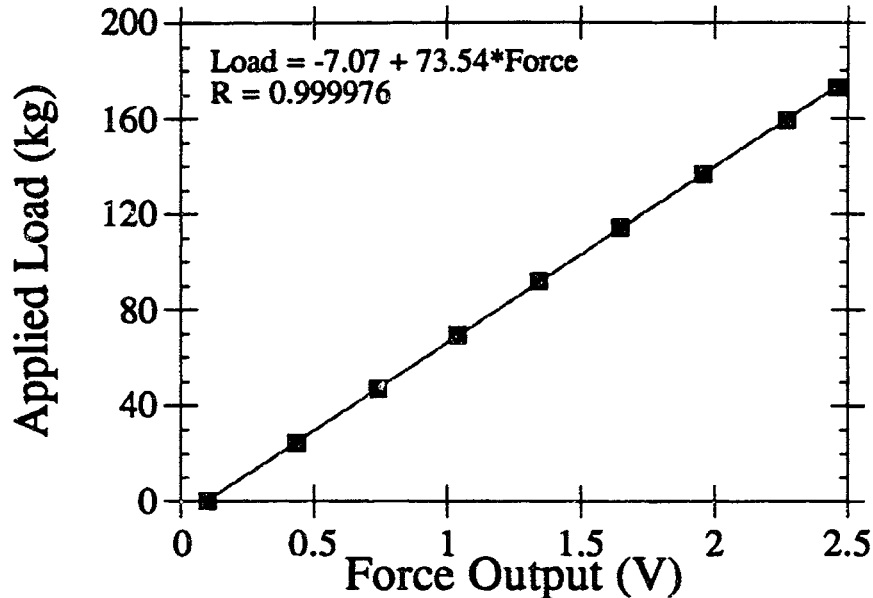


Figure 4.8 NASA Johnson Space Center's Del-Mar instrumented treadmill force calibration. The force platform shows a linear output response to applied load.

4.3.3 Data Acquisition and Analysis

For the underwater partial gravity experiments, vertical ground reaction forces are sampled at 1 kHz for each treadmill speed during each session while oxygen and carbon dioxide levels are continuously sampled at 0.1 Hz. For the parabolic flight experiments, vertical ground reaction forces are sampled at 250 Hz from the Del-Mar treadmill and recorded on a TEAC data acquisition system (shown in Figure 4.9) along with treadmill velocity. A microcomputer, computer programs for data acquisition, and a data acquisition board are used to record the raw force data⁶. All force data are low-pass filtered using a second order Butterworth filter with a corner frequency of 60 Hz, and then vertical ground reaction force profiles, $f(t)$, are averaged over stride cycles. Figure 4.10 illustrates the front panel of the icon level computer program, named Treadmill, written for force trace and gas analysis data acquisition.

Gait analysis is calculated from the force traces. This biomechanics analysis includes peak force, stride frequency, contact time t_c (the duration the support foot is in contact with the ground), aerial time t_a , and the angle of excursion of the limbs (Θ) measurements. Vertical velocity, $v(t)$, is

⁶ Macintosh IIfx microcomputer, Apple, Inc., Cupertino, CA; LabView 2™, National Instruments, Austin, TX; MacAdios II A/D board, GW Instruments, Inc., Somerville, MA.

calculated by integrating the force profile over the stride cycle; the mean vertical velocity for a stride cycle is equal to zero. The displacement of the center of mass, $y(t)$, during foot contact is taken as the double integral of the force profile. Data analysis is performed using programs written for time series and graphing software⁷. The measurements alluded to herein are presented in Chapter 5 Results and Discussion.

The statistical analysis of the experimental partial gravity locomotion data includes basic statistics, analysis of variance, and Student's t tests. Table 4.5 shows an example of basic statistical calculations for lunar gravity peak force data for six subjects when the treadmill velocity is 0.5 m/s. Analysis of variance and paired Student's t test calculations assess statistical significance and are acknowledged when used in Chapter 5 Results and Discussion.

Table 4.5 Basic Statistical Calculations for a Lunar Gravity Simulation.

F _{max} (N) V=0.5 m/s			
Minimum	256	RMS	386.44793
Maximum	495	Std Deviation	86.296388
Sum	2270	Variance	7447.0667
Points	6	Std Error	35.230353
Mean	378	Skewness	0.034503892
Median	364	Kurtosis	-1.0614767

⁷ Matlab™ software, The MathWorks, Inc., South Natick, MA; Kaleidagraph™ software, Synergy Software, Reading, PA.

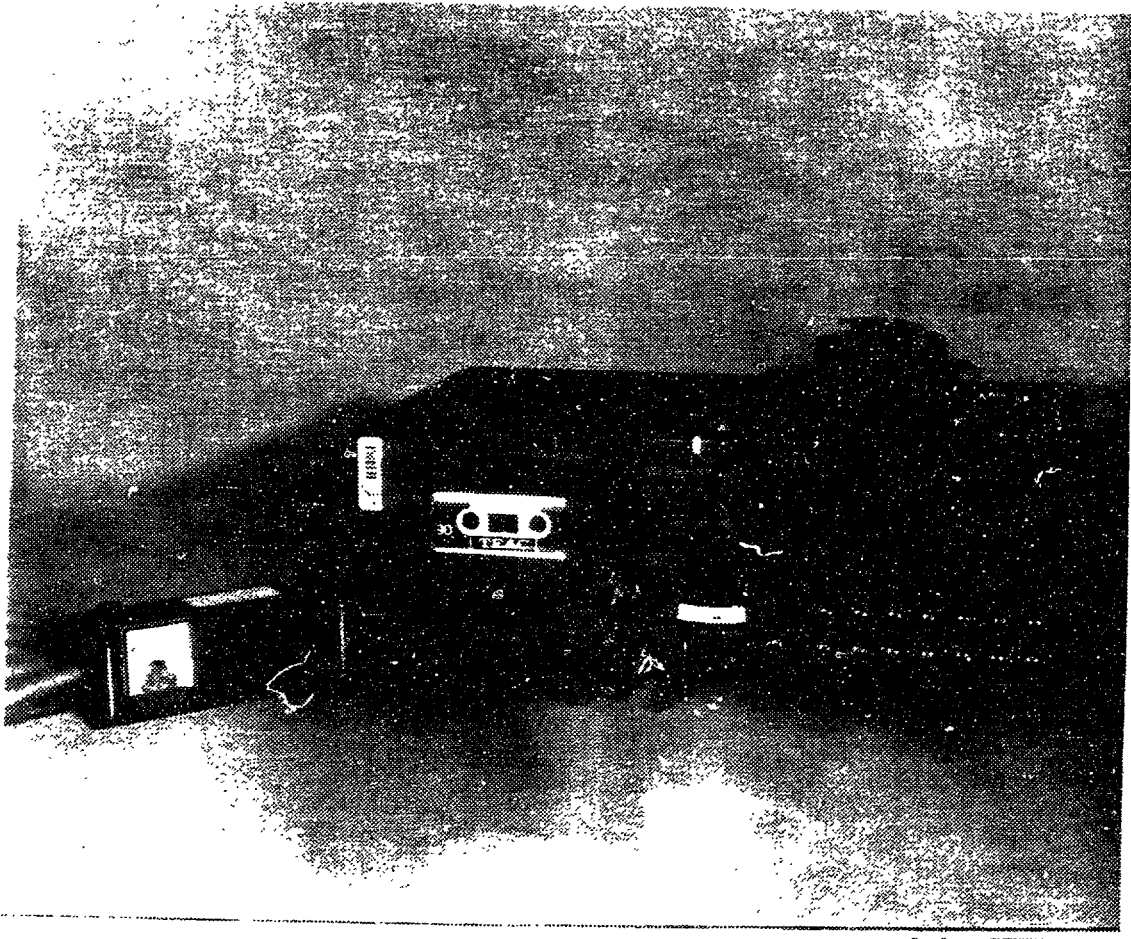
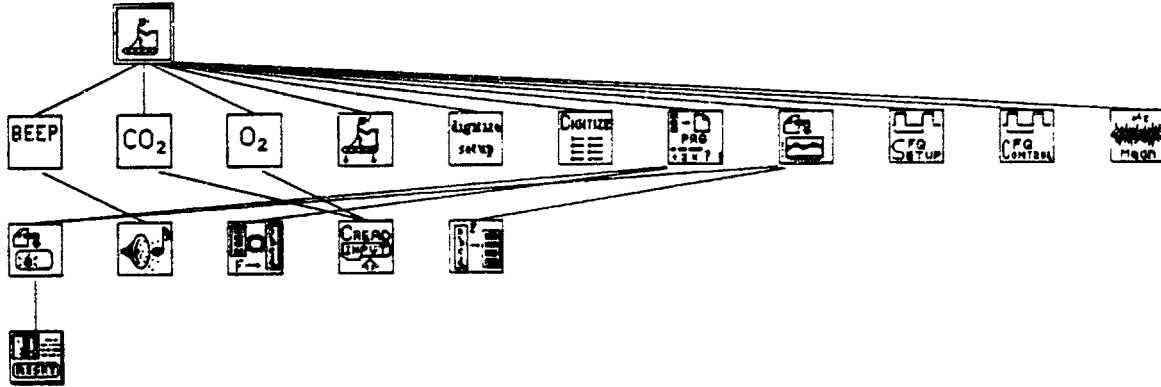


Figure 4.9 Data collection on the KC-135 using a TEAC recorder to measure force and velocity. The analog biomechanics signals are sampled at 250 Hz.

Position in hierarchy



Connector Pane



Front Panel

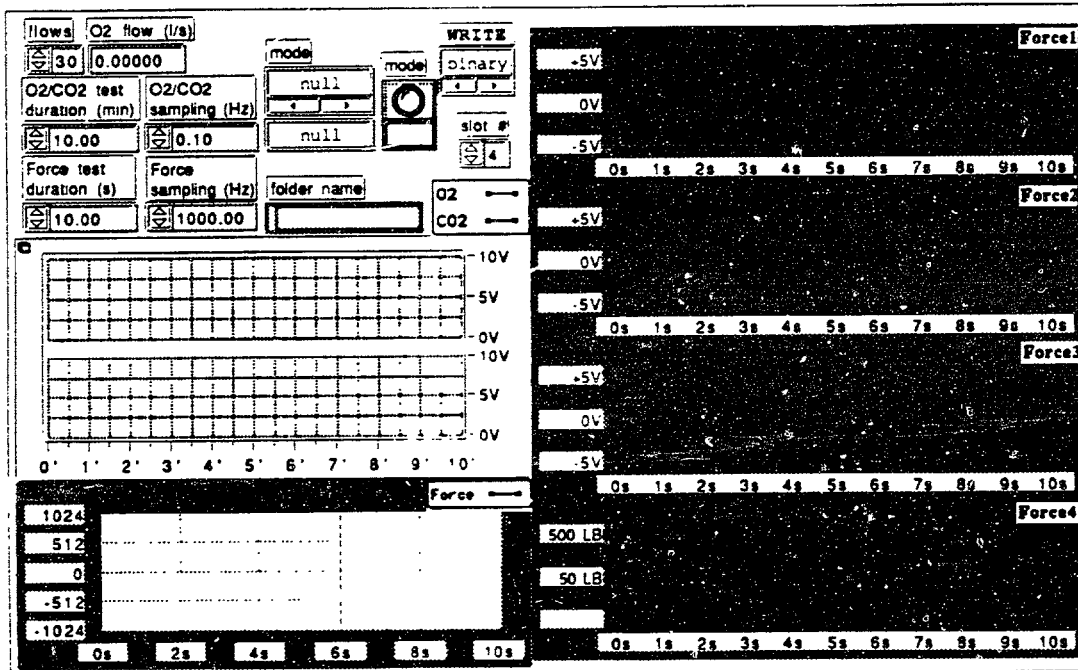
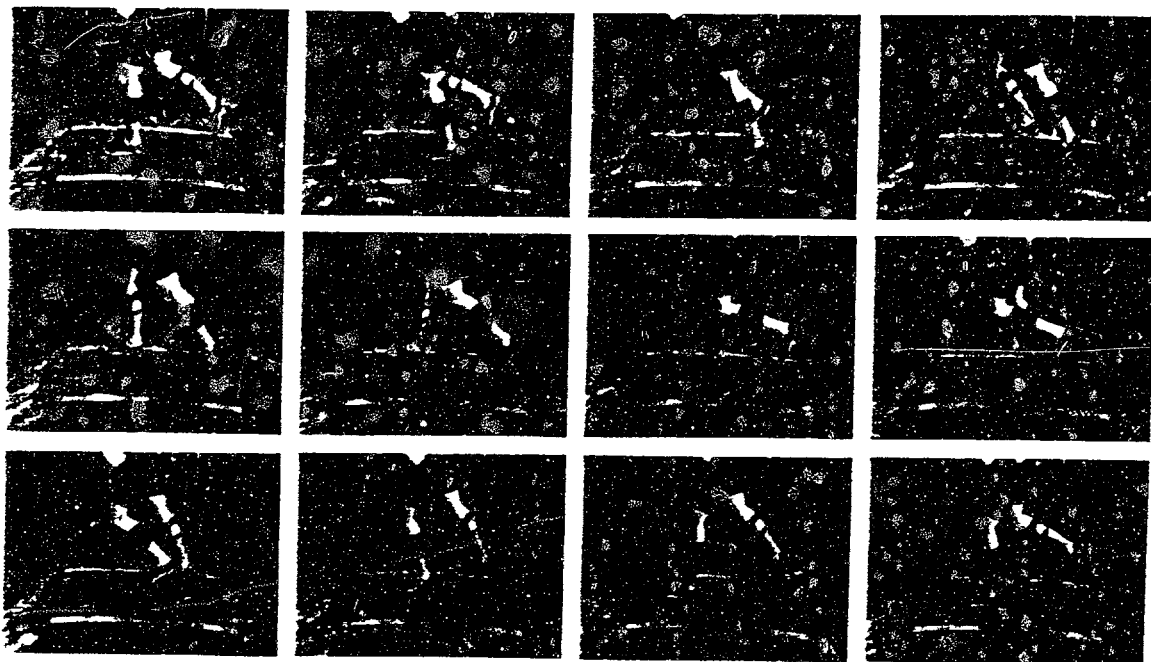


Figure 4.10 Data acquisition computer program front panel. Program combines both analog and digital biomechanics and energetic signals. Four analog signals from the treadmill force plate are sampled at 1 kHz, two analog signals of gas concentration are sampled at 0.1 Hz, and a digital pulse frequency of flow rate is sampled.

V. RESULTS AND DISCUSSION



*If the doors of perception were cleansed,
everything would appear as it is, infinite.*
- William Blake (1810), A Vision of the Last Judgment

*Joy lies in the fight, in the attempt, in the suffering involved,
not in the victory itself.*
- Gandhi

CHAPTER V. RESULTS AND DISCUSSION

This Chapter presents and discusses the experimental results of the partial gravity human locomotion study. Section 5.1.1, Biomechanics, presents results of the underwater experiments and parabolic flight experiments. Section 5.1.2, Energetics, reveals the energy expenditures associated with partial gravity locomotion. The first half of this Chapter offers a comprehensive report of experimental findings and the second half provides a discussion of the partial gravity locomotion study. Section 5.2, Discussion, addresses the shortcomings of the experimental techniques; introduces a theoretical model of running which enhances the interpretation of biomechanics results and verifies the simulation techniques; and compares metabolic expenditure results to results from a third simulation technique.

5.1 RESULTS

Experimental results from two partial gravity simulation techniques, underwater submersion and parabolic flight, are detailed in this Section. The water immersion partial gravity simulation technique provides biomechanics and steady-state workload measurements for locomotion in altered gravity environments. Unlike mechanical simulators, water immersion permits subjects to operate with six degrees of freedom unrestricted by attachment cables, springs, or yokes. Immersion also offers total body support and ensures task continuity. The hydrodynamic model of Section 3.2 shows that limb drag is negligible because it comprises less than three percent (< 3 %) of the total measured metabolic cost. The parabolic flight experiments complement the submersion experiments by offering a realistic simulation technique for lunar and Martian gravity environments. Whenever possible, the experimental results of both techniques are compared to published data from other partial gravity investigations.

The literature reviews in the Introduction predict changes in biomechanics and workload during partial gravity locomotion. Previous biomechanics research suggests that vertical force, stride frequency, contact time, vertical landing velocity, and limb angle tend to decrease for locomotion in partial gravity [He *et al.*, 1991; Hewes, 1969; Seminara and Shavelson, 1969; Hewes and Spady, 1964]. He *et al.* report an increase in vertical stiffness and stride length during partial gravity simulation [1991], and the study by Seminara and Shavelson supports the stride length finding [1969]. Results of the energetics measurements are expected to decrease as gravity level decreases. However, the literature reports conflicting trends for workload measures in partial gravity. Workload may not decrease as a linear function from 1 g to 0 g; rather a *gravity threshold* (or optimum gravity level) may exist where workload increases on both sides of this postulated

optimum. A study by Trout [1967] supports this notion and reports that optimal performance occurs at 1/12 g implying that some level of gravity is helpful for locomotion.

5.1.1 Biomechanics

The biomechanics measurements are derived from ground reaction force profiles, $f(t)$, over a stride cycle. Peak force, stride frequency, stride length, contact time, and aerial time are all biomechanics measures obtained from force profiles. An integration of the force profile yields vertical velocity, $v(t)$, with mean vertical velocity equal to zero for a complete stride cycle. The displacement of the center of mass, $y(t)$, during foot contact is taken as the double integral of the force profile. The biomechanics measurements provide the necessary data for partial gravity gait analysis. Figure 5.1 illustrates a typical filtered force trace from the treadmill-mounted force platform. After the force trace is low-passed filtered, single and double integrations of the signal yield vertical velocity and vertical displacement of the center of mass during foot ground contact, respectively. The figure displays the vertical force trace for the duration the foot is in contact with the ground, and the vertical velocity and displacement for the entire stride cycle. A noticeable reduction in force is seen from 1 g to Martian gravity. The Martian stride extends for a longer time than the 1 g stride and vertical displacement is greater for the Martian simulation than for 1 g.

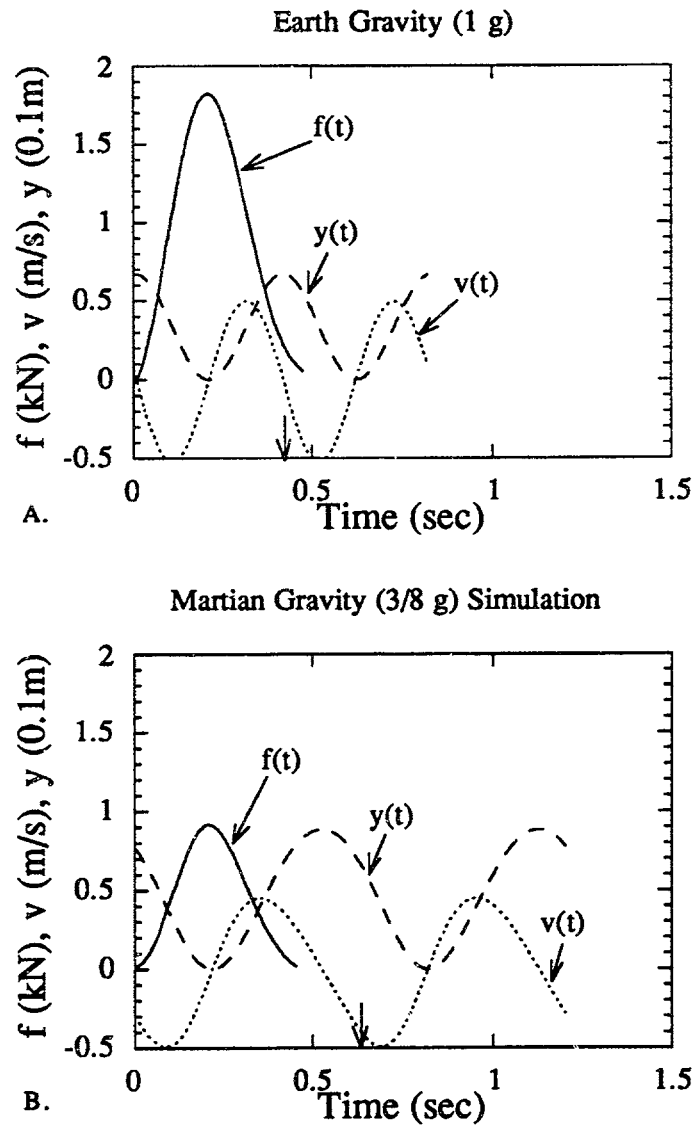


Figure 5.1 Typical traces for vertical ground reaction (f), vertical velocity (v), and vertical displacement (y) of the center of mass during foot contact for a subject traveling at 2.3 m/s plotted versus time. A) Earth gravity (1 g). B) Martian gravity (3/8 g) simulation results show a significant decrease in f , an extended stride time (e.g., 1.25 seconds), and an increase in y . Arrow shows the moment of contact of second foot and indicates an aerial phase for the Martian locomotion but not for terrestrial locomotion.

5.1.1.1 Underwater Locomotion Study

In order to further familiarize the reader with biomechanics nomenclature, an example illustrates the experimental biomechanics measurements. Recall, that the distance between foot prints of the same foot defines a single stride. In other words, a complete stride cycle includes ground contact with the right foot followed by an aerial phase (during running) then ground contact with the left foot and another aerial phase until the right contacts the ground again. Typical partial gravity force profiles (from Subject 1) show significant reductions ($p < 0.001$)* in peak force, f_{max} , when compared to 1 g data. The partial gravity peak forces for Subject 1 traveling at 2.3 m/s are 80%, 50%, and 26% of 1 g levels for two-thirds gravity (66% of 1 g), Martian gravity (38% of 1 g), and lunar gravity (16.7% of 1 g), respectively. There is no significant difference in t_c for various gravity levels. For locomotion at 1.5 m/s and 2.3 m/s, the time for a single stride, t_{stride} , increases as the gravity level decreases, thus, an increase in stride length and a decrease in stride frequency (strides/min) result from reductions in the gravitational acceleration.

Figure 5.2 shows an average stride cycle for Subject 1, and compares Martian gravity and lunar gravity with 1 g. The figure shows the airborne time, t_a , between toe-off of one foot and ground contact of the other foot for partial gravity locomotion, but there is no aerial phase for normal 1 g locomotion at 2.3 m/s. Low gravity levels change the mechanics of running and result in extended aerial phases. Subjects walk at 0.5 m/s and lope at 1.5 m/s and 2.3 m/s during lunar and Martian simulations. During the 2/3 g simulations, subjects walk at 0.5 m/s and 1.5 m/s and run at 2.3 m/s; and at 1 g, subjects walk at 0.5 m/s and 1.5 m/s and use slow jog without a significant aerial phase at 2.3 m/s.

* Convention for documenting statistically significant results is to show the confidence of the statistical measure. For example, published results must exhibit statistical significance greater than the 95th percentile, typically written $p < 0.05$. All results published in this thesis that claim statistical significance have a confidence interval greater than the 95th percentile.

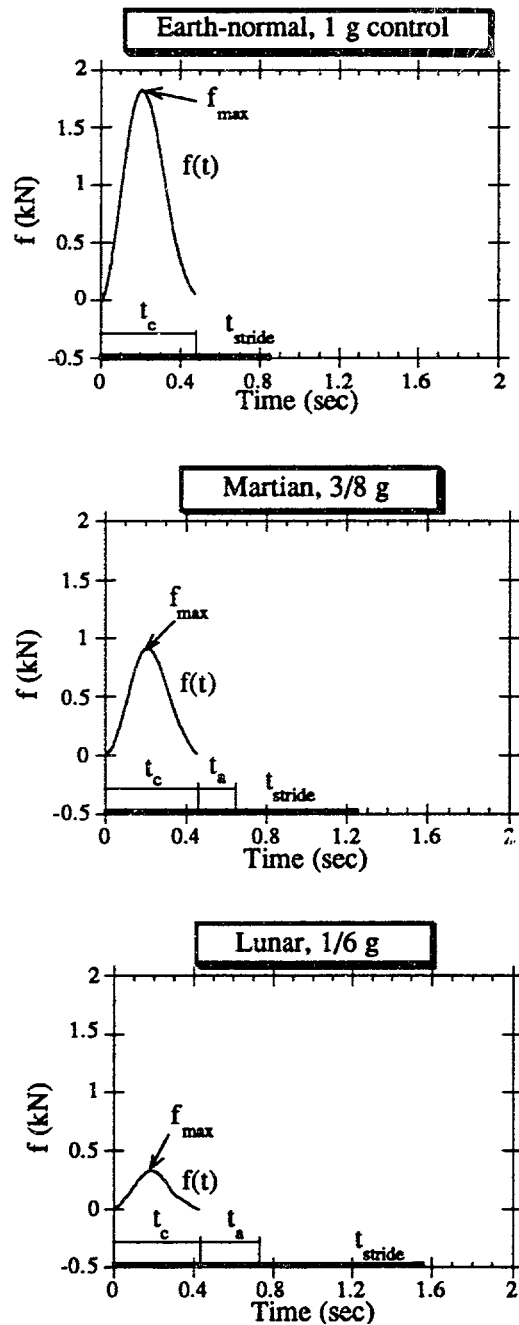


Figure 5.2 Biomechanics data of an average stride cycle (10 steps) for an individual subject on the submersible treadmill moving at 2.3 m/s. A comparison of partial gravity results with Earth gravity is shown. The data reveal a significant reduction ($p < 0.001$) in peak force, f_{max} , for a decrease in gravity level. There is a 50% reduction from 1 g to Martian gravity (3/8 g) and a 74% reduction in peak force from 1 g to lunar gravity (1/6 g). The contact time is the duration the support foot is in contact with the ground and is depicted by t_c . There is no significant difference in t_c for various gravity levels. The time for a single stride, t_{stride} , increases as the gravity level decreases, thus, a decrease in stride frequency (strides/min) is seen for a reduction in gravity level. A significant aerial time, t_a , (time between toe-off and ground contact of the opposite foot) exists for partial gravity locomotion whereas terrestrial locomotion elicits no significant aerial phase at this velocity.

5.1.1.1.1 Peak Force

The individual biomechanics measurements mentioned in the preceding example are discussed in detail in the following paragraphs. The data reveal significant nonlinear reductions in peak force ($p < 0.05$) with decreasing gravity level at all speeds. Figure 5.3 displays mean values of peak force for all six subjects. Figure 5.3 A) exclusively depicts partial gravity submersion experiments and Figure 5.3 B) plots 1 g control data along with the underwater data. A dimensionless force is attained by dividing the peak force by the subjects' weight ($m \cdot g$, where the gravitational constant is 9.8 m/s^2). Figure 5.4 A) and 5.4 B) show the mean value for the six subjects' normalized peak force versus four different simulated gravity levels for all three treadmill speeds. Figures 5.3 and 5.4 both show a significant reduction in partial gravity peak force and second and third order polynomials provide the best curve fits to the underwater force data, respectively. The literature review predicted this significant reduction in peak force, but the question remains (and is addressed further in Section 5.2 Discussion) as to the implications of these results for human performance on other celestial bodies.

Figure 5.5 further investigates the vertical force exerted on the ground by subjects ambulating in partial gravity. A second dimensionless force is attained by dividing peak force by the subjects' mass times the local gravitational acceleration ($m \cdot g_{\text{local}}$; for example, $g_{\text{local}} = 1.64 \text{ m/s}^2$ for the lunar environment). At 0.5 m/s there is a significant increase in dimensionless vertical force from 1 g to lunar gravity ($p < 0.001$) and from 9/10 g to lunar gravity ($p < 0.001$). There is no significant difference between the other gravity conditions. Locomotion at 1.5 m/s elicits a significant increase in dimensionless vertical force between Martian gravity and 1 g as well as between Lunar gravity and 1 g ($p < 0.05$). The same is true for locomotion at 2.3 m/s; dimensionless force (normalized by local gravitational acceleration) significantly increases for lunar and Martian gravity levels compared to 1 g levels ($p < 0.05$).

5.1.1.1.2 Stride Frequency and Contact Time

Stride frequency and contact time are two biomechanics measurements that determine gait. Reductions in stride frequency indicate a general trend toward loping as gravity level decreases from 1 g. For locomotion at 1.5 m/s and 2.3 m/s, the plot of average stride frequency versus gravity (Figure 5.6) depicts a linear reduction in stride frequency as gravity level decreases. Figure 5.6 A) shows a linear reduction in stride frequency as gravity decreases from 9/10 g to 1/6 g for the underwater locomotion experiments. Figure 5.6 B) adds results from the 1 g control session. A significant increase in stride frequency is seen for the 1 g case at all three treadmill velocities. This result makes sense in lieu of the different experimental environments.

The decrease in stride frequency for the underwater locomotion experiments is attributed to the added ballast on the subjects' bodies and the additional inertial effect of added mass to move the water column during locomotion. The underwater running experiments (characterized by the mass-spring model) yield damped oscillatory motions, whereas, the 1 g control experiments in air represent undamped harmonic motion. The natural frequency of a damped system is always less than that of an equivalent undamped system, therefore, the result of increased stride frequency for locomotion in air compared to underwater is explained by the inertial changes and the physics of harmonic motion.

Either an increase in stride length or an increase in the amount of time the foot is in contact with the ground would explain a decrease in stride frequency. Figure 5.7 shows no significant difference in foot contact time across simulated gravity levels, therefore, stride length must increase as gravity level is reduced.

Since the time available to apply muscular force to the ground during locomotion is constant across gravity levels, a reduction in metabolic costs for low gravity levels is anticipated because the results of Section 5.1.1.1.1, Peak Force, reveal that less muscular force is required for locomotion at reduced gravity levels. Section 5.1.2, Energetics, revisits this hypothesis and presents the energy expenditure data for partial gravity locomotion.

Figure 5.8 shows actual data from the Apollo 11 lunar mission. Stepping frequency is displayed for the Apollo 11 data, underwater simulated lunar gravity data, and 1 g data. There is scatter in the Apollo data, but the simulated lunar stepping rates are seen to correlate with the actual Apollo data. The stepping frequencies at 1 g are significantly higher than the lunar data at velocities of 1.5 m/s and 2.3 m/s ($p < 0.05$).

5.1.1.1.3 Aerial Time

The combination of decreases in stride frequency and constant values of contact time suggests an increase in aerial time for partial gravity locomotion. Figure 5.9 verifies an increase in aerial time at low gravity and illustrates the mean aerial phase for all six subjects during simulated partial gravity locomotion for all three treadmill velocities. A significantly extended aerial phase typifies loping in which subjects essentially propel themselves into an aerial trajectory for a few hundred milliseconds during the stride.

Results show no significant aerial phases during terrestrial 1 g locomotion for any of the treadmill speeds. Negative aerial times occur during walking (0.5 m/s) and categorize the dual stance phase.

During the stance phase of walking the second foot strikes the ground while the first foot is still on the ground (dual stance phase). The measurement between toe-off of the first foot and heel strike of the second foot has a negative value and can be thought of as the time during double foot contact.

Defining a locomotive index as the ratio of aerial time to duration of the stride cycle is useful to distinguish between walking and running. Walking elicits no aerial phase and has a locomotive index of zero, while running has a ratio greater than zero. To distinguish loping, a specific category of running, the additional qualification that the locomotive index exceed 0.20 is imposed. In other words, the subject is airborne for over one-fifth of the stride cycle. Terrestrial running at 3.0 m/s in 1 g (greater than all three treadmill velocities used in this experiment) elicits a locomotive index ratio less than 0.20, therefore, this value defines an altered gait, or a lope. Figure 5.10 shows gaits and locomotive indices for the partial gravity study. Walking is seen for a treadmill speed of 0.5 m/s. Subjects lope at lunar and Martian gravity levels when they move at 1.5 m/s and 2.3 m/s.

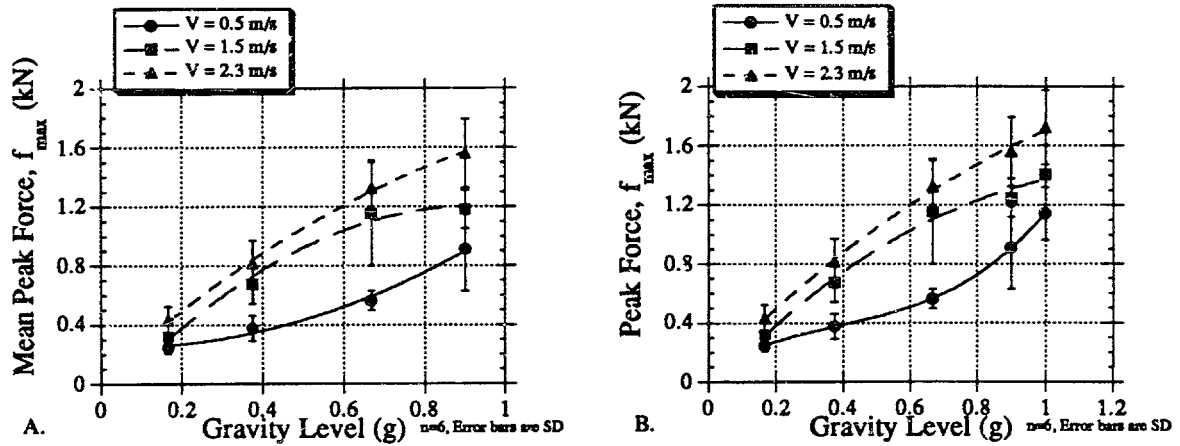


Figure 5.3 Mean peak force versus gravity level. Each point is the mean for all six subjects and the error bars are the standard deviations of the means. A) Results of underwater immersion experiments in which lunar (1/6 g), Martian (3/8 g), two-thirds (2/3 g), and close to Earth gravity (9/10 g) are simulated. A second order polynomial provides the best curve fit. Statistical comparisons using Student's t tests reveal a significant decrease ($p < 0.001$) in peak vertical force as gravity level is reduced from 9/10 g to lunar gravity (1/6 g). B) Data from the 1 g control session superimposed with the results from the underwater experiments. Data is fit with a third order polynomial. Experimental results show a significant decrease ($p < 0.001$) in peak vertical force as gravity level is reduced from 1 g to 1/6 g.

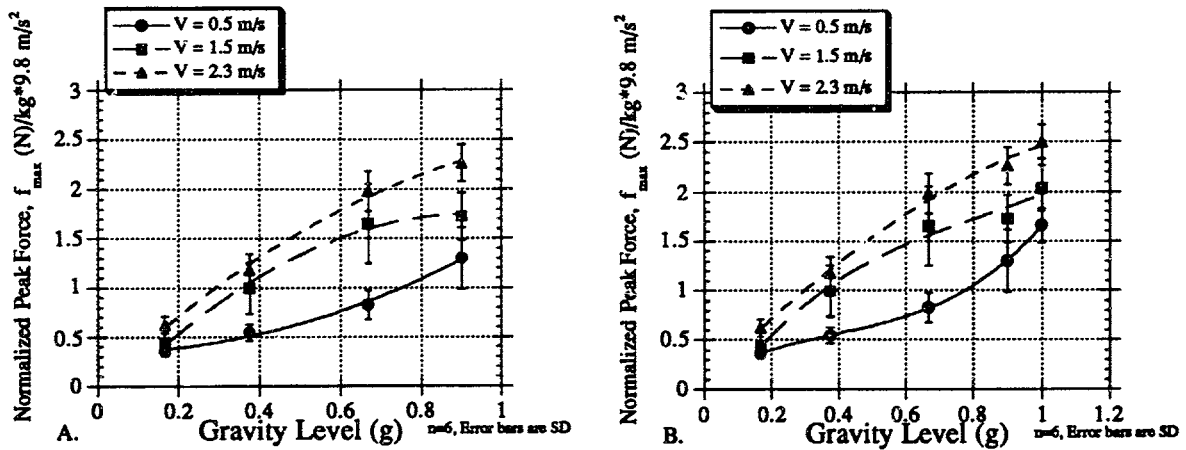


Figure 5.4 Dimensionless peak force versus gravity level. Each point is the mean for all six subjects and the error bars are the standard deviations of the means. Peak force is divided by individual subject mass and then divided by Earth's gravitational acceleration (9.8 m/s²). A) Results of underwater immersion experiments in which lunar (1/6 g), Martian (3/8 g), two-thirds (2/3 g), and close to Earth gravity (9/10 g) are simulated. B) Data from the terrestrial 1 g control session is shown with the immersion results. Both graphs show a significant reduction in dimensionless force as gravity is reduced from terrestrial levels toward lunar conditions.

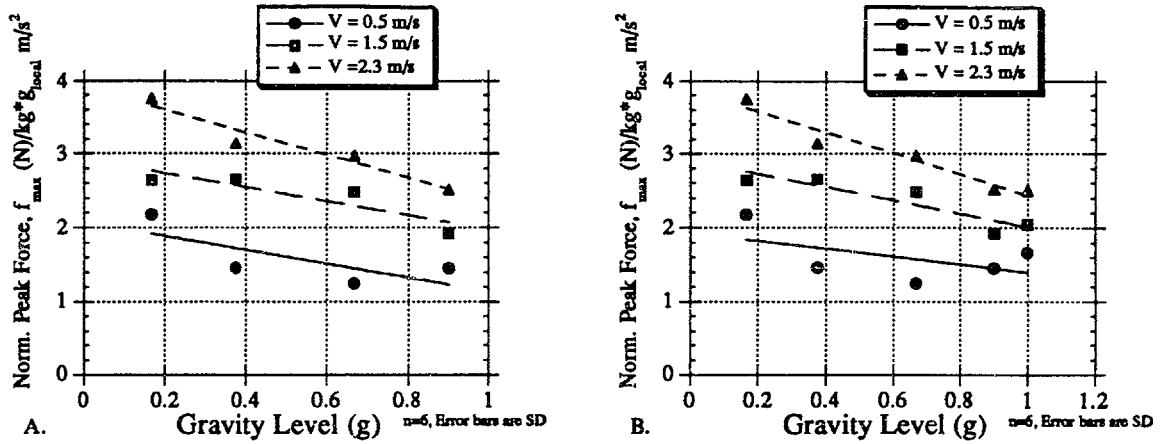


Figure 5.5 Dimensionless peak force normalized by local gravitational acceleration (i.e. g_{local} for Mars is $3/8 \cdot 9.81 \text{ m/s}^2 = 3.68 \text{ m/s}^2$) versus gravity level. Each point is the mean for all six subjects. A) Underwater immersion experiments. B) Results of underwater immersion experiments with the results of the 1 g control session. Statistical comparisons using Student's t tests reveal a significant increase in force from 1 g to 1/6 g and from 9/10 g to 1/6 g when the treadmill velocity is 0.5 m/s ($t=3.994$, $p<0.001$; $t=3.8263$, $p<0.001$, respectively). For locomotion at 1.5 m/s and 2.3 m/s dimensionless normalized force is significantly higher at Martian and lunar gravity conditions when compared to 1 g ($t=2.1458$, $p<0.05$ for comparisons when $v=1.5 \text{ m/s}$ and $t=2.5736$, $p<0.05$ for dimensionless force comparisons when $v=2.3 \text{ m/s}$).

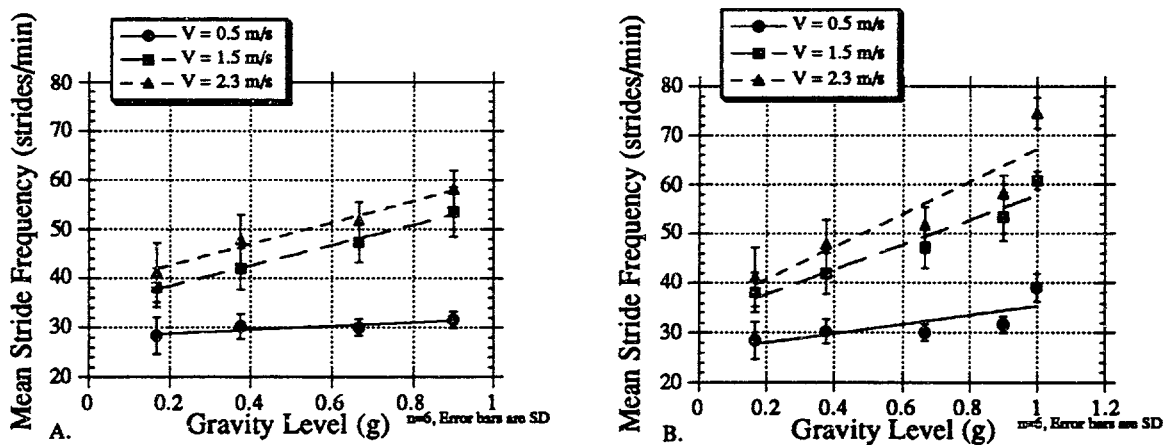


Figure 5.6 Stride frequency versus gravity level. Each point is the mean for all six subjects and the error bars are the standard deviations of the means. A) Results of underwater immersion experiments in which lunar (1/6 g), Martian (3/8 g), two-thirds (2/3 g), and close to Earth gravity (9/10 g) are simulated. Locomotion at the two fastest treadmill speeds elicits a significant linear reduction in stride frequency as gravity decreases from 9/10 g to 1/6 g. B) Results of underwater immersion experiments supplemented by results of the 1 g control session. A significant reduction in stride frequency is seen across all three speeds from 1 g to 1/6 g. Although, the data for the 1 g control fall outside of the curve fit. The inertial effects caused by the added ballast and added mass during underwater locomotion cause an enhanced decrease in stride frequency during underwater partial gravity locomotion as compared to the 1 g control experiment.

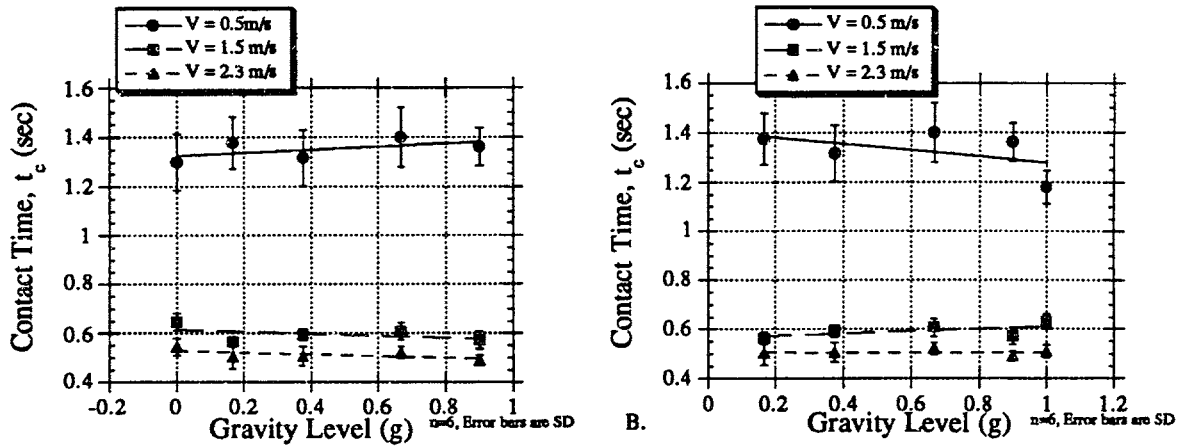
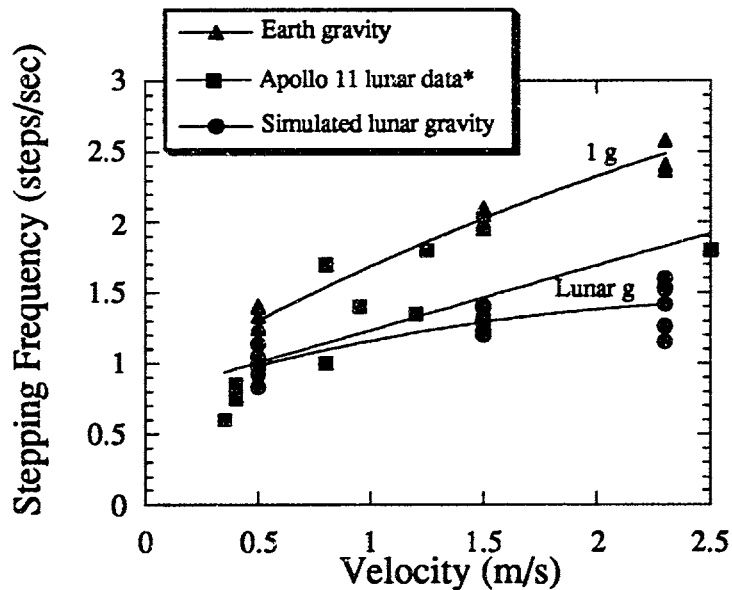


Figure 5.7 Contact time versus gravity level. Each point is the mean for all six subjects and the error bars are the standard deviations of the means. A) Data from the underwater immersion experiments shows no significant difference in t_c across gravity levels. B) 1 g control data is added to the underwater data. There is still no significant difference between t_c data across various gravitational accelerations.



* Stone, R.W. (1971) Man in Space.

Figure 5.8 Stepping frequency for Apollo 11 data and simulated lunar gravity. This is some of the only biomechanics data obtained from the Apollo lunar missions. Stepping frequency for terrestrial locomotion is also plotted. The Apollo data and simulated lunar data show a reduction in stepping frequency as compared to the terrestrial data, especially for locomotion at velocities of 1.5 m/s and 2.3 m/s.

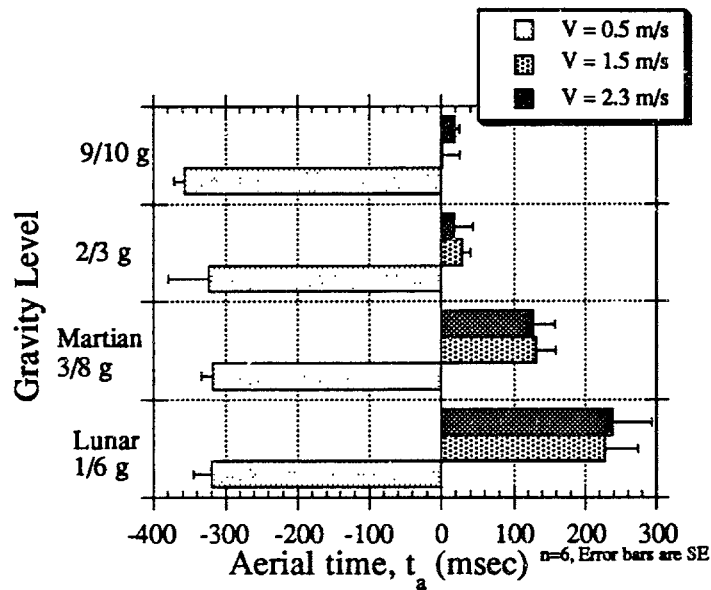


Figure 5.9 Aerial time for partial gravity immersion simulations. The mean for all six subjects is plotted and the error bars are the standard errors of the means. Negative aerial time measurements are calculated for walking at a treadmill velocity of 0.5 m/s because during the stance phase of walking the second foot strikes the ground while the first foot is still on the ground (dual stance phase), therefore the measurement between toe-off of the first foot and heel strike of the second foot has a negative value. This measurement can be thought of as the time for dual stance. A slight aerial phase is seen for locomotion at the faster velocities during 9/10 g and 2/3 g simulations. A significant aerial phase is depicted for locomotion at 1.5 m/s and 2.3 m/s for both Martian and lunar simulations.

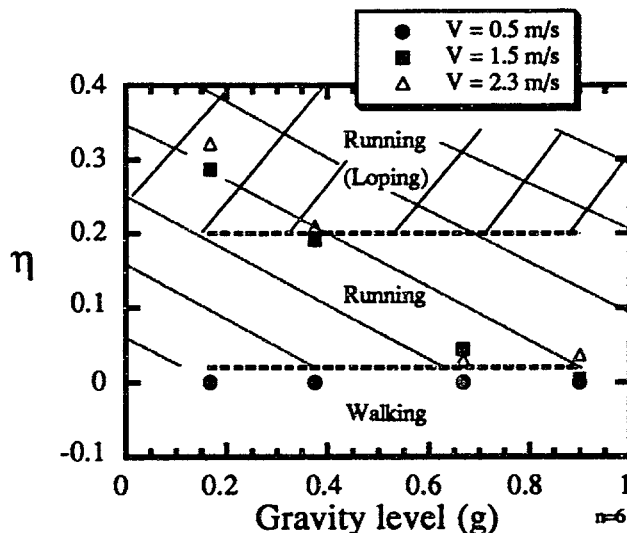


Figure 5.10 Locomotive index versus gravity level. The locomotive index, h , distinguishes between gaits and is defined as the ratio of time spent in the air to the duration of the stride cycle. Walking is seen for 0.5 m/s locomotion. Running has an index from 0.01 to 0.2 and is seen during 2/3 g and 9/10 g. Loping, a specific category of running, has a locomotive index of $h > 0.2$ and is seen during lunar and Martian simulations.

5.1.1.2 Parabolic Flight Pilot Study

The parabolic flight biomechanics data shown in this Section complement the underwater partial gravity results. Two men served as primary subjects for the lunar and Martian parabolic flights. As previously explained in Section 4.3.2, Parabolic Flight Pilot Equipment, the instrumented Del-Mar treadmill yields biomechanics results for running gaits, but not for walking because the force platform lies under the four corners of the tread and signals from walking gaits can not be differentiated between left and right foot. Figure 5.11 A) shows peak force for lunar and Martian locomotion at a velocity of 2.0 m/s. There is a significant reduction in peak force for ambulating in partial gravity. Figure 5.11 B) presents data from both underwater and parabolic flight simulation techniques and verifies that mean peak force is significantly reduced ($p < 0.05$) as gravity level is reduced. The force data from the parabolic experiments correlate extremely well with the immersion results.

Figure 5.12 illustrates a reduction in stride frequency for lunar and Martian parabolic flight gravity conditions. The general trend of a reduction in stride frequency is seen for both partial gravity simulation techniques. However, the superposition of underwater and parabolic flight data yields stride frequency results which are markedly higher for parabolic flight. This result makes sense in lieu of the simulation environments. As previously discussed, the decrease in stride frequency for the underwater locomotion experiments is attributable to the added ballast on the subjects' bodies and the additional inertial effect of added mass to move the water column during locomotion. The underwater running experiments characterized by the mass-spring model yield damped oscillatory motions, whereas, the experiments run on the KC-135 and the 1 g control experiments in air could be characterized by undamped harmonic motion. The natural frequency of a damped system is always less than that of an equivalent undamped system, therefore, the result of increased stride frequency for parabolic running and running in air compared to the underwater results was expected.

The contact time measurements for lunar and Martian parabolic flight show no variation across the two gravity conditions. Shorter contact times for parabolic flight as compared to the submersion technique are seen in Figure 5.13. The discrepancy between contact times for parabolic flight and submersion is again attributed to the inertial effects of added ballast and added mass during underwater partial gravity simulations. In sum, reducing the gravitational acceleration decreases stride frequency, increases stride length, and has no significant effect on contact time.

Subjects run at the fastest parabolic flight treadmill speed (2.0 m/s^2). The aerial times for lunar and Martian parabolas are less than the aerial times for underwater locomotion. Again, this difference is attributed to the different simulation environments. Intersubject variation might contribute to the results since the two parabolic flight subjects were different than the six underwater treadmill subjects. Individual aerial time measurements for the two subjects who participated in the parabolic flight experiments are plotted in Figure 5.14 A) and Figure 5.14 B) shows the mean aerial times for both simulation techniques. Overall, the results from both underwater submersion and parabolic flight techniques augment one another and yield similar biomechanics results for partial gravity locomotion.

Figure 5.15 illustrates the gaits and locomotive indices for the entire partial gravity study. A treadmill velocity of 0.5 m/s causes subjects to walk regardless of gravity level. For the immersion experiments, subjects lope at lunar and Martian gravity levels for the two fastest treadmill speeds. During parabolic flight, locomotion at 2 m/s produces a running gait. However, subjects comments suggest that they feel like they are loping during lunar and Martian parabolic flight. The locomotive index does not reveal a loping gait for parabolic flight because the aerial time and stride duration are much shorter than during underwater locomotion.

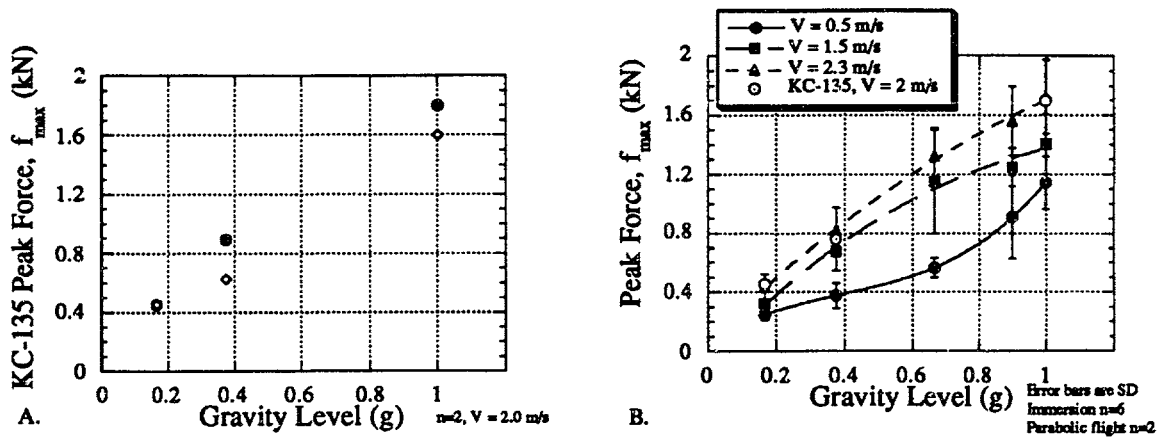


Figure 5.11 A) KC-135 peak force data versus gravity level for a treadmill speed of 2.0 m/s. Individual data points for Subject 1 (filled circles) and Subject 2 (open diamonds) are presented. B) Mean peak force versus gravity level for all partial gravity simulation experiments. Each point is the mean and the error bars are the standard deviations of the means. Peak force is significantly reduced as gravity level is decreased ($p < 0.05$) for all treadmill speeds.

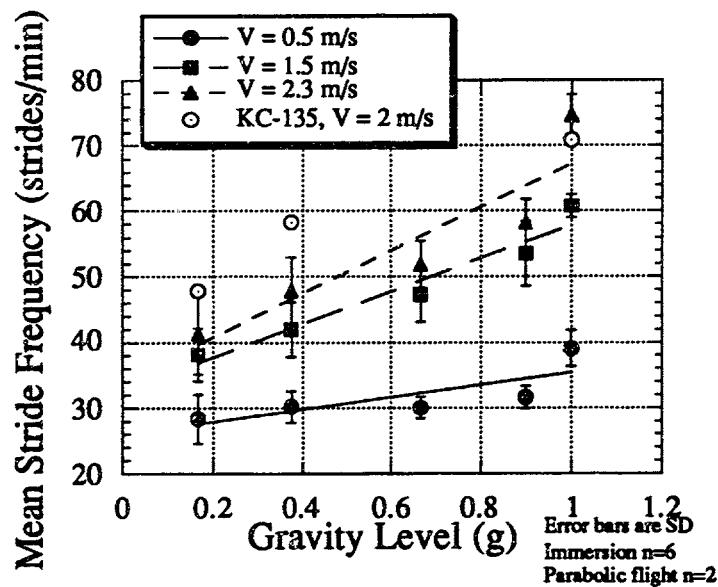


Figure 5.12 Mean stride frequency versus gravity level for all partial gravity simulation experiments. Each point is the mean and the error bars are the standard deviations of the means. During locomotion in parabolic flight the duration of stride cycles is measurably less than for simulated lunar and Martian locomotion underwater, resulting in an increase in stride frequency.

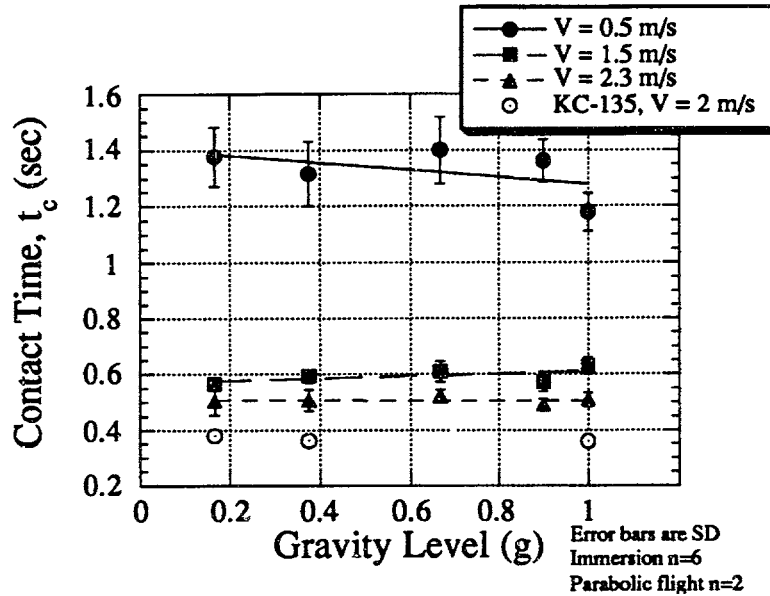


Figure 5.13 Contact time versus gravity level for all partial gravity simulation experiments. Each point is the mean and the error bars are the standard deviations of the means. There is no significant difference in t_c across gravity levels. The contact time measurements for parabolic flight gravity conditions are significantly less than those measured for underwater locomotion ($p < 0.05$).

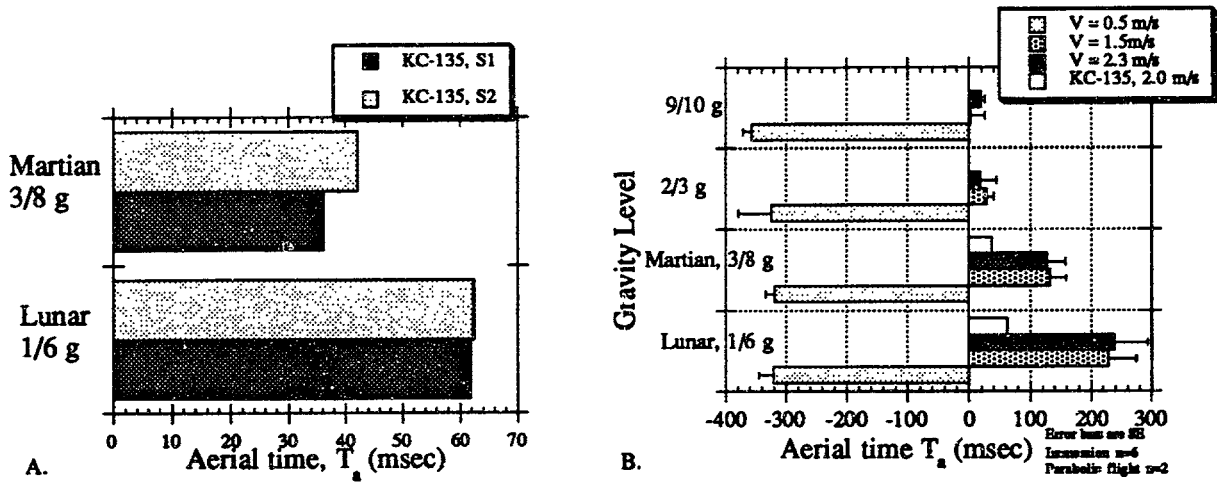


Figure 5.14 A) Aerial time versus gravity level for parabolic flight partial gravity experiments. Results from Subject 1 and Subject 2 are shown. B) Aerial time versus gravity level for all partial gravity simulation experiments. During walking at 0.5 m/s there is no aerial time, but the flight phase increases with a decrease in gravity level for locomotion at 1.5 m/s and 2.3 m/s.

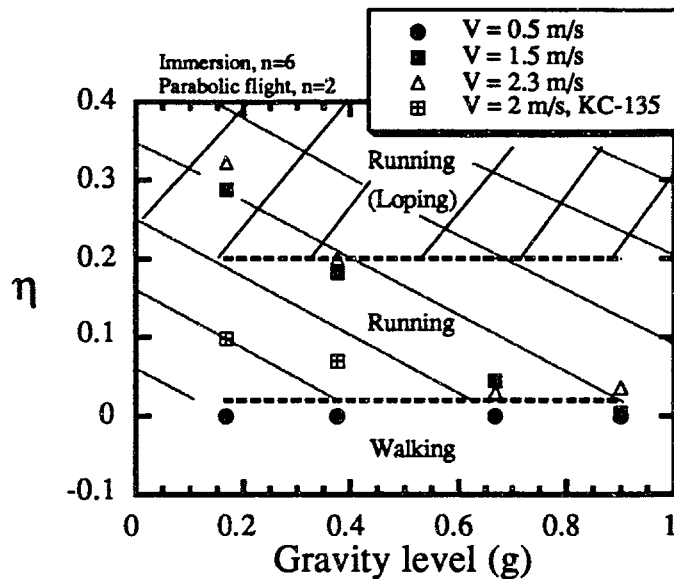


Figure 5.15 Locomotive index versus gravity level. The locomotive index, h , is defined as the ratio of aerial time to duration of the stride cycle and is useful to distinguish between walking and running. Walking is denoted for an index of zero, running has an index from 0.0 to 0.2, and loping (a specific category of running) has an index greater than 0.2. Lunar and Martian loping are seen for locomotion at both 1.5 m/s and 2.3 m/s.

5.1.2 Energetics

A few 1 g trends are mentioned in this introductory paragraph to provide the reader with a basis for comparison to partial gravity results. Recall from Section 2.1.1, Energetics Processes, that steady-state levels of oxygen consumption represent the energy required for locomotion because exercise below the maximum rate of oxygen consumption utilizes only the aerobic pathways. At 1 g steady-state oxygen consumption increases linearly with speed in 2, 4, 6, 8, 40, and even 100-legged runners [Full, 1989]. Oxygen consumption and heart rate are linearly related during dynamic exercise at 1 g [Gleim and Nicholas, 1989; Åstrand and Rodahl, 1977]. What effect does gravity have on the energetics of locomotion in reduced gravity environments? Results from the oxygen consumption and heart rate measurements address this question.

5.1.2.1 Partial Gravity Oxygen Uptake Measurements

In the partial gravity submersion study workload is primarily measured by oxygen uptake, \dot{V}_{O_2} , with heart rate taken as a secondary measure. For all energetics results, data from all six subjects are shown for lunar, Martian, and two-thirds gravity simulations, but not all of the subjects reached steady-state workload conditions under the 90% body weight loading condition (data for

9/10 g is designated by subject). The average resting metabolic rate is 0.06 ± 0.01 ml/(kg*s) and is independent across various simulated gravity levels (e.g., oxygen uptake at 3/8 g is 0.062 ± 0.013 ml/(kg*s)). The data from full body loading underwater and the 1 g control are not significantly different, matter-of-fact, the data are within one standard deviation. This result fortifies the claim of the hydrodynamics model that the drag effects are negligible for the experimental protocol of this study and lends credence to the validity of underwater partial gravity simulation for locomotion on a treadmill at low speeds.

Figure 5.16 shows mean \dot{V}_{O_2} , or the rate of oxygen consumed during exercise for all subjects as a function of gravity level for all three treadmill velocities. The error bars are the standard deviations of the mean. For all three speeds there is a reduction in oxygen uptake as gravity level is decreased. For locomotion at 1.5 m/s and 2.3 m/s, a significant decrease in \dot{V}_{O_2} is seen for a continuous reduction in gravity.

Basal metabolic rate is subtracted from oxygen uptake measurements to calculate the extra energy consumed for partial gravity locomotion at lunar (1/6 g) and Martian (3/8 g) simulations. When subjects run at 2.3 m/s average oxygen uptake decreases by 67% for 1/6 g (a 83% gravity reduction) and 41% for 3/8 g (a 63% gravity reduction) as compared to 1 g. The reductions in metabolic expenditure at 1.5 m/s are 66% and 31% for the lunar and Martian gravity simulations, respectively.

Figure 5.17 presents individual's workload measurements. Exercise at low gravity levels requires less energy consumption than at approximate Earth gravity (9/10 g). A few subjects (both female subjects and two of the male subjects) were unable to reach steady-state \dot{V}_{O_2} for 9/10 g loading for various treadmill velocities. However, this is not thought to be a gender dependent phenomenon because other women were able to reach steady-state workload following the same protocol. Unfortunately these women did not serve as primary subjects during formal data collection. Walking at 0.5 m/s produces interesting reductions in \dot{V}_{O_2} for half the subjects during Martian gravity simulation.

5.1.2.2 Partial Gravity Heart Rate Measurements

Figure 5.18 shows a reduction in mean heart rate for the partial gravity simulations as compared to the gravity level approaching 1 g. For locomotion at 1.5 m/s and 2.3 m/s, a continuous decrease in heart rate is seen with decreasing gravity level. However, for locomotion at 0.5 m/s, the results indicate an *increase* in heart rate for the lunar simulation as compared to the Martian simulation. A

resulting hypothesis is that at low velocities and low levels of gravity subjects expend proportionately more energy to maintain stability and posture control than in locomotion itself resulting in an increase in workload at the lowest partial gravity simulation.

Results from individual heart rate measurements and the relationship between $\dot{V}O_2$ and heart rate complete the workload analysis. Individual heart rates versus treadmill speed show a significant reductions in heart rate for complementary decreases in simulated gravity level. Linear curve fits provide the best fit for locomotion at 1.5 m/s and 2.3 m/s, but a second order polynomial best fits the 0.5 m/s data. This latter curve fit exhibits a distinct minimum in heart rate for the Martian simulation (See Figure 5.19). Recall, a linear relationship between $\dot{V}O_2$ and heart rate is documented for 1 g conditions. Figure 5.20 shows a linear relationship between oxygen consumption and heart rate (also known as oxygen pulse) for the partial gravity immersion experiments. This relationship offers future investigators of underwater locomotion a workload metric in case gas analysis measurements are unavailable.

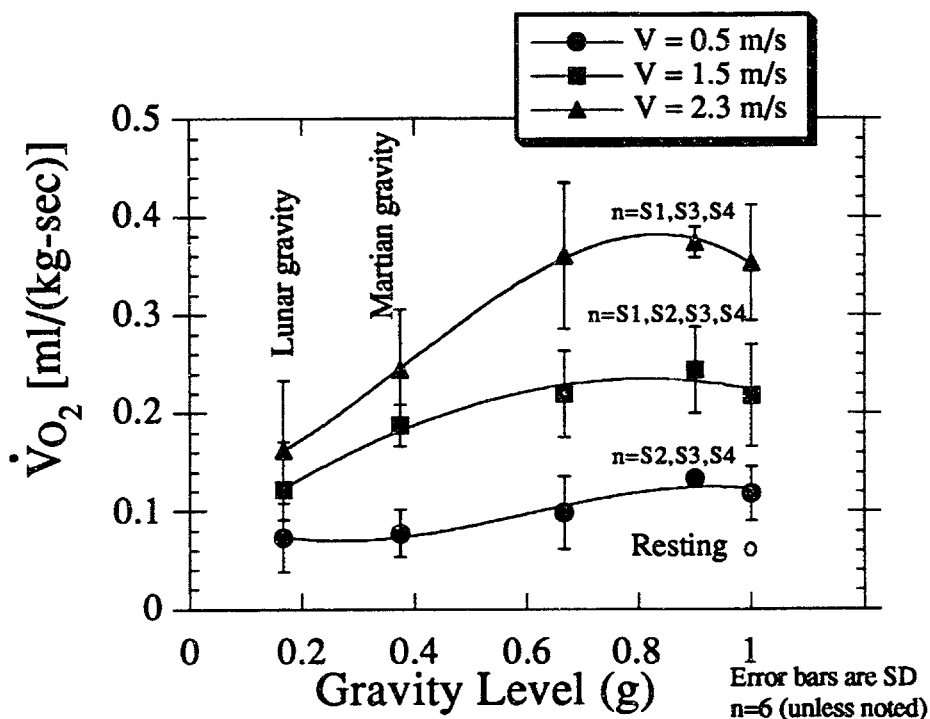


Figure 5.16 Workload, $\dot{V}O_2$, versus gravity level. Each point is the mean and the error bars are the standard deviations of the means. The mean resting workload value is 0.06 ± 0.01 ml/(kg-sec) and is independent of gravity (i.e., oxygen uptake at 3/8 g is 0.062 ± 0.013). Workload significantly decreases for locomotion at 1.5 m/s and 2.3 m/s from 1 g to lunar and Martian gravity levels ($p < 0.05$). Subjects 1, 2, 3, and 4 were unable to reach steady-state workload levels for all treadmill velocities while ballasted to 9/10 g. There is a reduction in oxygen uptake from the simulated 9/10 g underwater (filled markers) to the 1 g terrestrial (open markers) locomotion due to the hydrodynamic drag forces inherent in the submersion technique, but the difference is not significant and the values for both 9/10 g and 1 g are within one standard deviation.

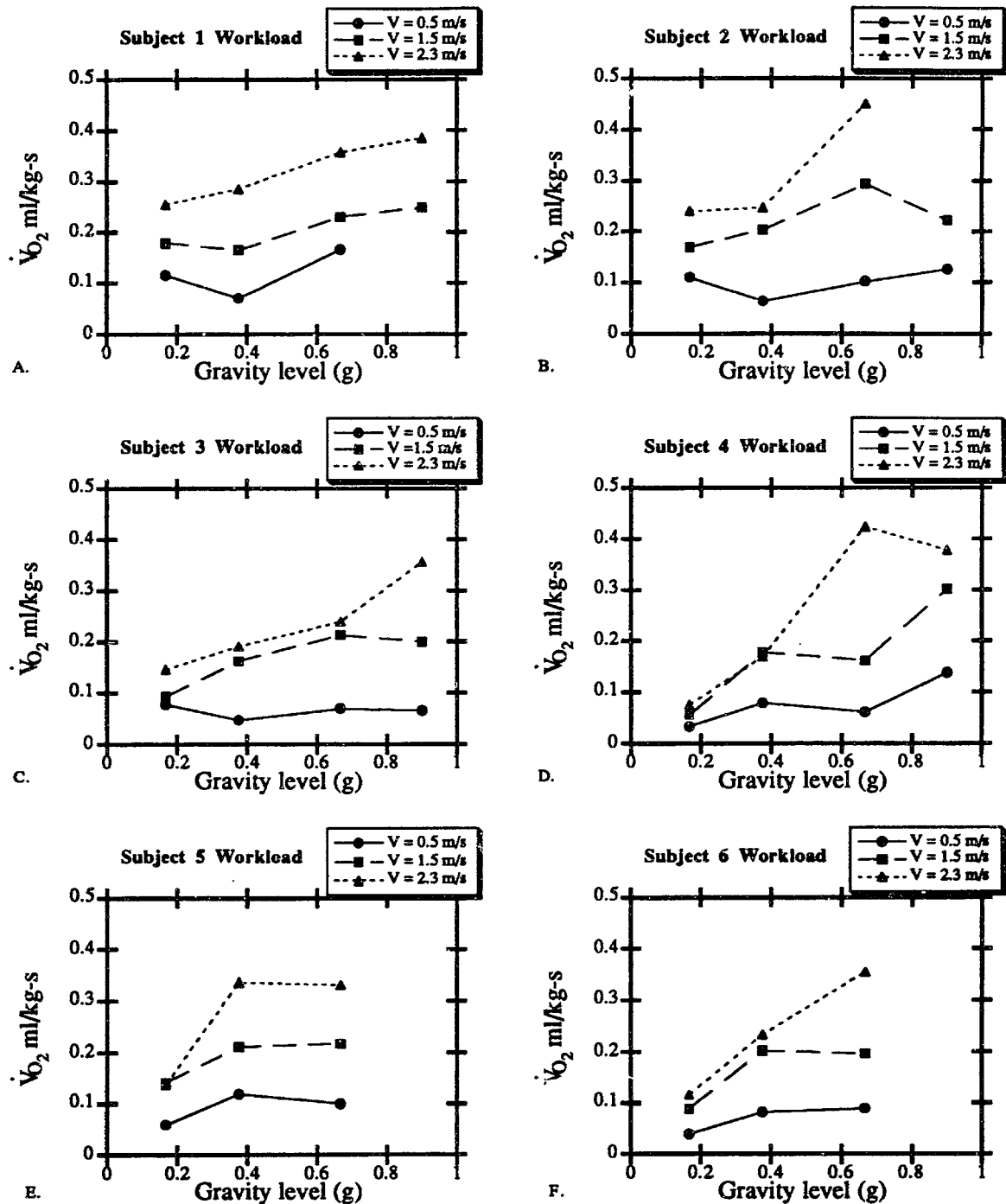


Figure 5.17 Workload, \dot{V}_{O_2} , versus gravity level for each of the six subjects. Each point is the mean steady-state oxygen consumption. In general, workload decreases as gravity level is reduced. Subjects 1-4 are men and Subjects 5 and 6 are women. Subject 1 was unable to reach steady-state \dot{V}_{O_2} for 9/10 g loading while walking at 0.5 m/s. Subject 2 was unable to reach steady-state \dot{V}_{O_2} for 9/10 g loading at the fastest velocity of 2.3 m/s. Subjects 3 and 4 completed the entire experimental protocol and Subjects 5 and 6 were unable to reach steady-state \dot{V}_{O_2} levels for the 9/10 g simulation. Subjects 1-3 show a decrease in oxygen uptake at Martian gravity compared to lunar gravity.

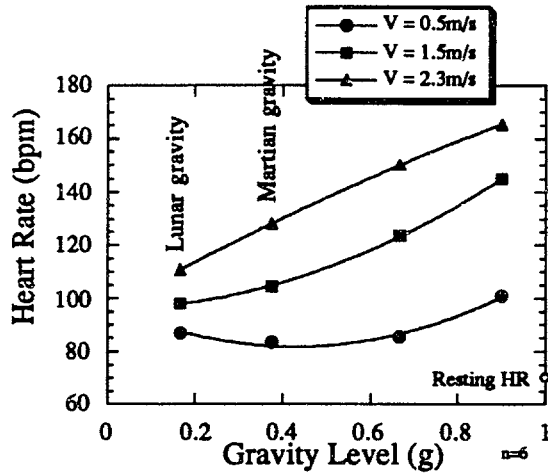


Figure 5.18 Heart rate versus gravity level. Each point represents the mean. Heart rate decreases linearly during running at 2.3 m/s and a 33% reduction is seen from 9/10 g to 1/6 g. Heart rate decreases nonlinearly for walking at 0.5 m/s and only a 12% reduction is seen from 9/10 g to 1/6 g, however, a 16% reduction is seen from 9/10 g to 3/8 g.

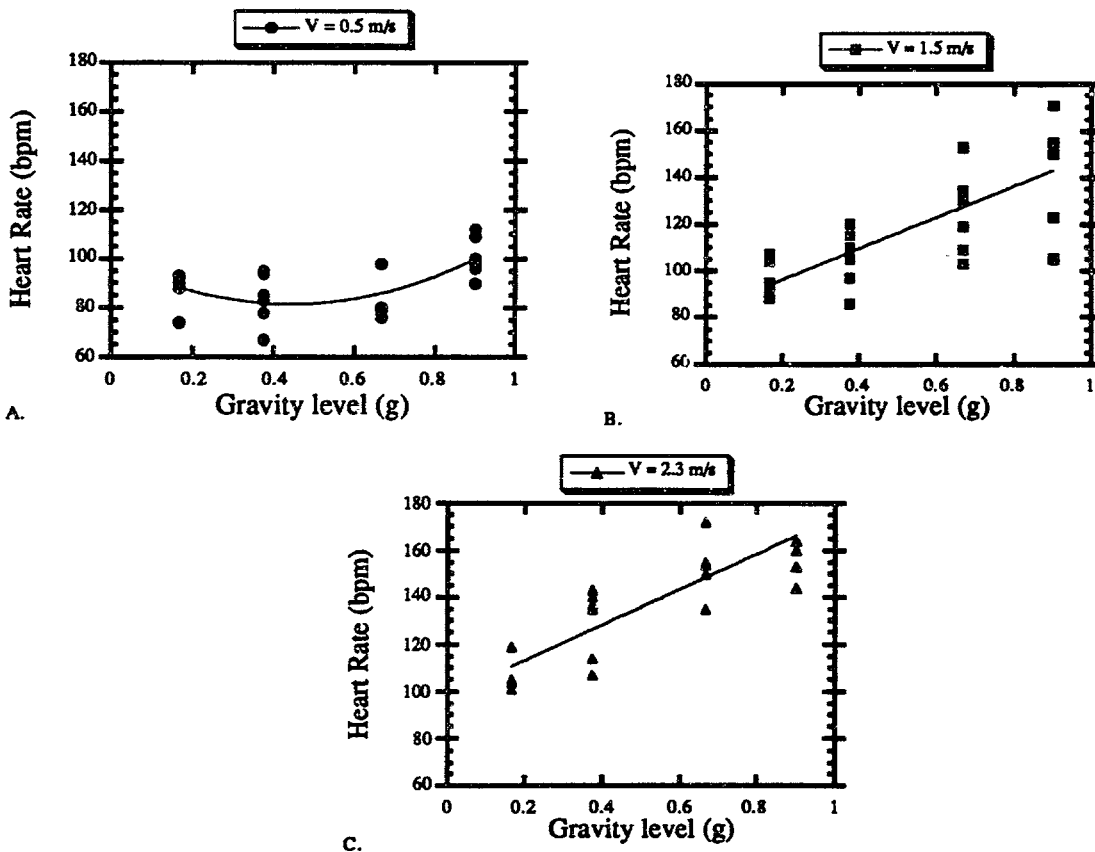


Figure 5.19 Individual heart rates versus gravity level for locomotion at A) 0.5 m/s B) 1.5 m/s and C) 2.3 m/s. A second order polynomial provides the best curve fit for the walking data (0.5 m/s) and a minimum heart rate is elicited at Martian gravity rather than lunar gravity. Linear curve fits are shown for heart rate data at the two higher treadmill velocities (1.5 m/s and 2.3 m/s).

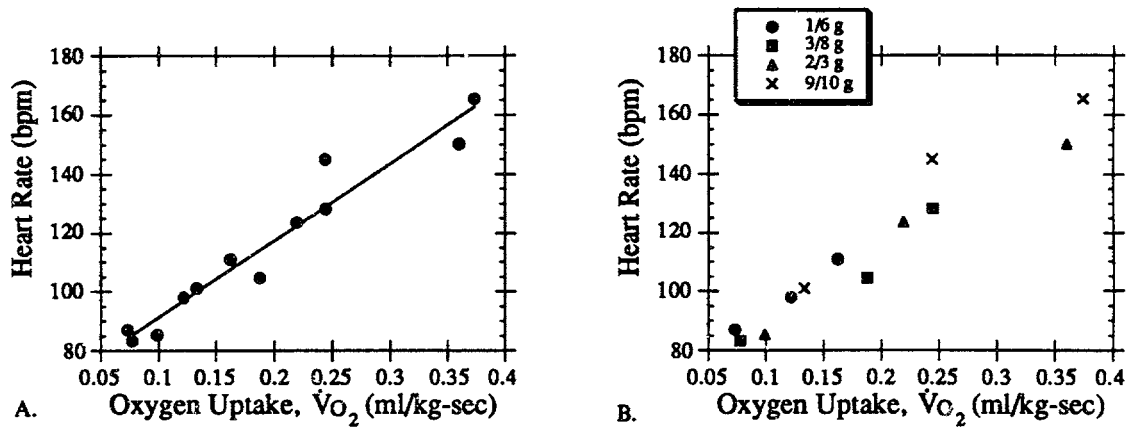


Figure 5.20 Linear relationship between oxygen uptake and heart rate for partial gravity locomotion experiments. A) Linear curve fit with each point representing the mean for all six subjects. B) Means for all subjects and markers differentiate between gravity levels. Data for all three treadmill velocities are shown. Circles represent lunar workload, squares represent Martian workload, triangles represent two-thirds gravity conditions, and crosses denote nine-tenths gravity workload results.

5.2 DISCUSSION

This Discussion Section starts by delineating the limitations of the experimental techniques. The results of this investigation show that walking, loping, and running are all possible in partial gravity. Subjects alter their mechanics and employ a loping gait for a wide range of speeds (~1.5 m/s to ~2.3 m/s) during lunar and Martian gravity simulations. Having evolved in our 1 g Earth environment using only two gaits, walking and running, this change to a more efficient lope is phenomenal and reinforces the idea that for specific speeds and gravity conditions, humans adopt optimal gaits. Section 5.2.2 introduces a mathematical model for running and theoretical analysis fortifies the experimental biomechanics results. The Chapter concludes with a discussion of the energetics. A difference is seen in workload as measured by energy consumption and heart rate. Subjects consume less oxygen for partial gravity simulations as compared to approximate 1 g levels. Section 5.2.3 discusses the nonmonotonic reduction in workload and suggests the existence of a gravity threshold. The concept of minimum cost of locomotion identifies optimal partial gravity gaits.

5.2.1 Limitations of Experimental Techniques

The submersion/ballasting technique and the parabolic flight technique offer partial gravity simulation environments to study locomotion. However, there are a few constraints that limit the realism of the simulations. The major constraint of the submersion technique is the inherent hydrodynamic viscosity. The major disadvantage of the parabolic flight partial gravity experiments is that data collection is limited to biomechanics, excluding steady-state workload measurements.

Subjects experience drag and damping forces while moving in water ; this hydrodynamic constraint could alter locomotion and workload. The design of the underwater treadmill enables the subject to move his/her limbs through the water without noticeably altering their center of gravity. If the treadmill were not present and subjects were required to translate their entire bodies through the water hydrodynamic forces could possibly invalidate the simulation. Section 3.2, Hydrodynamic Modeling, verifies that the drag energy of a subject moving his/her limbs through the water while traveling on the treadmill is a negligible percentage (< 6 %) of the overall measured energy expenditure.

5.2.2 Mathematical Model for Running

In order to further study the change of mechanics seen during partial gravity locomotion, this Section introduces McMahon and Cheng's [1990] mathematical model for running as a basis to interpret the experimental results. They present a comprehensive theory for running in terrestrial animals. This Section addresses the extent to which it predicts the biomechanics of partial gravity locomotion. The experimental data depict the dynamics of low gravity locomotion as differing from 1 g locomotion (i.e., increased stride length and aerial time).

A linear spring representing the muscles and tendons of the leg provides the basis for the mathematical running model (See Figure 5.21). Recall from Sections 2.2.2.1-2 that different mechanisms operate during walking and running gaits, specifically, the maximum vertical force occurs at mid-step and the vertical height of the CoM reaches a minimum at mid-step for running. The literature supports using spring-like systems to model the properties of muscle and tendons of the leg [Alexander, 1988; Cavagna *et al.*, 1988; Full, 1991; McMahon, 1984]. Results from animals and humans show that acceleration (which is proportional to vertical force) increases as the vertical displacement of the CoM decreases during ground contact. This finding leads to the idea that an undamped spring describes the stiffness of a running animal during the time the foot is in contact with the ground. The stiffer the spring the shorter the contact time and the higher the vertical force.

McMahon and Cheng describe initial model conditions to maintain a steady running cycle by assuming that forward speed u , is the same at the beginning and end of a step and that the magnitude of the angle between the leg and the vertical, Θ , is the same at the beginning and end of the step [1990, pg 66]. The input to the model includes dimensionless parameters that characterize running, they are: a horizontal Froude number (U) based on forward speed, u , and leg length, l_0 ; a vertical Froude number (V) based on vertical landing velocity, v , and leg length; a dimensionless leg spring stiffness (K_{leg}) based on the linear spring representation of the muscles and tendons of the leg, k_{leg} , defined as the ratio of maximum vertical force (f_{max}) to the change of leg spring length (Δl); and Θ , the angle of the leg with respect to the vertical at foot contact [McMahon & Cheng, 1990]. The definition of Froude numbers comes from the discipline of fluid dynamics and represent the ratio of inertial to gravitational forces. The leg spring stiffness K_{leg} is the square of the ratio of the natural frequency of the mass-spring system to the natural frequency of the leg during pendulum motion. Equations 5.1 through 5.3 define these dimensionless model parameters. Equation 5.4 calculates the angle between the leg and the vertical at the moment of foot contact.

$$U = u/(gl_o)^{1/2} \quad (5.1)$$

$$V = v/(gl_o)^{1/2} \quad (5.2)$$

$$K_{leg} = k_{leg}l_o/mg \quad (5.3)$$

$$\Theta_o = \sin^{-1}(ut_o/2l_o) \quad (5.4)$$

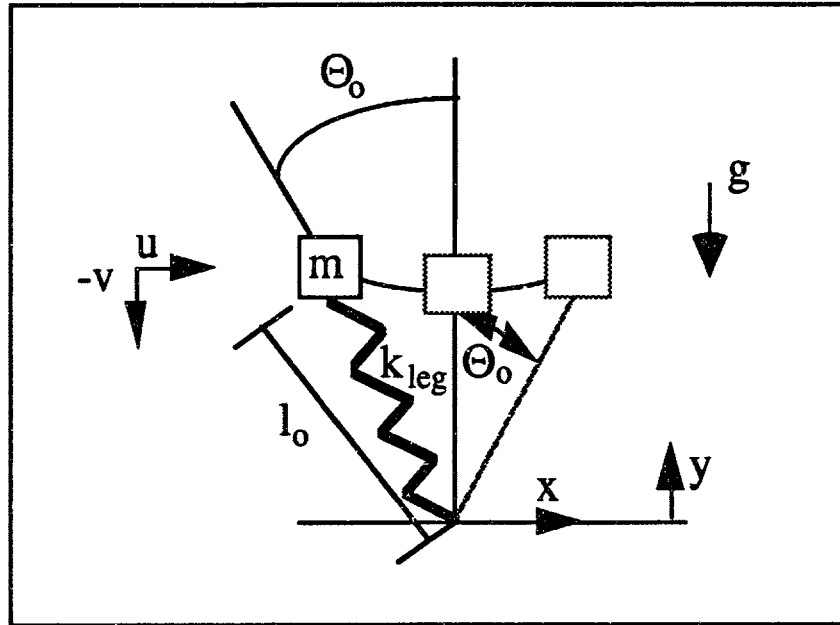


Figure 5.21 Schematic drawing of mass-spring model for forward running where u is forward velocity, v is vertical velocity, k_{leg} is leg stiffness, l_o is leg length, Θ_o is the angle between the leg and the vertical, and y is the vertical height of the mass during ground contact. (From McMahon and Cheng, 1990).

Interpretation of Experimental Results using the Mathematical Model

Investigating the entire range of partial gravity conditions represented in the underwater experiments requires a modification of the mathematical model. The local gravitational acceleration (for Mars, $g_{local} = 3/8 \cdot 9.81 \text{ m/s}^2 = 3.68 \text{ m/s}^2$) replaces the constant gravity condition of Earth ($g = 9.81 \text{ m/s}^2$) and Equations 5.1-5.3 become Equations 5.5-5.7.

An additional dimensionless group in the McMahon and Cheng model is a *vertical stiffness* parameter, or the peak vertical force divided by the vertical displacement during foot contact (See Equation 5.8). The McMahon and Cheng model lumps the body CoM at the hip, therefore, vertical displacement of the hip during contact period corresponds to the vertical displacement of the body. Recall from the Results Section that a double integration of the vertical trace yields displacement of the CoM. Table 5.1 shows the dimensionless variables of the model calculated

using experimental biomechanics data. Figures 5.22-5.25 present partial gravity results from theoretical predictions of the model and from experiments.

$$U = u/(g_{local}l_o)^{1/2} \quad (5.5)$$

$$V = v/(g_{local}l_o)^{1/2} \quad (5.6)$$

$$K_{leg} = k_{leg}l_o/mg_{local} \quad (5.7)$$

$$K_{vert} = k_{vert}l_o/mg = (\Delta f_y/\Delta y)l_o/mg \quad (5.8)$$

The Results Section shows significant changes in many variables during partial gravity locomotion. Peak force, stride frequency, and vertical landing velocity all decrease as gravity is reduced. Contact time stays relatively constant across the range of partial gravity. Stride length and aerial time increase as gravitational acceleration decreases. The purpose of the mathematical model is to verify and enhance the interpretation of partial gravity locomotion experimental results. The dimensionless parameters are functions of the local gravity level, thus the interactions and dependence of the biomechanics results on gravity is accounted for in these parameters.

Table 5.1 Input Parameters for Mathematical Model for Running.

Mass (kg)	Gravity	l_o (m)	u (km/hr)	u (m/s)	U	V	Θ_o
70	1/6•g	0.89	5.4	1.5	1.25	0.17	0.51
70	1/6•g	0.89	8.3	2.3	1.91	0.20	0.72
70	3/8•g	0.89	5.4	1.5	0.83	0.22	0.53
70	3/8•g	0.89	8.3	2.3	1.27	0.23	0.73
70	2/3•g	0.89	5.4	1.5	0.62	0.21	0.55
70	2/3•g	0.89	8.3	2.3	0.96	0.26	0.77
70	9/10•g	0.89	5.4	1.5	0.54	0.20	0.55
70	9/10•g	0.89	8.3	2.3	0.82	0.25	0.77
70	1•g	0.89	5.4	1.5	0.51	0.23	0.56
70	1•g	0.89	8.3	2.3	0.78	0.27	0.78

Peak Vertical Force

A theoretical value of peak force is attained from the McMahon and Cheng paper [1990]. The peak force is modeled as a function of the horizontal and vertical Froude numbers. Equation 5.9 represents peak force and is derived from the mass-spring model and interpolation of theoretical results in light of the experimental protocol followed in the partial gravity experiments.

$$f_{max} = (1.75 + 2.5UV)mg_{local} \quad (5.9)$$

When peak vertical force f_{max} , is plotted as a function of dimensionless horizontal velocity U , the model shows peak force to rise linearly with U . Recall that the peak force occurs during mid-step, or in the middle of the contact period. Figure 5.22 A)-E) present peak force as a function of horizontal velocity for the results of the mathematical model and experimental data across the entire

range of partial gravity. The mathematical model predicts the mechanics of running and only applies to the experimental results where subjects are seen to run (underwater treadmill speeds of 1.5 m/s and 2.3 m/s and parabolic flight treadmill speed of 2 m/s, ($U > 0.5$)). The predictions of the mathematical model represented by solid lines show strong correlation to the experimental data points. The model predicts f_{\max} to within one standard deviation across all gravity levels except for lunar and $2/3$ g locomotion at 2.3 m/s which are just over one standard deviation.

The physiological importance of the significant reduction in partial gravity peak force is deconditioning of the musculoskeletal system for long duration spaceflight or planetary habitation. Atrophy of the skeletal and muscular systems is one of the most serious spaceflight problems [Cavanagh *et al.*, 1992]. Will partial gravity cause permanent or irreversible physiological damage to humans or will the body adapt to living in partial gravity without irreparable damage? Maximal impact loading of the skeleton is often prescribed as a countermeasure to the harmful deconditioning effects of spaceflight. Maintaining skeletal and muscular integrity takes on the utmost importance to ensure human performance on planetary surfaces as well as upon return to the 1 g environment of Earth. This research study provides an initial database of peak forces to be expected during lunar and Martian locomotion.

Leg Spring Stiffness and Effective Vertical Stiffness

McMahon and Cheng's theoretical results of the leg spring model for 1 g verify that a constant leg spring is a valid assumption for human running. The biomechanical and neurological literature supports the hypothesis that mechanical stiffness of muscles remains relatively constant over an entire range of forces in humans [Greene and McMahon, 1979] and animals [Hoffer and Andreassen, 1981].

The effect of gravity on the spring properties of leg muscles and tendons is questioned in this Section. He *et al.* [1991] hypothesized that the leg spring stiffness k_{leg} would remain relatively constant under reduced gravity conditions. Inputs from the partial gravity study (See Table 5.1) allow the model to be run for a specified partial gravity condition. K_{leg} remains constant across dimensionless horizontal velocity, U (which includes the local gravity level) and K_{vert} increases as a function of U . The spring constants K_{leg} and K_{vert} are calculated from the experimental results and plotted as a function of U (See Figure 5.23). K_{leg} remains constant across dimensionless horizontal velocity, U (which includes the local gravity level) and K_{vert} increases as a function of U . Theoretical predictions of K_{vert} from the McMahon and Cheng are superimposed on the values attained from experimental data and a constant K_{leg} is plotted along with the experimental data. The theoretical results for partial gravity running at the low velocities of 1.5 m/s and 2.3 m/s agree

quite well with the trends seen at higher speeds (6 m/s to 20 m/s) and suggest that the model is useful for low speed running at partial gravity.

Leg Angle and Vertical Velocity

The leg angle, Θ_o , and vertical velocity, V , are two of the dimensionless parameters introduced in the McMahon and Cheng model that provide additional variables to interpret the experimental results. These two parameters are calculated from experimental data and plotted in Figure 5.24. The Figure presents Θ_o and V as functions of treadmill velocity, u . Data is plotted for the entire range of partial gravity (1/6 g through 9/10 g), and the values lie directly on top of one another. This result indicates that the calculated values of Θ_o and V (initial dimensionless leg angle and dimensionless vertical landing velocity, respectively) are invariant across gravity levels as a function of treadmill speed.

The initial leg angle increases with horizontal speed for the underwater experiments, but a significant decrease is seen for Θ_o during parabolic flight running. This is attributed to the contact time results from parabolic flight being shorter in duration than the contact times during underwater immersion. Recall that the vertical stiffness depends on the peak force and the displacement of the CoM during foot contact. Peak force increases with speed and displacement stays relatively constant which predicts a stiffer spring constant at higher speeds. As speed increases, an increase in initial leg angle is seen which indicates that a larger vertical stiffness contributes to increasing the speed of locomotion.

There is a slight increase in vertical landing velocity and experimental data from both underwater immersion and parabolic flight show a rise in V to 0.2 for the fastest horizontal speed of the protocol. The dimensionless vertical landing velocity is relatively independent of treadmill speed and gravity level. Equation 5.10 predicts the excursion of the center of mass during the flight phase of the stride cycle. Using a constant value of 0.2 for the vertical Froude number ($V=0.2=v/(g_{local}l_o)^{1/2}$) the conclusion is reached that the CoM rises approximately 2 cm (or 2% of the leg length).

$$\Delta y = (0.2)^2 g_{local} l_o / 2 g_{local} = 0.02 l_o \quad (5.10)$$

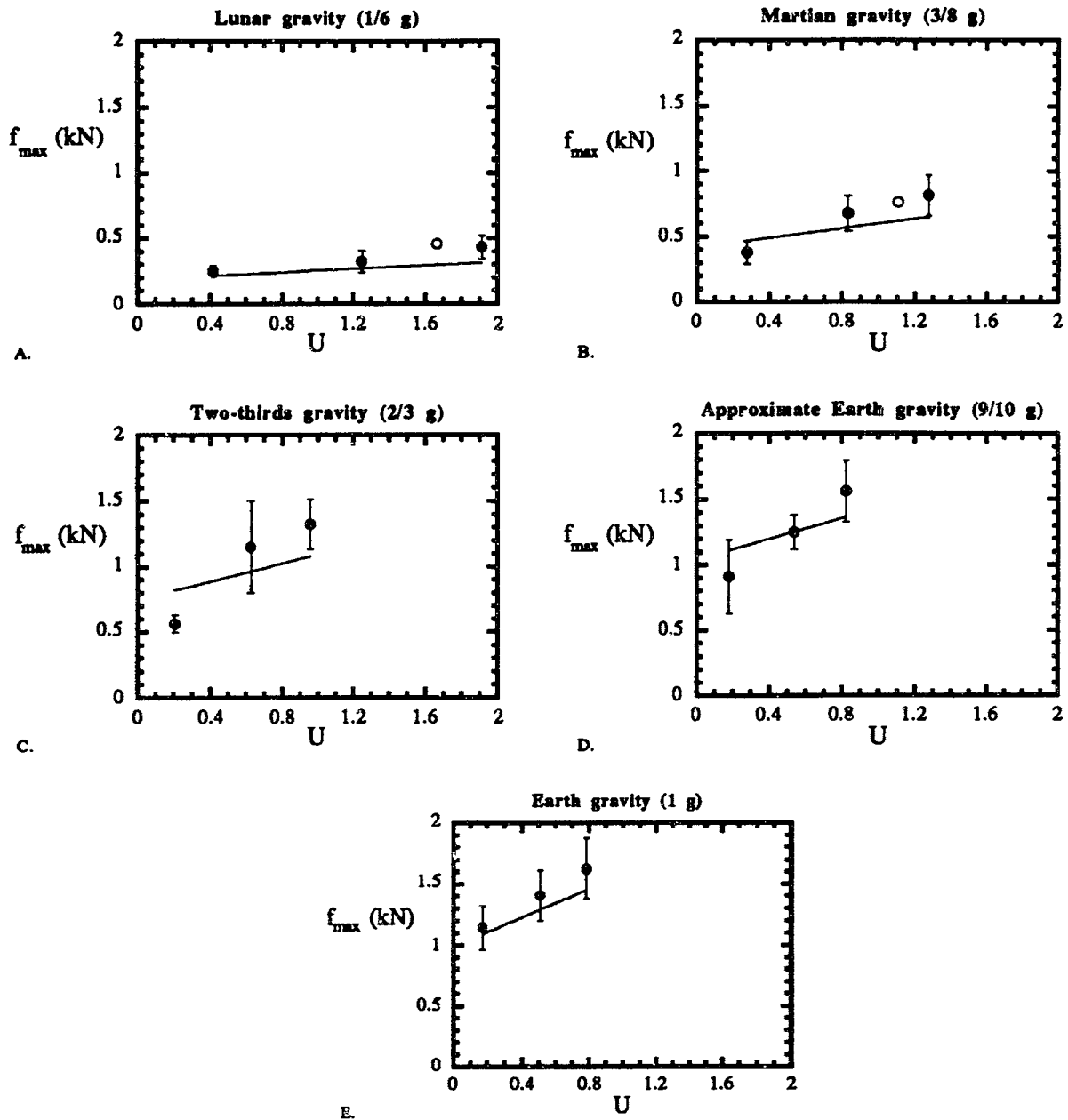


Figure 5.22 Peak force at midstep (f_{\max}) for a mathematical spring-model (solid lines) and experimental data (solid circles represent immersion data and an open circle represents parabolic flight) as a function of dimensionless horizontal speed U (Froude number). The horizontal Froude number is defined as $U = u/(g_{\text{local}}l_0)^{1/2}$ where u is the treadmill velocity, g_{local} is the partial gravity condition (i.e., $1/6 \cdot 9.81 = 1.635 \text{ m/s}^2$ for the lunar environment), and l_0 is leg length. The model only applies to running, therefore, experimental data when subjects were running ($U > 0.5$) is relevant. Both experimental data and the model show f_{\max} to rise linearly with U . There is high correlation between the model and experimental results to within one standard deviation for 1 g, simulated 9/10 g, and simulated 3/8 g, and just over one standard deviation for simulated 2/3 g and simulated 1/6 g.

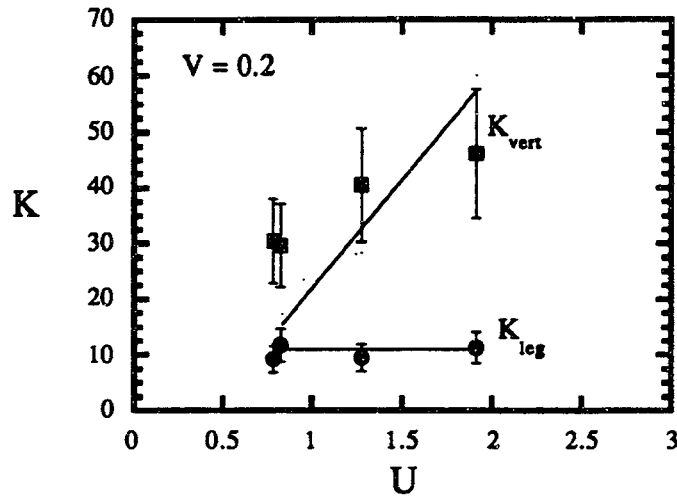


Figure 5.23 Leg spring stiffness, K_{leg} , and effective vertical stiffness, K_{vert} , as functions of dimensionless horizontal velocity, U , for constant dimensionless vertical landing velocity, V where K_{leg} is the square of the ratio of natural frequency of the mass-spring system to the natural frequency of the leg during pendulum motion ($K_{leg} = k_{leg}l_0/mg_{local} = (f_{max}/\Delta l)l_0/mg_{local}$); K_{vert} depends on the peak force and the vertical displacement of the CoM during the contact phase ($K_{vert} = k_{vert}l_0/mg_{local} = (\Delta f_y/\Delta y)l_0/mg$); $U = u/(g_{local}l)^{1/2}$, and $V = v/(g_{local}l)^{1/2}$. The dimensionless parameters are calculated from the experimental data and reveal constant K_{leg} (solid circles) and increasing K_{vert} (solid squares). Means are plotted with error bars representing a 25% deviation of the mean. The theoretical model predicts (solid lines) the vertical stiffness parameter increases as a function of dimensionless horizontal velocity with an assumed leg stiffness of $K_{leg} = 11$.

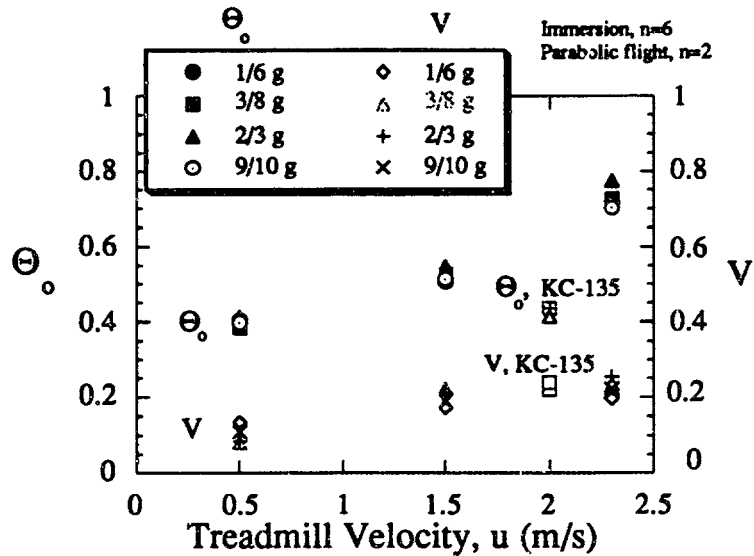


Figure 5.24 Leg angle, Θ , and vertical Froude number, V , as a function of treadmill velocity, u . Experimental results from immersion and parabolic flight partial gravity simulation techniques. Leg angle ($\Theta_0 = \sin^{-1}(ut/2l_0)$) increases with horizontal speed, but is extremely consistent for all gravity levels. The noticeable drop on leg angle for the parabolic flight experiments can be explained by the difference in contact times for parabolic flight and underwater locomotion. Dimensionless vertical landing velocity ($V = v/(gl_0)^{1/2}$) plateaus close to 0.2 and is consistent across all gravitational acceleration levels.

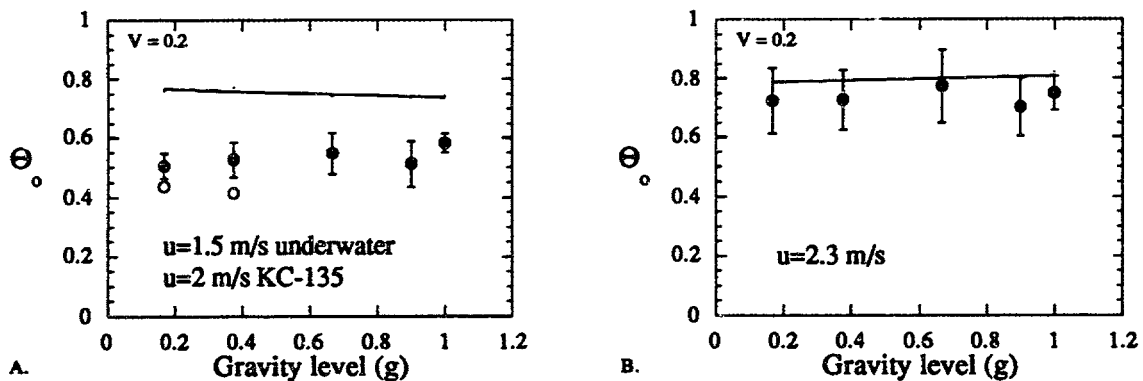


Figure 5.25 Initial leg angle upon landing as a function of gravity for different speeds. Solid line represents the running model prediction and experimental values are plotted with circular markers (filled for underwater experiments and open circles for KC-135 flights at a velocity of 2 m/s). Error bars signify standard deviations of the means. A) For a treadmill velocity of 1.5 m/s, the model significantly overpredicts the leg angle. This slow velocity is beyond the capabilities of the running model. B) The model makes an accurate prediction of leg angle for locomotion at a velocity of 2.3 m/s. Higher speeds of locomotion are attained via increases in the initial leg angle.

In sum, the dimensionless parameters introduced for the running model of McMahon and Cheng investigate the spring-like characteristics of muscular activity during running and analyze the interactions among gravity, speed, and stiffness parameters for locomotion. The equations are modified to reflect the experimental protocol of this partial gravity study. Significant findings reveal that the mass-spring model for running predicts some of the dynamics of partial gravity locomotion. The peak force is seen to be significantly reduced at reduced gravity levels both in theory and experiments, and force increases with dimensionless horizontal speed. The spring stiffness of the leg is independent of gravity level, while the effective vertical spring stiffness increases as a function of horizontal speed. The model predicts the initial leg angle for the mass-spring model at 2.3 m/s, but fails to predict the leg angle for locomotion at 1.5 m/s. The dimensionless vertical landing velocity calculated from experimental data is relatively constant at 0.2 and agrees with theoretical predictions.

5.2.3 Gravity Threshold and Optimal Gaits

The energetics data can be investigated further to reveal the possibility of a gravity level threshold for low speed walking at low gravity levels. The notion of minimum cost of locomotion identifies optimal gaits for partial gravity locomotion. It supplements the hypothesis that a change in mechanics takes place during partial gravity locomotion.

The energy consumption data reveal that subjects consume less oxygen for partial gravity simulations as compared to approximate 1 g levels, but there is a nonmonotonic reduction in workload for locomotion at 0.5 m/s (Recall Figures 5.16 and 5.19). Averaging the data across all subjects shows a slight gravity effect on \dot{V}_{O_2} for walking at 0.5 m/s. Although, half of the individual subjects' (3/6) oxygen consumption measurements show significantly lower \dot{V}_{O_2} ($p < 0.05$) when comparing Martian and lunar simulations. Figure 5.26 depicts the workload results of these three subjects.

The data suggest a gravity level threshold, or optimum loading level, close to Martian gravity (3/8 g). Lunar locomotion at 0.5 m/s could elicit higher oxygen uptake due to energy expenditure for walking as well as energy expenditure for retaining stability and posture control. Auxiliary evidence that supports the gravity level threshold idea is that during training sessions some subjects skull the water with their hands to provide additional stability during the lowest gravity simulations (i.e., microgravity and lunar gravity). Subjects are not allowed to skull the water under any gravity condition once they are considered trained and formal data collection commenced. While walking at 0.5 m/s during the Martian simulations, subjects' comments reveal that 3/8 g is the

"optimal, and most comfortable" simulated partial gravity level. These findings recommend further studies regarding increased energy expenditure for locomotion in low gravity levels (between 0 g and 3/8 g). Also, supplemental physiological measuring techniques, such as, EMG recordings from the antigravity postural muscles might show increases in muscle activity for locomotion at low gravity levels.

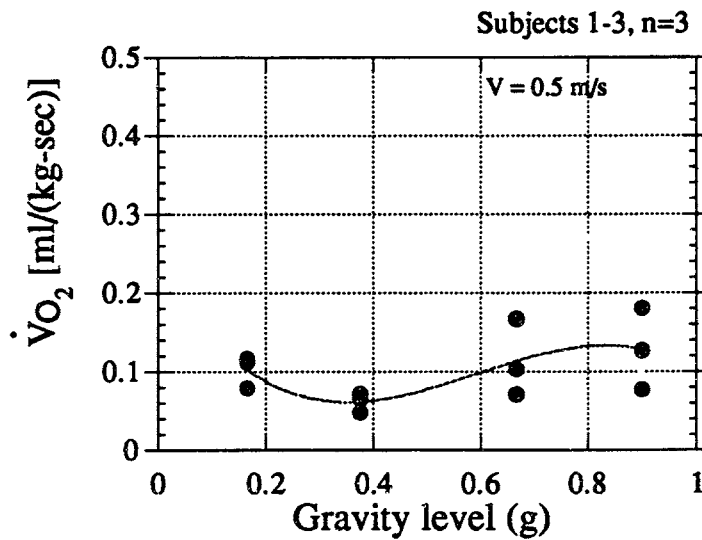


Figure 5.26 Oxygen uptake, \dot{V}_{O_2} , for Subject 1-3 walking at 0.5 m/s versus simulated gravity level. Workload decreases as gravity level is reduced from 9/10 g to 3/8 g. A slight increase in \dot{V}_{O_2} is seen from 3/8 g to 1/6 g which leads to the hypothesis of a gravity level threshold. For erect locomotion, some gravitational loading may be helpful. Subjects might require energy at 1/6 g to maintain stability and posture control in addition to energy used for walking.

Minimum Cost of Locomotion and Specific Resistance

Choosing the most efficient gait during movement minimizes the energetic cost of locomotion. The notions of minimum cost of transport and specific resistance offer additional dimensions to interpret the underwater locomotion energetics measurements. Also, the underwater results are compared to published results in which a suspension system is used to simulate partial gravity.

Recall that Section 2.2.1, Introduction to the Determinants of Human Gait, claims the functional significance of the characteristics of gait is to minimize energy expenditures. The minimum cost of locomotion (or cost of transport) per unit distance can be defined as the ratio of steady-state oxygen consumption over speed. Each subject requires a different metabolic expenditure to travel the same distance, therefore, in order to compare across subjects the energy expenditures are normalized by the mass of each subject. Equation 5.11 defines the minimum cost of transport.

$$\text{Minimum Cost of Transport} = \frac{\text{Energy Required}}{\text{Velocity} \cdot \text{Mass}} \quad (5.11)$$

Historically, the notion of minimum cost of locomotion is derived from a dimensionless engineering metric known as specific resistance. Full [1991] notes that specific resistance finds utility in comparisons of economies of vehicles and is defined as the amount of energy required to travel a given distance per unit weight and therefore includes a gravity term (See Equation 5.12). Specific resistance can be thought of as a tractive force per unit weight.

$$\text{Specific Resistance} = \frac{\text{Energy Required}}{\text{Velocity} \cdot \text{Mass} \cdot \text{Gravitational Acceleration}} \quad (5.12)$$

There exists a well documented optimal cost of transport for terrestrial walking at the speed of 1 m/s [Margaria, 1976]. In terms of metabolic expenditure, it costs about half the amount of energy to walk 1.67 km (1 mile) as compared to running 1.67 km. Is there a similar optimal cost of transport for locomotion on other planets and is walking the most economical gait?

Walking at 1 m/s is not the least expensive method of transporting one kg of body mass over one meter in partial gravity. Figure 5.27 verifies this claim and shows the cost of transport versus speed of locomotion for partial gravity. Surprisingly enough, running at the intermediate and fast speeds elicits a cheaper cost of transport. For the 9/10 g and 2/3 g gravity levels, the minimum cost of transport seems to occur at the intermediate speed of 1.5 m/s. For gravity levels approaching 1 g (9/10 g simulation), the cost of transport is similar for the intermediate and fast treadmill velocities. Cost of transport for the lunar (1/6 g) and Martian (3.8 g) conditions decreases as speed increases, suggesting that quicker locomotion is cheaper in terms of cost of transport. This result finds support in the literature when a suspension system is used to impart partial gravity [Farley, 1991]. Results from the suspension system at the Harvard University Field Station (HFS) indicate that "walking is not the cheapest way to travel a unit distance at all gravity levels" [Farley, 1991, pg. 50]. Above 1/2 g, the study reports a lower cost of transport for walking than for running, but from 1/4 g to 1/2 g running is cheaper than walking in terms of cost of transportation [Farley, 1991].

Figure 5.28 plots CoT versus gravity level and shows that walking a unit distance is less economical in terms of energetics than running at higher speeds. The mean for all subjects is plotted and the error bars are the standard errors of the means. The cost of transport is lower at 2.3 m/s than at 1.5 m/s and walking at 0.5 m/s. Table 5.2 displays statistical analysis using the

Student's *t* test measure to determine the significance of differences in cost of transport calculations. Statistical measures are reported to be significant if the *t* statistic is greater than the 95th percentile, often denoted $p < 0.05$.

During the underwater experiments, the cost of transport for moving at 1.5 m/s and 2.3 m/s is significantly less than walking at 0.5 m/s for lunar gravity (1/6 g). For Martian gravity (3/8-g), the cost of transport for loping at 2.3 m/s is significantly lower than walking at 0.5 m/s. For 2/3 g, there is a 26% reduction in the cost of transport between walking and running, but the difference is not statistically significant at the 95% level. For close to 1 g loading (9/10 g) a 26.4% reduction in cost of transport is seen, but the difference is not statistically significant. Figure 5.29 compares the underwater cost of transport data to data from the HFS suspension system partial gravity simulator. The HFS data reveals running to be the most economical gait at low gravity while walking is more economical at 1 g.

These results answer the question previously posed regarding the most efficient gait for planetary locomotion. Loping and running on other planets, specifically, the moon and Mars, are optimal gaits while walking at a two-thirds gravity simulation and Earth gravity is optimal in terms of cost of transport.

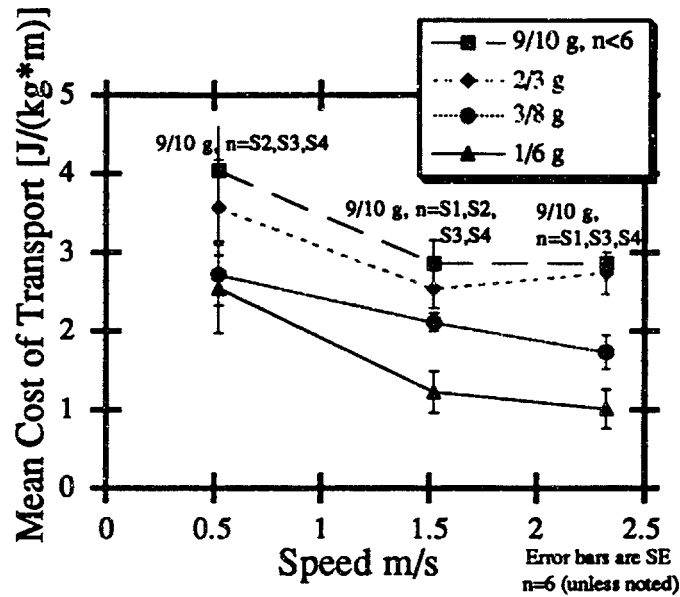


Figure 5.27 Cost of transport (CoT) versus treadmill velocity. Each point is the mean and the error bars are the standard errors of the means. Cost of transport decreases as speed increases and as gravity level is reduced. The cost of transport has units of $J/(kg \cdot m)$ and is calculated by multiplying the energy expenditure [$ml/(kg \cdot sec)$] by the energetic equivalent of 20.1 J per ml O_2 and then dividing by the treadmill velocity [Farley, 1991]. This is a standard conversion factor to convert oxygen uptake to an energy measurement [Blaxter, 1989].

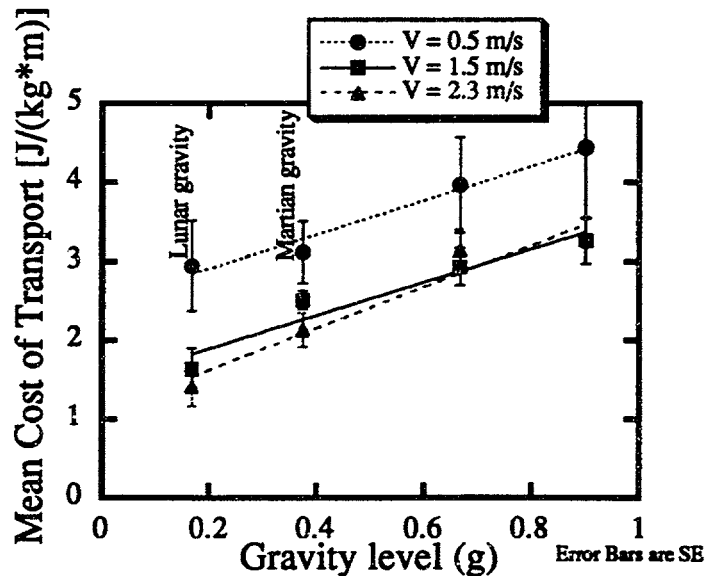


Figure 5.28 Cost of transport (CoT) versus gravity level. Each point is the mean and the error bars are the standard errors of the means. The fastest gaits (running and loping) cost significantly less in terms of CoT than walking at low gravity levels ($p < 0.05$).

Table 5.2 Statistical Values for Cost of Transport Measures Across Gravity Levels.

Gravity	Treadmill Velocity	Student's <i>t</i> Value	CoT Statistics
1/6 g	0.5 m/s	<i>t</i> = 2.08	<i>p</i> < 0.05
	1.5 m/s		
3/8 g	0.5 m/s	<i>t</i> > 2.08	<i>p</i> < 0.05
	2.3 m/s		
2/3 g	0.5 m/s	<i>t</i> = 2.22	<i>p</i> < 0.05
	2.3 m/s		
9/10 g	0.5 m/s	<i>t</i> = 1.58	<i>p</i> < 0.1
	2.3 m/s		

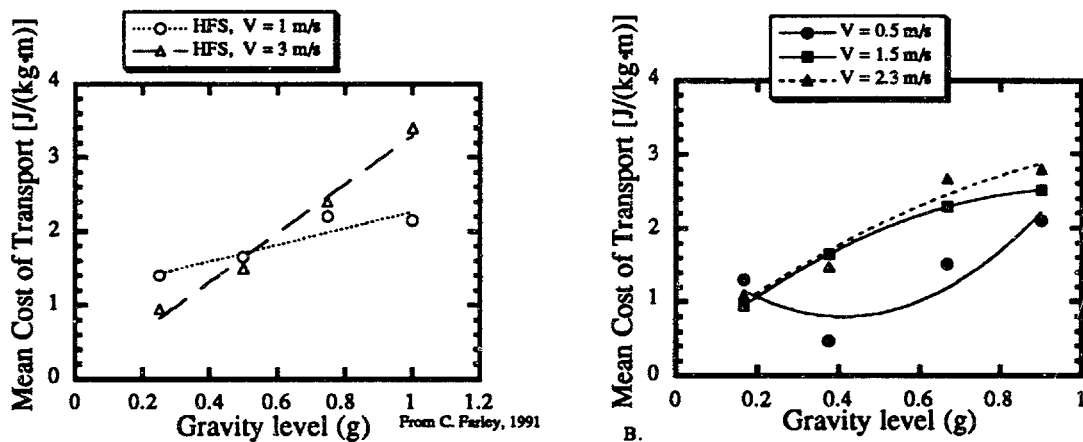
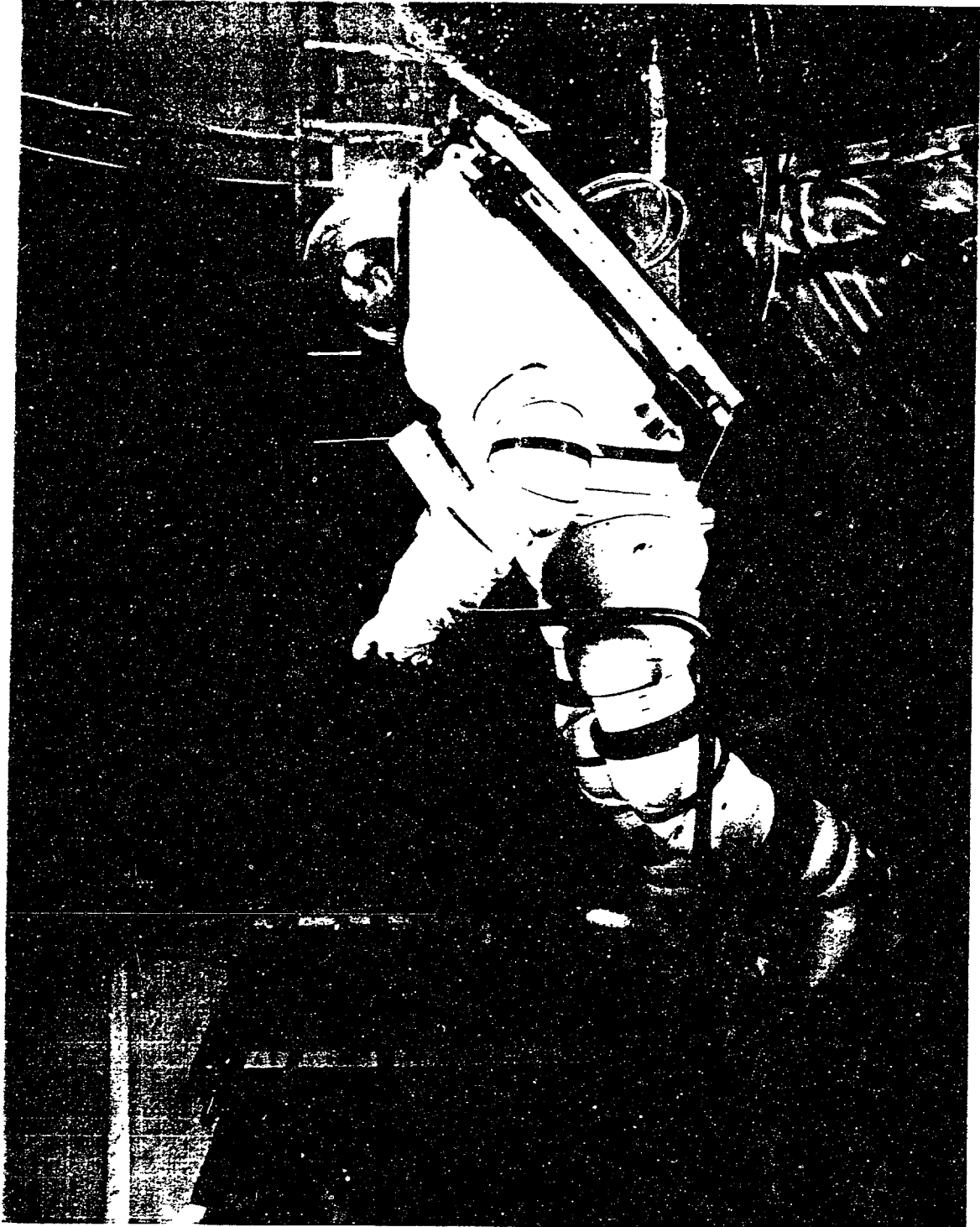


Figure 5.29 Cost of Transport (CoT) versus gravity level. All data points have the resting metabolic cost subtracted out, thus the CoT results show the extra energy cost of locomotion for the various gravity levels. A) Data extrapolated from HFS suspension system [Farley, 1991]. Running at 3 m/s is seen to be more economical at gravity levels below 1/2 g and walking at 1 m/s is the most economical gait from 1/2 g to 1 g. B) Mean CoT data from underwater partial gravity simulation for the subjects who were able to reach steady-state workload levels for every gravity condition (n=3). For immersion, running (specifically, a loping gait) is seen to be the most economical for lunar gravity. Walking is seen to be most economical at higher gravitational accelerations. The discrepancy in the HFS and submersion data is attributable to differences in simulation environment and experimental protocols (i.e., treadmill velocity).

VI. SUMMARY AND CONCLUSIONS



*"What are you? From where did you come? I have never seen anything like you."
The Creator Raven looked at the Human and was...surprised to find that this
strange new being was so much like himself.*

- An Eskimo creation myth

CHAPTER VI. SUMMARY AND CONCLUSIONS

This thesis investigates the role gravity plays in the mechanics and energetics of human locomotion. Gravity plays a crucial role in human locomotion, but there is no clear understanding of this role. Humans have evolved in an Earth-normal one gravity (1 g) environment and the development of our 1 g musculoskeletal system optimizes performance under Earth gravity conditions where the gravitational acceleration is constant at 9.8 m/s^2 . Chapter I, Introduction, provides a review of the literature and presents the main hypothesis of the thesis, namely, that the mechanics and energetics vary for partial gravity conditions compared to terrestrial 1 g conditions. If the hypothesis is true, then compensating mechanisms take place during partial gravity locomotion. The goal of the thesis was to investigate the mechanics of locomotion for a variety of simulated partial gravity levels and to reveal the associated energetic expenditures for partial gravity locomotion.

The Introduction identifies the important research questions and presents the contributions of the thesis. A research effort is proposed to 1) identify the natural gaits for partial gravity locomotion at given speeds; 2) investigate transitions between gaits; and 3) assess the metabolic cost of partial gravity locomotion. The contributions of the thesis include 1) a scientific investigation of biomechanics and energetics for a full range of partial gravity simulations (including lunar and Martian environments); 2) a comparison of multiple simulation techniques; 3) a unique submersible treadmill design that provides comprehensive analysis for every gait; 4) quantification of metabolic cost during partial gravity walking and running; and 5) a database to be used in future designs of advanced spacesuits, vehicles, and planetary habitats.

Chapter Two presents background on work physiology and locomotion and discusses models for walking and running. The energy conserving mechanism in human walking, similar to an inverted pendulum, results in an exchange of gravitational potential energy and forward kinetic energy. Humans vault over their stance limbs making this exchange of energy possible [Farley, 1991]. The magnitudes of PE and KE are roughly equivalent and opposite in phase, which result in very efficient energy exchange. The muscles and skeleton must support the body during walking. Fluctuations in gravitational potential energy and forward kinetic energy for humans running are different from walking. Gravitational PE and forward KE are in phase during running which suggests that the energy conserving inverted pendulum mechanism used in walking is not a valid model for human running. The lack of an energy conserving mechanism explains why running elicits twice the energy consumption of walking on the level (in 1 g).

Muscles, ligaments, and tendons are recruited during running and humans spring off the ground much the same as a hopping kangaroo. The elastic storage of energy seems to govern running gaits and the leg-spring model emulates the storage and release of elastic energy. In order to support the weight of the body during running, muscles are activated and the associated energetic cost is proportional to the amount of force generated [Farley, 1991; McMahon and Cheng, 1990; and Full, 1991]. Assuming that force generation reflects metabolic cost, then the energetics of running should vary directly with gravitational acceleration.

Chapter III, Simulation Environment and Modeling, describes the partial gravity simulation techniques with a focus on underwater submersion since it is the primary simulation technique of this study. A hydrodynamics model assesses the magnitude of the drag force acting on a subject's limbs during partial gravity locomotion (See computer program in Appendix A). The hydrodynamic drag force is negligible in this study, and low speed underwater locomotion on a treadmill provides a viable partial gravity simulation technique.

The Methods Chapter describes the subjects who participated in the experiments (both underwater and parabolic flights), outlines the experimental protocol, and describes the equipment used for the study. Six healthy paid subjects, four men and two women, participated in the underwater locomotion and energetics experiments while two healthy males volunteered to serve as the primary subjects in the complementary parabolic flight experiments. Subjects range in age from 24 to 39 years, height from 1.66 to 1.83 m, and weight from 578 to 801 N. Subjects participated in underwater experiments at the Neutral Buoyancy Test Facility (NBTF) located at NASA Ames Research Center (ARC), Moffett Field, California. The underwater experiments assess human performance for numerous partial gravity levels (1/6 g, 3/8 g, 2/3 g, and 9/10 g) and are complemented by parabolic flight experiments for lunar (1/6 g) and Martian (3/8 g) gravity levels. Parabolic flights using NASA's KC-135 aircraft took place in conjunction with NASA Johnson Space Center (JSC) and were flown out of Ellington Field, Texas.

The major design contribution of this research effort is the patent-pending human-rated submersible treadmill. The novel design incorporates a split-plate force platform embedded under the belt to provide biomechanics analysis for partial gravity locomotion. The split-plate design allows for a complete biomechanics analysis of all gaits. In other words, peak force, stride length, contact time, and aerial time measurements can be made from the force traces of a subject walking, loping, or running. The treadmill-mounted force platform offers many advantages over standard laboratory force platforms. A plethora of force traces are collected in only a few seconds and altered stride frequency and gait transitions are studied.

Chapter Five presents and discusses the experimental results. Subjects are capable of walking, loping, and running during partial gravity locomotion. A change in the mechanics of progression from typical walking and running to loping is seen for the lunar and Martian gravity level simulations at 1.5 m/s and 2.3 m/s. Peak forces are significantly reduced as gravity level is decreased. Contact time remains constant across gravity levels and stride frequency decreases as gravity is reduced, resulting in longer strides. The energetics results reveal a significant reduction in oxygen consumption for locomotion at low gravity compared to Earth normal 1 g. At extremely low gravity levels, subjects may be below the threshold for legged locomotion. It is hypothesized that they use energy to attain posture control and stability besides using energy for locomotion.

A mathematical model for running in terrestrial animals [McMahon and Cheng, 1990] was applied to the experimental results to assess the extent to which theory predicts the biomechanics of partial gravity locomotion. The dimensionless parameters introduced for the running model of McMahon and Cheng investigate the spring-like characteristics of muscular activity during running and analyze the interactions among gravity, speed, and stiffness parameters for locomotion. The mathematical model was modified to reflect the experimental protocol of this partial gravity study. Significant findings reveal that the mass-spring model for running predicts some of the dynamics of partial gravity locomotion. The peak force is seen to be significantly reduced at low gravity levels both in theory and experiments, and force increases with dimensionless horizontal speed. The spring stiffness of the leg is independent of gravity level, while the effective vertical spring stiffness increases as a function of horizontal speed. The model predicts the initial leg angle for the model at 2.3 m/s, but fails to predict the leg angle for locomotion at 1.5 m/s. The dimensionless vertical landing velocity calculated from experimental data is relatively constant at 0.2 and agrees with theoretical predictions.

Steady-state energy expenditures are revealed through gas analysis of oxygen consumption and heart rate measurements. In concurrence with theoretical predictions, the experimental energy expenditure results for lunar gravity (1/6 g), Martian gravity (3/8 g), and two-thirds gravity (2/3 g) are less than energy requirements for 1 g locomotion. Oxygen uptake measurements, \dot{V}_{O_2} , decrease as gravity level changes from 1 g to 1/6 g, however, the decrease is nonmonotonic in over half the subject population for walking at low gravity levels. It is hypothesized that a gravity threshold may exist, and energy expenditures below this threshold increase for low speed locomotion as excess energy is spent maintaining posture control and stability besides the energy expended for walking. Also, the most economical means of transportation in partial gravity are questioned. For 1 g locomotion walking is the most economical means of transportation, but it

turns out that loping for lunar and Martian gravity conditions is the most efficient gait in terms of cost of transportation.

A notable change in the mechanics of running stems from a reduction in the vertical component of force that significantly decreases with the acceleration of gravity. Assuming that energy expenditure is a function of the muscular force required to support the weight of the body during running, the reduction in energy expenditure makes sense for partial gravity locomotion because less weight has to be supported, therefore, less leg muscle recruitment is necessary. Less energy is required as a result of the reduced work against gravity. If the amount of force produced is a major determinant of metabolic cost and the kinematics of locomotion show little alteration, then cost of running should vary directly with gravitational acceleration. However, the experimental results show changes in the kinematics of running (i.e., altered accelerations of the center of mass and reductions in stride frequency), thus the rate at which muscles must develop force to support the body's mass against gravity is altered. The nonlinear reduction in metabolic cost suggests that both the amount of force produced and the rate of force developed are important variables in understanding the dynamic adjustments taking place during partial gravity locomotion.

The results of this study are applicable to planetary spacesuit design, artificial gravity vehicle design, and planetary habitat design. The designers of lunar and Martian locomotion spacesuits can use the data revealing reductions in peak force and stride frequency in their concepts. Spacesuits should provide uninhibited locomotion during planetary EVAs by incorporating the necessary characteristics of gait into the design. For example, a waist bearing should be included to provide pelvic rotation and pelvic tilt during locomotion; boots should have an ankle joint to allow for ankle plantar flexion. The data presented herein serves as an initial biomechanics database and additional studies could assess the total impact partial gravity has on the musculoskeletal system; these data could help solve the debate over artificial gravity space vehicles for a human mission to Mars. Although it is possible for subjects to perform *superhuman tasks* like jumping 6-7 times higher in partial gravity, bipeds are seen to travel similarly to terrestrial means. People typically travel by using a one foot take-off, then they apply enough force on the ground to fly-up in the air a few centimeters (incorporating a slightly elongated stride length), and then use the other leg in the same manner. Designers of planetary habitats should consider these partial gravity human performance characteristics. Life support system requirements for advanced spacesuits, vehicles, and planetary habitats should incorporate data from partial gravity simulations and not rely solely on extrapolation from 1 g data. This is an important contribution because significant reductions in oxygen consumption seen during lunar and Martian simulations can be

realized in smaller, lighter life support system designs, rather than using conventional designs which accommodate subjects for terrestrial oxygen consumption needs.

For all that has been -- Thanks!

To all that shall be -- Yes!

- Dag Hammarskjöld

APPENDIX A : COMPUTER PROGRAMS

A.1 HYDRODYNAMICS MODEL

A computer program named "Legs"^{A.1} was written in the C programming language to calculate the hydrodynamic drag energy of a subject moving his/her legs through the water during the underwater partial gravity locomotion study.

Section 3.2.2.1, Calculating the Drag Energy, described the mathematical calculations that are implemented in the Legs program. A listing of the Legs program is included in this Appendix. The main program is entitled legsmain.c. The calculations are based on input data from subjects' anthropometric measurements and digitized video images of underwater locomotion. The three main sections of the program are input, drag calculation, and output.

Legs contains numerous subprograms. A listing of the primary subprograms follows and the program itself contains descriptive comments for each subprogram.

abc	gen_dim	outfile
adjust	getname	outxv
calc_const	get_stride_name	simpson
current_results	input	stime
dig_data	makefile	stride
dim_read	make_dims	take_names
eqsol	make_mot	time_read
fill_position	mot_read	wabc
fill_velocity	outdim	wx
final_result	outdt	

^{A.1} Acknowledgment of thanks to Mark P. Hurst, Man-Vehicle Laboratory UROP, M.I.T.

Legs Project

Dava Newman

Mark Hurst (UROP)

All procedures include the two libraries `stdio.h` and `def.h`

```
#include <stdio.h>
#include <def.h>

/* legsmain.c */

double v[JNT][DIR][MAXT]; /* array of velocity vectors for each of 3 joints */
double x[JNT][DIR][MAXT]; /* array of position vectors for each of 3 joints */
double al[DIR][SEG]; /* A,B,C for segments 1 -> 2 */
double as[DIR][SEG]; /* a,b,c for segments 1 -> 2 */
double fl[SEG]; /* upper and lower leg lengths (respectively) */
int curtime; /* current simulation time increment */
double height,thihd,kneed,ankd; /* four model dimensions, as it is now --
/* height and three diameters - thigh, knee, and ankle */
char dimname[CHAR], motname[CHAR], outname[CHAR];
/* names of program files:dimension,motion,output */

main ()
{
    int ndt; /* number of time increments in simulation */
    double limdrag = 0.0; /* drag energy on limbs and torso */
    double totdrag = 0.0; /* final sum of drag energy for entire simulation */
    double const; /* something to do with drag coefficient and RHO */

    /* *****
    /* Assemble all model data by reading data files and
    /* making some calculations
    /* *****

    take_names ();
    /* take_names gives the user the option of making new input (dimension
    /* or motion) files. If the user chooses not to make new files and instead
    /* chooses to begin a drag calculation, the functions below are called. */

    input(); /* input names of motion and dimension files */
    dim_read (); /* read in dimensions from dimfile */
    mot_read (&ndt); /* get ndt and v and x data from motion file */

    /* Output model data to output file */
    outfile(ndt);

    /* *****
    /* Calculate model drag for entire simulation
    /* *****
    for (curtime = 0; curtime<ndt; curtime++) {
        calc_const (&const); /* calc drag constant */
        abc (); /* calc a,b,c,A,B,C for 2 segs */
        legdrag (const, &limdrag); /* calc drag on one leg */
        current_results (limdrag); /* writeout drag for curtime */
        totdrag += limdrag; /* increment total drag */
        limdrag = 0.0; /* reset value of limdrag */
    }
    final_result (totdrag); /* writeout final drag total */
}
```

```

abc()
{
extern int curtime;
extern double fl[SEG];
extern double al[DIR][SEG]; /* actually the [DIR] term refers not to the number of */
extern double as[DIR][SEG]; /* directions but to the number of vars: A,B,C; a,b,c. */
extern double v[JNT][DIR][MAXT];
extern double x[DIR][JNT][MAXT];
double xa[DIR], xb[DIR], va[DIR], vb[DIR];
/* position and velocity vectors of endpoint
joints of currently integrated segment */
double xab[DIR], vba[DIR]; /* vectors of the difference of velocity
between endpoint joints */
int loop, loop2, iseg; /* loop counters */
int ia, ib; /* distinguish the zero "reference" joint for
the integration of each segment */

double ans1,ans2,ans3;
iseg = 0; /* counter for segments - goes from 0 to SEG-1 */
loop = 0;
/* Initialize arrays */
for (loop2=0; loop2<SEG; loop2++)
    for (loop=0; loop<DIR; loop++) {
        al[loop][loop2]=0.0;
        as[loop][loop2]=0.0;
    }
for (iseg=0; iseg<SEG; iseg++) {
/* Begin loop to calculate A,B,C,a,b,c for each of
the segments - in the leg.π case, numbering 2 */
    ia = iseg;
    ib = iseg+1;
    for (loop=0; loop<DIR; loop++) {
        xa[loop] = x[loop][ia][curtime];
        xb[loop] = x[loop][ib][curtime];
        va[loop] = v[ia][loop][curtime];
        vb[loop] = v[ib][loop][curtime];
    }
/* Calculate A, B, and C for current segment */
    for (loop=0; loop<DIR; loop++) {
        xab[loop] = xb[loop] - xa[loop];
        vba[loop] = va[loop] - vb[loop];
        al[0][iseg] += SQR ( vba[loop] );
        al[1][iseg] += - (vba[loop] * va[loop]);
        al[2][iseg] += SQR (va[loop]);
    } /* for loop */
    al[0][iseg] /= SQR(fl[iseg]);
    al[1][iseg] *= 2.0 / fl[iseg];
/* al[2][iseg] isn't a function of segment length */
    cross(vba,xab,&ans1);
    cross(va,xab,&ans2);
    cross2(vba,xab,va,&ans3);
    as[0][iseg] = ans1 / SQR(fl[iseg]);
    as[1][iseg] = 2.0 * ans3 / fl[iseg];
    as[2][iseg] = ans2;
} /* iseg segment loop */
}
abstest (element,amax,flag)
double element;
double amax;

```

```

    int *flag;
{
    double temp1 = element;
    double temp2 = amax;
    absval (&temp1);
    absval (&temp2);

    if (temp1 > temp2)
        *flag = 1;
    else
        *flag = 0;
}
absval (x)
    double *x;
{
    if (*x<0.0)
        *x = -*x;
}
void adjust()
{
    double k = 375.0; /* pixels per meter */
    extern int numframes;
    extern double pt[JNT][DIR][MAXT];
    int i;

    for (i=0; i<numframes; i++) {
        pt[2][0][i] /= k;
        pt[1][0][i] /= k;
        pt[0][0][i] /= k;
        pt[2][1][i] = (300.0 - pt[2][1][i])/k;
        pt[1][1][i] = (300.0 - pt[1][1][i])/k;
        pt[0][1][i] = (300.0 - pt[0][1][i])/k;
    }
}
calc_const (const)
    double *const;

{
    extern int curtime;
    double cdx = 1.0; /* drag coefficient as function of time - right now, */
                    /* without exper. data, always set it to 1.0 */
    *const = 0.5 * RHO * cdx * DT_SIZE;
}
cross (vba,xab,answer)
    double *vba, *xab, *answer;

{
    double temp1, temp2, temp3; /* temporary variables to make documentation better */
    temp1 = *(vba+1) * (*(xab+2)) - *(vba+2) * (*(xab+1));
    temp2 = *(vba+2) * (*xab) - *vba * (*(xab+2));
    temp3 = *vba * (*(xab+1) - *(vba+1) * (*xab);
    *answer = SQR(temp1) + SQR(temp2) + SQR(temp3);
    /* Yields the SQUARE OF THE MAGNITUDE of the cross product of vba and xab:
    /*
    /*
    /*      | i   j   k |
    /* vba X xab = det | *vba *(vba+1) *(vba+2) |
    /*      | *xab *(xab+1) *(xab+2) | */

```



```

}
cross2 (vba,xab,vo,answer)
    double *vba, *xab, *vo, *answer;
{
int add1,add2,add3;
int m1,m2;
m1 = *(vo+1) * (*(xab+2)) - *(vo+2) * (*(xab+1));
m2 = *(vba+2) * (*(xab+1)) - *(vba+1) * (*(xab+2));
add1 = m1*m2;
m1 = *(vo+2) * (*(xab+0)) - *(vo+0) * (*(xab+2));
m2 = *(vba+0) * (*(xab+2)) - *(vba+2) * (*(xab+0));
add2 = m1*m2;
m1 = *(vo+0) * (*(xab+1)) - *(vo+1) * (*(xab+0));
m2 = *(vba+1) * (*(xab+0)) - *(vba+0) * (*(xab+1));
add3 = m1*m2;
*answer = (add1 + add2 + add3);
}
current_results (limdrag)
    double limdrag;
{
    extern int curtime;
    extern char outname[CHAR];
    FILE *fpin = NULL;
    printf ("curtime = %d\n", curtime);
    printf ("limdrag = %lf\n\n", limdrag);
    fpin = fopen (outname, "a");
    fcheck (fpin, "In current_results() - can't open output file.");
    fprintf (fpin, "\nTime interval %d\n", curtime);
    fprintf (fpin, "legdrag = %9.5lf\n", limdrag);
    fclose(fpin);
}
/* Reads in digitized data from a stride file by opening
stride file, reading in numframes, and reading in all
(unconverted) stride position data. */
/* REMEMBER that
/* JOINT = 0 --> HIP
/* JOINT = 1 --> KNEE
/* JOINT = 2 --> HEEL
/* Easily remembered by remembering that at Media Lab, first
/* point digitized was the HEEL - so, the first number in the
/* stride file is the HEEL coordinate. And, the first number
/* read from the stride file is joint 2. */
void dig_data (fname)
    char fname[CHAR];

{
    extern double pt[JNT][DIR][MAXT];
    extern int numframes;
    int counter;
    FILE *fpin3 = NULL;
    fpin3 = fopen(fname, "r");
    fcheck (fpin3, "Error -- Unable to open stride file.");
    skipline(fpin3);
    fscanf (fpin3, "%d", &numframes);
    printf ("\nnumframes = %d\n\n", numframes);
    skipline(fpin3);
    skipline(fpin3);
}

```

```

        for (counter=0; counter<numframes; counter++) {
            fscanf (fpin3, "%lf", &pt[2][0][counter]);
            fscanf (fpin3, "%lf", &pt[2][1][counter]);
            fscanf (fpin3, "%lf", &pt[1][0][counter]);
            fscanf (fpin3, "%lf", &pt[1][1][counter]);
            fscanf (fpin3, "%lf", &pt[0][0][counter]);
            fscanf (fpin3, "%lf", &pt[0][1][counter]);
        }
    fclose(fpin3);
}
/* dim_read
/* Opens and reads the dimension file being used
/* in the drag calculation, and reads in the four
/* parameter values. ABSTRACTION VIOLATION: Remember
/* that if more segments are added that the fl[] array,
/* which is filled here, will have to be modified. */
dim_read ()
{
    FILE *fpin = NULL; /* file pointer to dimension file being read */
    extern double height; /* height value in dimension file */
    double ankc, thihc, xneec; /* values in dimension file */
    extern double thihd, kneed, ankd; /* upper, middle, lower leg joint diameters */
    extern char dimname[CHAR]; /* name of dimension file to be read */
    extern double fl[SEG]; /* upper and lower leg lengths ([0] and [1]), resp. */
    char ignore[6]; /* string used in skipping over text in dimension file */

    fpin = fopen (dimname,"r");
    fcheck (fpin, "Error -- Unable to open the dimensionfile.");
    printf ("\nUsing dimensionfile named %s.\n", dimname);
    fscanf (fpin, "%s%lf", ignore,&height);
    fscanf (fpin, "%s%lf", ignore,&ankc);
    fscanf (fpin, "%s%lf", ignore,&thihc);
    fscanf (fpin, "%s%lf", ignore,&xneec);
    fclose (fpin);

    thihd=thihc/PI;
    kneed=xneec/PI;
    ankd=ankc/PI;

    /* put upper and lower leg lengths into fl array */
    fl[0]= 0.245 * height; /* upper leg length */
    fl[1]= 0.246 * height; /* lower leg length */
}

dot (product,vx,x12)
    double *product;
    double vx[3];
    double x12[3];
{
    double temp1,temp2,temp3;
    temp1 = x12[1]*vx[1];
    temp2 = x12[2]*vx[2];
    temp3 = x12[3]*vx[3];
    *product = temp1 + temp2 + temp3;

#include <stdio.h>
eqsol (ary,n,x)

```

```

    double ary[3][4];
    int n;
    double x[3];
{
    int m[3], lp1, lp2, lp3;
    double amax=0;
    int flag=0;
    int nn;
    int mmm, zmult;
    int no;
int i, j;
    for (lp1=0; lp1<n; lp1++) {
        m[lp1] = 0;
        amax = ary[lp1][0];
        for (lp2=1; lp2<n; lp2++) {
            abtstest(ary[lp1][lp2], amax, &flag);
            if (flag==1) {
                m[lp1]=lp2;
                amax=ary[lp1][lp2];
            }
        }
        if (amax==0) no_solution();
        nn=n+1;
        for (lp2=0; lp2<nn; lp2++)
            ary[lp1][lp2] /= amax;
        for (lp3=0; lp3<n; lp3++)
            if (lp3 != lp1) {
                mmm = lp1;
                zmult = ary[lp3][mmm];
                for (lp2=0; lp2<nn; lp2++) {
                    if (lp2!=mmm)
                        ary[lp3][lp2] += (-zmult*ary[lp1][lp2]);
                    else
                        ary[lp3][lp2] = 0.0;
                }
            }
    }
    for (lp1=0; lp1<n; lp1++) {
        no=m[lp1];
        x[no] = ary[lp1][nn];
    }
}
/* fcheck
/* If a given file pointer is equal to NULL,
/* print to the screen a given error message.
/* The user should then exit the program. */

#include <stdio.h>
#include <def.h>

void fcheck(fp, error)
    FILE *fp;
    char *error;

{
if (fp == NULL) {

```

```

    printf ("%s\n\n", error);
    printf ("Please exit the program now.");
    hitakey2();
    hitakey2();
    hitakey2();
}

/* fill_position
/* Inserts position (pt[][][]) data into the
/* motion file being created. */
void fill_position()
{
    /* x[][][] is the position array for all the segments for all
    the simulation time.

    TIME 0:
           DIR
           0   1   2
    JNT  0 x[0][0][0] x[1][0][0] x[2][0][0]
        1 x[0][1][0] x[1][1][0] x[2][1][0]
        2 x[0][2][0] x[1][2][0] x[2][2][0]
    TIME 1:

        another 3x3 array.
    TIME t:
        another 3x3 array, until numframes-1 is reached. */
    extern double pt[JNT][DIR][MAXT];
    extern double x[JNT][DIR][MAXT];
    extern char motname[CHAR];
    extern int numframes;
    double temp;
    int t,j,d; /* counters for time, joints, and direction */
    FILE *fpin;
    fpin = fopen (motname, "a");
    fprintf (fpin, "Position array for %d increments\n", numframes-1);
    /*
    for (t=0; t<numframes-1; t++) /* use numframes-1 positions for the array */
        for (j=0; j<JNT; j++) {
            for (d=0; d<DIR; d++) {
                temp = pt[j][d][t];
                fprintf (fpin, "%.3e %t", temp);
            }
            fprintf (fpin, "\n");
        }
        fprintf (fpin, "\n\n");
    }
    fclose (fpin);
}

/* fill_velocity
/* Inserts velocity data into the motion file being
/* created from stride data. DT_SIZE is accessed
/* from def.h. This is OK, and should be kept so. */
#include <stdio.h>
#include <def.h>
void fill_velocity()
{

```

```

/* v[][] is the velocity array for all the segments for all
the simulation time.

TIME 0:
          DIR
          0   1   2
0 v[0][0][0] v[1][0][0] v[2][0][0]
JNT 1 v[0][1][0] v[1][1][0] v[2][1][0]
      2 v[0][2][0] v[1][2][0] v[2][2][0]

TIME 1:
another 3x3 array.
TIME t:
another 3x3 array, until numframes-1 is reached. */
extern double x[JNT][DIR][MAXT];
extern double v[JNT][DIR][MAXT];
extern double pt[JNT][DIR][MAXT];
extern char motname[CHAR];
extern int numframes;
double temp;
int t,j,d; /* counters for time, joints, and direction */
FILE *fpin;
fpin = fopen (motname, "a");
fcheck (fpin, "Can't append to the motion file.");
printf ("Appending motionfile named %s.\n", motname);
for (t=0; t<numframes-1; t++) { /* use numframes-1 positions for the array */
    for (j=0; j<JNT; j++) {
        for (d=0; d<DIR; d++) {
            temp = (pt[j][d][t+1] - pt[j][d][t])/DT_SIZE;
            fprintf (fpin, "%.3e %t", temp);
        }
        fprintf (fpin, "\n");
    }
    fprintf (fpin, "\n\n");
}
fclose (fpin);
}

final_result (totdrag)
double totdrag;
{
    extern char outname[CHAR];
    FILE *fpin = NULL;
    fpin = fopen (outname, "a");
    fprintf (fpin, "\n\ntotal simulation drag = %9.5lf\n", totdrag);
    fclose (fpin);
    printf ("\ntotdrag = %9.5lf\n", totdrag);
    printf ("End program.\n");
    hitakey20;
}

/* gen_dim
/* Prompts the user for a value (type long float,
/* or double) for a given parameter name (type
/* string). It then prints the value to a file
/* with a given file pointer. */

```

```

gen_dim (param, fpin)
char *param;
FILE *fpin;
{
    double temp;
    printf ("%s ", param);
    scanf ("%lf", &temp);
    fprintf (fpin, "%s\\%.2e\\n", param, temp);
}

void getline (s, lim)
char s[],
int lim;
{
    int c, i;
    i=0;
    while (--lim<0 && (c=getchar()) != EOF && c != '\\n')
        s[i++] = c;
    if (c == '\\n')
        s[i++] = c;
    s[i] = '\\0';
}

getline (name)
char name[CHAR];
{
    char c;
    int i;
    printf ("\\n");
    for (i=0; (c = getch()) != '\\n'; ++i) {
        if (c == '/') {
            name[i-1] = ";";
            i-=2;
        }
        else
            name[i] = c;
        printf ("%s\\n", name);
    }
}

void get_stride_name (name)
char name[CHAR];
{
    FILE *fpin2 = NULL;
    int i;
    for (i=0; i<15; i++)
        name[i]=" ";
    printf ("\\nTo construct a motion file, you need a formatted \\n");
    printf (" file of digitized stride data.\\n");
    printf ("\\nInput the name of the stride file.\\n");
    printf ("If the file is somewhere but in the current directory,");
    printf ("you won't be able to input the file.\\n");
    printf ("\\nStride file name : ");
    scanf ("%s", name);
    printf ("\\n");
    fpin2 = fopen(name, "r");
    if (fpin2 == NULL) {
        printf ("Error -- Unable to open file.\\n");
        printf ("Try another name.\\n\\n");
        get_stride_name (name);
    }
}

```

```

        else
            fclose(fpin2);
    }
    hitakey2 ()

    {
        char trash;
        printf ("\nHit RETURN to continue.\n");
        scanf ("%c", &trash);
        printf ("\n");
    }

void initialize()
{
    extern double pt[JNT][DIR][MAXT];
    int j,d,t;
    for (j=0; j<JNT; j++)
        for (d=0; d<DIR; d++)
            for (t=0; t<MAXT; t++)
                pt[j][d][t] = 0.0;
}

/* input
/* This subroutine simply gets the NAMES of the four input files
/* that will be used in the simulation. It gets names only, not
/* any data. The only other subroutine it calls is getname(). */
input ()
{
    extern char dimname[CHAR], motname[CHAR], accname[CHAR], timename[CHAR];
    /* input one of four files: dimensions, motions, accels, time */
    printf ("\nInput names of the two input files :\n\n");
    printf ("Dimension file: ");
    scanf ("%s", dimname);
    printf ("Motion file: ");
    scanf ("%s", motname);
}

int coef[NUMPOINTS]; /* array of coefficients for integration by Simpson's
method; the number of elements equal the number of
integrating points along the integrated segment */

legdrag (const,ed)
double const;
double *ed; /* leg drag energy in current time increment */
{
    extern int curtime;
    extern double fl[SEG];
    int flag;
    double sum; /* integration approximation by Simpson's rule */
    int loop;
    *ed = 0.0; /* redundant - limdrag already set to zero on in legsmain - */
    /* but better safe than sorry in this case. */
    for (loop = 0; loop < SEG; loop++) {
        flag = loop + curtime;
        simpson (fl[loop],flag,&sum,loop);
        *ed += sum * const / fl[loop];
    }
    /* Here we double *ed, the drag energy for one leg, so that it equals */
}

```

```

        /* the drag energy for TWO legs. This is the ONLY place in */
        /* the program where the energy should be doubled for two */
        /* legs. */
        *ed *= 2.0;
    }
    /* makefile
    /* Gives the user a choice of creating a new motion
    /* or dimension file, or of quitting the program.
    /* makefile appropriately calls the make_() procedure
    /* for whichever file the user wants to create.
    /* Note that procedure info() is listed after makefile.*/

makefile ()
{
    int choice = 0;
    info();
    scanf ("%d", &choice);
    if (choice == 1) make_mot();
    else if (choice == 2) make_dims();
    while (choice != 3) {
        info();
        scanf ("%d", &choice);
        if (choice == 1) make_mot();
        else if (choice == 2) make_dims();
    }
}

/* make_dims
/* Creates a new dimension file with a
/* user-specified name. The file contains
/* four parameter names (height, ankc, thihc,
/* and xnec) and corresponding values. */
make_dims ()

{
    FILE *fpin = NULL;
    extern char dimname[CHAR];
    printf ("Making dimension file:\n\n");
    printf ("What will be the name of your new dimension file? ");
    scanf ("%s", dimname);
    printf ("\n");
    fpin = fopen (dimname, "w");
    printf ("\n");
    gen_dim ("height", fpin);
    gen_dim ("thihc", fpin);
    gen_dim ("xnec", fpin);
    gen_dim ("ankc", fpin);
    printf ("End of input for %s.\n", dimname);
    fclose (fpin);
}

/* make_mot
/* Creates a motion file containing
/* position and velocity data from the
/* stride data of a stride file. */
double pt[JNT][DIR][MAXT];
/* double nath = 0.03; */
int numframes;

```



```

char stridename[CHAR];
void make_mot()

{
    FILE *fpin = NULL;
    extern char motname[CHAR], accname[CHAR], timename[CHAR];
    get_stride_name (stridename);
    printf ("Using stridename %s.\n", stridename);
    stride_convert();
    stime();
    fill_position();
    fill_velocity();
}

/* mot_read
/* Given a motion file name, opens the file
/* and reads: (1) ndt, the number of time increments
/* in the simulation; (2) position data, which proceeds to
/* fill the x[][][] array; and (3) velocity data, which
/* fills the v[][][] array. */

void mot_read (ndt)
    int *ndt;

{
    FILE *fpin = NULL;
    extern double x[JNT][DIR][MAXT], v[JNT][DIR][MAXT];
    extern char motname[CHAR];
    int tinc; /* counter showing current time increment (1->*ndt)*/
    int dir; /* counter showing current direction (xyz) */
    int joint; /* counter showing current joint (1->3) */
    fpin = fopen(motname, "r");
    fcheck (fpin, "Error -- Unable to open the motion file.");
    printf ("Using motion file named %s.\n", motname);
    /**** ndt gets read here *****/
    /* (gets one number at varying yields) */
    fscanf (fpin, "%d", ndt);
    /**** read in x[][][] (position) array here *****/
    for (tinc=0; tinc<*ndt; tinc++)
        for (joint=0; joint<JNT; joint++)
            for (dir=0; dir<DIR; dir++)
                fscanf (fpin, "%lf", &x[joint][dir][tinc]);
    /**** read in v[][][] (velocity) array here *****/
    for (tinc=0; tinc<*ndt; tinc++)
        for (joint=0; joint<JNT; joint++)
            for (dir=0; dir<DIR; dir++)
                fscanf (fpin, "%lf", &v[joint][dir][tinc]);

    fclose (fpin);
}

outdim(fpin,name,dim)
    FILE *fpin;
    char name[CHAR];
    double dim;

{
    fprintf (fpin, "\t%s \t%.2lf\n", name, dim);
}

/* outdims

```

```

/* Outputs to output file (with given file
/* pointer) the four model dimensions. */
outdims (fpin)
    FILE *fpin;

{
    extern double height, thihd, kneed, ankd;
    double thihc, xneec, ankc;
    thihc = PI * thihd;
    xneec = PI * kneed;
    ankc = PI * ankd;
    fprintf (fpin, "\nmodel dimensions\n");
    outdim (fpin, "height", height);
    outdim (fpin, "thihc", thihc);
    outdim (fpin, "xneec", xneec);
    outdim (fpin, "ankc", ankc);
    fprintf (fpin, "\n\n");
}

/* outdt
/* Outputs to the output file the number
/* of time increments and the size of all
/* of the increments in simulation to which
/* the data pertains. */

outdt (fpin, ndt)
    FILE *fpin;
    int ndt;

{
    int j;
    fprintf (fpin, "time increment data\n\n");
    fprintf (fpin, "%d time increments.\n", ndt);
    fprintf (fpin, "For all time increments, DT_SIZE = %.4f\n\n", DT_SIZE);
}

/* outfile
/* Prompts the user for the name of an output file to
/* which to output all relevant simulation data, and then
/* creates a file with that name and outputs the data to
/* the file. Data includes dimension, position, velocity,
/* and number and size of time increments data. */

outfile (ndt)
    int ndt;

{
    extern char outname[CHAR];
    FILE *fpin = NULL;
    int t, joint, dir;
    extern double v[JNT][DIR][MAXT];
    printf ("What will be the name of your new output file? ");
    scanf ("%s", outname);
    printf ("\n");
    fpin = fopen (outname, "w");
    fcheck (fpin, "Can't create a new output file.");
    fprintf (fpin, "Output file name: %s\n", outname);
    outdims(fpin);
    outxv(fpin,ndt);
    outdt(fpin, ndt);
}

```

```

    fprintf (fpin, "\n");
    printf ("\nCreated output file named %s.\n", outname);
    fclose (fpin);
}

/* outxv
/* Given a file pointer to an output file being made,
/* outputs position and velocity data of the simulation
/* about to be run. */

outxv (fpin,ndt)
    FILE *fpin;
    int ndt;
{
    extern double x[JNT][DIR][MAXT], v[JNT][DIR][MAXT];
    int joint, dir, time;

    fprintf (fpin, "x array\n");
    for (time=0; time<ndt; time++) {
        for (joint=0; joint<JNT; joint++) {
            for (dir=0; dir<DIR; dir++)
                fprintf (fpin, " %.3lf", x[joint][dir][time]);
            fprintf (fpin, "\n");
        }
        fprintf (fpin, "\n\n");
    }
    fprintf (fpin, "\n\n");

    fprintf (fpin, "v array\n");
    for (time=0; time<ndt; time++) {
        for (joint=0; joint<JNT; joint++) {
            for (dir=0; dir<DIR; dir++)
                fprintf (fpin, " %.3lf", v[joint][dir][time]);
            fprintf (fpin, "\n");
        }
        fprintf (fpin, "\n\n");
    }
    fprintf (fpin, "\n\n");
}

simpson (x1,flag,sum,iseg)
    double x1; /* length of the current segment */
    int flag; /* tells if coefficients have been generated yet */
    double *sum; /* incremental sum of drag energy */
    int iseg; /* current segment undergoing integration */
{
    extern int coef[NUMPOINTS];
    int loop = 0;
    int leap = 1;
    double dl;
    double integrand=0.0;
    double x;

    /* NUMPOINTS = number of points of integration - now set to 21 */
    if (flag<1) {
        for ( loop = 0; loop < NUMPOINTS; loop++) {
            if ( (loop==0) || (loop == NUMPOINTS-1) )

```

```

        else {
            coef[loop]=1;
            if (leap == 1) {
                coef[loop]=4;
                leap = 2;
            }
            else /* if leap is 2 */ {
                coef[loop]=2;
                leap=1;
            }
        }
    }
}

/* Initialize the drag sum and current segment position */
*sum = 0;
x = 0;
/* Set value for delta length: dl. It equals NUMPOINTS-1 because this:
   imagine you wanted three points of integration. You would divide
   the segment in half, to yield two endpoints and a point in the middle.
   Therefore, to divide the segment into NUMPOINTS parts, divide its length
   by NUMPOINTS-1. */
dl = x1/(NUMPOINTS-1);
/* Begin x, current segment position, at -dl ; it gets incremented
   positively when the following loop begins. */
x = -dl;

/* Calculate integrand with weighted coefficients (which are functions
of NUMPOINTS) and A,B,C,a,b,c (which are functions of current velocity, position,
and segment (and time, of course)) at each of the NUMPOINTS points along
the segment. */
for (loop = 0; loop<NUMPOINTS; loop++) {
    x += dl;
    wabc (&integrand,x,iseq);
    /* The integrand is wx, a function of the current segment and the
       current integrating position x, times the ABCabc term. */
    *sum += (coef[loop]*integrand);
}
/* Divide the drag energy by three; this is just part of the
definition of Simpson's rule. */
*sum *= dl / 3.0;
}

/* skipline
/* moves a file pointer one line down in a file */
void skipline (fpin4)
FILE *fpin4;
{
    char c;
    while ((c = getc (fpin4)) != '\n')
        if (c == EOF) break;
}

/* stime
/* Prompts the user for a motionfile name, opens the new
/* motionfile, and inserts the number of time increments */
void stime()

```

```

{
    extern int numframes;
    extern char motname[CHAR];
    FILE *fpin = NULL;
    int i;
    printf ("What will be the name of your new motion file? ");
    scanf ("%s", motname);
    printf ("\n");
    fpin = fopen (motname, "w");
    fcheck (fpin, "Error -- Can't write to motion file.");
    printf ("Making motionfile named %s.\n", motname);
    /* write to the file the number of time increments */
    /* remember that number of time increments, ndt, equals
       the number of frames, numframes, minus 1 ....
       ndt = numframes - 1 */
    fprintf (fpin, "%d\n", numframes-1);
    /* close the motion file */
    fclose(fpin);
}
/* variables external to stride */
double pt[JNT][DIR][MAXT];
double nath = 0.03;
int numframes;
void stride()

{
    FILE *fpin = NULL;
    extern char motname[CHAR], accname[CHAR], timename[CHAR];
    char stridename[CHAR];
    int t;
    get_stride_name (stridename);
    printf ("stridename = %s\n", stridename);
    /* z values are zeroed for all motion here */
    initialize();
    /* 1. Get numframes.
       /* 2. Fill heel, knee, and hip arrays. */
    /* NOTE: Remember that ndt = numframes - 1. */

    dig_data (stridename);
    /* Convert units of pixels to "real" units of meters */
    adjust();
    stime();
    fill_position();
    fill_velocity();
}

/* Fills the pt[][][] (position) array by
reading in digitized data from a stride file
and adjusting the data by setting the origin
correctly. */
void stride_convert()

{
    extern double pt[JNT][DIR][MAXT];
    extern int numframes;
    extern char stridename[CHAR];
    /* z values are zeroed for all motion here */
    initialize();
}

```

```

    /* open the stride file.
    /* 1. Get numframes.
    /* 2. Fill heel, knee, and hip arrays. */
    /* NOTE: Remember that ndt = numframes - 1. */
    dig_data (stridename);
    /* Convert units of pixels to "real" units of meters */

    adjust();
}

/* take_names
/* Gives the user the choice of creating new
/* input files or conducting a drag calculation
/* using already existent input files. Also calls
/* the appropriate procedure to allow the user
/* to carry out his/er choice. */

FILE *fpin;
take_names ()

{

    int choice;
    while (choice != 2) {
        printf ("Leg project\n by Mark Hurst and Dava Newman\n\n");
        printf ("\n\n***** MAIN MENU *****\n\n");
        printf ("Options:\n");
        printf (" (1) Construct new input files to be used in drag calculations.\n");
        printf ("     - An input file is a DIMENSION file or a MOTION file.\n");
        printf ("     One of each is needed for a drag calculation.\n");
        printf (" (2) Conduct a drag calculation using already made files.\n");
        printf ("\nPlease type 1 or 2.\n");
        printf ("If you wish to exit the program, type command-Q.\n");
        scanf ("%d", &choice);
        printf ("\n");
        if (choice == 1) makefile();
    }
}

time_read (ndt)
int *ndt;
/* returns number of time increments: ndt */
/* fills dt[] and outputs (to the screen) the size of each time increment */

{

    FILE *fpin = NULL;
    extern double dt[MAXT];
    extern char motname[CHAR];
    int loop; /* loop counter */
    double incsize;
    fpin = fopen(motname, "r");
    if (fpin == NULL) { /* check to see if timefile exists */
        printf ("Error--Unable to open file.\n");
        hitakey20;
    }

    fscanf (fpin, "%d", ndt);

```

```

fscanf (fpin, "%lf", incsize);
printf ("Using motionfile named %s.\n", motname);
/* fill dt array with all elements equal to the time increment size incsize */
for (loop=0; loop<*ndt-1; loop++)
    dt[loop] = incsize;
fclose (fpin);
}

wabc (answer, x, iseg)
double *answer; /* points to &integrand */
double x;
int iseg;
{
    extern double al[DIR][SEG];
    extern double as[DIR][SEG];
    double wx_result;
    wx (x,&wx_result,iseg);
    *answer =
        wx_result *
            ( (al[0][iseg] * SQR(x)) + (al[1][iseg] * x) + (al[2][iseg]) )
                *
                    ( ROOT
                        (as[0][iseg]*SQR(x)) + (as[1][iseg]*x) + (as[2][iseg]));
}

wx (y,result,iseg)
double y;
double *result;
int iseg;
{
    extern double thhd,kneed,ankd;
    extern double fl[2];

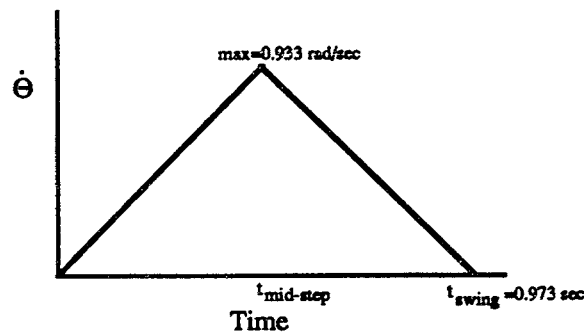
    if (iseg == 0)
        *result = thhd - y*(thhd-kneed)/fl[iseg];

    else /* if segment is lower legs, iseg = 1... */
        *result = kneed - y*(kneed-ankd)/fl[iseg];
}

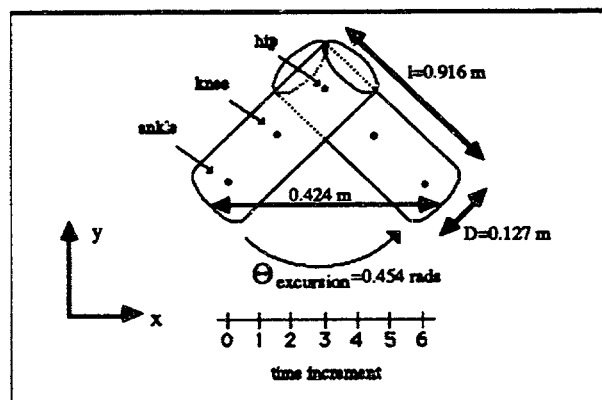
```

A.2 HYDRODYNAMICS MODEL VERIFICATION

An analytical solution to a simplified drag energy problem (using the Bernoulli equation) is compared to the mathematical computer analysis. The simplified geometric model introduced in Section 3.1.3.2, Immersion Assumptions, is used for the comparison. Results are within a factor of 2.6, thus validating the computer program since the two methods of solution are quite different. The velocity profile and geometric model are presented below as a review.



Velocity profile of the swing phase of the leg assumed during comparison between analytical calculations and computer modeling analysis of the legs moving through a fluid medium.



Model of the leg as a cylinder moving through the water. This simplified geometric model is assumed in the calculations of the inertial forces.

A summary of the analytical calculations follows:

$$P_1 + \frac{1}{2}\rho V^2)_1 + \rho gy = P_2 + \frac{1}{2}\rho V^2)_2 + \rho gy$$

$$P_2 = P_1 - \frac{1}{2}\rho V^2)_2$$

$$\text{Energy} = \int \text{Force} \cdot dx$$

$$= \frac{1}{2}\rho C_D \int_0^l \omega^2 l^2 dl \int l d\Theta$$

$$= \frac{1}{2} \rho C_D \frac{l^4}{4} \int_0^T \omega^2 d\Theta$$

where $d\Theta = \omega dt$ (or $\dot{\Theta} = \omega$) and $\omega = \alpha t$ (or $\ddot{\Theta} = \alpha$)

$$\int \omega^2 d\Theta = \int \omega^3 dt = \int_0^{T_0} \alpha^3 t^3 dt = \frac{1}{4} \omega_{\max}^3 T$$

$$E_D = \frac{1}{16} \rho C_D l^4 \omega_{\max}^3 T (\text{width of cylinder}) = 2.06 \text{ Joules}$$

where $l = 0.916 \text{ m}$, $\omega_{\max} = 0.933 \text{ rad/s}$, $T_s = 0.487 \text{ sec}$, and width = 0.127 m

Using the mathematical computer model to analyze the same parameters yields a drag energy of: $E_D = 0.849 \text{ Joules/stride}$. Therefore, the two methods yeild similar results within a factor of 2.6.

The incremental drag calculations for the computer program as shown below:

```

Hydrodynamic Drag program Output
Comparison between Analytical analysis and Computer Program
model dimensions
  height  1.78
  thihc   0.54
  xneec   0.39
  ankc    0.25

                                For all time increments
                                (6 time increments), DT_SIZE = 0.1620

position array (x, y, z)      velocity array (Vx, Vy, Vz)      Time interval 0
0.212  0.916  0.000           0.000  0.002  0.000           legdrag = 0.06110
0.098  0.451  0.000           0.235 -0.012  0.000
0.000  0.024  0.000           0.432 -0.049  0.000

                                Time interval 1
                                legdrag = 0.05719
0.212  0.916  0.000           0.000 -0.002  0.000
0.136  0.449  0.000           0.235 -0.025  0.000
0.070  0.016  0.000           0.438 -0.049  0.000

                                Time interval 2
                                legdrag = 0.06347
0.212  0.916  0.000           0.000  0.000  0.000
0.174  0.445  0.000           0.235 -0.043  0.000
0.141  0.008  0.000           0.438 -0.049  0.000

                                Time interval 3
                                legdrag = 0.11822
0.212  0.916  0.000           0.000  0.000  0.000
0.212  0.438  0.000           0.290  0.043  0.000
0.212  0.000  0.000           0.494  0.049  0.000

                                Time interval 4
                                legdrag = 0.09910
0.212  0.916  0.000           0.000  0.000  0.000
0.259  0.445  0.000           0.265  0.025  0.000
0.292  0.008  0.000           0.469  0.049  0.000

                                Time interval 5
                                legdrag = 0.02518
                                total simulation drag =
                                0.42427x2 = 0.84854
0.212  0.916  0.000           0.000  0.000  0.000
0.302  0.449  0.000           0.142  0.012  0.000
0.368  0.016  0.000           0.346  0.049  0.000

```

A.3 DATA ACQUISITION PROGRAM

The data acquisition program named "treadmill" was written in LabView2TMA.3 an icon level computer programming package. The data acquisition program records analog and digital data in real-time during the underwater locomotion experiments. The program records force traces from the submersible treadmill, samples gas concentrations from the subject's expired air, and calculates the flow rate of expired air.

The icon level program is comprised of a hierarchy of subprograms called VIs (virtual instruments). Each VI contains a front panel and a block diagram. The front panel is an electronic representation of what the actual instrument control panel might look like. The block diagram is essentially an electronic presentation of the wiring diagram for the VI. The Appendix illustrates all of the VIs that comprise the treadmill data acquisition program.

A narrative description of the primary VIs follows. The *treadmill* icon integrates all of the subVIs and is at the top of the data acquisition hierarchy. The *treadmill* front panel displays the 4 load cell channels, the O₂ channel, the CO₂ channel, and a numeric display of O₂ flow rate. Additionally, the *treadmill* front panel allows the user to select the program mode (i.e., null, set-up, session, flow, write file, quit), set the duration of force trace and gas analysis sampling, and select the sampling frequency for all measurements. The *treadmill* block diagram illustrates all modes of operation of the data acquisition program.

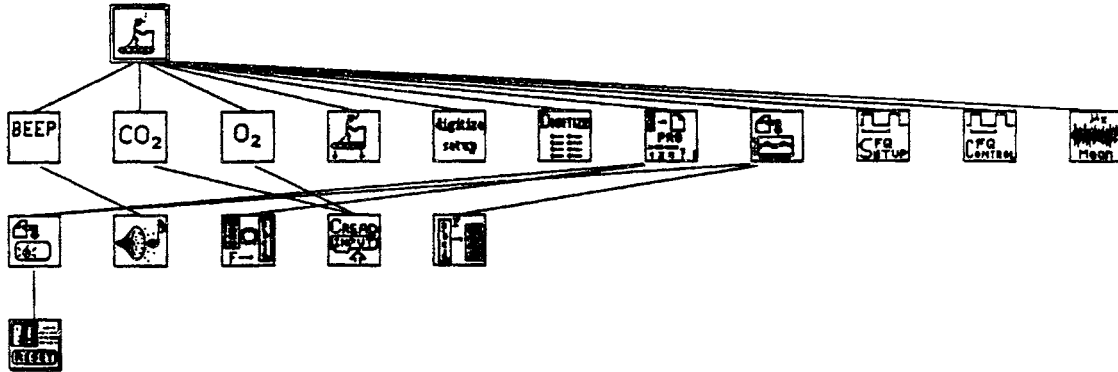
The CO₂ VI specifies the requirements for collection of carbon dioxide concentration. The O₂ VI is similar to the CO₂ VI, but records the concentration of oxygen consumed. Carbon dioxide and oxygen concentrations were sampled at 0.1 Hz continuously throughout the experimental session, but the program allows the user to specify both duration and sampling frequency.

The *digitize setup* and *digitize* VIs establish the digitization of recorded signals. The *Write ASCII array* VI allows for data to be recorded in ASCII format. The *read one data file* VI assists in storing the recorded signals. The *FqSetup* and *FqControl* VIs are programmed to record the digital flow rate signals. The *mean* VI calculates the mean (average) value of the input sequence.

A.3 LabView2 software, National Instruments, Austin, TX. Acknowledgment for programming goes to Nick Groleau, Man-Vehicle Laboratory, M.I.T.



Position in hierarchy



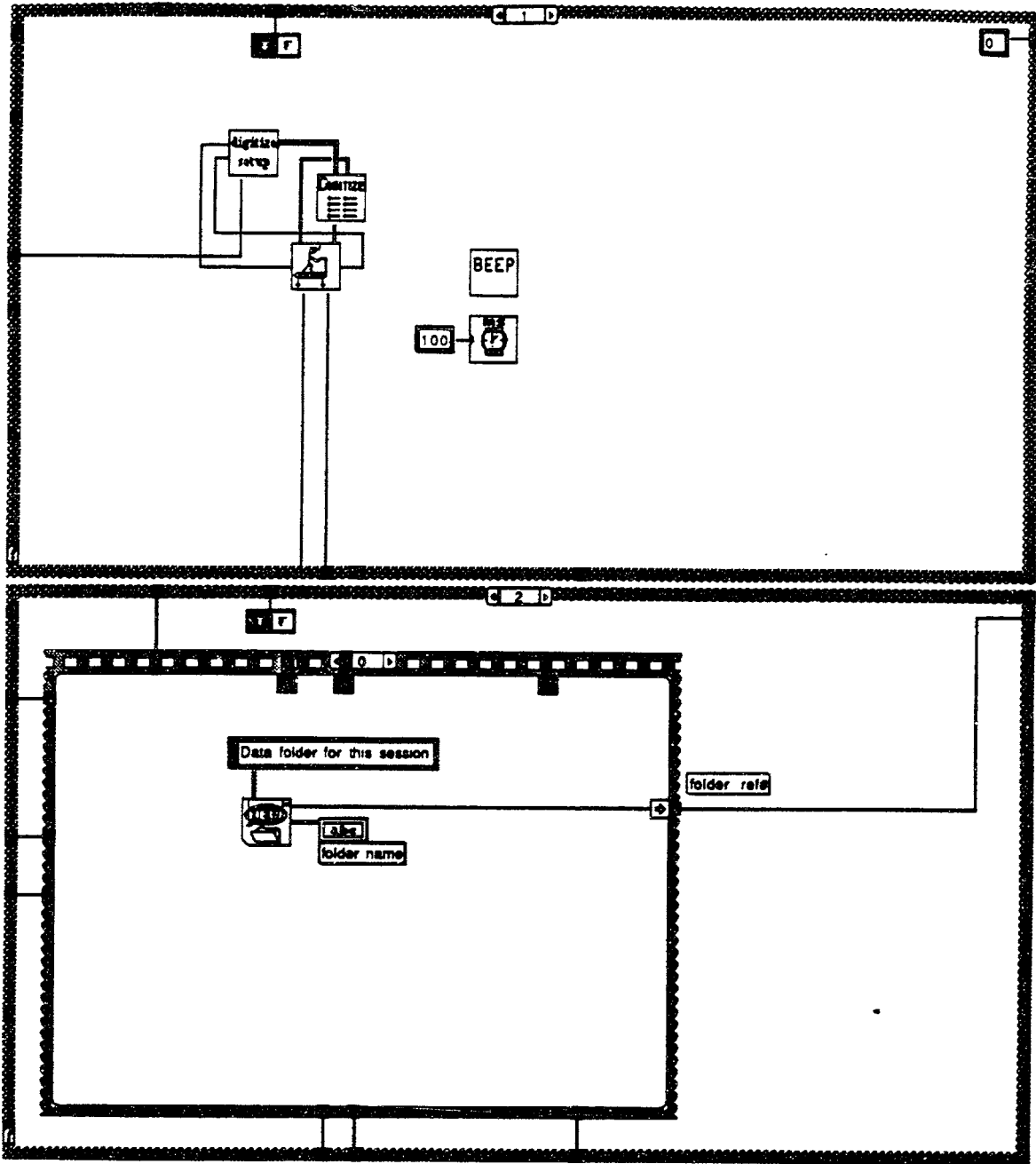
Connector Pane



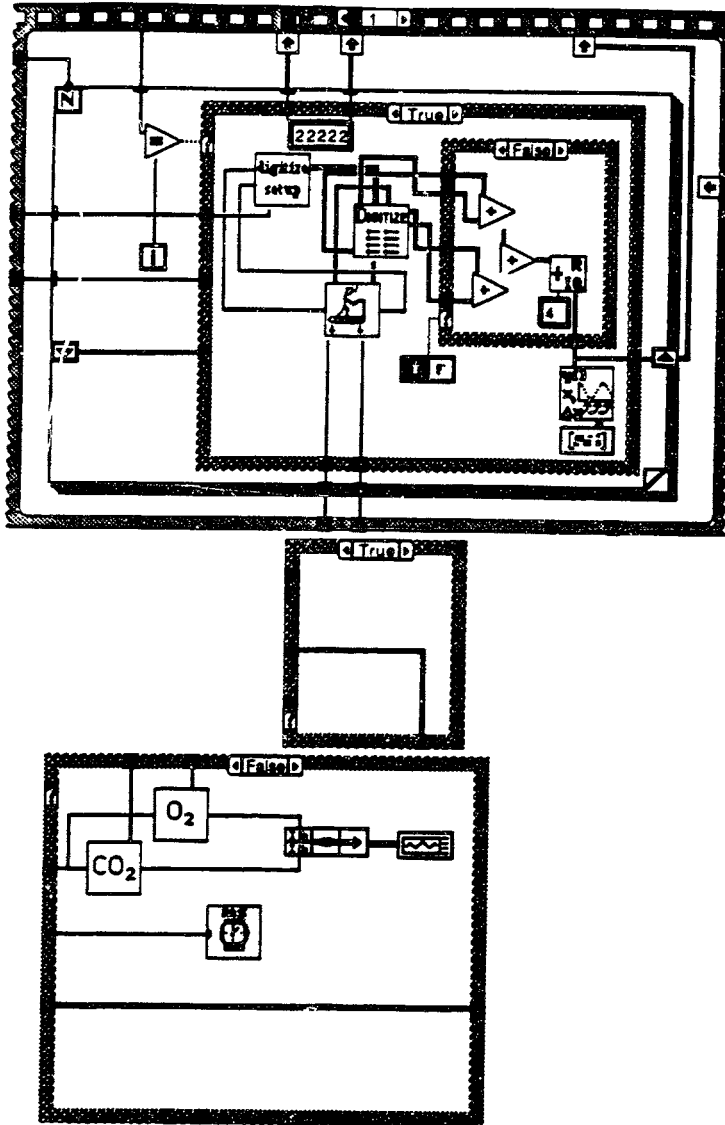
treadmill

Front Panel

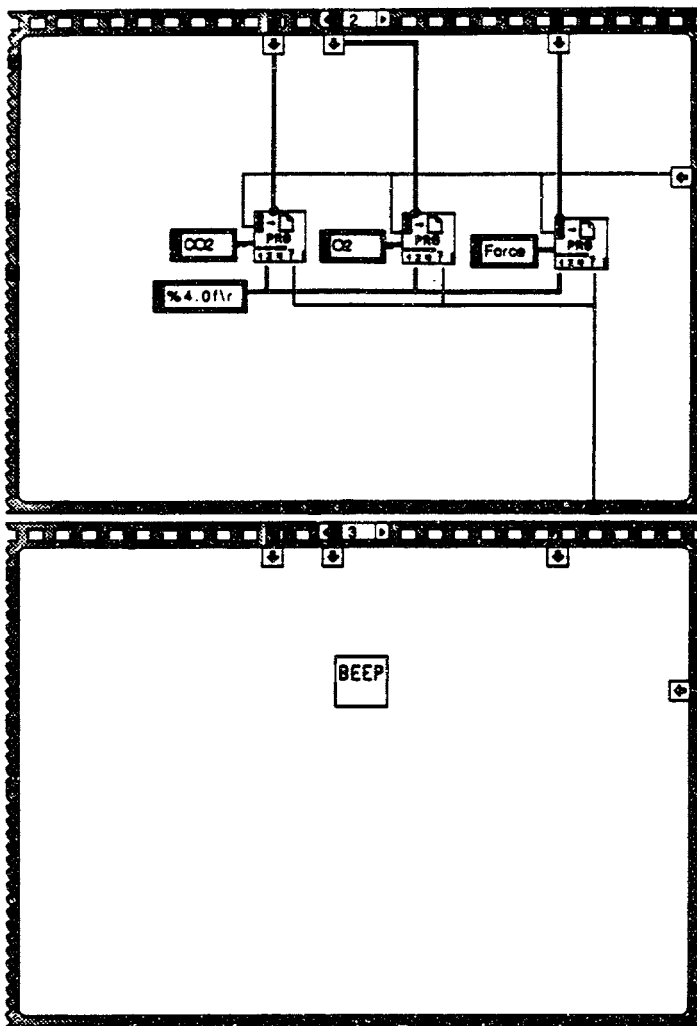
Block Diagram



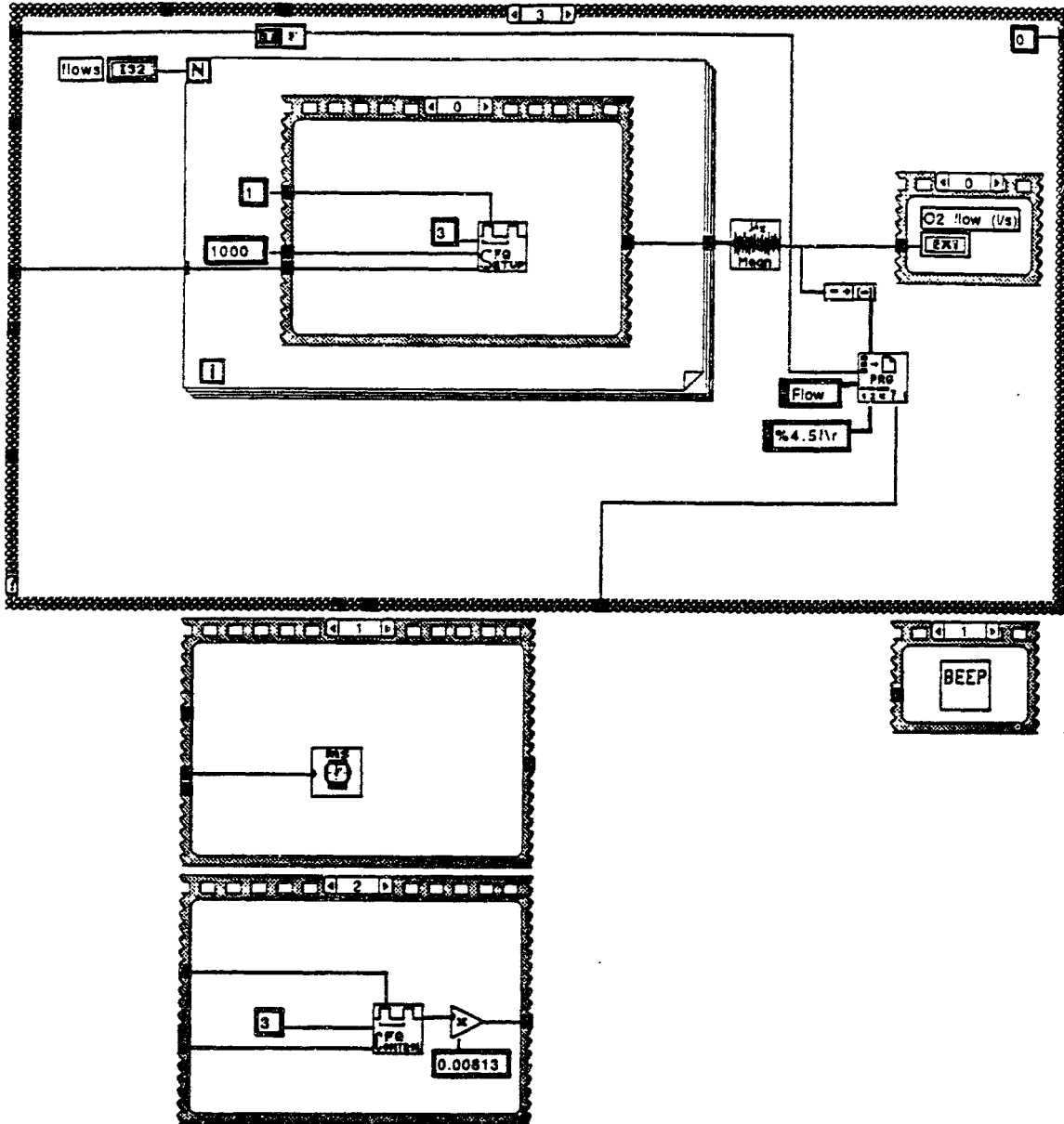
treadmill
Tuesday, September 24, 1991 11:03



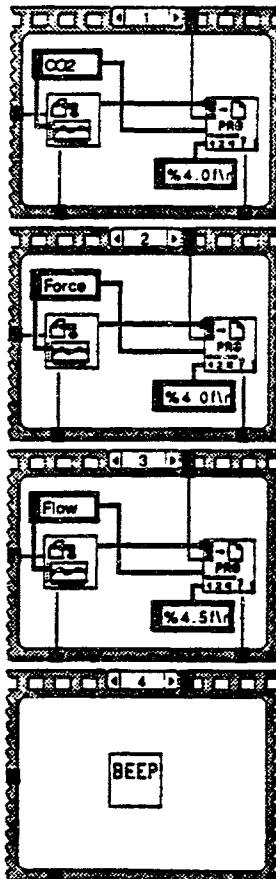
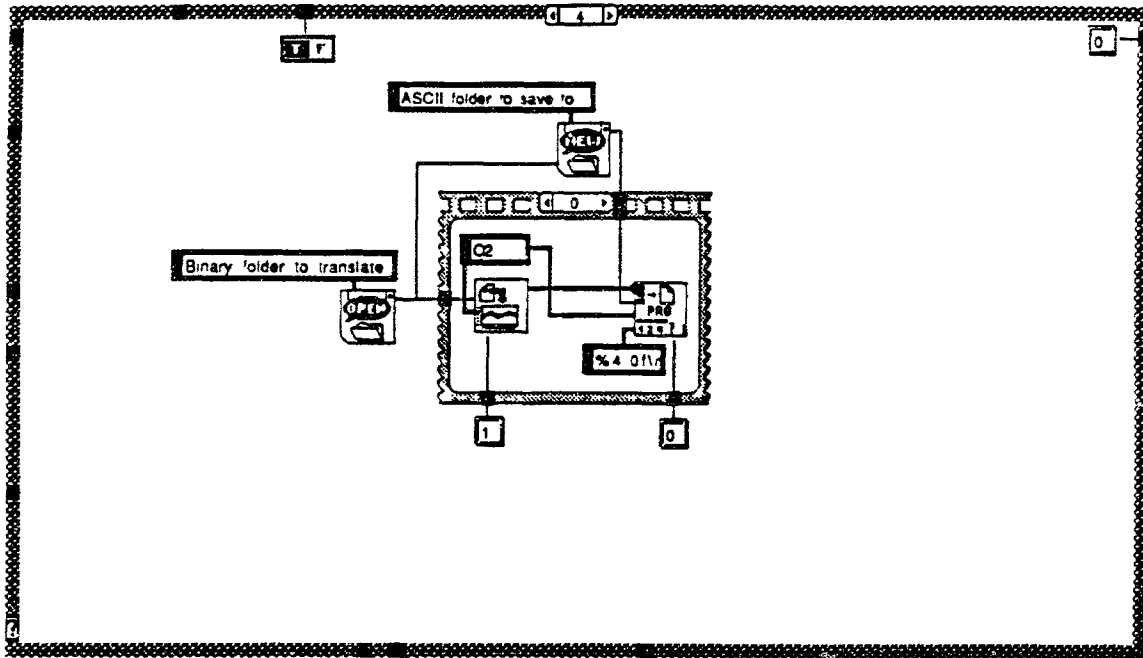
treadmill
Tuesday, September 24, 1991 11:03



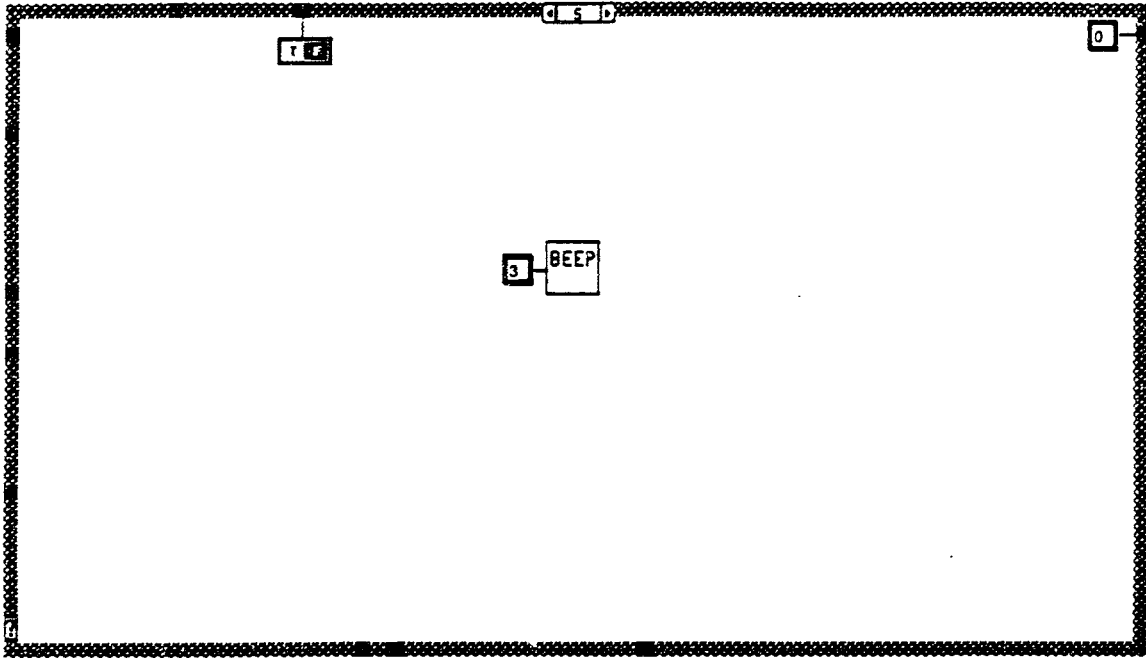
treadmill
Tuesday, September 24, 1991 11:03



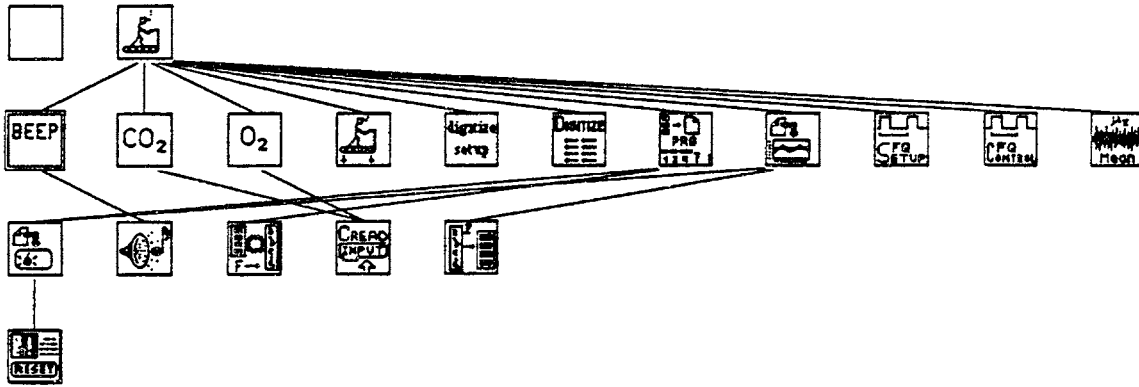
treadmill
Tuesday, September 24, 1991 11:03



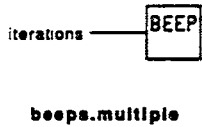
treadmill
Tuesday, September 24, 1991 11:03



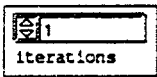
Position in hierarchy



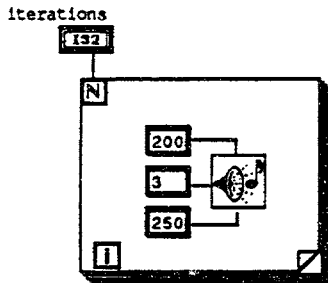
Connector Pane



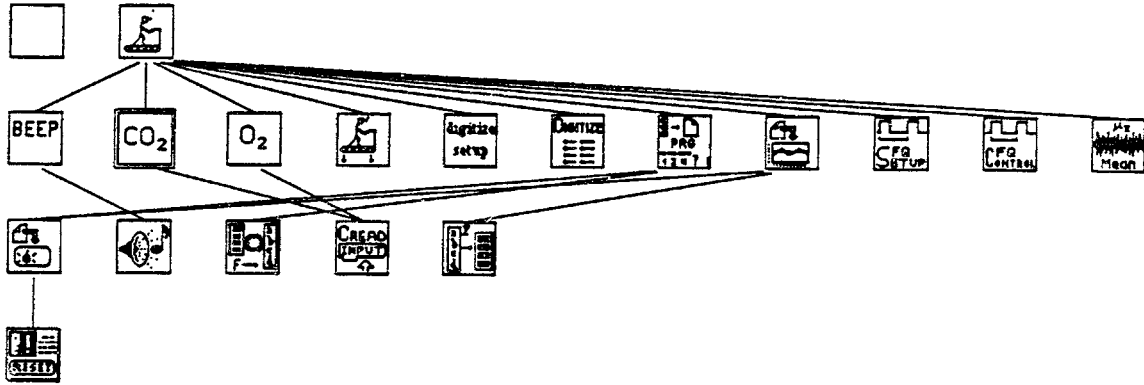
Front Panel



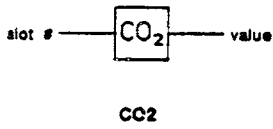
Block Diagram



Position in hierarchy



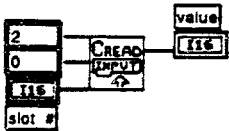
Connector Pane



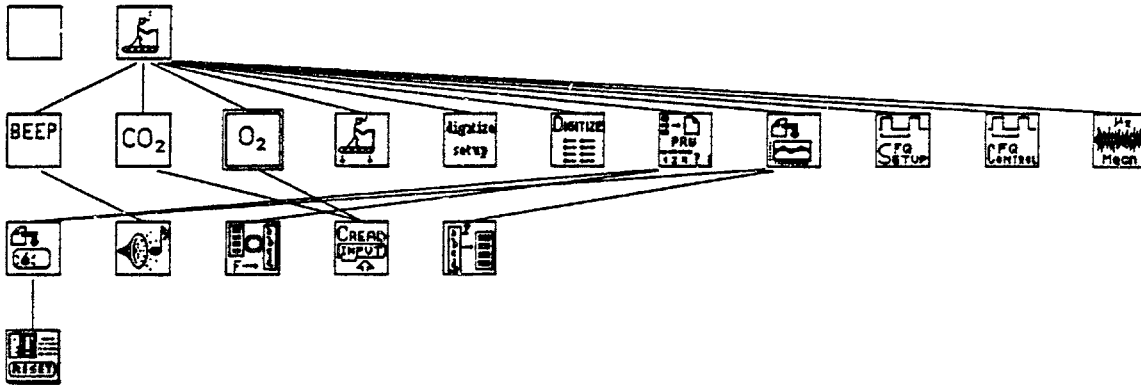
Front Panel



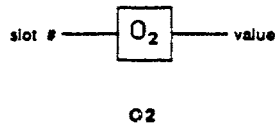
Block Diagram



Position in hierarchy



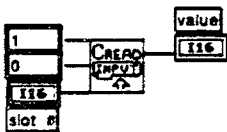
Connector Pane



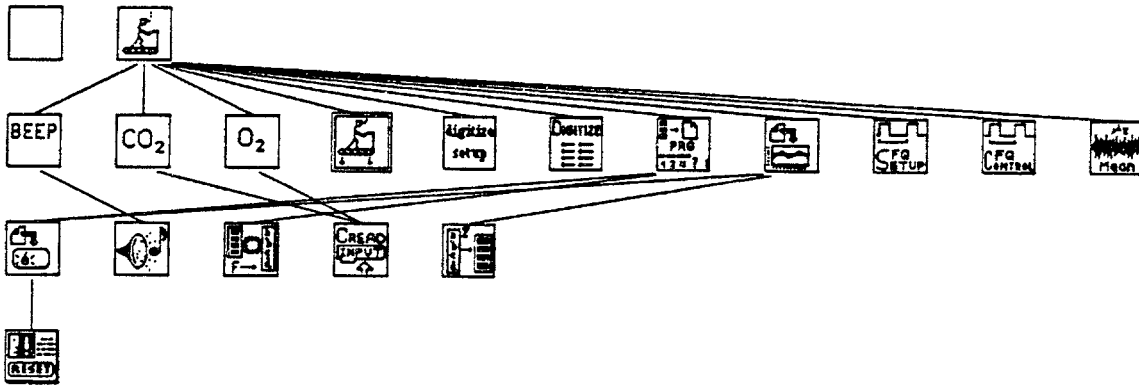
Front Panel



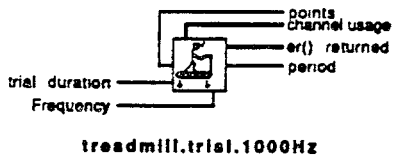
Block Diagram



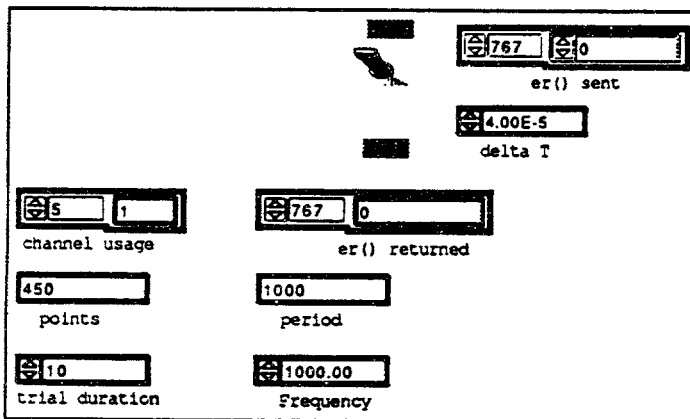
Position in hierarchy



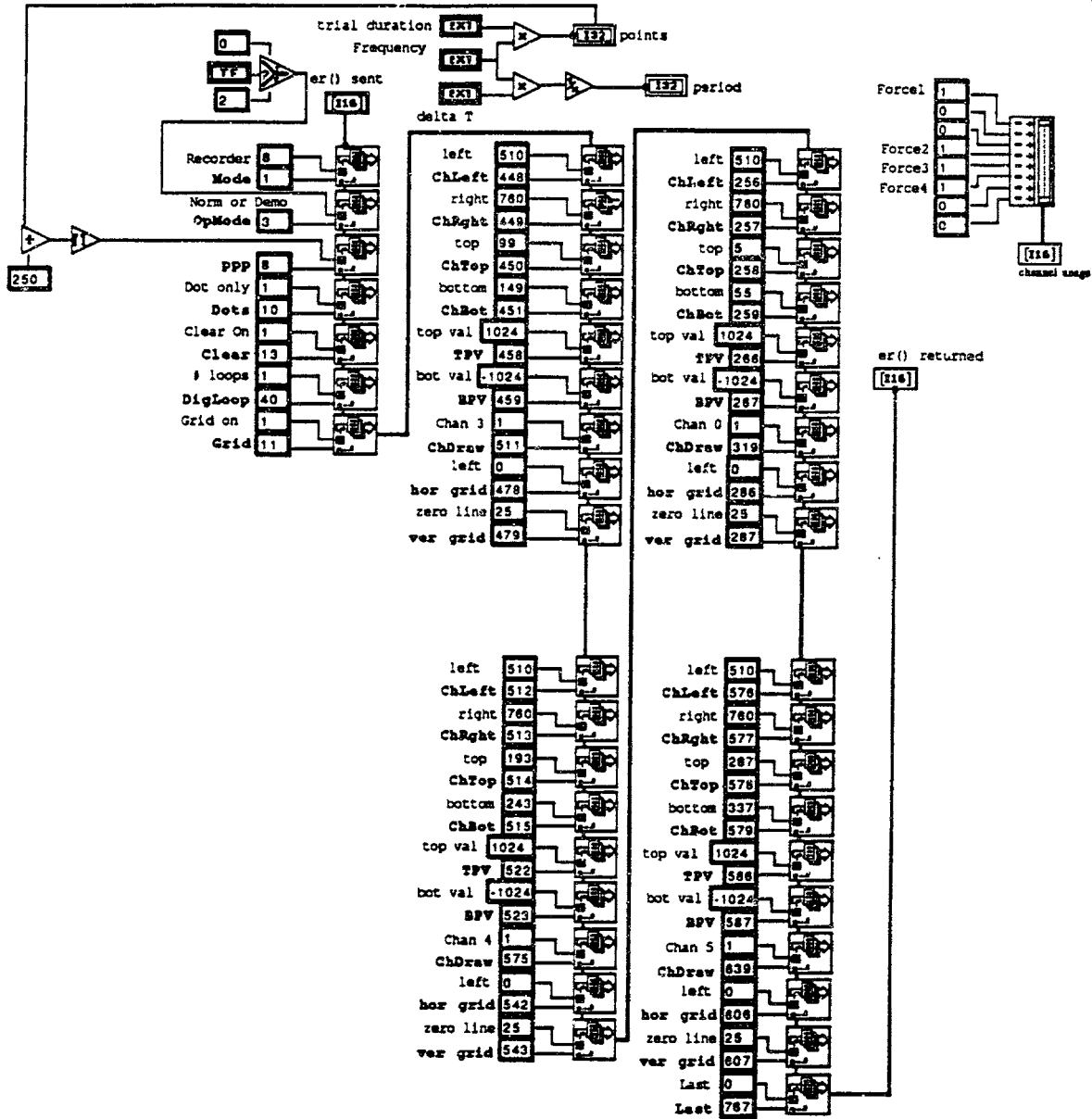
Connector Pane

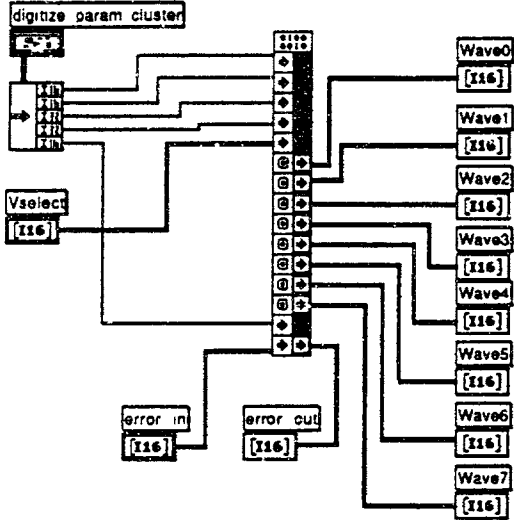


Front Panel

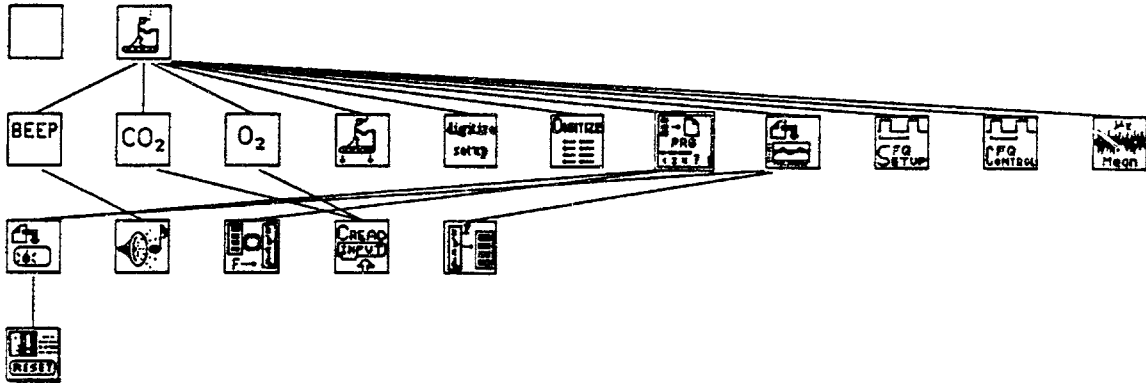


Block Diagram

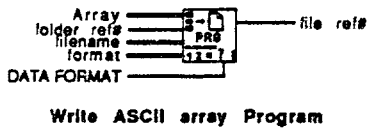




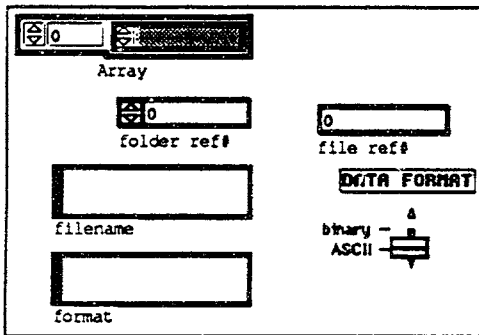
Position in hierarchy



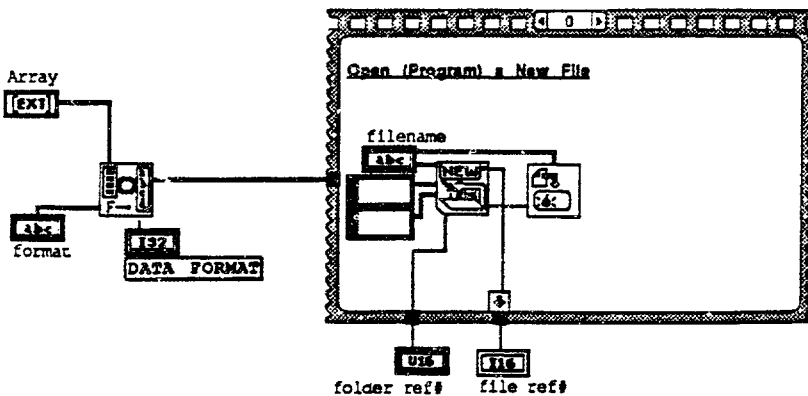
Connector Pane

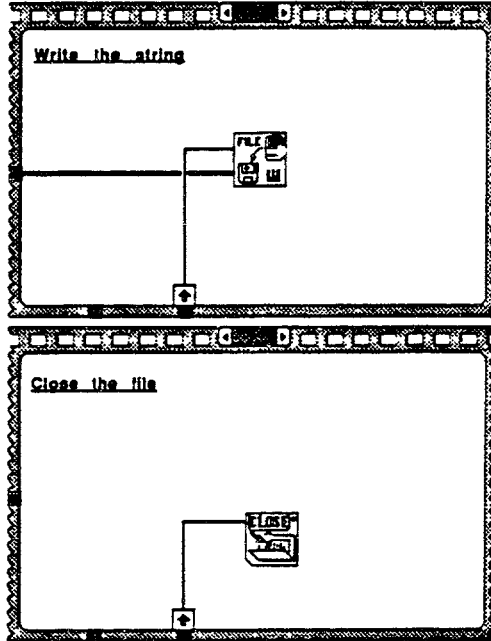


Front Panel

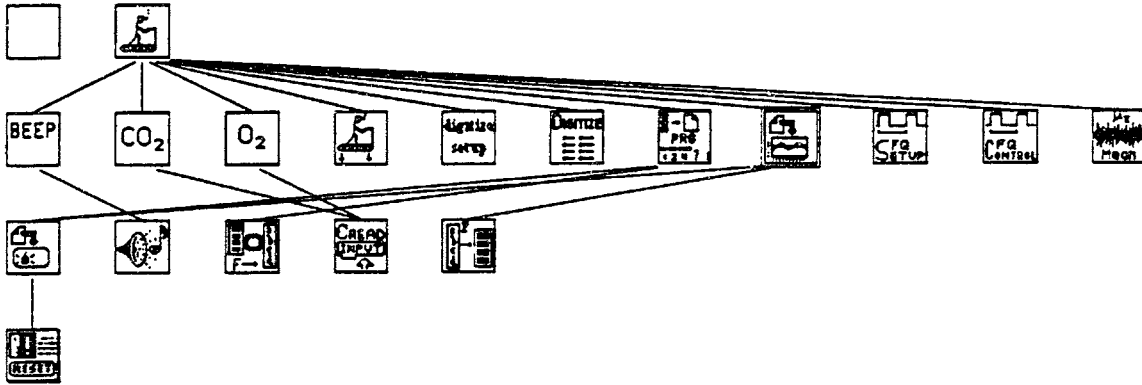


Block Diagram





Position in hierarchy



Connector Pane



read one data file

Front Panel

Dostoevsky:DATA:run 1 0

Run folder path data array

Run folder ref # data graph

Flow

filename

DATA FORMAT

binary

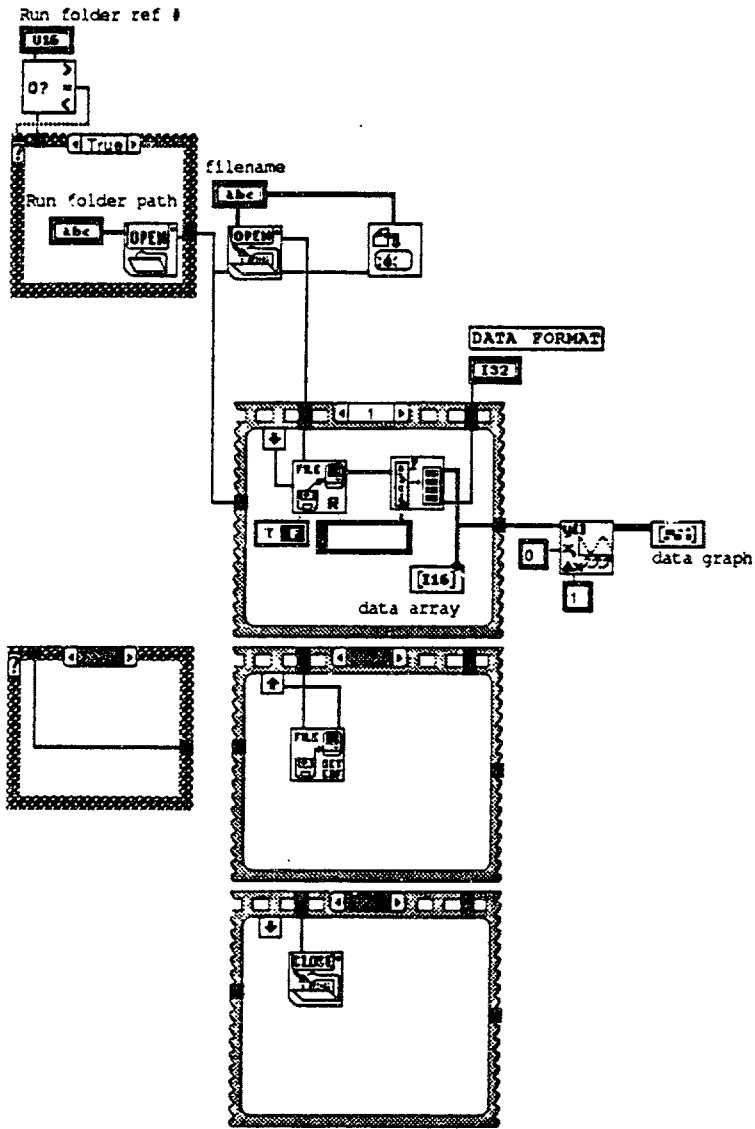
ASCII

500.0							
505.0							
510.0							
515.0							
520.0							
525.0							
530.0							
	0	5000	10000	15000	20000	25000	30000

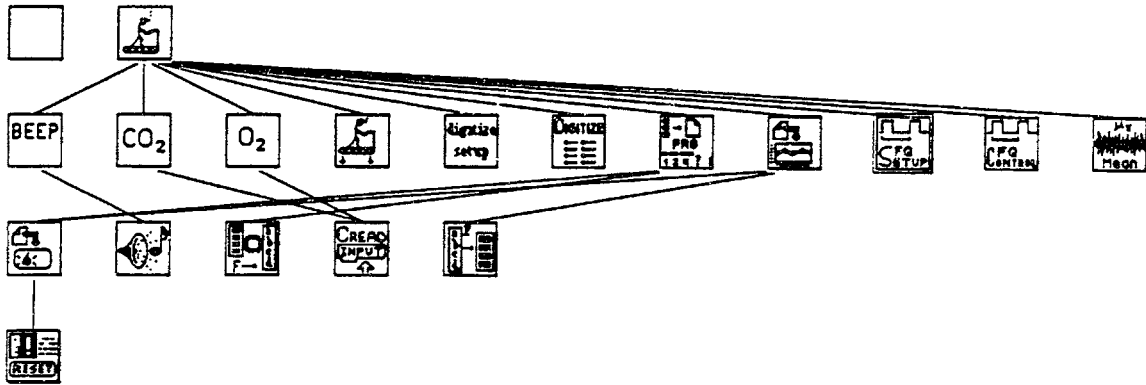
Cursor	X	Y	ΔX	ΔY
0	130.00	-108.27		
1	485.00	102.00	355.00	210.27

Block Diagram

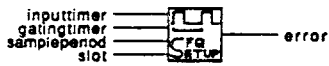
read one data file
Friday, September 13, 1991 20:41



Position in hierarchy

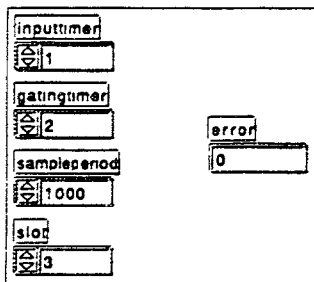


Connector Pane

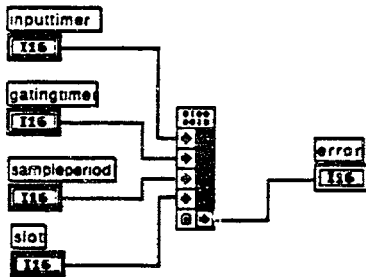


FqSetupVI

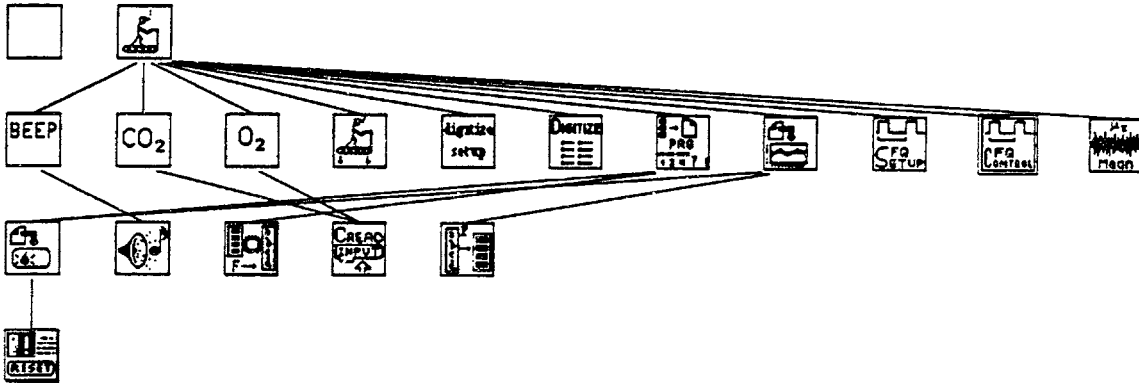
Front Panel



Block Diagram



Position in hierarchy

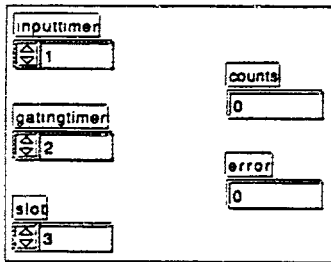


Connector Pane

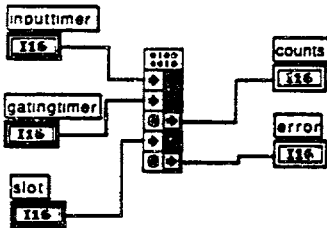


FqControlVI

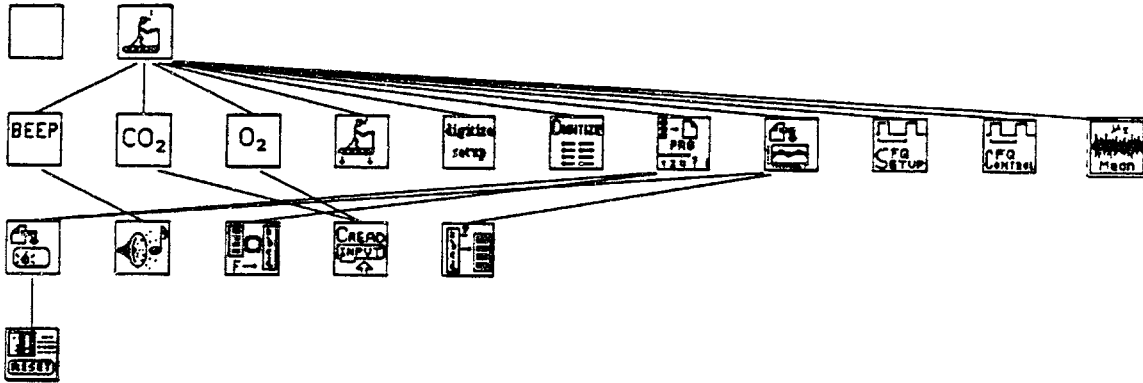
Front Panel



Block Diagram



Position in hierarchy



Connector Pane



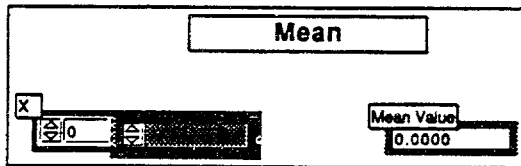
Mean

Mean:

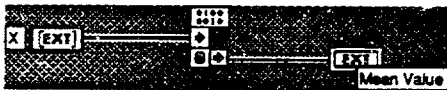
Compute the mean (average) value of the input sequence X.

January 19, 1990.

Front Panel

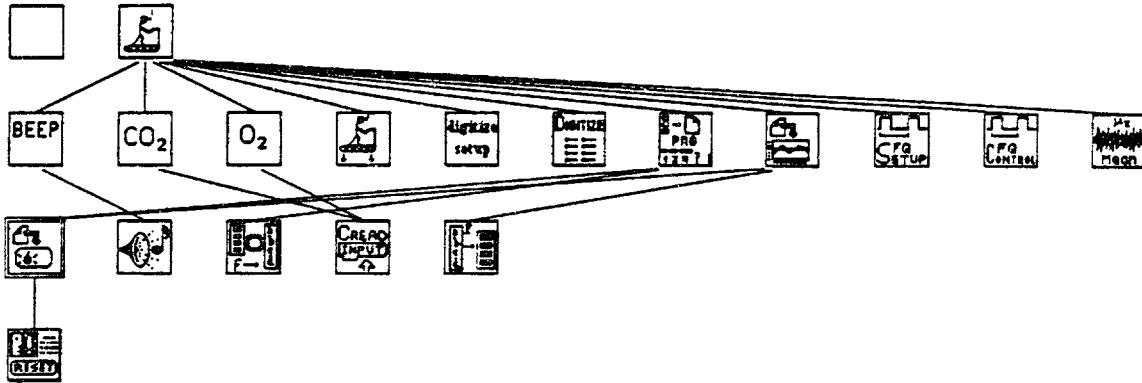


Block Diagram

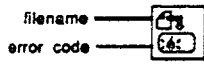




Position in hierarchy

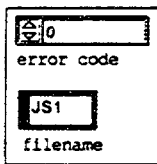


Connector Pane

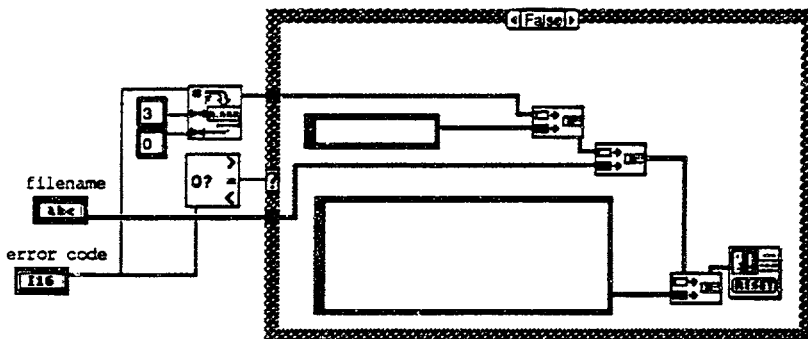


open.file.error

Front Panel



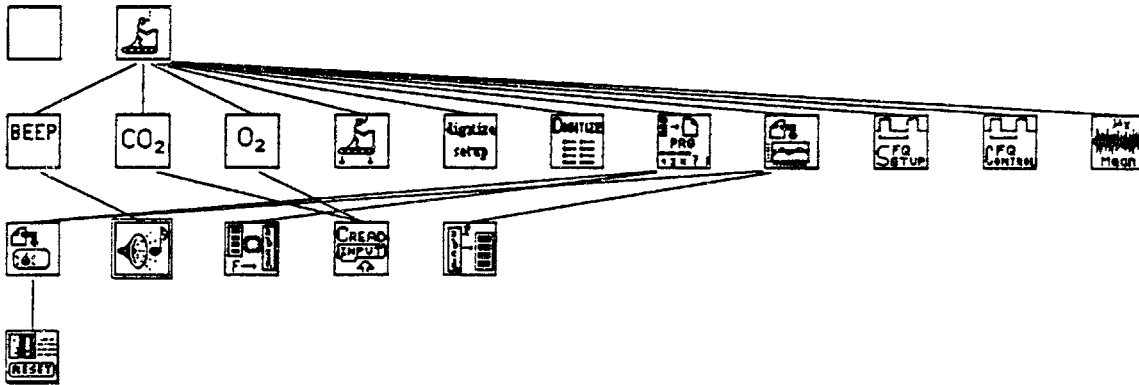
Block Diagram



open.file.error
Friday, September 13, 1991 20:41



Position in hierarchy



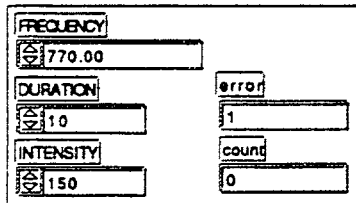
Connector Pane



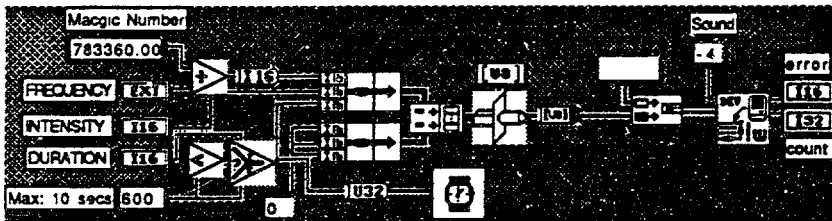
BEEP

Beep once with the given frequency (pitch), intensity (volume, also depends on the speaker volume set in the control panel), and duration (number of 1/60ths of a second, up to 600 (10 secs)).

Front Panel

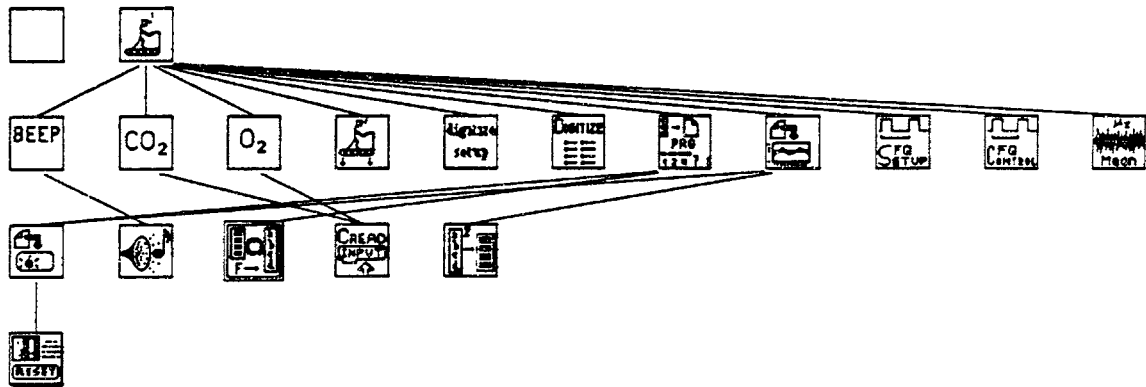


Block Diagram

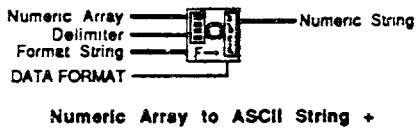




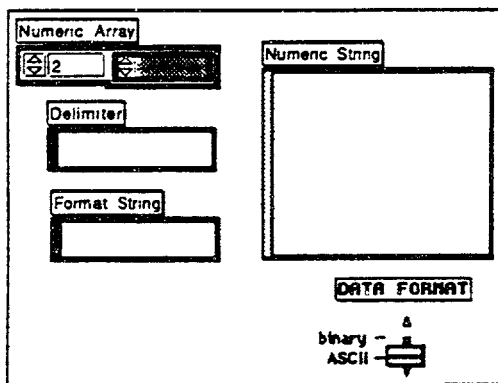
Position in hierarchy



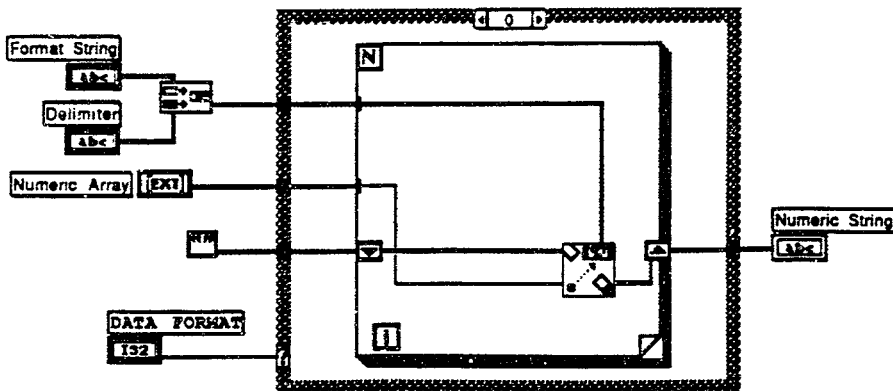
Connector Pane

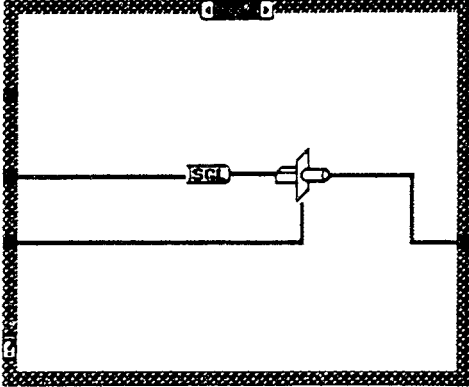


Front Panel

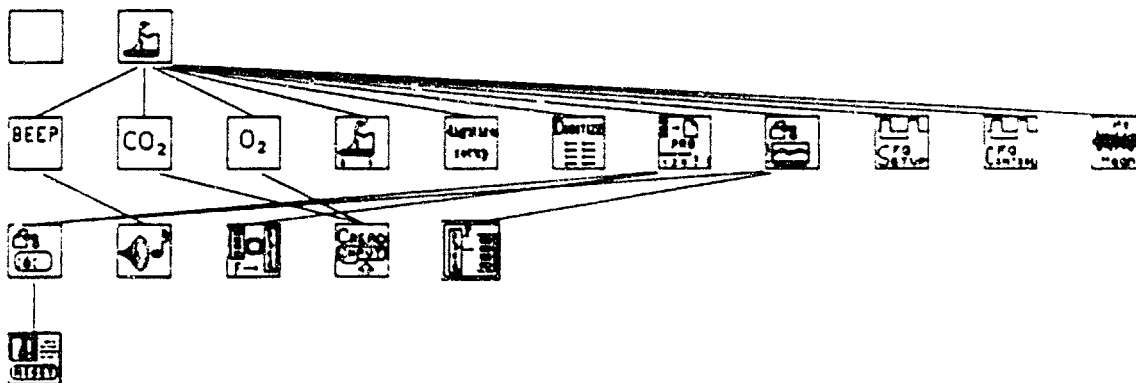


Block Diagram

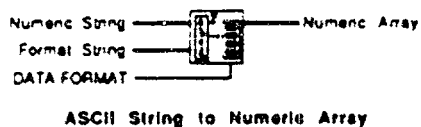




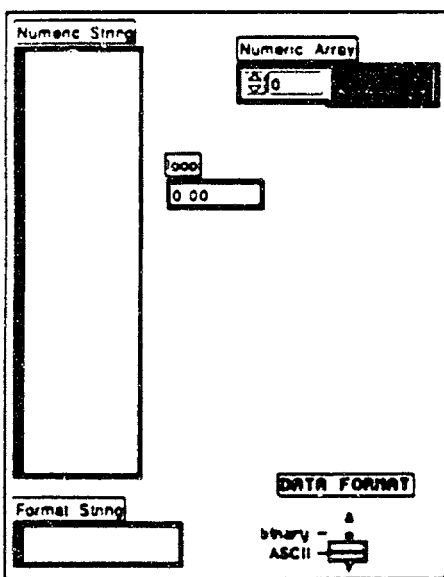
Position in hierarchy



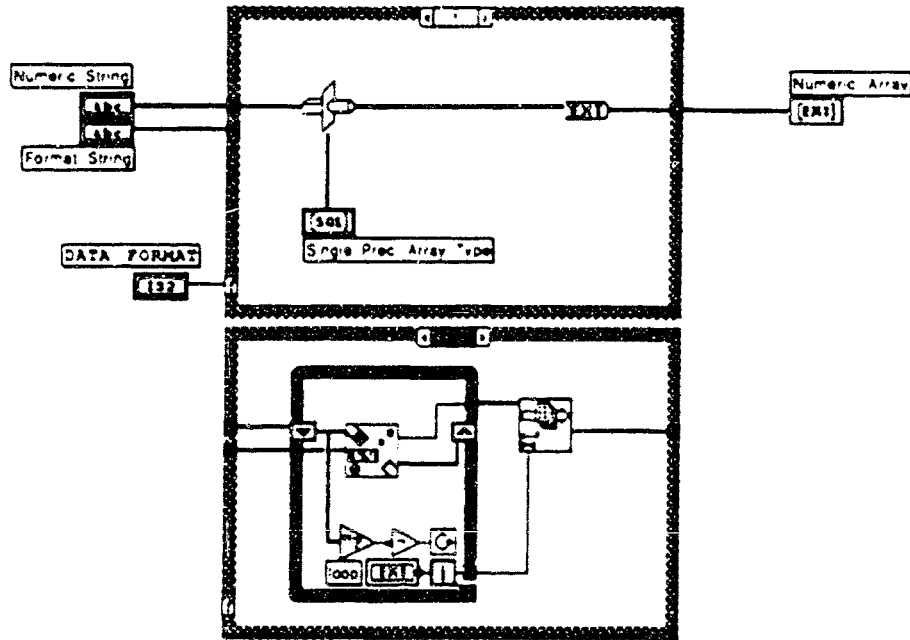
Connector Pane



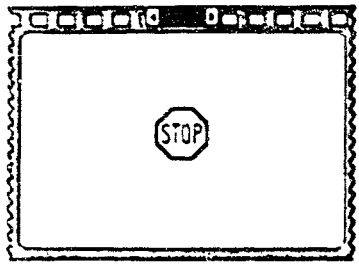
Front Panel



Block Diagram



Reset Dialog
Saturday, December 22, 1990 14:13



APPENDIX B : SUBJECTS

B.1 ANTHROPOMETRIC DATA

The subjects' anthropometric databases listed in this Appendix were obtained from a spreadsheet computer program. The necessary ballast for the adjustable harness and pockets is calculated from measurements of the subjects' mass and height (in SI units). The ballast calculations are based on the geometric hydrodynamics model. Limb segment dimensions are calculated and moments of inertia (i.e., I_{xx}) are calculated and displayed in the database.

Subject 1: Anthropometric Data

	A	B	C	D	E	F	G	H
1	Subj. Mass/Ht	Segment	Model	Mass (kg)	Mass lb	2.3 lb	Mars lb	Moon lb
2								
3	72.4	Head	Ellipsoid	4.67544	10.31	6.872	3.865	1.718
4	1.8	Neck	Cylinder	1.65704	3.653	2.435	1.37	0.609
5		Torso	Ellip. Cylinder	36.5566	80.59	53.73	30.22	13.43
6		Upper Arm	Conic Frustrum	1.97376	4.351	2.901	1.632	0.725
7		Lower Arm	Conic Frustrum	1.20836	2.664	1.776	0.999	0.444
8		Upper Leg	Conic Frustrum	7.37116	16.25	10.83	6.094	2.708
9		Lower Leg	Conic Frustrum	3.095	6.823	4.549	2.559	1.137
10		Hand	Sphere	0.4682	1.032	0.688	0.387	0.172
11		Foot	Rec. Parallel	0.96956	2.138	1.425	0.802	0.356
12	Total/Ave.			73.0612	161.1	107.4	60.4	26.85
13	Volume (ft ³)							
14	Volume (m ³)							

	I	J	K	L	M	N
1	Density kg/m ³	Length L (m)	COM Nu	Width W	Depth D	Radius R
2						
3	1110	0.2154152	0.5	2.05535973	2.05535973	
4	1110	0.08616608	0.5			0.79522209
5	1030	0.56007952	0.5	0.3438	0.33350144	
6	1070	0.30820944	0.436			
7	1130	0.24132784	0.43			
8	1050	0.4059748	0.433			
9	1090	0.40763184	0.433			
10	1160		0.5			0.66097566
11	1100	0.25187008	0.5	0.099	0.0702	
12	1094.44444					
13	2.35748067	0.81360564				
14	0.06675643					

	O	P	Q	R	S	T
1	Sigma	Parameter A	Parameter B	I _{xx}	I _{yy}	I _{zz}
2						
3				1.67750542	1.67750542	1.97514133
4				0.31315935	0.31315935	0.26196898
5				549.922456	549.906519	0.52418029
6	1.626096	0.09453812	0.07108927	0.38501047	0.38501047	0.62242051
7	1.6149	0.09494617	0.07076401	0.32941017	0.32941017	0.62510699
8	1.620489	0.09474124	0.0709273	4.14710949	4.14710949	0.62375778
9	1.620489	0.09474124	0.0709273	0.59577924	0.59577924	0.62375778
10				0.08182054	0.08182054	0.08182054
11				0.01104636	0.01065264	0.00119006
12						
13						
14						

Subject 3: Anthropometric Data

	A	B	C	D	E	F	G	H
1	Subj. Mass/Ht	Segment	Model	Mass (kg)	Mass (23 lb)	Mass (3 lb)	Mars lb	Moon lb
2								
3	74	Head	Ellipsoid	4.7244	10.42	6.944	3.906	1.736
4	1.78	Neck	Cylinder	1.6804	3.705	2.47	1.389	0.617
5		Torso	Ellip. Cylinder	37.4264	82.51	55.01	30.94	13.75
6		Upper Arm	Conic Frustrum	2.0176	4.448	2.965	1.668	0.741
7		Lower Arm	Conic Frustrum	1.2386	2.731	1.82	1.024	0.455
8		Upper Leg	Conic Frustrum	7.5566	16.66	11.11	6.247	2.777
9		Lower Leg	Conic Frustrum	3.155	6.956	4.637	2.608	1.159
10		Hand	Sphere	0.477	1.052	0.701	0.394	0.175
11		Foot	Rec. Parallel	0.9806	2.162	1.441	0.811	0.36
12	Total/Ave.			74.682	164.6	109.8	61.74	27.44
13	Volume (ft ³)							
14	Volume (m ³)							

	I	J	K	L	M	N
1	Density kg/m ³	Length L (m)	COM Nu	Width W	Depth D	Radius R
2						
3	1110	0.218452	0.5	2.04468192	2.04468192	
4	1110	0.0873808	0.5			0.78967537
5	1030	0.5679752	0.5	0.33998	0.32941125	
6	1070	0.3125544	0.436			
7	1130	0.2453384	0.43			
8	1050	0.4361	0.433			
9	1090	0.4133784	0.433			
10	1160		0.5			0.66097566
11	1100	0.2554208	0.5	0.0979	0.06942	
12	1094.4444					
13	2.40977935	0.8494784				
14	0.06823736					

	O	P	Q	R	S	T
1	Sigma	Parameter A	Parameter B	I _{xx}	I _{yy}	I _{zz}
2						
3				1.69940764	1.69940764	1.97514133
4				0.31535497	0.31535497	0.26196898
5				590.09578	590.079231	0.52419924
6	1.626096	0.09453812	0.07108927	0.39003813	0.39003813	0.62242051
7	1.6149	0.09494617	0.07076401	0.33070766	0.33070766	0.62510699
8	1.620489	0.09474124	0.0709273	4.44390702	4.44390702	0.62375778
9	1.620489	0.09474124	0.0709273	0.61261256	0.61261256	0.62375778
10				0.08335839	0.08335839	0.08335839
11				0.01139197	0.01100257	0.00117701
12						
13						
14						

Subject 2: Anthropometric Data

	A	B	C	D	E	F	G	H
1	Subj. Mass/Ht	Segment	Model	Mass (kg)	Mass c 2 3 lb	Mars lb	Moon lb	
2								
3	72.6	Head	Ellipsoid	4.68156	10.32	6.881	3.87	1.72
4	1.8	Neck	Cylinder	1.65996	3.66	2.44	1.372	0.61
5		Torso	Ellip. Cylinder	36.6654	80.83	53.89	30.31	13.47
6		Upper Arm	Conic Frustrum	1.97924	4.364	2.909	1.636	0.727
7		Lower Arm	Conic Frustrum	1.21214	2.672	1.782	1.002	0.445
8		Upper Leg	Conic Frustrum	7.39434	16.3	10.87	6.113	2.717
9		Lower Leg	Conic Frustrum	3.1025	6.84	4.56	2.565	1.14
10		Hand	Sphere	0.4693	1.035	0.69	0.388	0.172
11		Foot	Rec. Parallel	0.97094	2.141	1.427	0.803	0.357
12	Total/Ave.			73.2638	161.5	107.7	60.57	26.92
13	Volume (ft ³)							
14	Volume (m ³)							

	I	J	K	L	M	N
1	Density kg/m ³	Length L (m)	COM Nu	Width W	Depth D	Radius R
2						
3	1110	0.2157948	0.5	2.05401585	2.05401585	
4	1110	0.08631792	0.5			0.79452235
5	1030	0.56106648	0.5	0.3438	0.33251254	
6	1070	0.30875256	0.436			
7	1130	0.24235416	0.43			
8	1050	0.4066902	0.433			
9	1090	0.40835016	0.433			
10	1160		0.5			0.66097566
11	1100	0.25231392	0.5	0.099	0.0702	
12	1094.4444					
13	2.364018	0.81504036				
14	0.06694154					

	O	P	Q	R	S	T
1	Sigma	Parameter A	Parameter B	lxx	lyy	lzz
2						
3				1.68021828	1.68021828	1.97514133
4				0.31343045	0.31343045	0.26196898
5				554.841882	554.824398	0.52422992
6	1.626096	0.09453812	0.07108927	0.38562688	0.38562688	0.62242051
7	1.6149	0.09494617	0.07076401	0.32956886	0.32956886	0.62510699
8	1.620489	0.09474124	0.0709273	4.1834052	4.1834052	0.62375778
9	1.620489	0.09474124	0.0709273	0.59784814	0.59784814	0.62375778
10				0.08201277	0.08201277	0.08201277
11				0.01109134	0.01069706	0.00119175
12						
13						
14						

Subject 4: Anthropometric Data

	A	B	C	D	E	F	G	H	
1	Subj. Mass	Ht	Segment	Model	Mass kg	Mass lb	23 lb	Mars lb	Moon lb
2									
3	81.7	Head	Ellipsoid	4.96002	10.94	7.29	4.101	1.823	
4	1.83	Neck	Cylinder	1.79282	3.953	2.635	1.482	0.659	
5		Torso	Ellip. Cylinder	41.6121	91.74	61.16	34.4	15.29	
6		Upper Arm	Conic Frustrum	2.22858	4.913	3.275	1.842	0.819	
7		Lower Arm	Conic Frustrum	1.38413	3.052	2.034	1.144	0.509	
8		Upper Leg	Conic Frustrum	8.44903	18.63	12.42	6.985	3.105	
9		Lower Leg	Conic Frustrum	3.44375	7.592	5.061	2.847	1.265	
10		Hand	Sphere	0.51935	1.145	0.763	0.429	0.191	
11		Foot	Rec. Parallel	1.03373	2.279	1.519	0.855	0.38	
12	Total/Ave.				82.4821	181.8	121.2	68.19	30.31
13	Volume (ft ³)								
14	Volume (m ³)								

	I	J	K	L	M	N
1	Density kg/m ³	Length L (m)	COM Nu	Width W	Depth D	Radius R
2						
3	1110	0.2330666	0.5	1.99552592	1.99552592	
4	1110	0.09322664	0.5			0.76451601
5	1030	0.60597316	0.5	0.34953	0.28818114	
6	1070	0.33346452	0.436			
7	1130	0.26175172	0.43			
8	1050	0.4392409	0.433			
9	1090	0.44103372	0.433			
10	1160		0.5			0.66097566
11	1100	0.27250864	0.5	0.10065	0.07137	
12	1094.44444					
13	2.66146677	0.88027462				
14	0.07536436					

	O	P	Q	R	S	T
1	Sigma	Parameter A	Parameter B	I _{xx}	I _{yy}	I _{zz}
2						
3				1.81131197	1.81131197	1.97514133
4				0.32680247	0.32680247	0.26196898
5				810.996577	810.894828	0.53372639
6	1.626096	0.09453812	0.07108927	0.41744321	0.41744321	0.62242051
7	1.6149	0.09494617	0.07076401	0.33788807	0.33788807	0.62510699
8	1.620489	0.09474124	0.0709273	6.08757752	6.08757752	0.62375778
9	1.620489	0.09474124	0.0709273	0.70297078	0.70297078	0.62375778
10				0.09075928	0.09075928	0.09075928
11				0.01330095	0.01286706	0.00131147
12						
13						
14						

Subject 5: Anthropometric Data

	A	B	C	D	E	F	G	H
1	Subj. Mass:Ht	Segment	Model	Mass (kg)	Mass (lb)	23 lb	Mars lb	Moon lb
2								
3	61.5	Head	Ellipsoid	4.3419	9.572	6.382	3.59	1.595
4	1.7	Neck	Cylinder	1.4979	3.302	2.202	1.238	0.55
5		Torso	Elip. Cylinder	30.6314	67.53	45.02	25.32	11.26
6		Upper Arm	Conic Frustrum	1.6751	3.693	2.462	1.385	0.615
7		Lower Arm	Conic Frustrum	1.00235	2.21	1.473	0.829	0.368
8		Upper Leg	Conic Frustrum	6.10785	13.47	8.977	5.05	2.244
9		Lower Leg	Conic Frustrum	2.68625	5.922	3.948	2.221	0.987
10		Hand	Sphere	0.40825	0.9	0.6	0.338	0.15
11		Foot	Rec. Parallel	0.89435	1.972	1.314	0.739	0.329
12	Total/Ave.			62.0195	136.7	91.15	51.27	22.79
13	Volume (ft3)							
14	Volume (m3)							

	I	J	K	L	M	N
1	Density (kg/m ³)	Length L (m)	COM Nu	Width W	Depth D	Radius R
2						
3	1110	0.194727	0.5	2.13284443	2.13284443	
4	1110	0.0778908	0.5			0.83639903
5	1030	0.5062902	0.5	0.3247	0.42142541	
6	1070	0.2786094	0.436			
7	1130	0.2186934	0.43			
8	1050	0.3669855	0.433			
9	1090	0.3684834	0.433			
10	1160		0.5			0.66097566
11	1100	0.2276808	0.5	0.0935	0.0663	
12	1094.44444					
13	2.00119588	0.7354689				
14	0.05666756					

	O	P	Q	R	S	T
1	Sigma	Parameter A	Parameter B	l _{xx}	l _{yy}	l _{zz}
2						
3				1.54013139	1.54013139	1.97514133
4				0.29978169	0.29978169	0.26196898
5				323.564488	323.702654	0.5418493
6	1.626096	0.09453812	0.07108927	0.35632275	0.35632275	0.62242051
7	1.6149	0.09494617	0.07076401	0.32217496	0.32217496	0.62510699
8	1.620489	0.09474124	0.0709273	2.4938503	2.4938503	0.62375778
9	1.620489	0.09474124	0.0709273	0.49749824	0.49749824	0.62375778
10				0.07134394	0.07134394	0.07134394
11				0.0087	0.00837605	0.00097916
12						
13						
14						

Subject E. Anthropometric Data

	A	B	C	D	E	F	G	H	
1	Subj.	Mass/Ht	Segment	Model	Mass (kg)	Mass (lb)	2 3 lb	Mars lb	Moon lb
2									
3		58.8	Head	Ellipsoid	4.25928	9.39	6.26	3.521	1.565
4		1.66	Neck	Cylinder	1.45848	3.215	2.144	1.206	0.536
5			Torso	Ellip. Cylinder	29.1637	64.3	42.86	24.11	10.72
6			Upper Arm	Conic Frustrum	1.60112	3.53	2.353	1.324	0.588
7			Lower Arm	Conic Frustrum	0.95132	2.097	1.398	0.786	0.35
8			Upper Leg	Conic Frustrum	5.79492	12.78	8.517	4.791	2.129
9			Lower Leg	Conic Frustrum	2.585	5.699	3.799	2.137	0.95
10			Hand	Sphere	0.3934	0.867	0.578	0.325	0.145
11			Foot	Rec. Parallel	0.87572	1.931	1.287	0.724	0.322
12	Total/Ave.				59.2844	130.7	87.13	49.01	21.78
13	Volume (ft ³)								
14	Volume (m ³)								

	I	J	K	L	M	N
1	Density kg/m ³	Length L (m)	COM Nu	Width W	Depth D	Radius R
2						
3	1110	0.1896024	0.5	2.15343116	2.15343116	
4	1110	0.07584096	0.5			0.84762682
5	1030	0.49296624	0.5	0.31706	0.45330037	
6	1070	0.27127728	0.436			
7	1130	0.21293808	0.43			
8	1050	0.3573276	0.433			
9	1090	0.35878608	0.433			
10	1160		0.5			0.66097566
11	1100	0.22168896	0.5	0.0913	0.06474	
12	1094.44444					
13	1.91294185	0.71611368				
14	0.05416849					

	O	P	Q	R	S	T
1	Sigma	Parameter A	Parameter B	l _{xx}	l _{yy}	l _{zz}
2						
3				1.50918454	1.50918454	1.97514133
4				0.29687423	0.29687423	0.26196898
5				279.255245	279.446549	0.55777045
6	1.626096	0.09453812	0.07108927	0.35060572	0.35060572	0.62242051
7	1.6149	0.09494617	0.07076401	0.32077901	0.32077901	0.62510699
8	1.620489	0.09474124	0.0709273	2.17536561	2.17536561	0.62375778
9	1.620489	0.09474124	0.0709273	0.47729035	0.47729035	0.62375778
10				0.06874883	0.06874883	0.06874883
11				0.00816419	0.00786175	0.00091418
12						
13						
14						

Parabolic Flight Subject 1: Anthropometric Data

	A	B	C	D	E	F	G	H
1	Subj. Mass/Ht	Segment	Model	Mass (kg)	23 lb	Mars lb	Moon lb	Mars Moon
2								
3	73.8	Head	Ellipsoid	4.71828	6.935	3.901	1.734	2.16710024
4	1.74	Neck	Cylinder	1.67748	2.465	1.387	0.616	0.77046452
5		Torso	Ellip. Cylinder	37.3177	54.85	30.85	13.71	17.1399649
6		Upper Arm	Conic Frustrum	2.01212	2.957	1.663	0.739	0.92416426
7		Lower Arm	Conic Frustrum	1.23482	1.315	1.021	0.454	0.56715132
8		Upper Leg	Conic Frustrum	7.53342	11.07	6.228	2.768	3.46009061
9		Lower Leg	Conic Frustrum	3.1475	4.626	2.602	1.157	1.44564291
10		Hand	Sphere	0.4759	0.699	0.393	0.175	0.21858029
11		Foot	Rec. Parallel	0.97922	1.439	0.81	0.36	0.44975455
12	Total/Ave.			74.4794	109.5	61.57	27.37	34.2082975
13	Volume (ft ³)							
14	Volume (m ³)							

	I	J	K	L	M	N	O	P
1	Density k	Length L (COM)	Nu	Width W	Depth D	Radius R	Sigma	Parameter A
2								
3	1110	0.21807	0.5	2.04601	2.04601			
4	1110	0.08723	0.5			0.79036		
5	1030	0.56699	0.5	0.33234	0.33797			
6	1070	0.31201	0.436				1.6261	0.09453812
7	1130	0.24491	0.43				1.6149	0.09494617
8	1050	0.41098	0.433				1.62049	0.09474124
9	1090	0.41266	0.433				1.62049	0.09474124
10	1160		0.5			0.66098		
11	1100	0.25498	0.5	0.0957	0.06786			
12	1094.44							
13	2.40324	0.82364						
14	0.06805							

	Q	R	S	T
1	Parameter B	lxx	lyy	lzz
2				
3		1.69664487	1.69664487	1.97514133
4		0.31507715	0.31507715	0.26196898
5		584.957777	584.966572	0.52401178
6	0.07108927	0.38939756	0.38939756	0.62242051
7	0.07076401	0.33054195	0.33054195	0.62510699
8	0.0709273	4.40599834	4.40599834	0.62375778
9	0.0709273	0.61047296	0.61047296	0.62375778
10		0.08316616	0.08316616	0.08316616
11		0.01131139	0.01093982	0.00112312
12				
13				
14				

Parabolic Flight Subject 2 Anthropometric Data

	A	B	C	D	E	F	G	H
1	Subj. Mass/Ht	Segment	Model	Mass (kg)	Mass lb	2 3 lb	Mars lb	Moon lb
2								
3	69.85	Head	Ellipsoid	4.59741	10.14	6.757	3.801	1.689
4	1.78	Neck	Cylinder	1.61331	3.571	2.381	1.339	0.595
5		Torso	Ellip. Cylinder	35.17046	77.54	51.69	29.08	12.92
6		Upper Arm	Conic Frustrum	1.90339	4.197	2.798	1.574	0.7
7		Lower Arm	Conic Frustrum	1.160165	2.558	1.705	0.959	0.426
8		Upper Leg	Conic Frustrum	7.075615	15.6	10.4	5.85	2.6
9		Lower Leg	Conic Frustrum	2.999375	6.613	4.408	2.48	1.102
10		Hand	Sphere	0.454175	1.001	0.668	0.375	0.167
11		Foot	Rec. Parallel	0.951965	2.099	1.399	0.787	0.35
12	Total/Ave.			70.47805	155.4	103.6	58.27	25.9
13	Volume (ft ³)							
14	Volume (m ³)							

	I	J	K	L	M	N	O	P
1	Mars-Moon	Density k	Length L (COM)	Nu	Width W	Depth D	Radius R	Sigma
2								
3	2.1115848	1110	0.21058	0.5	2.07273	2.07273		
4	0.74397676	1110	0.08423	0.5			0.80431	
5	16.1537493	1030	0.5475	0.5	0.33998	0.35054		
6	0.87445435	1070	0.30128	0.436				1.6261
7	0.53286237	1130	0.23649	0.43				1.6149
8	3.24982133	1050	0.39685	0.433				1.62049
9	1.37760928	1090	0.39847	0.433				1.62049
10	0.20860202	1160		0.5			0.66098	
11	0.43723636	1100	0.24621	0.5	0.0979	0.06942		
12	32.3704823	1094.44						
13		2.27413	0.79533					
14		0.0644						

	Q	R	S	T	U
1	Parameter A	Parameter B	l _{xx}	l _{yy}	l _{zz}
2					
3			1.64353506	1.64353506	1.97514133
4			0.30978589	0.30978589	0.26196898
5			489.721121	489.737151	0.52418312
6	0.09453812	0.07108927	0.37744718	0.37744718	0.62242051
7	0.09494617	0.07076401	0.32747258	0.32747258	0.62510699
8	0.09474124	0.0709273	3.70404061	3.70404061	0.62375778
9	0.09474124	0.0709273	0.57026923	0.57026923	0.62375778
10			0.07936959	0.07936959	0.07936959
11			0.0104666	0.01008857	0.00114264
12					
13					
14					

B.2 INFORMED CONSENT FORM

This Appendix shows the informed consent form that all subjects read and signed before participating in the simulated partial gravity locomotion study. The informed consent form was part of the documentation presented to the NASA ARC Human Research Experiments Review Board (HRERB) in order to obtain permission to run the locomotion experiments.

Workload and Biomechanics for EVA: Simulated Microgravity and Partial Gravity, H.R. No. 89.

National Aeronautics and Space Administration

AMES RESEARCH CENTER
Moffett Field, California 94035

HUMAN RESEARCH CONSENT FORM

Part 1

Workload and Biomechanics for EVA: Simulated Microgravity and Partial Gravity, H.R. No. 89.

A. PURPOSE

The purpose of this study is to measure your body's reaction to specific exercise that is similar to an astronaut's work in space or on celestial bodies (i.e. the Moon or Mars). The amount of oxygen you consume and some biomechanical (forces you impart while walking) data will be measured. Your specific task will be to perform locomotive tasks on an underwater treadmill equipped with a force platform. The information will be useful for unveiling unanswered questions regarding how gravity affects human locomotion. The results will help us understand human performance in light of earth normal gravity (1-g), and impact the design of advanced space suits and the portable life support system (PLSS).

B. INVESTIGATORS

D. Newman, M.S.A.E., M.S., Principal Investigator
B. Webbon, PhD., Co-Investigator

C. NATURE OF TESTS AND EXPERIMENTS

In order to measure the body's reaction to locomotion for simulated microgravity and partial gravity, you will walk on an underwater treadmill. The exercise involves using your legs to walk along the treadmill belt at a specified speed. You will be ballasted with weights in order to load your body through a range from 0 to 100% of your body weight. You will be supplied with breathing air via a facemask and Hookah apparatus.

You are required to partake in six experimental sessions after being fully trained on the treadmill device. You will be given at least one practice session on the treadmill device in the 1-g environment. Following this training session, you will be given two or three additional practice sessions on the treadmill submerged in water to familiarize yourself with the device. Training sessions will continue until you are completely comfortable with the ballasting system and the underwater treadmill device.

A different simulated gravity level will be employed in each of the six experimental sessions. The first session will be a 1-g control experiment and you will exercise outside of the NBTF on the treadmill. The remaining sessions will take place underwater in the NBTF. Five gravity conditions will be simulated by ballasting you with weights. The five conditions are: 0-g, 1/6-g, 3/8-g, 2/3-g, and 1-g. You will perform a total of six experimental sessions: the five simulated gravity sessions in addition to the 1-g control session.

During each experimental session, you will exercise through a variable workload range of your maximum oxygen uptake. You will exercise at workload levels corresponding to 10%, 40%, and 70% until equilibrium values are reached (typically 20-40 minutes), then

Workload and Biomechanics for EVA: Simulated Microgravity and Partial Gravity, H.R. No. 89.

the subject will be asked to slowly cool down until coming to a complete stop on the treadmill. The treadmill speed will be controlled by the test monitor to insure that the range of workload values are safely realized.

The approximate length of the experimental sessions will be 2 hours, including over 3/4 of an hour for preparation and cool down, and 1 to 1 1/2 hours of exercise. You will have at least 2 days of rest between sessions.

D. MANNER IN WHICH TEST OR EXPERIMENTS WILL BE CONDUCTED

You will be asked to arrive at the test site dressed in a swimsuit. You will then be shown into a private room where you will measure your body weight (unclothed) and put on the heart rate chest transmitter belt. Then, you will be ballasted for the appropriate simulated gravity level. Once ballasted, you and the test monitor will walk to the NBTF platform. Here you will be supplied with breathing air. Once the airflow system is checked and operational, communication signals will be reviewed. Now you are ready to enter the tank.

You should proceed into the water after the safety diver. The safety diver will help you get positioned on the treadmill device. The force platform signals will be verified. You will be asked to relax for approximately 30 to 60 seconds. The test monitor controls the speed of treadmill, insuring a very slow speed (i.e. 1/2 mph) at the beginning. Once you are comfortable with the moving treadmill belt, you are to perform the 10-70% workload protocol. This is accomplished by keeping pace with the treadmill belt. Workload will be continuously monitored. After reaching steady state conditions (20 to 40 minutes) you will be asked to keep pace with a different treadmill speed. You will encounter three treadmill speeds per session. Then you are asked to slowly cool down until coming to a complete stop on the treadmill.

Upon completion of a session, the safety diver will help you ascend to the water surface. Once you reach the surface you can take-off the facemask and air supply. The technician will help you remove the ballast. You will be asked for subjective comments. You are asked to remain in the test area for an additional 30 minute rest period to fully recover. We will encourage you to sit down, drink some water or juice, and relax. Before leaving the site, you should confirm your schedule for the next session.

E. DURATION

The experiment sessions (practice sessions included) are scheduled to run for less than 3 hours each, and will start on July 1st, 1990, and run through August 31st, 1990.

F. FORESEEABLE INCONVENIENCE, DISCOMFORT, AND RISKS:

- a. The breathing air may produce a feeling of "dry mouth".
- b. Delayed-onset muscle soreness may occur due to locomotion and stabilization efforts.
- c. The weights may initially cause soreness or discomfort.
- d. Current literature dealing with treadmill exercise states that the chances of a cardiac emergency (non-fatal heart attack or serious arrhythmia) are 3 in 10,000, and the chances of sudden death are 1 in 10,000 [Guidelines for Exercise Testing and Prescription, 3rd Edition, 1986].

Workload and Biomechanics for EVA: Simulated Microgravity and Partial Gravity, H.R. No. 89.

G. RIGHT TO WITHDRAW FROM THE STUDY; HAZARDS ASSOCIATED WITH WITHDRAWAL

You have the right to withdraw from the study at any time for any reason. However, we hope that you will not volunteer for the study unless you intend to complete it. There are no hazards associated with withdrawal at any time during this study. You will be paid for time served up through departure from the study, but not thereafter.

H. ANSWERS TO QUESTIONS

You may receive answers to any questions related to this study by contacting the Principal Investigator at (415) 604-5719. Should any problems related to the study occur during its course, please contact the Principal Investigator at that number.

I. REMEDY IN THE EVENT OF INJURY

You will be covered by Worker's Compensation insurance during the course of your participation in this study. If you sustain an injury caused by this study, the benefits you will receive are those currently provided under the Worker's Compensation law in California. You cannot sue your employer because the law makes Worker's Compensation your only remedy against him. You may have other remedies against persons or organizations depending on the circumstances of your injury.

I certify that the series of tests for which _____ is to serve as a subject have been explained to him/her in detail.

Principal Investigator

Date

Medical Monitor

Date

REFERENCES

- Akin, D., Bowden, M., Cousins, D., and Paines, J. (1988), Biomechanics of Extravehicular Activity and Neutral Buoyancy Simulation. MIT Space Systems Laboratory, Prepared for NASA-JSC under NAS9-17266, Report Number 9-88.
- Alexander, R.M. (1988), *Elastic Mechanisms in Animal Movement*. © by Cambridge University Press, Cambridge, England.
- Asmussen, E. (1965), Muscular Exercise. In: *Handbook of Physiology. Respiration*. American Physiological Society. Washington D.C., 939-978.
- Åstrand, P-O., Ekholm, B., Messin, R., Saltin, B., and Sternberg, J. (1965), Intra-Arterial Blood Pressure During Exercise with Different Muscle Groups. *J. Appl. Physiol.*, **20**, 253-255.
- Åstrand, P-O. and Rodahl, K. (1977), *Textbook of Work Physiology: Physiological Bases of Exercise*. © by McGraw-Hill, Inc., New York.
- Baldwin, E. (1967), *Dynamic Aspects of Biochemistry*. 5th Edition, © by Cambridge University Press, New York.
- Blaxter, K. (1989), *Energy metabolism in animals and man*. © by Cambridge University Press, Cambridge, England, 16-17.
- Blickhan, R. and Full, R.J. (1987), Locomotion energetics of the ghost crab: II. Mechanics of the center of mass during walking and running. *J. exp. Biol.*, **130**, 155-174.
- Boslough, J. (1989), Searching for the Secrets of Gravity. *National Geographic*, **May**, 563-583.
- CRC Standard Mathematical Tables* (1984), 27th Edition, W.H. Beyer, ed., CRC Press, Boca Raton, Florida.
- Cavagna, G.A., Saibene, F., and Margaria, R. (1964), Mechanical work in running. *J. Appl. Physiol.*, **19**, 249-56.
- Cavagna, G.A., Zamboni, A., Faraggiana, T., and Margaria, R. (1972), Jumping on the moon: Power output at different gravity values. *Aerospace Med.*, **43**, 408-414.
- Cavagna, G.A., Thys, H., and Zamboni, G.A. (1976), The sources of external work in level walking and running. *J. Physiol.* **262**, 639-657.
- Cavagna, G.A., Heglund, N.C., and Taylor, C.R. (1977), Mechanical work in terrestrial locomotion: two basic mechanisms for minimizing energy expenditure. *American J. Physiology*, **233**: R243-R261.
- Cavagna, G.A. (1985), Force platforms as ergometers. *J. Appl Physiol.*, **39**(1), 174-179.
- Cavagna, G.A., Franzetti, P., Heglund, N.C., and Willems, P. (1988), The determinants of the step frequency in running, trotting, and hopping in man and other vertebrates. *J. Physiol.* **399**, 81-92.
- Cavanagh, P.R., Davis, B.L., and Miller, T.A. (1992), A biomechanical perspective on exercise countermeasures for long term space flight. Submitted to *Aviat. Space Environ. Med.*

- Chakraborty, S. (1990), Experimental Modeling of EVA Tasks and Workload Using Force-Torque Sensing Apparatus. Massachusetts Institute of Technology (MIT) Master's thesis, Department of Aeronautics and Astronautics.
- Cousins, D. (1987), *Biomechanics of Extravehicular Activity and its Neutral Buoyancy Simulation*. Massachusetts Institute of Technology (MIT) Dissertation, © by MIT, Cambridge, Massachusetts.
- de Bergerac, C., 1619-1655, *Other worlds; the comical history of the states and empires of the worlds of the moon and sun*. © 1965 by Oxford University Press, Cambridge, England.
- DeJours, P. (1964). Control of Respiration in Muscular Exercise. In: Handbook of Physiology. Respiration. American Physiological Society, Washington D.C.
- de Tolnay, C., (1975), *Michelangelo: Sculptor, Painter, Architect*. © 1975 by Princeton University Press, Princeton, New Jersey.
- Deutsch, S. (1969), Human Factors Review of Reduced-Gravity Simulators. *Human Factors*, 11(5), 417-418.
- Di Giovanni, C., Chambers, R.M. (1964), Physiologic and Psychologic Aspects of the Gravity Spectrum. *New England J. of Med*, 270(2), 88-94.
- Duddy, J.H. (1969), The Simulation of Weightlessness Using Water Immersion Techniques: An Annotated Bibliography. *Human Factors*, 11(5), 507-540.
- Einstein, A. (1879-1955), *Relativity: The Special and The General Theory; A Popular Exposition*. 17th Ed. © 1961. Crowne Publishers, New York.
- Farley, C.T. (1991), Energetics of walking and running: Insights from simulated reduced gravity experiments. Chapter 3, Harvard University Doctoral Dissertaion.
- Fox, E.L., Bartels, R.L., Chaloupka, E.C., Klinzing, J.E., and Hoche, J. (1975), Oxygen cost during exercise in simulated subgravity environments. *Aviat. Space Environ. Med.* 46(3), 300-303.
- Full, R.J. (1989), Mechanics and Energetics of Terrestrial Locomotion: From Biped to Polypeds. In: Energy Transformation in Cells and Animals. W. Wieser and E. Gnaiger, eds. Thieme, Stuttgart, 175-182.
- Full, R.J., (1991), Animal Motility and Gravity. *The Physiologist*, 34, Suppl. 1.
- Gleim, G.W. and Nicholas, J.A. (1989), Metabolic costs and heart rate responses to treadmill walking in water at different depths and temperatures. *The American Journal of Sports Medicine.*, 17(2), 248-252.
- Greene, P.R. and McMahon, T.A. (1979), Reflex stiffness of man's anti-gravity muscles during kneebends while carrying extra weight. *J. Biomechanics*, 12, 881-891.
- Hanavan, E.P. (1964), A Mathematical model of the Human Body. AMRL-TR-64-102, Aerospace Medical Research Laboratory, Wright-Patterson AFB, Ohio.

- He, G., Kram, R., and McMahon, T.A. (1991), Mechanics of running under simulated low gravity. *J Appl Physiol.*, **71**(3), 863-870.
- Heglund, N.C., Cavagna, G.A., and Taylor, C.R. (1982), Energetics and Mechanics of terrestrial locomotion. III. Energy changes of the center of mass as a function of speed and body size in birds and mammals. *J. exp. Biol.*, **79**, 41-56.
- Hewes, D.E. and Spady, A.A., Jr. (1964), Evaluation of Gravity Simulation Techniques for Studies of Man's Self-Locomotion in the Lunar Environment. NASA, TN D-2176.
- Hewes, D.E., Harris, R.L., and Spady, A.A., Jr. (1966), Comparative Measurements of Man's Walking and Running Gaits in Earth and Simulated Lunar Gravity. NASA, TN D-3363.
- Hewes, D.E. (1967), Analysis of Self-Locomotive Performance of Lunar Explorers Based on Experimental Reduced-Gravity Studies. NASA, TN D-3934.
- Hewes, D.E. (1969), Reduced-Gravity Simulators for Studies of Man's Mobility in Space and on the Moon. *Human Factors*, **11**(5), 419-432.
- Hoerner, S.F. (1958), *Fluid-Dynamic Drag*. Published by the author, 148 Busted Drive, Midland Park, New Jersey.
- Hoffer, J.A. and Andreassen, S. (1981), Regulation of soleus muscle stiffness in pre-mammillary cats: intrinsic and reflex components. *J. Neurophysiol.*, **45**, 267-285.
- Jenkins, (1991) Human Anatomy, Harvard University Medical School Lectures, Fall term.
- Keim, S.R. (1956), Fluid Resistance to Cylinders in Accelerated Motion. *Journal of the Hydraulics Div.*, ASCE, **83**, No. HY6.
- Kram, R. and Powell, A.J. (1989), A Treadmill-Mounted Force Platform. *J. Appl. Physiology*, **67**(4), 1692-1998.
- Kram, R. and Taylor, C.R. (1990), The energetics of running: a new perspective. *Nature*, **346**: 265-267.
- Kuehneggar, W., Roth, H.P., and Thiede, F.C. (1965), A Study of Man's Physical Capabilities on the Moon (III). Work Physiology Research Program, Doc. No. NSL 65-153 (NASA CR-66119), Northrop Space Laboratories.
- Lamb (1945), *Hydrodynamics*. 6th Edition. © by Dover Publications, New York.
- Letko, W., Hewes, D.E., and Spady, A.A., Jr. (1966), The Problems of Man's Adaptation to the Lunar Environment. Paper presented at a workshop sponsored by the National Academy of Sciences, National Research Council Committee on Heating, Bioacoustics, and Biomechanics, at the Ames Research Center, Moffett Field, California, January 25-27.
- Levine, S. (1978), Ventilatory Response to Muscular Exercise., In: Regulation of Ventilation and Gas Exchange. D.G. Davies and C.D. Barnes, eds. © by Academic Press, New York, 31-68.
- Lombrozo, P.C., Barr, R. E., and Abraham, L.D. (1988), Smoothing of noisy human motion data using digital filtering and spline curves. In the proceedings of the Tenth Annual Conference of IEEE Engineering and Medicine and Biology Society. New Orleans, Louisiana, November.

- Lomonaco, T., Scano, A., and Meineri, G. (1962), Physiological remarks on man's mobility upon partial or total relief of body weight. *Riv. Med. Aero.*, **25**, 623-635.
- Margaria, R., Cerretelli, P., Aghemo, P., and Sassi, G. (1963), Energy cost of running. *J. appl. Physiol.*, **18**, 367-370.
- Margaria, R. and Cavagna, G.A. (1964), Human locomotion in subgravity. *Aerospace Med.*, **35**, 1140-1146.
- Margaria, R. (1976), *Biomechanics and Energetics of Muscular Exercise*. © by Cambridge University Press, Cambridge, England.
- McDougall, W., (1985), *...the Heavens and the Earth: A Political History of the Space Age*. © by Basic Books, Inc., New York.
- McMahon, T.A. (1984), *Muscles, Reflexes, and Locomotion*. © by Princeton University Press, Princeton, New Jersey.
- McMahon, T.A. (1985), The Role of Compliance in Mammalian Running Gaits. *J. exp. Biol.*, **115**, 264.
- McMahon, T.A. and Cheng, G.C. (1990), The Mechanics of Running: How Does Stiffness Couple with Speed? *J. Biomech.*, **23**, Suppl. 1, 65-78.
- Mochon, S. and McMahon, T.A. (1981), Ballistic Walking: An Improved Model. *Mathematical Biosciences*, **52**, 241-260.
- Moran, M.J. (1969), Reduced-Gravity Human Factors Research with Aircraft. *Human Factors*, **11**(5), 463-472.
- Morlock, J.F. and Dressendorfer, R.H. (1974), Modification of a standard bicycle ergometer for underwater use. *Undersea Biomedical Research*, **1**(4), 335-342.
- Muybridge, E. (1957), *Animals in Motion*. © by Dover Publications, Inc., New York.
- NASA Man-Systems Integration Standards*. (1987), NASA-STD-3000, **1**, March.
- Newman, D.J. (1990), NASA Ames Research Center Hazard Report #ARCX-01-NB01. Advanced Life Support Division, EVA Systems Branch, Moffett Field, California.
- Newton, Isaac, Sir (1642-1727), *The Mathematical Papers of Isaac Newton*. © 1967, Cambridge, England.
- Nicogossian, A.E., Huntoon, C.L., and Pool, S.L. (1989), *Space Physiology and Medicine*, 2nd Edition. © by Lea and Febiger, Philadelphia, Pennsylvania.
- Oxford Dictionary of Quotations*. Third Edition. © 1979 by Oxford University Press, New York.
- Paines, J.D.B. (1986), A Review of Hydrodynamic Forces in Neutral Buoyancy Simulation of Microgravity EVA of IVA. MIT SSL Report Number 17-86, NASA/Johnson Contract No. NAS9-17266.

Pietrangeli, C., Chastel, A., Shearman, J., et al., *The Sistine Chapel: The Art, the History, and the Restoration*. © 1986 by Nippon Television, published in the U.S. by Harmony Books, New York.

Roberts, J.F. (1963), Walking Responses under Lunar and Low-Gravity Conditions. AMRL-TDR-63-112, Aerospace Medical Research Laboratory, Wright-Patterson AFB, Ohio.

Robertson, W.G. and Wortz, E.C. (1968), The Effect of Lunar Gravity on Metabolic Rates. AiResearch Report LS 67-2174, Contract NASA 6494. *Aerospace Med.*, **39**(8), 799-805.

Rodahl, K., Vokac, Z., Fugelli, P., Vaage, O., and Maehlum, S. (1974), Circulatory Strain: Estimated Energy Output and Catecholamine Excretion in Norwegian Coastal Fishermen. *Ergonomics*, **17**, 585-602.

Sanborn, W.G. and Wortz, E.C. (1967), Metabolic Rates During Lunar Gravity Simulation. *Aerospace Med.*, **38**(4), 380-382.

Sarpkaya, T. and Garrison, C.J. (1963), Vortex Formation and Resistance in Unsteady Flow. *Journal of Applied Mechanics*, **30**, Series E, No. 1, 16-24.

Sawka, M.N., Miles, D.S., Petrofsky, J.S., Wilde, S.W., and Glaser, R.M. (1982), Ventilation and Acid-Base Equilibrium for Upper and Lower Body Exercise. *Aviat. Space Environ. Med.*, **April**, 354-359.

Schilling, C.W., Werts, M.F., and Schandelmeier, N.R., eds. (1976), *The Underwater Handbook*. © by Plenum Press, New York.

Seminara, J.L. and Shavelson, R.J. (1969), Lunar Simulation. *Human Factors*, **11**(5), 451-462.

Spady, A.A., Jr. and Krasnow, W.D. (1966), Exploratory Study of Man's Self-Locomotion Capabilities with a Space Suit in Lunar Gravity. NASA, TN D-2641.

Springer, W.E., Stephens, T.L., and Streimer, I. (1962), The Metabolic Cost of Performing a Specific Exercise in a Low-Friction Environment. *Aerospace Med.*, **34**, 486-488.

Sternberg, J., Åstrand, P-O., Ekholm, B., Royce, J., and Saltin, B. (1967), Hemodynamic Responses to Work with Different Muscle Groups, Sitting and Supine. *J. Appl. Physiol.*, **42**, 61-70.

Stone, R.W. (1971), Man's motor performance including acquisition of adaptation effects in reduced gravity environments. In *Человек в Космосе*. Distributed by UNIVELT, Inc., P.O. Box 28130, San Diego, California, 92128.

Taylor, C.R. (1980), Mechanical efficiency: a useful concept? in *Aspects of Animal Movement*. H.Y. Elder and E.R. Trueman, eds. © by Cambridge University Press, Cambridge, England. 235-244.

Taylor, C.R., Heglund, N.C., McMahon, T.A., Looney, T.R. (1980), Energetic cost of generating muscular force during running: a comparison of large and small animals. *J. exp. Biol.*, **86**, 9-18.

- Thornton, W., Smith, R., Harris, J. (1990) Testing of the MKI/Kistler, MKII and Del-Mar Treadmill Instrumentation Systems. Exercise Countermeasure Facility, Crew Health Care System, McDonnell Douglas Space Systems Company, MDSS Reports I-1 and I-2, November 12, 1990.
- Trout, O.F., Jr., Loats, Jr., H.L., and Mattingly (1966), A Water-Immersion Technique for the Study of Mobility of a Pressure-Suited Subject Under Balanced-Gravity Conditions. NASA TND-3045, January.
- Trout, O.F. (1967), Water Immersion Simulation of Extravehicular Activities by Astronauts. *J. Spacecraft*, **4(6)**, 806-808.
- Trout, O.F. and Bruchey, W.J. (1969), Water Immersion Reduced-Gravity Simulation. *Human Factors*, **11(5)**, 473-488.
- Vern, J., 1828-1905, *From the earth to the moon*. Written in 1865. © 1960 by Dover Publications, New York.
- Vokac, Z., Bell, H., Bautz-Holter, E., and Rodahl, K. (1975), Oxygen Uptake/Heart Rate Relationship in Leg and Arm Exercise, Sitting and Standing. *J. Appl. Physiol.*, **39**, 54.
- Wahren, J. and Bygdeman, S. (1971), Onset of Angina Pectoris in Relation to Circulatory Adaptation During Arm and Leg Exercise. *Circulation*, **44**, 432-441.
- Waligora, J.M. and Horrigan, D.J. (1977), Metabolic Cost of Extravehicular Activities. Chapter 38, NASA document N77-33818, 395-399.
- Webbon, B.W. (1987), Neutral Buoyancy Test Facility Standard Operating Procedures. NASA Ames Research Center, Document # PN-86-7104-519-05.
- Whitman, W. (1900), *Leaves of Grass*. © by David McKay, Philadelphia, Pennsylvania.
- Whitsett, C.E. (1963), Some Dynamic Response Characteristics of Weightless Man. AMRL-TDR-63-18, Aerospace Medical Research Laboratory, Wright-Patterson AFB, Ohio.
- Wilkins, J. (1638). *The Discovery of a World in the Moone*.
- Wortz, E.C., Browne, L.E., Gafvert, M.R., Macek, A.J., Robertson, W.G., and Schreck, W.H. (1966), Study of Astronaut Capabilities to Perform Extravehicular Maintenance and Assembly Functions in Weightless Conditions. Prepared under NASA Contract NAS 1-5875. NASA CR-859, July.
- Wortz, E.C. and Prescott, E.J. (1966), The Effects of Subgravity Traction Simulation on the Energy Costs of Walking. *Aerospace Med.*, **37(12)**, 1217-1222.
- Wortz, E.C., Browne, L.E., Shreck, W.H., Macek, A.J., Robertson, W.G., and Gafvert, M.R. (1967), Study of Astronaut Capabilities to Perform Extravehicular Maintenance and Assembly Function in Weightless Conditions. NASA CR-859, September, 20.
- Wortz, E.C. (1968), Effects of reduced gravity environments on human performance. *Aerospace Med.*, **39**: 963-965.
- Wortz, E.C. (1969), Work in Reduced-Gravity Environments. *Human Factors*, **11(5)**, 433-440.